

**The influence of cyst nematodes on the plant secretory
pathway**

Ashley Hayes

Submitted in accordance with the requirements for the degree of
Doctor of Philosophy

The University of Leeds

School of Biology

December 2022

The candidate confirms that the work submitted is their own and that appropriate credit has been given where reference has been made to the work of others.

This copy has been supplied on the understanding that it is copyright material and that no quotation from the thesis may be published without proper acknowledgement.

The right of Ashley Hayes to be identified as Author of this work has been asserted by her in accordance with the Copyright, Designs and Patents Act 1988.

Acknowledgements

Firstly, I'd like to thank my two supervisors, Prof. Peter Urwin and Prof. Jurgen Denecke, whose combined knowledge and expertise made this project possible. I'm highly grateful to have been supervised by them both.

I'd like to specially thank Dr. Catherine Lilley. She is a great asset to the Urwin lab, I'm beyond appreciative of all of the advice and support she has given to me over the years.

Thank you to the other members, both past and present in the Urwin and Denecke labs, for all of the help you've given me and for the friendships I've made. You have made both labs such a happy and welcoming environment to be in.

Thanks to everyone else in the Centre for Plant Sciences who has helped me or made me smile along the way, I will be taking so many fond memories away with me!

Finally, I'd like to thank my partner, family and friends for their endless support throughout my project, especially during the final year.

This project was funded by the Biotechnology and Biological Sciences Research Council (BBSRC).

"A journey of a thousand miles begins with one step"

Lao Tzu

Abstract

Cyst nematodes are economically important plant pathogens that induce vast subcellular changes in host root cells to form a specialised feeding site, the syncytium. Previously characterised changes to the plant secretory pathway during syncytial formation include the proliferation of the endoplasmic reticulum (ER) and Golgi apparatus, and the replacement of the large central vacuole with numerous smaller vacuoles. To further characterise the plant secretory pathway in plant-cyst nematode interactions, novel dual fluorescence marker constructs were developed. Each construct contained a Golgi marker fused to YFP and an additional plant secretory pathway marker fused to RFP. Stable *Arabidopsis* marker lines expressing these constructs were infected with the beet cyst nematode *Heterodera schachtii* to provide a model host-cyst nematode system.

Fluorescence microscopy evidenced small vacuoles throughout the syncytium as expected. However, all other plant secretory markers within the dual fluorescence lines were undetectable in syncytia, suggesting disruption to the plant secretory pathway. To support this, gene expression analysis of a subset of plant secretory pathway genes was conducted using published RNA-seq data. Results from this suggest the altered regulation of genes involved in the early secretory pathway and post-Golgi trafficking, validating the fluorescence microscopy observations.

Another aim of this work was to identify novel cyst nematode effectors containing a single C-terminal transmembrane domain (TMD), that are predicted to localise to the ER. For this, a multi-step bioinformatics pipeline was created, using the proteomes of *Heterodera schachtii* and the potato cyst nematode *Globodera pallida*. Eight screened nematode cDNAs were cloned, with tobacco leaf epidermal cells transformed to analyse subcellular localisation, and in-situ hybridisations conducted to validate gland cell expression indicative of effector activity. From this, five novel putative effector genes were identified, localising to varied subcellular compartments, including the ER, nucleus, and peroxisomes. This effector screen has contributed to growing evidence that plant pathogen effectors can have transmembrane domains, and if studied further, these genes could provide cyst nematode target genes for RNA interference.

Table of Contents

| | |
|---|-------------|
| Abstract | iii |
| Table of Contents | iv |
| List of Figures | ix |
| List of Tables | xiii |
| List of abbreviations | xv |
| Chapter 1 General Introduction | 1 |
| 1.1 Nematoda | 1 |
| 1.1.1 Plant Parasitic Nematodes (PPNs) | 1 |
| 1.1.2 Sedentary endoparasitic PPNS | 2 |
| 1.1.3 Cyst nematodes | 2 |
| 1.1.4 The cyst nematode feeding site, the syncytium | 4 |
| 1.2 The plant secretory pathway | 7 |
| 1.2.1 Overview | 7 |
| 1.2.2 The conventional plant secretory pathway in more detail | 9 |
| 1.2.3 Unconventional Protein Secretion Pathways | 12 |
| 1.3 The plant secretory pathway during pathogen infection | 12 |
| 1.3.1 The ER and Golgi | 12 |
| 1.3.2 Intermediate organelles: the TGN and PVCs | 13 |
| 1.3.3 Vacuoles | 14 |
| 1.3.4 The exocyst | 15 |
| 1.3.5 Changes to the plant secretory pathway during nematode feeding site formation | 15 |
| 1.4 Cyst nematode effectors | 20 |
| 1.4.1 Cyst nematode effector secretion and delivery | 20 |
| 1.4.2 Cell biology of nematode effectors | 21 |
| 1.4.3 PPN effectors which interact with the plant secretory pathway | 23 |
| 1.5 Research gaps | 25 |
| 1.5.1 The plant secretory pathway during syncytial formation | 25 |
| 1.5.2 Cyst nematode effectors | 25 |
| 1.6 Aims and objectives | 26 |
| Chapter 2 Materials and Methods | 27 |
| 2.1 Nematode cyst collection and hatching | 27 |
| 2.2 Arabidopsis infection with <i>H. schachtii</i> in tissue culture | 27 |
| 2.3 Media | 27 |

| | | |
|--|---|-----------|
| 2.3.1 | Luria-Bertani LB Growth Medium | 27 |
| 2.3.2 | ½ MS 10 Media | 28 |
| 2.3.3 | 0.5 X TBE Buffer | 28 |
| 2.3.4 | Tobacco leaf infiltration buffer | 28 |
| 2.4 | Molecular Cloning Techniques | 28 |
| 2.4.1 | Transformation of competent <i>Escherichia coli</i> cells | 28 |
| 2.4.2 | Transformation of competent <i>Agrobacterium tumefaciens</i> Gv3101 cells | 28 |
| 2.4.3 | Colony PCRs | 29 |
| 2.4.4 | DNA minipreps | 29 |
| 2.4.5 | Preparative and qualitative restriction digests | 29 |
| 2.4.6 | Filling sticky ends | 29 |
| 2.4.7 | Dephosphorylation of 5' ends | 30 |
| 2.4.8 | DNA fragment isolations | 30 |
| 2.4.9 | Ligations | 30 |
| 2.4.10 | Polymerase Chain Reaction (PCR) | 30 |
| 2.4.11 | Sanger Sequencing | 31 |
| 2.5 | Arabidopsis transformation by floral dip | 31 |
| 2.6 | <i>Agrobacterium</i> -mediated transient gene expression within tobacco | 32 |
| 2.7 | Confocal Laser Scanning Microscopy (CLSM) | 32 |
| Chapter 3 The development of dual fluorescence reporter constructs to monitor the plant secretory pathway | | 33 |
| 3.1 | Introduction | 33 |
| 3.2 | Methods | 34 |
| 3.2.1 | Organelle markers within the double fluorescent constructs | 34 |
| 3.2.2 | Promoters used for marker expression | 35 |
| 3.2.3 | DNA plasmid construction | 36 |
| 3.2.4 | Primers for sequencing | 40 |
| 3.2.5 | The selection of primary transformants | 40 |
| 3.2.6 | Screening transgene expression using confocal microscopy | 40 |
| 3.3 | Results | 41 |
| 3.3.1 | Qualitative restriction digests | 41 |
| 3.3.2 | Subcellular localisation of the double fluorescent reporter constructs | 43 |
| 3.4 | Discussion | 65 |
| 3.4.1 | Construct Design | 65 |

| | | |
|--|--|------------|
| 3.4.2 | <i>Agrobacterium</i> -mediated tobacco leaf infiltrations and transgenic Arabidopsis lines | 65 |
| 3.4.3 | Conclusions | 73 |
| Chapter 4 Imaging syncytia within fluorescent Arabidopsis marker lines | | 75 |
| 4.1 | Introduction | 75 |
| 4.2 | Methods | 76 |
| 4.2.1 | Arabidopsis marker lines infected with <i>H. schachtii</i> | 76 |
| 4.2.2 | Confocal microscopy of Arabidopsis syncytia | 77 |
| 4.2.3 | The analysis of secretory pathway related genes in Arabidopsis syncytia | 77 |
| 4.3 | Results | 79 |
| 4.3.1 | Expression analysis of secretory pathway related genes in Arabidopsis syncytia | 79 |
| 4.3.2 | Confocal imaging of syncytia in fluorescent Arabidopsis lines | 89 |
| 4.4 | Discussion | 105 |
| 4.4.1 | General observations using fluorescence microscopy in Arabidopsis syncytia | 105 |
| 4.4.2 | The ER and Golgi in syncytia | 106 |
| 4.4.3 | Post-Golgi organelles in syncytia: the TGN, PVCs and LPVCs .. | 110 |
| 4.4.4 | The vacuoles in syncytia | 112 |
| 4.4.5 | Conclusions | 114 |
| Chapter 5 Identifying novel cyst nematode effectors containing C-terminal transmembrane domains | | 115 |
| 5.1 | Introduction | 115 |
| 5.1.1 | ER-targeting pathogen effectors containing a C-terminal TMD ... | 115 |
| 5.1.2 | Evidence of ER-targeting effectors in cyst nematodes | 116 |
| 5.2 | Materials and Methods | 117 |
| 5.2.1 | Effector screen pipeline | 117 |
| 5.2.2 | Gene cloning | 119 |
| 5.2.3 | In-situ hybridisation | 121 |
| 5.2.4 | Subcellular localisation analysis | 124 |
| 5.3 | Results | 128 |
| 5.3.1 | Overview of the effector screen pipeline | 128 |
| 5.3.2 | Cluster analysis for the expression of tail-anchored cyst nematode proteins containing signal peptides | 130 |
| 5.3.3 | Genes chosen for further analysis | 133 |
| 5.3.4 | Subcellular localisation prediction for each gene | 135 |
| 5.3.5 | The positive control gene GPLIN_000854400 | 137 |

| | | |
|---|--|------------|
| 5.3.6 | Hsc_gene_15040 | 141 |
| 5.3.7 | Hsc_gene_2739 | 145 |
| 5.3.8 | GPLIN_001269700 | 149 |
| 5.3.9 | Hsc_gene_19069 | 153 |
| 5.3.10 | Hsc_gene_19059 | 157 |
| 5.3.11 | Hsc_gene_14672 | 161 |
| 5.3.12 | Hsc_gene_10206 | 165 |
| 5.3.13 | GPLIN_000933000 | 169 |
| 5.4 | Discussion | 174 |
| 5.4.1 | Putative ER-targeting cyst nematode effectors | 174 |
| 5.4.2 | Putative effectors targeting other subcellular compartments | 175 |
| 5.4.3 | Proteins discounted as putative effectors | 177 |
| 5.4.4 | The efficacy of the effector screen | 178 |
| 5.4.5 | Conclusions | 181 |
| Chapter 6 General Discussion | | 182 |
| 6.1 | Dual fluorescence reporters provide new insight into the plant secretory pathway | 182 |
| 6.2 | Common aspects of the plant secretory pathway across plant-pathogen interactions | 183 |
| 6.2.1 | The early secretory pathway reveals features of both plant defence and susceptibility | 183 |
| 6.2.2 | Atypical secretion and vacuolar sorting occurs across plant-pathogen interactions | 184 |
| 6.2.3 | The vacuoles of syncytia have both unique and common features to other plant-pathogen interactions | 185 |
| 6.2.4 | A novel model for the plant secretory pathway in syncytia | 185 |
| 6.3 | Nematode effectors target diverse subcellular compartments in the host | 187 |
| 6.3.1 | ER-targeting cyst nematode effectors reveal conserved and potentially unique functions | 187 |
| 6.3.2 | A putative <i>H. schachtii</i> effector with potential ROS-modulating function | 188 |
| 6.3.3 | A putative <i>H. schachtii</i> effector hypothesised to target host gene expression | 188 |
| 6.3.4 | Putative effectors potentially targeting COPII and COPI cycling, or vacuolar sorting | 189 |
| 6.3.5 | Research gaps on plant pathogen effector delivery | 189 |
| 6.4 | Conclusions | 190 |

References 192

List of Figures

| | |
|---|----|
| Figure 1. 1. Schematic representation of the life cycle of a cyst nematode | 4 |
| Figure 1. 2. The ultrastructure of a syncytium induced by a male J3 <i>Heterodera schachtii</i> within <i>Arabidopsis</i> | 6 |
| Figure 1. 3. An overview of the plant secretory pathway | 8 |
| Figure 1. 4. Schematic representation of SNARE-mediated membrane fusion | 11 |
| Figure 1. 5. Diagram of the anterior portion of a cyst nematode J2, showing the position of the dorsal and subventral pharyngeal glands | 20 |
| Figure 3. 1. The development of pTASH1, a precursor to pTASH2, which is the backbone for all dual reporter constructs made | 36 |
| Figure 3. 2. The development of pTASH2, a backbone construct for all pTASH dual fluorescence constructs | 37 |
| Figure 3. 3. pTASH2 plasmid features | 38 |
| Figure 3. 4. The development of the dual reporter construct pTASH3, used to demonstrate how all dual fluorescence constructs were created | 39 |
| Figure 3. 5. Qualitative EcoRI-HindIII restriction digests performed on the pTASH constructs | 42 |
| Figure 3. 6. Qualitative NheI restriction digest performed on the pTASH constructs | 42 |
| Figure 3. 7. Tobacco leaf epidermal cells infiltrated with pTASH2, expressing the Golgi marker secYFP-ERD2b alone | 43 |
| Figure 3. 8. pTASH3, co-expressing the Golgi marker secYFP-ERD2b and the LPVC marker RFP-Rha1, within infiltrated tobacco leaves | 44 |
| Figure 3. 9. pTASH4, co-expressing the Golgi marker secYFP-ERD2b and the PVC marker RFP-BP80 under the control of the 35S promoter, within infiltrated tobacco leaves | 46 |
| Figure 3. 10. Tobacco leaf epidermis cells infiltrated with pTASH5, co-expressing the Golgi marker secYFP-ERD2b and the PVC marker pNOS:RFP-BP80 | 47 |
| Figure 3. 11. pTASH6, co-expressing the cis-Golgi marker secYFP-ERD2b and the PVC marker TR2:RFP-BP80, within infiltrated tobacco leaves | 48 |
| Figure 3. 12. pTASH7, co-expressing the Golgi marker secYFP-ERD2b and the ER marker RFP-HDEL within infiltrated tobacco leaf epidermis cells | 49 |
| Figure 3. 13. pTASH8, co-expressing the Golgi marker secYFP-ERD2b and the ER marker secRFP-p24a TM within infiltrated tobacco leaf epidermis cells | 50 |
| Figure 3. 14. pTASH9, co-expressing the Golgi marker secYFP-ERD2b with the TGN marker RFP-BP80(Tyr) within infiltrated tobacco leaf epidermis cells | 51 |
| Figure 3. 15. pTASH10, co-expressing the Golgi marker secYFP-ERD2b and the TGN marker RFP-SYP61 within infiltrated tobacco leaves | 53 |

| | |
|---|-----|
| Figure 3. 16. pTASH11, co-expressing the Golgi marker secYFP-ERD2b with the LPVC marker RFP-BP80(Leu) within infiltrated tobacco leaf epidermis cells | 54 |
| Figure 3. 17. pTASH12, co-expressing the Golgi marker secYFP-ERD2b with the vacuole marker Aleu-RFP within infiltrated tobacco leaf epidermis cells | 55 |
| Figure 3. 18. pTASH13, co-expressing the Golgi marker secYFP-ERD2b and the tonoplast marker CBL6-RFP within infiltrated tobacco leaves | 56 |
| Figure 3. 19. Primary transformed, T ₁ seedlings grown on ½ MS10 plates containing kanamycin and cefotaxime, after two weeks of growth | 57 |
| Figure 3. 20. Confocal images of the roots of selected T ₂ transgenic lines ... | 58 |
| Figure 3. 21. Continued confocal images of root cells of the best expressing T ₂ transgenic lines | 59 |
| Figure 3. 22. Confocal images of the cotyledons of selected T ₂ transgenic Arabidopsis lines | 60 |
| Figure 3. 23. Continued confocal images of the cotyledons of selected T ₂ transgenic lines | 61 |
| Figure 4. 1. The expression clusters of plant secretory pathway genes in Arabidopsis syncytia induced by <i>H. schachtii</i> , across various parasitic life stages | 81 |
| Figure 4. 2. The uninfected control roots of pTASH8 Arabidopsis lines, expressing the ER marker secRFP-p24aTM with secYFP-ERD2b | 91 |
| Figure 4. 3. 8 days post infection (dpi) syncytia induced by <i>H. schachtii</i> within Arabidopsis roots expressing pTASH8 | 92 |
| Figure 4. 4. Uninfected Arabidopsis roots expressing the ER marker GFP-HDEL | 93 |
| Figure 4. 5. 13 dpi syncytia induced by <i>H. schachtii</i> in Arabidopsis lines expressing GFP-HDEL | 94 |
| Figure 4. 6. pTASH12 expression within uninfected Arabidopsis root cells ... | 95 |
| Figure 4. 7. 10 dpi syncytia in pTASH12 Arabidopsis roots | 96 |
| Figure 4. 8. pTASH13 expression in uninfected Arabidopsis root cells | 97 |
| Figure 4. 9. The expression of pTASH13 within Arabidopsis syncytia induced by <i>H. schachtii</i> , at 17 dpi | 98 |
| Figure 4. 10. The expression of pTASH10 in uninfected Arabidopsis root cells | 99 |
| Figure 4. 11. The expression of pTASH10 within Arabidopsis syncytia induced by <i>H. schachtii</i> , at 12 dpi | 100 |
| Figure 4. 12. The expression of pTASH3 in uninfected Arabidopsis root cells | 101 |
| Figure 4. 13. The expression of pTASH3 within Arabidopsis syncytia induced by <i>H. schachtii</i> , at 18 dpi | 102 |

| | |
|---|-----|
| Figure 4. 14. The expression of pTASH5 in the roots of uninfected <i>Arabidopsis</i> | 103 |
| Figure 4. 15. The expression of pTASH5 within <i>Arabidopsis</i> syncytia induced by <i>H. schachtii</i> , at 13 dpi | 104 |
| Figure 5. 1. A plasmid map of the pGEM®-T Easy vector | 120 |
| Figure 5. 2. Plasmid maps for the entry and destination gateway constructs, which were used to develop the N- and C- terminal GFP fusions | 126 |
| Figure 5. 3. A schematic of the effector screen pipeline | 129 |
| Figure 5. 4. The gene expression clusters of <i>H. schachtii</i> genes containing a signal peptide and a C-terminal TMD | 131 |
| Figure 5. 5. The gene expression clusters of <i>G. pallida</i> genes containing a signal peptide and a C-terminal TMD | 132 |
| Figure 5. 6. The analysis of GPLIN_000854400, the ER-localised 16H02 effector used as a positive control | 138 |
| Figure 5. 7. Tobacco leaf epidermal cells <i>Agro</i> -infiltrated with GFP-16H02 . | 139 |
| Figure 5. 8. Tobacco leaf epidermal cells co-infiltrated with GFP-16H02 and the ER marker secRFP-24aTM | 139 |
| Figure 5. 9. Tobacco leaf epidermal cells <i>Agro</i> -infiltrated with 16H02-GFP . | 140 |
| Figure 5. 10. Tobacco leaf epidermal cells co-infiltrated with 16H02-GFP and the ER marker secRFP-p24aTM | 140 |
| Figure 5. 11. The analysis of Hsc_gene_15040, a <i>H. schachtii</i> gene with no annotation | 142 |
| Figure 5. 12. Tobacco leaf epidermal cells <i>Agro</i> -infiltrated with the N-terminal GFP fusion for Hsc_gene_15040 | 143 |
| Figure 5. 13. Tobacco leaf epidermal cells co-infiltrated with GFP-Hsc_gene_15040 and the ER marker secRFP-p24aTM | 143 |
| Figure 5. 14. Tobacco leaf epidermal cells <i>Agro</i> -infiltrated with the C-terminal GFP fusion of Hsc_gene_15040 | 144 |
| Figure 5. 15. Tobacco leaf epidermal cells co-infiltrated with Hsc_gene_15040-GFP and the ER marker secRFP-p24aTM | 144 |
| Figure 5. 16. The analysis of Hsc_gene_2739, a <i>H. schachtii</i> protein with no annotation | 146 |
| Figure 5. 17. Tobacco leaf epidermal cells <i>Agro</i> -infiltrated with GFP-Hsc_gene_2739 | 147 |
| Figure 5. 18. Tobacco leaf epidermal cells co-infiltrated with GFP-Hsc_gene_2739 and the nucleus marker NLS-mCherry | 147 |
| Figure 5. 19. Tobacco leaf epidermal cells <i>Agro</i> -infiltrated with Hsc_gene_2739-GFP | 148 |
| Figure 5. 20. Tobacco leaf epidermal cells co-infiltrated with Hsc_gene_2739-GFP and the nucleus marker NLS-mCherry | 148 |
| Figure 5. 21. The analysis of GPLIN_001269700, a <i>G. pallida</i> gene with no annotation | 150 |

| | |
|--|-----|
| Figure 5. 22. Tobacco leaf epidermal cells <i>Agro</i> -infiltrated with GFP- GPLIN_001269700 | 151 |
| Figure 5. 23. Tobacco leaf epidermal cells co-infiltrated with GFP- GPLIN_001269700 and the ER marker secRFP-p24aTM | 151 |
| Figure 5. 24. Tobacco leaf epidermal cells <i>Agro</i> -infiltrated with GPLIN_001269700-GFP | 152 |
| Figure 5. 25. Tobacco leaf epidermal cells co-infiltrated with GPLIN_001269700-GFP and the ER marker secRFP-p24aTM | 152 |
| Figure 5. 26. The analysis of Hsc_gene_19069 (putative esophageal gland cell secretory protein 28) | 154 |
| Figure 5. 27. Tobacco leaf epidermal cells <i>Agro</i> -infiltrated with GFP- Hsc_gene_19069 | 155 |
| Figure 5. 28. Tobacco leaf epidermal cells co-infiltrated with GFP- Hsc_gene_19069 and the mitochondria marker ScCOX4sp-mCherry .. | 155 |
| Figure 5. 29. Tobacco leaf epidermal cells <i>Agro</i> -infiltrated with Hsc_gene_19069-GFP | 156 |
| Figure 5. 30. Tobacco leaf epidermal cells co-infiltrated with Hsc_gene_19069- GFP and the mitochondria marker ScCOX4sp-mCherry | 156 |
| Figure 5. 31. The analysis of Hsc_gene_19059 (no annotation) | 158 |
| Figure 5. 32. Tobacco leaf epidermal cells <i>Agro</i> -infiltrated with GFP- Hsc_gene_19059 | 159 |
| Figure 5. 33. Tobacco leaf epidermal cells of GFP-Hsc_gene_19059 co- infiltrated with the peroxisome marker mCherry-SKL | 159 |
| Figure 5. 34. Tobacco leaf epidermal cells <i>Agro</i> -infiltrated with Hsc_gene_19059-GFP | 160 |
| Figure 5. 35. Tobacco leaf epidermal cells co-infiltrated with Hsc_gene_19059- GFP and the peroxisome marker mCherry-SKL | 160 |
| Figure 5. 36. The analysis of Hsc_gene_14672, the Ran binding protein-1 .. | 162 |
| Figure 5. 37. Tobacco leaf epidermal cells <i>Agro</i> -infiltrated with GFP- Hsc_gene_14672 | 163 |
| Figure 5. 38. Tobacco leaf epidermal cells <i>Agro</i> -infiltrated with 35S:GFP, used a control for cytoplasm localisation | 163 |
| Figure 5. 39. Tobacco leaf epidermal cells <i>Agro</i> -infiltrated with Hsc_gene_14672-GFP | 164 |
| Figure 5. 40. Tobacco leaf epidermal cells co-infiltrated with Hsc_gene_14672- GFP and the peroxisome marker mCherry-SKL | 164 |
| Figure 5. 41. The analysis of Hsc_gene_10206, predicted to be a homologue for the <i>H. avenae</i> effector Ha-acp1 | 166 |
| Figure 5. 42. Tobacco leaf epidermal cells <i>Agro</i> -infiltrated with GFP- Hsc_gene_10206 | 167 |
| Figure 5. 43. Tobacco leaf epidermal cells <i>Agro</i> -infiltrated with Hsc_gene_10206-GFP | 167 |

| | |
|---|-----|
| Figure 5. 44. Tobacco leaf epidermal cells co-infiltrated with Hsc_gene_10206-GFP and the plasmodesmata marker PCDB-mCherry | 168 |
| Figure 5. 45. The analysis of GPLIN_000933000, the <i>H. glycines</i> G17G01 effector homologue | 170 |
| Figure 5. 46. Tobacco leaf epidermal cells <i>Agro</i> -infiltrated with GFP-GPLIN_000933000 | 171 |
| Figure 5. 47. Tobacco leaf epidermal cells co-infiltrated with GFP-GPLIN_000933000 and the Golgi marker RFP-MNS3 | 171 |
| Figure 5. 48. Tobacco leaf epidermal cells co-infiltrated with GFP-GPLIN_000933000 and the ER marker secRFP-p24aTM | 172 |
| Figure 5. 49. Tobacco leaf epidermal cells <i>Agro</i> -infiltrated with GPLIN_000933000-GFP | 172 |
| Figure 5. 50. Tobacco leaf epidermal cells co-infiltrated with GPLIN_000933000-GFP and the Golgi marker RFP-MNS3 | 173 |
| Figure 5. 51. Tobacco leaf epidermal cells co-infiltrated with GPLIN_000933000-GFP and the ER marker secRFP-p24aTM, showing co-localisation | 173 |
| Figure 6. 1. A novel model for the plant secretory pathway in Arabidopsis syncytia induced by <i>H. schachtii</i> | 186 |

List of Tables

| | |
|--|-----|
| Table 1. 1. A list of previously characterised cyst nematode effectors that target diverse cellular processes | 22 |
| Table 2. 1. The PCR conditions for each DNA polymerase enzyme used | 31 |
| Table 3. 1. A list of the double fluorescence organelle marker constructs developed | 35 |
| Table 3. 2. Primer sequences used for the DNA sequencing of pTASH constructs | 40 |
| Table 3. 3. A summary of the localisation of each marker gene across the transient and stable expression systems | 72 |
| Table 3. 4. A summary of the stable transgenic lines that were selected for use in Chapter 4 | 74 |
| Table 4. 1. The names of the plant secretory pathway genes selected for expression analysis, and the reason why they were selected | 78 |
| Table 4. 2. The expression of ER-related genes in Arabidopsis syncytia | 84 |
| Table 4. 3. The expression of ER and Golgi trafficking components in Arabidopsis syncytia | 85 |
| Table 4. 4. The expression of Golgi-related trafficking genes in Arabidopsis syncytia | 85 |
| Table 4. 5. The expression of genes related to post-Golgi trafficking to the plasma membrane (PM) in Arabidopsis syncytia | 86 |
| Table 4. 6. The expression of vacuolar trafficking genes in Arabidopsis syncytia | 87 |
| Table 4. 7. The expression of vacuolar processing genes and tonoplast membrane proteins in Arabidopsis syncytia | 88 |
| Table 5. 1. The forward (F) and reverse (R) primers used to amplify each gene from the cDNA | 119 |
| Table 5. 2. In-situ probe synthesis reaction conditions using the Onetaq polymerase enzyme (New England Biolabs) | 122 |
| Table 5. 3. The forward (F) and reverse (R) primers used to generate in-situ probes | 122 |
| Table 5. 4. The sequences of the forward (F) and reverse (R) primers used to clone each gene into the pCR™8/GW/TOPO™ gateway entry vector .. | 125 |
| Table 5. 5. The selection of <i>H. schachtii</i> and <i>G. pallida</i> genes containing a signal peptide and C-terminal TMD, identified as homologues of cyst nematode effectors | 134 |
| Table 5. 6. The selection of <i>H. schachtii</i> and <i>G. pallida</i> genes containing a signal peptide and C-terminal TMD | 134 |
| Table 5. 7. The subcellular localisation prediction of each protein, using the three servers PSORTII, MultiLoc2 and MULocDeep | 136 |

List of abbreviations

| | |
|--------------------|--|
| ARF | ADP ribosylation factor |
| ADAS | Agricultural development and advisory service |
| ADH | Alcohol dehydrogenase |
| BLAST | Basic local alignment search tool |
| BP80 | Vacuolar-sorting receptor 1 |
| CBL6 | Calcineurin B-like protein 6 |
| CCV | Clathrin-coated vesicle |
| CIP | Calf-intestinal alkaline phosphatase |
| CLSM | Confocal laser scanning microscopy |
| COG complex | Conserved oligomeric Golgi (COG) complex |
| COPI | Coatomer protein I coated |
| COPII | Coatomer protein II coated |
| CRT | Calreticulin |
| DIG | Digoxigenin |
| DOG box | Dorsal gland promoter element motif |
| Dpi | Days post infection |
| EGF | Epidermal growth factor |
| EM | Electron microscopy |
| ER | Endoplasmic reticulum |
| ERD2 | Endoplasmic reticulum retention defective 2 |
| ERES | Endoplasmic reticulum exit sites |
| ESCRT | Endosomal sorting complex required for transport |
| EVs | Extracellular vesicles |
| EXPO | Exocyst-positive organelle |
| FP | Fluorescent protein |
| GFP | Green fluorescent protein |
| ISC | Initial syncytial cell |
| LB | Luria-Bertani |
| LOESS | Locally estimated scatterplot smoothing |
| LPVC | Late prevacuolar compartment |
| LSP | Leaderless secretory protein |
| MAPK | Mitogen-activated protein kinase |
| MS | Murashige and Skoog |
| NASC | Nottingham Arabidopsis Stock Centre |
| NCBI | National Center for Biology Information |
| NEB | New England Biolabs |

| | |
|--------------|--|
| NLS | Nuclear localisation signal |
| NOS | Nopaline synthase |
| PCD | Programmed cell death |
| PCR | Polymerase chain reaction |
| PDCB1 | Plasmodesmata callose-binding protein 1 |
| PDF1 | Plant Defensin type 1 |
| PDI | Protein disulfide-isomerase |
| PM | Plasma membrane |
| PPN | Plant-parasitic nematode |
| PR1 | Pathogenesis-related 1 |
| PSV | Protein storage vacuole |
| PVC | Prevacuolar compartment |
| QTL | Quantitative trait locus |
| RBP | RNA-binding protein 1 |
| RER | Rough endoplasmic reticulum |
| RFP | Red fluorescent protein |
| ROS | Reactive oxygen species |
| SCN | Soybean cyst nematode |
| SER | Smooth endoplasmic reticulum |
| SNAP | Soluble NSF attachment protein |
| SNARE | Soluble N-ethylmaleimide-sensitive-factor attachment protein receptor |
| SYP61 | Syntaxin 61 |
| TGN | Trans-Golgi network |
| TM | Transmembrane |
| TMD | Transmembrane domain |
| TMHMM | Transmembrane prediction using Hidden Markov Models |
| UPR | Unfolded protein response |
| UPS | Ubiquitin proteasome system |
| VSR | Vacuolar sorting receptor |
| YFP | Yellow fluorescent protein |

Chapter 1 General Introduction

1.1 Nematoda

Nematodes, also known as roundworms, comprise the Nematoda phylum. This is amongst the most numerous animal phyla, with over 28,000 species described, identified in almost every habitat on earth (Hodda, 2022; Bongers and Ferris, 1999; Hodda et al, 2009). This phylum is broadly categorised into two groups; free-living nematodes and parasitic nematodes. Free-living nematodes feed on bacteria, algae, fungi, dead organisms and living tissues, whereas parasitic nematodes depend on animal or plant hosts for survival, inducing disease or mortality. Free-living nematodes have large ecological benefits within aquatic and terrestrial environments, including the decomposition of organic matter, nutrient cycling in the soil and disease suppression (Neher, 2010; Moens et al, 2013). Contrastingly, parasitic nematodes pose a large threat to human, animal and plant health (Jones et al, 2013; Jasmer et al, 2003).

1.1.1 Plant Parasitic Nematodes (PPNs)

The global crisis in food security has been driven by various factors, including exponential population growth and changing diets (Godfray et al, 2010; Tilman et al, 2011). To solve this crisis, food production will need to increase by an estimated 50-70% by 2050 (Bruce, 2010). Thus, it will be essential to improve crop productivity through reducing crop losses. This includes reducing losses to pests and disease, which account for a loss of 20-40% of global crop yields each year (Teng and Krupa 1980; Oerke, 2006; Savary et al, 2019). Plant parasitic nematodes (PPNs) are major crop pests, causing annual global yield losses worth \$80 billion (Nicol et al, 2011). PPNs are associated with most agriculturally important crop species (Jones et al, 2013). Moreover, the extent of the global impact of PPNs is likely to be an underestimation. This is due to many factors, such as lack of awareness, the microscopic size of PPNs, and the symptoms resembling those induced by water and nutrient deficiency (Oka et al, 2000). Concerningly, the damaging effects of PPNs may increase with climate change, with some species predicted to increase in abundance and distribution (Franco et al, 2019; Ghini et al, 2008).

Several sustainable PPN control strategies have been developed. This includes resistant crop varieties (Ali et al, 2017), biological control agents (Davies and Spiegel, 2011), crop rotation (Rashidifard et al, 2021) and cover crops (Chauvin et al, 2015). Yet despite these current strategies, PPNs still remain a large problem. The development of novel control strategies, such as HD-RNAi (host delivered RNA interference), have been facilitated by an increased molecular understanding of the plant-nematode interaction. HD-RNAi

suppresses essential nematode genes, through the delivery of double-stranded RNAs (dsRNAs) into feeding PPNs (reviewed in Joshi et al, 2022; Banerjee et al, 2017). Therefore, increased knowledge on the molecular mechanisms underlying PPN pathogenicity will identify novel target genes for RNAi, and potentially enable the development of additional control strategies.

1.1.2 Sedentary endoparasitic PPNs

PPNs display a wide range of feeding strategies. Some are migratory ectoparasites, which never enter the host, feeding externally on host root tissue as they move through the soil (Wyss, 1981). Other PPNs are migratory endoparasites, entering the host and migrating through host root tissue as they feed (Moens and Perry, 2009). Contrastingly, some PPNs are sedentary endoparasites, which are the most economically important group of PPNs, thus are the most important to control (Jones et al, 2013). Sedentary endoparasitic PPNs are the most evolved and successful group of nematodes, forming complex interactions with their hosts. These nematodes exploit key host developmental and physiological pathways to establish specialised feeding sites within the root (Siddique and Grundler, 2018). Sedentary PPNs become immobile after feeding site formation, using specialised feeding cells as their sole source of nutrients for the rest of their life (Wyss and Grundler, 1992). Therefore, one of the main targets for PPN control is feeding site development (Tytgat et al, 2000).

The feeding sites formed by sedentary endoparasitic PPNs are unique and specialised organs within the host root. Different types of feeding sites are formed by different sedentary endoparasitic PPNs, with those formed by root-knot nematodes and cyst nematodes being the best studied (reviewed in Kyndt et al, 2013). Root-knot nematodes form giant cells within the host root. These consist of a group of 4-8 multinucleate, hypertrophied 'giant' cells within the root, formed through repeated rounds of cell division and growth in the absence of cytokinesis (Jones and Payne, 1978). Contrastingly, cyst nematodes form syncytia within host roots that consist of large, multinucleate cells formed through partial cell wall dissolution and protoplast fusion (Jones and Northcote, 1972).

1.1.3 Cyst nematodes

Cyst nematodes are one of the most economically important groups of plant parasitic nematodes, with species belonging to *Heterodera* and *Globodera* genera impacting globally important crops (Jones et al, 2013). For instance, the soybean cyst nematode *H. glycines* reduces soybean yields in the US by over \$1.5 billion per year (Wrather et al, 2001), the sugar beet cyst nematode *H. schachtii* results in a crop loss worth \$95 million in EU countries each year (Müller, 1999), and potato cyst nematodes, *G.*

rostochiensis and *G. pallida*, result in an annual crop loss of \$80 million in the UK (Haydock and Evans, 1998).

Cyst nematodes develop intimate and prolonged relationships with their hosts (**Figure 1.1**). They hatch from their eggs as infective second stage juveniles, J2s, and locate host roots in the soil via chemotaxis (Clemens et al, 1994). J2s enter the host preferentially behind the root tip in the elongation zone, and intracellularly migrate towards the vascular cylinder (Holtmann et al, 2000). Once within the vascular cylinder, cyst nematodes initiate the formation of the specialised feeding site, the syncytium. Following syncytial formation, J2s moult three times to reach the J3, J4 then adult life stages. Shortly before the moult into J3, sexual differentiation occurs. After the J3 phase, the male stops feeding, and the adult male begins to develop within the J4 cuticle. During the moult into the adult phase, the males regain their vermiform shape and become motile to enable mating. Contrastingly, the adult female remains sedentary, producing eggs at the end of the feeding stage. The female then dies, forming a protective case around the eggs. Cysts can contain hundreds of eggs (Sipes et al, 1992), and in the absence of a host, these can remain dormant for many years (Evans and Stone, 1977).

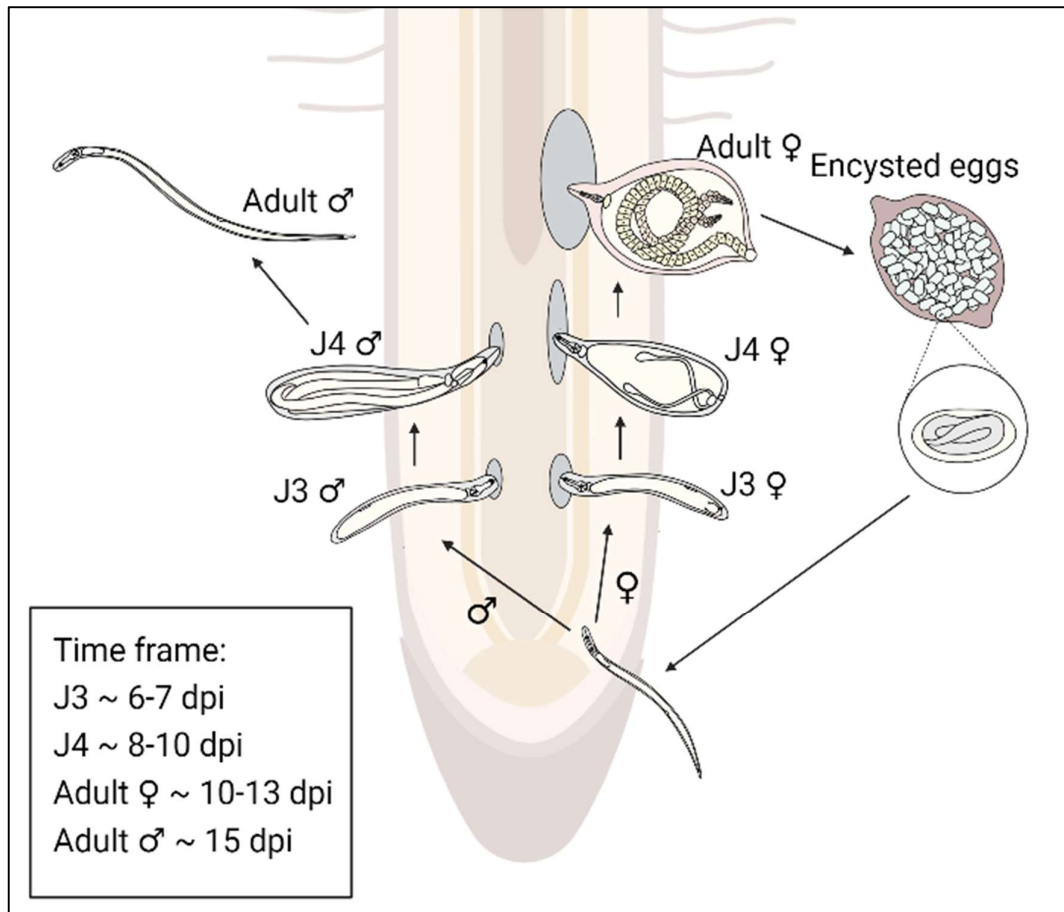


Figure 1. 1. Schematic representation of the life cycle of a cyst nematode. The life cycle begins as infective stage juveniles (J2) hatch from eggs. J2s enter the root behind the root tip, and migrate intracellularly until they reach the vascular cylinder. The initial syncytial cell is chosen, as the J2 starts to feed and the syncytium develops. The J2 becomes immobile, moulting into J3 then J4 stages. Adult males leave the root to mate with adult females, who remain sedentary. The adult female then dies to form a cyst filled with eggs. For each parasitic life stage, an estimated time frame is given in days post infection (dpi), using information based on *Heterodera glycines* (Thapa et al, 2019). Diagram is not drawn to scale.

1.1.4 The cyst nematode feeding site, the syncytium

The syncytium is initiated from a single cell (Golinowski et al, 1996). This is usually located within the inner cortex, pericycle or parenchyma (Golinowski et al, 1996; Jones and Northcote, 1972; Sijmons et al, 1991). Once the initial syncytial cell (ISC) has been selected, the nematode uses its stylet to pierce the ISC cell wall (Endo, 1991). Esophageal gland secretions are then released from the stylet. These are hypothesised to reach the host's cell cytoplasm through a small pore in the plasma membrane, located at the stylet's orifice (Sobczak et al, 1999). Cyst nematode secretions contain a vast range of effector molecules that trigger the re-differentiation of the ISC and surrounding cells (Ali et al, 2018). Plasmodesmata of the ISC widen to create cell wall openings, followed by protoplast fusion of the ISC with adjacent cells (Bohlmann and Sobczak,

2014). Partial cell wall dissolution and protoplast fusion then occurs in surrounding cells to create a large, multinucleate feeding site (Ohtsu et al, 2017). After maturation, syncytia induced by adult cyst nematodes consist of around 200 cells, although those induced by females are typically larger than those induced by males (Goverse et al, 2000). Despite this, the ultrastructure of male and female syncytia are similar (Sobczak et al, 1997).

During syncytial formation, root cells are reprogrammed into highly metabolically active feeding cells to provide the nematode with lipids, carbohydrates, vitamins and other nutrients that are essential for its survival (Goheen et al, 2013). The high metabolic status of syncytial cells is evidenced by their ultrastructure. For instance, within 24 hrs of infection, syncytial cells have a dense and granular cytoplasm (Hussey and Grundler, 1998), containing abundant mitochondria (Melillo et al, 1990), lipid bodies (Golinowski et al, 1996), and plastids (Jones and Northcote, 1972).

In addition to aspects of high metabolic activity, root cells undergo a range of other subcellular changes during syncytial formation (**Figure 1.2**). This includes large changes to the host cell wall composition. For example, cell wall ingrowths appear in syncytial cells next to xylem vessels, increasing the surface area for solute transfer (Hoth et al, 2008; Rodiuc et al, 2014). Also, the outer cell wall of the syncytium is thickened to cope with the increased turgor pressure (Doucet et al, 2004). Another remarkable ultrastructural feature of syncytial cells is the enlargement of the nucleus and nucleolus (Sobczak and Golinowski, 2009; Burrows, 1992). Changes to nuclei in syncytial cells are in conjunction with large changes to host transcription. For example, over 7000 *Arabidopsis* genes are differentially regulated upon infection with *H. schachtii* (Szakasits et al, 2009). Changes to the cell cytoskeleton are also essential for syncytial formation, with strong disruption to actin and tubulin cytoskeletons observed (Engler et al, 2004). Finally, large changes to plant secretory pathway organelles occur during syncytial formation. This includes the replacement of the large central vacuole with numerous smaller vacuoles (Doucet et al, 2004), and proliferation of the ER and Golgi apparatus (Jones and Northcote, 1972).

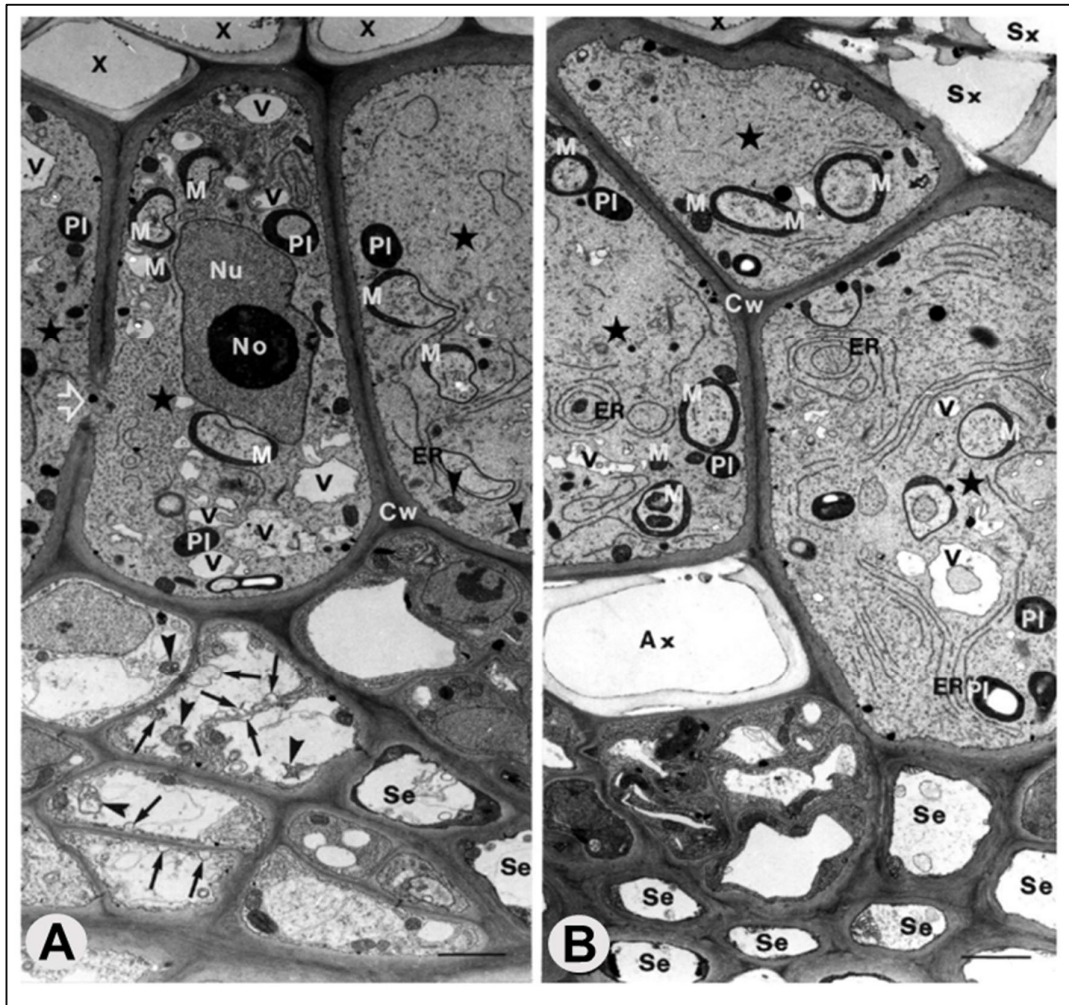


Figure 1. 2. The ultrastructure of a syncytium induced by a male J3 *Heterodera schachtii* within *Arabidopsis*. Syncytial cells are labelled with an asterisk. Images A and B show a dense cytoplasm within syncytial cells, containing abundant endoplasmic reticulum (ER), mitochondria (M) and plastids (PI). **A.** Small vacuoles have replaced the large central vacuole. The nucleus (Nu) is hypertrophied and lobed, with the nucleolus (No) darkly stained. Abundant paramural bodies (arrows) and multivesicular bodies (arrow heads) are present in neighbouring cells. Cell wall (Cw) openings, labelled with an open arrow, are rare within syncytial cells. **B.** The ER is arranged in parallel rows or concentric swirls. Fully differentiated sieve tubes (Se) and xylem elements (Ax) are abundant surrounding the syncytium. Scale bars represent 3 μm . Figure modified from Sobczak et al. (1997).

1.2 The plant secretory pathway

1.2.1 Overview

The plant secretory pathway consists of a network of organelles that are responsible for the synthesis, processing and transport of cargo — including proteins, lipids and polysaccharides — to various subcellular locations (Foresti and Denecke, 2008). This pathway is essential for many biological processes, including cell wall formation and maintenance (Kim and Brandizzi, 2014), plant development (Philippe et al, 2022; Preuss et al, 2004) and responses to abiotic and biotic stress (Sampaio et al, 2022; Wang et al, 2020b; Kwon et al, 2008a).

The conventional plant secretory pathway starts at the ER, where cargo is assembled and exported to the Golgi (**Figure 1.3**). From the Golgi, cargo is transported to the trans-Golgi network (TGN) which is the final pit stop for secreted proteins before the plasma membrane (Wang et al, 2018; Hu et al, 2021). Secretion at the plasma membrane is the default secretory pathway route in the absence of sorting signals or retention signals (Denecke et al, 1990). An alternative destination for proteins of the secretory pathway is the vacuoles, mediated by the presence of vacuolar sorting signals (Hadlington and Denecke, 2000). Vacuolar cargo is sorted at the TGN, where it is trafficked to the prevacuolar compartments (PVCs) which mature into late PVCs (LPVCs) before fusing with the vacuole. There are two types of vacuoles within plant cells, lytic vacuoles and protein storage vacuoles (PSVs) (Zhang et al, 2021b; Hara-Nishimura et al, 1998a). Lytic vacuoles typically receive material from the conventional vacuolar trafficking route, and can store ions and metabolites that are involved in several cellular processes, including homeostasis, degradation and stress responses (Zhang et al, 2014; Marty, 1999). These are found in almost all plant vegetative tissues. Contrastingly, PSVs receive cargo directly from the ER or Golgi as an alternative trafficking route (Hara-Nishimura et al, 1998b; Jiang et al, 2000; **Figure 1.3**). This type of vacuole stores nutrients such as proteins and lipids, with specialised roles in seed development and maturation (Marty, 1999).

In addition to secretion and vacuolar sorting, endocytosis is another key trafficking pathway within the plant endomembrane system (Fan et al, 2015). During endocytosis, extracellular material is captured at the plasma membrane then trafficked in the retrograde direction to the TGN (Lam et al, 2007). From the TGN, endocytosed cargo can be trafficked to the lytic vacuoles via the PVCs, or it can be recycled back to the plasma membrane (Reyes et al, 2011). Retrograde trafficking within the endomembrane system is also essential for the recycling of receptors, and the targeting of proteins to their resident organelles (Johannes and Popoff, 2008).

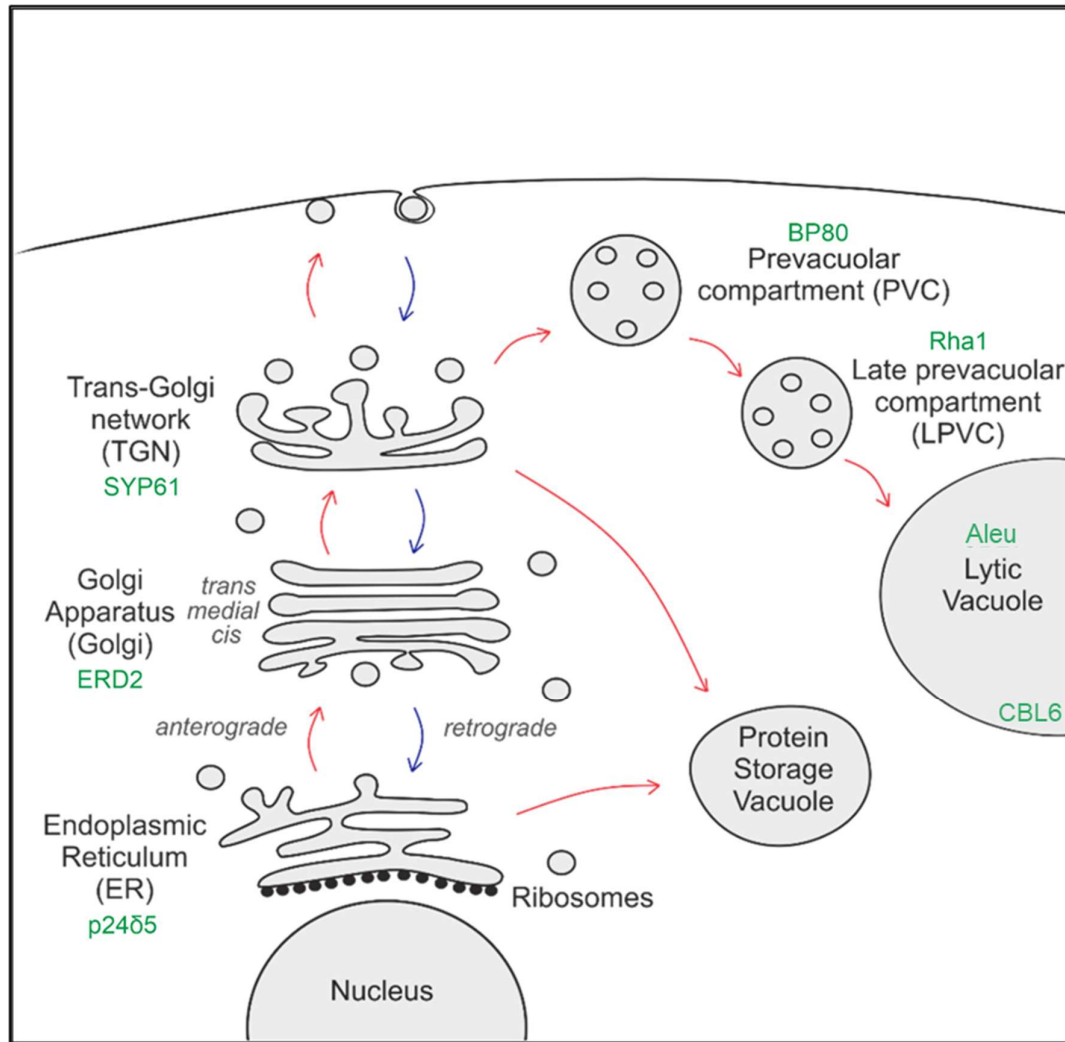


Figure 1. 3. An overview of the plant secretory pathway. Red arrows represent anterograde transport, which includes the classical secretory pathway. This starts at the Endoplasmic Reticulum (ER), before reaching the Golgi Apparatus, then the Trans-Golgi Network (TGN). From the TGN, cargo can be secreted at the plasma membrane, or progress to the Prevacuolar Compartments (PVCs). The PVCs then mature into late PVCs (LPVCs), before fusing with the vacuoles, which are often lytic. Anterograde transport also describes the transport of cargo from the ER or TGN to protein storage vacuoles. Contrastingly, blue arrows represent retrograde transport, which includes the endocytic pathway. Endocytosed cargo is captured at the TGN, to either be recycled back to the cell surface, or transported to the lytic vacuole via the PVCs. Retrograde transport also allows for escaped proteins and lipids to be recycled back to their resident compartment, and allows for the recycling of receptors. The genes listed in green are characterised markers for the respective organelle.

1.2.2 The conventional plant secretory pathway in more detail

The conventional plant secretory pathway begins as proteins are synthesised within the ribosomes and co-translationally enter the ER (Walter and Lingappa, 1986). The N-terminal signal peptide is removed as the protein emerges into the ER lumen (Vitale et al, 1993). Protein folding and assembly occurs in the ER lumen, in addition to modifications such as N-linked glycosylation and disulphide bond formation (Vitale et al, 1993). Proteins are exported from the ER at endoplasmic reticulum export sites (ERES; Hanton et al, 2007), and packaged into COPII-coated vesicles which fuse with cis-Golgi cisternae, located closest to the ER (Barlowe and Brandizzi, 2013). Within the cis-Golgi cisternae, ER resident proteins are recognised and recycled back to the ER. This can occur via the presence of a tetrapeptide H/KDEL ER retention signal, that binds to the transmembrane receptor protein ERD2 (ER retention defective 2) at the cis-Golgi. Binding to ERD2 initiates the packaging of ER resident proteins into COPI-coated vesicles, to be recycled back to the ER (Silva-Alvim et al, 2018).

The Golgi is the hub of the endomembrane system, receiving material from the ER and sorting proteins destined for secretion from those destined for the vacuoles. Moreover, the Golgi is also an important biosynthetic compartment, responsible for the synthesis of carbohydrates and complex cell wall polysaccharides (Nebenführ and Staehelin, 2001), and post-translational modifications such as glycosylation and phosphorylation (Stanley, 2011). Proteins destined for secretion or vacuolar sorting progress from cis- to trans-Golgi cisternae. There are two models proposed for Golgi cisternal formation and maintenance. The first model is cisternal progression, with the cis-Golgi cisternae maturing to become medial, then trans cisternae. Here, Golgi stacks are maintained through the continuous de-novo formation of cis-Golgi cisternae and disassembly of trans-Golgi cisternae (Hawes and Satiat-Jeunemaitre, 2005). Contrastingly, the vesicular transport model proposes that Golgi cisternae are permanent, stable structures, with proteins shuttling between the cisternae in vesicles (Rothman, 1981). The cisternal progression model for Golgi maintenance is currently the most accredited (Robinson, 2020). However, evidence to support and constrain both models within plants exists (Glick and Luini, 2011).

Once at the trans-most Golgi cisternae, proteins progress to the trans-Golgi network (TGN). The TGN is hypothesised to be formed through the maturation of trans-Golgi cisternae (Renna and Brandizzi, 2020; Kang et al, 2011). This organelle has distinct characteristics, such as its low pH (Demaurex et al, 1998), despite being located a few μm from the Golgi (Foresti and Denecke, 2008). The TGN plays a key role in the secretory pathway, being a hub for endocytosis, secretion and vacuolar sorting. Proteins destined for secretion are packaged into secretory vesicles, which bud off from the TGN to fuse with the plasma membrane. Endocytosed proteins are packaged into clathrin-

coated vesicles (CCVs) at the plasma membrane, which traffic to the TGN (McMahon and Boucrot, 2011).

For vacuolar sorting at the TGN, two models have been proposed. These hypothesise how vacuolar cargo reaches the prevacuolar compartment (PVC). The first and most supported model describes the presence of vacuolar sorting receptors (VSRs) at the TGN, such as BP80. VSRs bind to vacuolar sorting signals that are present in pro-peptides, including sporamin and aleurain (Matsuoka and Nakamura, 1991; Di Sansebastiano et al, 2001), to induce the sorting of vacuolar cargo into CCVs that fuse with the PVC (Sanderfoot et al, 1998). Within the PVCs, VSRs dissociate from the cargo and are recycled back to the TGN (Foresti et al, 2010). Contrastingly, the second model for vacuolar trafficking from the TGN hypothesises that vacuolar sorting occurs in a receptor independent manner. This model describes the TGN maturing into PVCs, rather than cargo shuttling between the two organelles within vesicles (Niemes et al, 2010). However, this model doesn't explain how secretory cargo is segregated from vacuolar proteins at the TGN.

Nevertheless, once within the PVCs, cargo destined for the lytic vacuoles is sequestered into intraluminal vesicles via the presence of ESCRT (endosomal sorting complexes required for transport) degradation signals (Cai et al, 2014). The PVCs then mature into LPVCs which fuse with the tonoplast to release cargo into the vacuole, via the sequential action of Rab5 and Rab7 GTPases (ras-related in brain guanosine triphosphatases; Bottanelli et al, 2011 & 2012).

A key aspect of the conventional plant secretory pathway is vesicular transport. Cargo is selected and packaged into vesicles that form through the self-assembly of coat proteins at the donor organelle membrane (Bonifacino and Glick, 2004; Sanderfoot and Raikhel, 1999). Vesicles are then trafficked along the cytoskeleton to the target membrane (Boutté et al, 2007). Vesicle fusion to the target membrane is facilitated by various proteins including Rab GTPases, tether factors and SNAREs (soluble N-ethylmaleimide-sensitive factor attachment receptor proteins; Bonifacino and Glick, 2004; **Figure 1.4**). SNAREs play a crucial role in vesicle fusion (Martiniere and Moreau, 2020; Kim and Brandizzi, 2012). They are categorised into vesicle associated SNAREs (R-SNAREs) and target membrane associated SNAREs (Q-SNAREs). R-SNAREs interact with Q-SNAREs, forming a trans-SNARE complex that catalyses vesicle fusion to the target membrane (McNew et al, 2000). Following this, SNARE recycling machinery, such as α -SNAP proteins, mediates the disassembly of the trans-SNARE complex (Marz et al, 2003; **Figure 1.4**).

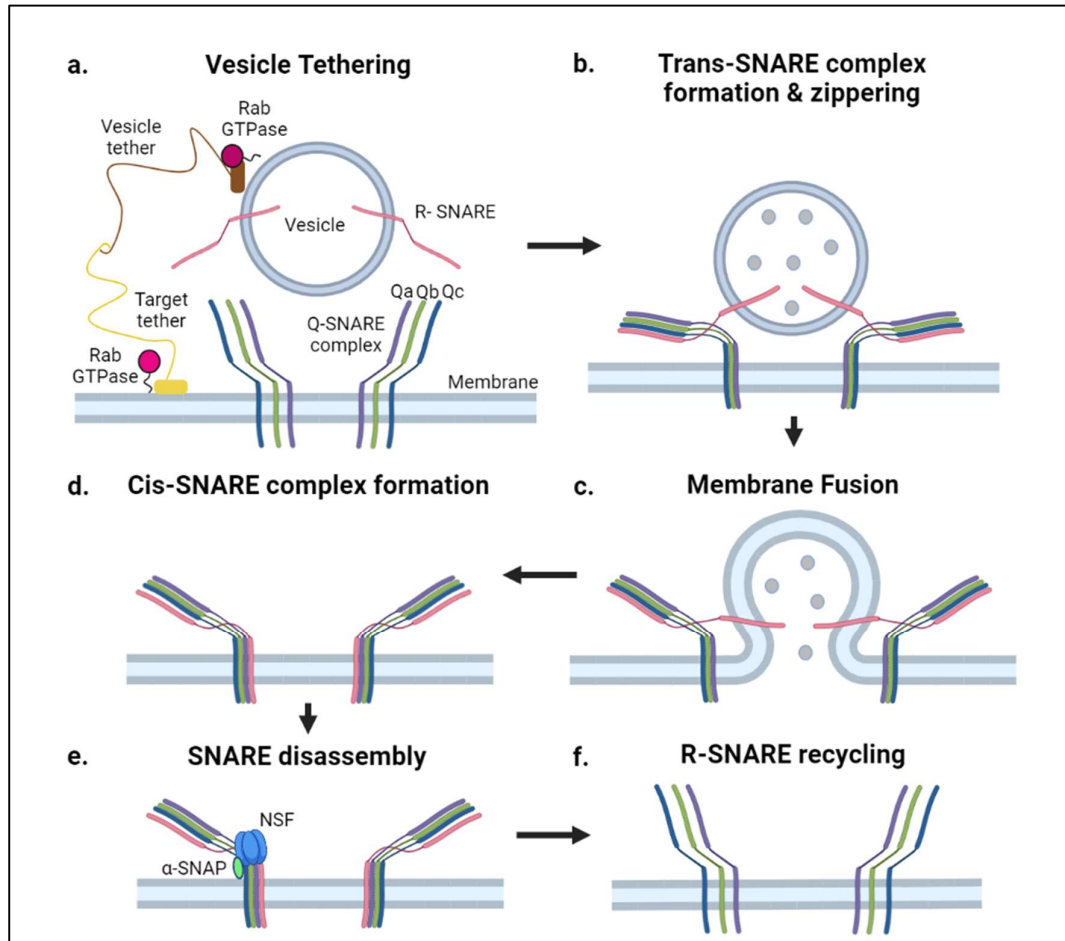


Figure 1. 4. Schematic representation of SNARE-mediated membrane fusion. **a.** Vesicle and target membrane tethers interact with the aid of Rab GTPases. **b.** Vesicle tethering is followed by the formation of a quaternary- α -helical trans-SNARE complex, consisting of the vesicle associated R-SNARE and the target membrane associated Q-SNARE complex. Zippering of the trans-SNARE complex occurs, pulling the vesicle membrane towards the target membrane. **c.** Membrane fusion occurs, allowing for the contents of the vesicles to be released. **d.** After membrane fusion, all SNAREs reside on the target membrane, referred to as the cis-SNARE complex. **e.** The adaptor protein α -SNAP binds to the cis-SNARE complex and recruits the ATPase NSF from the cytosol, which disassembles the cis-SNARE complex. **f.** R-SNAREs are recycled back to their original membrane to enable future membrane fusion events.

1.2.3 Unconventional Protein Secretion Pathways

The importance of unconventional secretion pathways (UPS pathways) in plants is beginning to be unravelled. By definition, these pathways bypass one or more pit stops of the conventional secretory pathway (Davis et al, 2016). Most proteins that undertake UPS are 'leaderless secretory proteins' (LSPs), lacking a signal peptide. These peptides cannot co-translationally enter the ER, and often bypass the Golgi (Davis et al, 2016). A significant portion of the proteins within the plant secretome are predicted to be LSPs (Alexandersson et al, 2013). Thus, UPS likely plays a large role within the plant endomembrane system.

Several UPS pathways in plants have been described (reviewed in Robinson et al, 2016; Ding et al, 2014). These pathways are categorised into non-vesicular and vesicular routes (Ding et al, 2014). Non-vesicular routes describe the direct translocation of cytosolic proteins across the plasma membrane (Nickel, 2010). Vesicular routes can be independent of the ER and/or the Golgi (Cheng et al, 2009), and can also include the direct fusion of the PVCs with the plasma membrane (Meyer et al, 2009). Another vesicular UPS route is the EXPO pathway. This route describes protein transport from the ER to the Golgi, then to the exocyst-positive organelle (EXPO), a double-membrane-bound organelle that tethers secretory vesicles to the plasma membrane (Poulsen et al, 2014; Robinson et al, 2016). UPS is generally associated with stress in yeast and mammalian cells (Cohen et al, 2020; Rabouille, 2017). Evidence supports this within plants, with the EXPO pathway involved in abiotic stress including salt stress (Hayashi et al, 2001), oxidative stress (Zhou et al, 2011) and cold temperature stress (Gupta and Deswal, 2012), and in response to pathogen infection (reviewed in Ruano and Scheuring, 2020).

1.3 The plant secretory pathway during pathogen infection

1.3.1 The ER and Golgi

The plant secretory pathway is crucial in the response to plant pathogens such as fungi (reviewed in Yun et al, 2016), oomycetes (reviewed in Hardham et al, 2007) and bacteria (reviewed in Ivanov et al, 2010). The ER is a key organelle involved in plant immune responses. This organelle is highly active during pathogen infection, due to the increased synthesis and folding of defence related proteins (Wang et al, 2005). Consequently, various ER chaperones, involved in ER quality control and protein folding, are involved in resistance to various pathogens. For example, the expression of heat shock protein70 binding proteins (BiPs) and lectin-type calreticulins (CRTs) are required for tomato resistance to *Cladosporium fulvum* fungus (Liebrand et al, 2012). Additionally, protein disulfide isomerases (PDIs) NbERp57 and NbP5 and the calreticulins NbCRT2 and NbCRT3 are required for resistance in *Nicotiana benthamiana* against tobacco mosaic

virus (Caplan et al, 2009). Increased activity of the ER during pathogen infection can trigger ER stress to activate the unfolded protein response (UPR; Eichmann and Schäfer, 2012). UPR is a cellular stress response that functions to increase the folding capability of the ER and to reduce the number of unfolded or misfolded proteins (Read and Schröder, 2021). UPR is also associated with the induction of defence responses such as programmed cell death (PCD) in resistance to several types of plant pathogens including viruses and bacteria (Manghwar and Li, 2022; Kørner et al, 2015).

Thus unsurprisingly, some pathogens have adapted to disrupt the ER during infection. For example, within *Arabidopsis* infected by the fungi *Golovinomyces orontii*, restricted intraluminal ER transport, evidenced by swollen ER, is observed surrounding fungal haustoria (Micali et al, 2011; Tolley et al, 2008). Moreover, some plant pathogens have adapted to inhibit ER-stress, to prevent the downstream induction of plant defence responses. For example, several pathogen effectors, such as the oomycete *Phytophthora infestans* Pi03192 effector, the bacteria *Pseudomonas syringae* HopD1 effector, and the fungi *Bremia lactucae* BLR05 and BLR09 effectors bind to ER-localised NAC transcription factors to prevent the downstream activation of PCD (McLellan et al, 2013; Block et al, 2014; Meisrimler et al, 2019).

Another organelle key to plant-pathogen interactions is the Golgi. This organelle plays a key role in the biosynthesis, modification and trafficking of defence related compounds. This includes the N-glycosylation and secretion of cell wall components (Wan et al, 2021), antimicrobial compounds (Lin et al, 2020) and pattern recognition receptors (Häweker et al, 2010). Golgi-mediated trafficking is also altered during plant pathogen infection. For example, the conserved oligomeric Golgi (COG) membrane protein complex is involved in plant pathogen resistance, such as barley resistance to the fungi *Blumeria graminis* (Ostertag et al, 2013). The COG is hypothesised to act as a tether for retrograde vesicles within intra-Golgi trafficking (Blackburn et al, 2018). Another Golgi related trafficking component altered during plant pathogen infection includes the ADP-ribosylation factor (ARF) GTPase ARF1, which is involved in the formation of COPI vesicles (Yang et al, 2002) and Golgi assembly (Nakai et al, 2013). ARF1 functions in tobacco resistance to tobacco mosaic virus, triggering cell death via the activation of MAPK signalling cascades (Coemans et al, 2008). ARF1 is also target of pathogen effectors, including the red clover necrotic mosaic virus p27 protein, shown within *Nicotiana benthamiana* (Hyodo et al, 2013). This further supports the role of Golgi related subcellular trafficking in plant-pathogen interactions.

1.3.2 Intermediate organelles: the TGN and PVCs

Post-Golgi organelles including the TGN are important in plant-pathogen interactions. For example, during immune responses, vacuolar defence related compounds such as hydrolytic enzymes are sorted at the TGN (Hatsugai et al, 2018). Moreover, the

exocytosis of defence related compounds from the TGN to the PM plays a key role in plant-pathogen interactions, evidenced by the role of TGN-PM trafficking components in resistance. For example, the Q-SNAREs Syp61, Syp121 and the R-SNARE VAMP722 contribute to Arabidopsis resistance to *Blumeria graminis* fungi (Drakakaki et al, 2012). In addition to exocytosis, TGN-mediated endocytosis is important within plant pathogen responses. Endocytosis enables the recycling of cell surface immune receptors, such as FLS22, upon binding to pathogen effectors (Spallek et al, 2013). However, endocytosis can act to deliver pathogen effectors into the plant cell to support pathogen infection, as observed within plant-fungal and plant-oomycete interactions (Leborgne-Castel et al, 2010).

Several plant pathogen effectors have been identified which target TGN mediated trafficking components, such as RabA GTPases and SNAREs. For example, the *Phytophthora infestans* effector RxLR24 binds to the Rab GTPase RABA1a in potato and Arabidopsis. This inhibits the trafficking of two antimicrobial compounds — the pathogenesis-related PR1 and defensin PDF1.2 — from the TGN to the plasma membrane (Tomczynska et al, 2018). Additionally, the oomycete *Phytophthora sojae* effector, PsAvh181, interacts with the soybean SNARE GmSNAP-1 to disrupt the exocytosis of defence related compounds such as the pathogenesis-related proteins P69B and PR1 (Wang et al, 2021b).

In addition to the TGN, the PVC plays a large role within responses to plant pathogens. During plant pathogen infection, increased endocytic trafficking to the lytic vacuoles can occur. This functions to balance the increased secretion (Zhang et al, 2019b), to degrade membrane materials damaged during oxidative defence (An et al, 2006b), and to degrade internalised cell surface immune receptors (Gu et al, 2017). Additionally, there is evidence of increased unconventional fusion of the PVCs with the PM during plant pathogen infection, as observed within barley in response to the fungus *Blumeria graminis* (An et al, 2006a), and within Arabidopsis in response to the bacterium *Pseudomonas syringae* (Wang et al, 2014a). PVCs in these interactions unconventionally fuse with the plasma membrane to secrete defence related compounds to the site of pathogen entry (An et al, 2006a; Wang et al, 2014a). The importance of PVCs in plant pathogen responses is also evidenced by the role of the Arabidopsis LYST INTERACTING PROTEIN 5 (LIP5) within immune signalling. LIP5 positively regulates PVC biogenesis and is required in Arabidopsis for basal resistance to *Pseudomonas syringae* (Wang et al, 2014a).

1.3.3 Vacuoles

The vacuoles have a prominent role in plant immune responses, mainly due to the presence of antimicrobial and hydrolytic compounds inside the vacuole that can trigger rapid cell death upon disruption of the vacuolar membrane (Hara-Nishimura and

Hatsugai, 2011). This is shown within tobacco against tobacco mosaic virus (Hatsugai et al, 2004) and within *Arabidopsis* in response to the *Fusarium moniliforme* fungus (Kuroyanagi et al, 2005). Hydrolytic compounds in vacuoles include nucleases (Ito and Fukada, 2002) and cysteine proteases (Rojo et al, 2004) that are involved in cell death. Antimicrobial compounds in vacuoles include albumins, kunitz proteinase inhibitors, lectins, glycine-rich proteins, vicilins, patatins, tarins, and ocatins (de Souza Cândido et al, 2011).

1.3.4 The exocyst

The exocyst positive organelle (EXPO), and its associated trafficking pathway, plays a role within plant immunity. For instance, key exocyst subunits are associated with immunity to bacteria, as within *Arabidopsis-Pseudomonas syringae*, and within fungi, as observed within *Arabidopsis-Hyaloperonospora arabidopsidis* (Stegmann et al, 2013), barley-*Blumeria graminis* (Ostertag et al, 2013), and rice-*Magnaporthe oryzae* interactions (Hou et al, 2020). Defence related compounds including cell wall material and antimicrobial proteins are trafficked from the Golgi to the exocyst, which fuses directly with the plasma membrane (Poulsen et al, 2014; Robinson et al, 2016). The EXPO pathway has a characterised role in the formation of cell wall appositions during pathogen infection, as observed within *Arabidopsis* infected with the *Pseudomonas syringae* bacterium and the *Blumeria graminis* fungus (Pecenková et al, 2011). Counteractively, exocysts are manipulated by pathogen effectors, including the *Magnaporthe oryzae* fungus Avr-Pii effector which targets two rice Exo70 genes (Fujisaki et al, 2015), that are key members of the exocyst complex (Zhao et al, 2018).

1.3.5 Changes to the plant secretory pathway during nematode feeding site formation

1.3.5.1 Changes to the early secretory pathway: the ER and Golgi

Vast changes to the plant secretory pathway occur during cyst nematode feeding site formation, including large changes to the ER. For example, during early stages of syncytial development, rough endoplasmic reticulum (RER) is proliferated and arranged in concentric layers. This is observed within the susceptible *Arabidopsis-H. schachtii* and soybean- *H. glycines* interactions (Golinowski et al, 1996; Kim et al, 1987; Blev-Zacheo and Zacheo, 1987) and the resistant soybean- *H. glycines* interaction (Kim et al, 2012). Proliferation of the RER suggests high levels of protein synthesis occurs during early syncytial formation. This is supported by increased transcriptional activity of protein synthesis genes within syncytia of *Arabidopsis-H. schachtii* (Szakasits et al, 2009) and tomato- *G. rostochiensis* (Filipecki et al, 2021). Moreover, as syncytia develop, tubular smooth ER (SER) increases in abundance (Kim et al, 1987; Golinowski and Magnusson,

1991). This is a feature of both susceptible and resistant soybean- *H. glycines* interactions (Kim et al, 2012). Increased SER may reflect increased lipid and carbohydrate synthesis, detoxification or Ca²⁺ signalling (Chen et al, 2012).

The increased activity of the ER within syncytia may result in ER stress, which is involved within plant immune signalling (Kørner et al, 2015). This is supported by observations of dilated RER cisternae, an indicator of ER stress, within soybean resistance to *H. glycines* (Kim et al, 2012; Endo, 1991; Vitale and Boston, 2008). ER stress triggers the unfolded protein response (UPR) to trigger immune signalling cascades, resulting in PCD (Simoni et al, 2022). UPR genes are upregulated within soybean cultivars resistant to *H. glycines* (Kandoth et al, 2011), and PCD is involved in resistance within several plant-cyst nematode interactions, such as soybean- *H. glycines* (Wang et al, 2020b), potato- *G. pallida* (Sacco et al, 2009) and Arabidopsis- *H. schachtii* interactions (Matuszkiewicz et al, 2018). This supports the role of the ER within plant resistance to cyst nematodes.

The Golgi is an important organelle within plant responses to cyst nematodes. Golgi proliferate during syncytial formation and display structural evidence of high biosynthetic activity observed in both susceptible and resistant plant-cyst nematode interactions (Fudali et al, 2007; Endo, 1991; Melillo et al, 1990). Golgi are responsible for the synthesis and secretion of cell wall matrix polysaccharides (Driouich et al, 2012), that are abundant in the cell walls of syncytial cells. For example, xyloglucan, methyl-esterified homogalacturonan and pectic arabinan are abundant in potato syncytia induced by *Globodera pallida* and soybean syncytia induced by *Heterodera glycines* (Zhang et al, 2017c). Additionally, wheat syncytia induced by *Heterodera avenae* and *Heterodera filipjevi* contain abundant feruloylated xylan and arabinan residues (Zhang et al, 2017c). Therefore, the increased abundance of Golgi in syncytia may function to increase its biosynthetic output to enable the alteration of cell wall composition during syncytial formation. Additionally, Golgi-mediated trafficking is also involved in the plant response to cyst nematodes. For example, the conserved oligomeric golgi (COG) complex contributes to soybean resistance to *H. glycines* (Klink et al, 2022; Klink et al, 2021; Lawaju et al, 2020). The COG complex plays a key role in glycosylation within the Golgi (Smith and Lupashin, 2008), maintaining Golgi structure (Rui et al, 2020), and retrograde trafficking (Tan et al, 2016), implicating that these functions are involved in plant defence responses to cyst nematodes.

1.3.5.2 Changes to post-Golgi organelles: the TGN and PVC

Although ultrastructural evidence of the TGN is unavailable within syncytia (Baranowski et al, 2019), this organelle is likely involved in the response to cyst nematodes. As with responses to other pathogens, the TGN is probably involved with the trafficking of antimicrobial compounds, immune receptors, and cell wall components to the cell

surface (LaMontagne and Heese, 2017). This is supported by the role of TGN mediated trafficking components within cyst nematode resistance (see **section 1.4.3**).

Abundant PVCs, described as multivesicular bodies, are observed within *Arabidopsis* syncytia induced by *H. schachtii*. These are associated with strongly lobed and subdivided vacuoles, suggesting fusion of the LPVCs with fragmented vacuoles (Golinowski et al, 1996). Additionally, unconventional fusion of PVCs with the plasma membrane may occur within syncytia, as is typical during the response to other plant pathogens. This is supported by the observation of paramural bodies, vesicles located between the plasma membrane and cell wall, in the syncytia of susceptible *Arabidopsis*-*H. schachtii*, and tomato-*G. rostochiensis* interactions (Golinowski et al, 1996; Fudali et al, 2007), and also within syncytia of the resistant soybean-*H. glycines* interaction (Riggs et al, 1973). Paramural bodies arise from the fusion of PVCs with the plasma membrane (Marchant and Robards, 1968). This suggests that the secretion of defence related compounds into the apoplast, as observed in several plant-pathogen interactions (Nielsen et al, 2012; Böhlenius et al, 2010; Meyer et al, 2009; An et al, 2006a), also occurs in plant-cyst nematode interactions.

1.3.5.3 Changes to the vacuoles

Loss of the large central vacuole, and the formation of numerous smaller vacuoles during early syncytial formation is observed in both susceptible and resistant plant-cyst nematode interactions (Kim et al, 1987). This is a feature of cells with high metabolic activity (Rodiuc et al, 2014) and hasn't been observed during infection with any plant pathogens other than cyst nematodes. It is hypothesised that small vacuoles are formed de novo through the widening of ER cisternae during early syncytial development. As the syncytia mature, larger vacuoles are hypothesised to form through the fusion of vesicles/tubules surrounding organelle free pre-vacuole regions (Baranowski et al, 2019). Lytic vacuoles within syncytia may function in programmed cell death. Some of these vacuoles are lytic, as described during *Arabidopsis* infection with *H. schachtii* (Baranowski et al, 2019). In syncytia, lytic vacuoles may induce PCD through the release of antimicrobial and hydrolytic compounds into the cytoplasm (Hara-Nishimura and Hatsugai, 2011). During cell death, increased lytic vacuole size occurs (Van Doorn, 2011). Cell death is a common feature of cyst nematode resistance (Wang et al, 2020b; Ali et al, 2015a), and ultrastructural evidence suggests that vacuoles are larger within syncytia resistant to cyst nematodes. This is shown within barley-*H. avenae* (Aditya et al, 2015), radish-*H. schachtii* (Wyss et al, 1984), potato-*G. rostochiensis* (Bleve-Zacheo et al., 1990), wheat-*H. avenae* (Williams & Fisher, 1993). Thus, the increased vacuole size observed in resistance to cyst nematodes could be associated with PCD.

In addition to their role in PCD, vacuoles may function to alter osmoregulation, nutrient availability, detoxification and indole metabolism within syncytia. Vacuole-mediated osmoregulation may support syncytial development. For example, tonoplast aquaporins are downregulated within syncytia (Baranowski et al, 2019; Szakasits et al, 2009). These aquaporins regulate water balance within the cell (Johansson et al, 2000); their downregulation hypothesised to increase turgor pressure during syncytial formation (Baranowski et al, 2019; Böckenhoff and Grundler 1994). Additionally, vacuolar nutrient transporters may support syncytial development. For example, the vacuolar amino acid transporters AAP6 and AAP8 are upregulated within *Arabidopsis* syncytia induced by *H. schachtii* (Szakasits et al, 2009). This may increase the transport of amino acids from the vacuoles into the cytoplasm, to enhance nutrient uptake by the nematode. Moreover, vacuolar transport of auxin may also support syncytia. For instance, downregulation of the *Arabidopsis* auxin transporter WAT1 is associated with resistance to *H. schachtii* (Chopra et al, 2021). WAT1 downregulation decreases the export of indole from the vacuoles into the cytoplasm, resulting in failed syncytial development (Chopra et al, 2021). Also, vacuole mediated detoxification, through fragmentation of the large central vacuole, may be a resistance response within syncytia. Fission of the large central vacuole into several smaller vacuoles increases the total vacuolar surface to volume ratio within the plant cell, allowing for a more efficient removal of toxic metabolic compounds from the cytoplasm (Martinoia et al, 2007).

1.3.5.4 Changes to the exocyst

The exocyst-positive organelle is associated with cyst nematode resistance. The expression of 27 exocyst genes were studied in soybean in response to *H. glycines* infection. 14 of these were expressed exclusively during parasitism, suggesting a role of this organelle within cyst nematode resistance (Sharma et al, 2020). During plant defence responses, trafficking of antimicrobial compounds and cell wall material to the plasma membrane via the exocyst is often observed (Du et al, 2018; see **section 1.3.4**), with cargo trafficked from the TGN to the exocyst before fusing with the plasma membrane (Žárský et al, 2013). This further supports the role of the plant secretory pathway in the secretion of defence related compounds in syncytia.

1.3.5.5 Altered vesicle trafficking in resistance to cyst nematodes

Vesicle trafficking in the endomembrane system likely facilitates immune responses to cyst nematodes, such as hormone signalling and the secretion of defence related compounds. For example, two soybean Qa SNAREs, SYP22-3 and SYP22-4, are associated with resistance to *H. glycines* (Aljuaifari et al 2019). SYP22 proteins, typically involved in PVC to vacuole transport (Uemura et al, 2010), are hypothesised to control

the cell surface brassinosteroid hormone receptor BRI1 (Zhu et al, 2019), thus may control brassinosteroid signalling within syncytia to enhance resistance.

Most research on vesicle trafficking within syncytia is based on the soybean Rhg1 major resistance quantitative trait locus (QTL) which confers resistance to *H. glycines* (Kandath et al, 2011). Within this QTL, the α -SNAP adaptor protein GmSNAP18 is the strongest candidate gene conferring resistance (Liu et al, 2017). α -SNAP proteins are essential to vesicle trafficking, mediating the binding of NSF to SNARE protein complexes (Choi et al, 2018, see **section 1.2.2**). GmSNAP18 within the Rhg1 QTL has impaired binding to wildtype NSF (Bayless et al, 2018). Instead, GmSNAP18 binds to an atypical NSF protein, NSFRan07, which is also associated with the Rhg1 locus (Bayless et al, 2018). Therefore, defective vesicle trafficking within the host may function in resistance to cyst nematodes.

SNARE proteins that interact with the Rhg1 GmSNAP18 have been identified, all of which are involved in the secretion of defence related compounds. Yeast two-hybrid assays have identified two t-SNAREs, Syn12, Syn16, which interact with GmSNAP18 to confer *H. glycines* resistance (Dong et al, 2020). Within Arabidopsis, Syn12 is involved in callose deposition in Arabidopsis resistance to *Plectosphaerella cucumerina* fungus (Gamir et al, 2018). Additionally, *Nicotiana benthamiana* Syn16 traffics pathogenesis-related proteins to the cell wall (Kalde et al, 2007). The atypical GmSNAP18 is also co-expressed with other SNAREs, including the Qa-SNARE PEN1, the v-SNAREs VAMP721, VAMP722, the t-SNARE SNAP33 and the regulatory protein sec11. PEN1 forms a SNARE complex with VAMP721, VAMP722 and SNAP33 (Kwon et al, 2008), which interacts with Sec11 to enable recycling of the SNARE complex (Karnik et al, 2015). This SNARE complex is involved in post-Golgi trafficking to the plasma membrane, and is associated with immune responses, including callose deposition and the release of antimicrobial compounds in response to fungal and oomycete pathogens (Kwon et al, 2008). RNAi and overexpression confirms the role of each of the above genes in resistance to *H. glycines* (Sharma et al, 2016). Therefore, this SNARE complex may also be involved in the deposition of callose and the secretion of antimicrobial compounds in the defence against cyst nematodes.

Contrary to the soybean α -SNAP resistance mechanism, altered regulation of a different SNAP protein within the soybean wild relative *Glycine soja* contributes towards nematode susceptibility. The major resistance QTL within *G. soja*, cqSCN-006, encodes a γ -SNAP (Butler et al, 2021), which acts in synergy with α -SNAP to recruit NSF (Bitto et al, 2007). Only *G. soja* lines susceptible to *H. glycines* showed increased γ -SNAP expression upon nematode infection, suggesting a role of this protein within nematode susceptibility (Butler et al, 2021).

1.4 Cyst nematode effectors

1.4.1 Cyst nematode effector secretion and delivery

Cyst nematodes secrete effector proteins into the host to suppress immune responses and initiate or maintain syncytia (Siddique and Grundler, 2018). Although some cyst nematode effectors are secreted from the amphids (Eves-van den Akker et al, 2014) and the hypodermis (Jones et al, 2004), most are secreted from the esophageal glands. These are enlarged, specialised cells consisting of two subventral glands and one dorsal gland (Endo, 1984; **Figure 1.4**). Generally, effector proteins are synthesised in the nucleus of the esophageal gland cells, with the presence of an N-terminal signal peptide allowing for their translocation across the gland cell ER membrane and into the secretory pathway. Once within the nematode secretory pathway, effectors are packaged into membrane-bound secretory granules, which bud off from the TGN (Mitchum et al, 2013; Hussey and Mims, 1990).

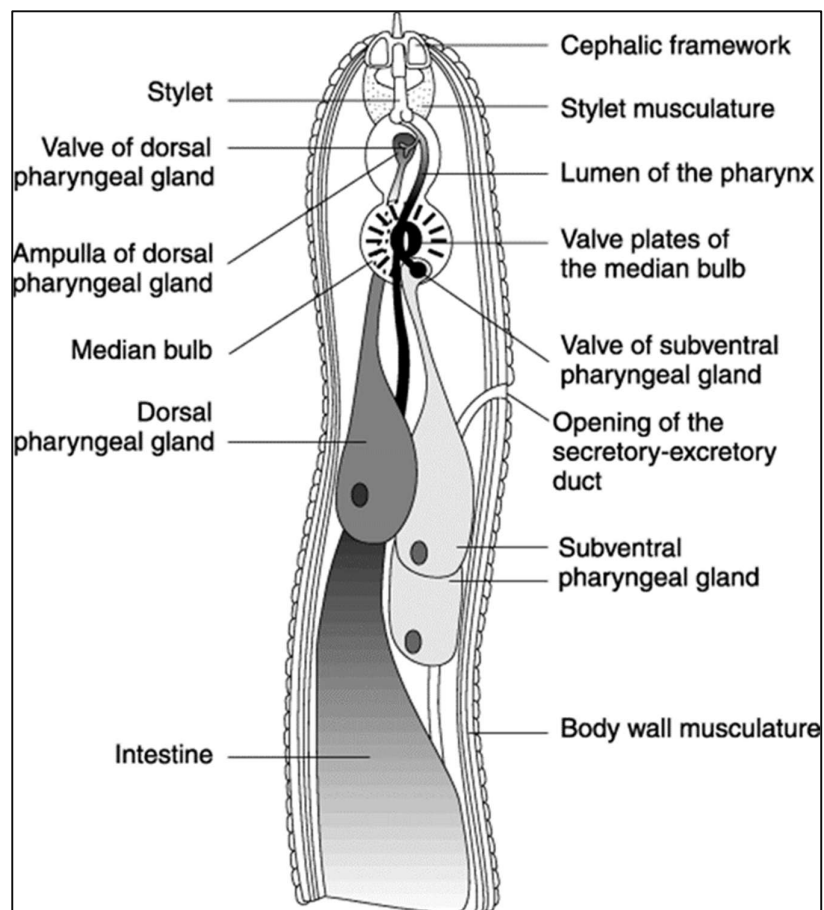


Figure 1. 5. Diagram of the anterior portion of a cyst nematode J2, showing the position of the dorsal and subventral pharyngeal glands. Secretory granules from the dorsal pharyngeal gland are loaded into the ampulla, which is emptied upon stylet protrusion into the host cell. Diagram taken from Lilley et al. (2005).

Effector containing membrane-bound granules accumulate within the ampulla of cyst nematode esophageal gland cells (Wyss and Grundler, 1992). Expanding of the ampulla valve membranes allows for the release of the granules into the nematode's stylet, which is a hollow and protrusible needle-like structure. Nematode secretions from the stylet start during the J2 stage, mostly from the subventral glands (Tytgat et al, 2002; Wyss and Zunke, 1986). This is supported by a peak in the expression of subventral gland cell effector genes within J2s (Thorpe et al, 2014). This suggests that subventral gland cell effectors have a role in root invasion, intracellular migration and other early parasitic processes. Contrastingly, dorsal gland cell secretions are observed later on in infection, during the nematode's sedentary phases (Tytgat et al, 2002; Wyss and Grundler, 1992), as supported by expression analyses of dorsal gland cell effector proteins (Thorpe et al, 2014). This suggests that dorsal gland effectors are involved in syncytial induction and maintenance.

As the cyst nematode stylet perforates the ISC cell wall but not the plasma membrane (Sobczak et al, 1999), multiple modes of effector delivery are hypothesised. Effectors may be delivered directly into the apoplast (Eves-van den Akker et al, 2014). Alternatively, effectors may be translocated across the plasma membrane and into the cytoplasm via a small pore in the plasma membrane at the stylet's orifice (Hussey et al, 1992). Evidence for direct translocation into the host cell cytoplasm are cyst nematode CLE effectors. These function within the apoplast, binding to extracellular receptors. To reach the apoplast, cyst nematode CLE effectors enter the host cell cytoplasm where they post-translationally enter the host ER to be transported through the secretory pathway (Wang et al, 2021a). Other indirect evidence of cyst nematode translocation across the plasma membrane into the cytoplasm is the diverse host subcellular targets of cyst nematode effectors which have been identified, including the nucleus (Elling et al, 2007) and peroxisomes (Thorpe et al, 2014).

1.4.2 Cell biology of nematode effectors

Cyst nematode effector proteins target important host molecular components or pathways to promote infection (Vieira and Gleason, 2019). Many cyst nematode effectors have been described to date. These manipulate processes such as plant developmental pathways, immune responses, and other key cellular processes (summarised in **Table 1.1**).

Table 1. 1. A list of previously characterised cyst nematode effectors that target diverse cellular processes. The name of each effector/effector family is given, in addition to the species of cyst nematodes they have been characterised from, their *in planta* subcellular localisation, targeted cellular process and publication.

| Species | Effector name/family | <i>In planta</i> localisation | Targetted cellular process | Publication |
|---|----------------------|-------------------------------|--|-----------------------------------|
| <i>Heterodera</i> and <i>Globodera</i> spp. | CLEs | Apoplast | CLE hormone signalling | Guo et al, 2017 |
| <i>H. schachtii</i> | HsTyr | Cytoplasm | Auxin homeostasis | Habash et al, 2017a |
| <i>Heterodera</i> spp. | 19C07 | Plasma membrane | Auxin homeostasis | Lee et al, 2011 |
| <i>H. schachtii</i> | HsPDI | Apoplast | Cell redox status | Habash et al, 2017b |
| <i>H. schachtii</i> | Hs32E03 | Nucleus | Histone acetylation | Vijayapalani et al, 2018 |
| <i>Globodera</i> spp. | SPRY-SECs | Nucleus/cytoplasm | Immune signalling/microtubule dynamics | Sacco et al, 2009/Mei et al, 2018 |
| <i>H. glycines</i> | Hg-SLP-1 | Unknown | Exocytosis | Bekal et al, 2015 |
| <i>H. schachtii</i> | 4E02 | Nucleus | Vacuole-mediated PCD | Lampl et al, 2013 |
| <i>H. avenae</i> | HaCRT1 | ER | Calcium signalling | Liu et al, 2020 |

Cyst nematode effectors that manipulate plant hormone and development pathways include CLE peptides. These mimic the endogenous B-type CLE peptide hormone to promote the proliferation of procambial meristem cells during syncytial formation (Guo et al, 2017). Additionally, the *H. schachtii* effector HsTyr encodes a tyrosinase which modulates hormone homeostasis, promoting plant growth and altering root architecture. RNAi of HsTyr results in decreased syncytial cell size (Habash et al, 2017a). Another example is the *H. glycines* and *H. schachtii* effector 19C07, which manipulates the plant hormone auxin. 19C07 interacts with the Arabidopsis auxin influx transporter LAX3 to increase auxin influx. This stimulates cell wall hydrolysis to support syncytial development (Lee et al, 2011). In addition to hormone signalling pathways, cyst nematode effectors target other key cellular processes, such as redox homeostasis. For example, the *H. schachtii* effector HsPDI encodes a disulfide isomerase, which alters the redox status within syncytia (Habash et al, 2017b), to decrease the production of reactive oxygen species (ROS) that are toxic to cyst nematodes.

Several cyst nematode effectors which suppress host immune responses have been identified. This includes the *H. schachtii* effector Hs32E03, which modifies histone acetylation to suppress the expression of genes involved in plant immunity (Vijayapalani et al, 2018). SPRY domain-containing effector proteins from *G. rostochiensis* also suppress plant immunity, some interacting with nucleotide-binding leucine-rich repeat (NB-LRR) receptors to prevent the induction of effector-triggered immunity (Sacco et al, 2009).

1.4.3 PPN effectors which interact with the plant secretory pathway

Limited cyst nematode effectors have been identified that target the plant endomembrane system. However, a *H. glycines* SNARE-like protein, HgSLP-1, has been identified which alters vesicle trafficking (Bekal et al, 2015). Interestingly, HgSLP-1 is highly similar to a protein from the bacterium *Paenibacillus dendritiformis*. Both proteins contain a SNARE domain characteristic of bacterial t-SNARE-like effectors (Bekal et al, 2015; Delevoye et al, 2008). Thus, HgSLP-1 may act similarly to bacterial t-SNARE-like effectors, mimicking host t-SNAREs to bind to host v-SNAREs, subsequently suppressing defence related membrane fusion. However, HgSLP-1 may also function as an avirulence protein. HgSLP-1 co-localises with the Rhg1-associated dysfunctional α -SNAP protein, GmSNAP18 (Bekal et al, 2015). GmSNAP18 largely contributes towards resistance against *H. glycines* (Liu et al, 2017). Therefore, in the absence of GmSNAP18, HgSLP-1 may manipulate membrane fusion to promote virulence (Bekal et al, 2015).

Another cyst nematode effector which targets the secretory pathway is the *H. schachtii* effector 4E02. This effector induces the re-localisation of the Arabidopsis vacuolar papain-like cysteine protease RD21A from the vacuole to the nucleus and cytoplasm. RD21A plays a key role in vacuole-mediated PCD (Lampl et al, 2013). Thus, the effector induced re-localisation of this protein may prevent or delay vacuole-mediated PCD within syncytia (Pogorelko et al, 2019). Another cyst nematode effector which targets the plant secretory pathway is the *H. avenae* effector HaCRT1. This effector encodes a calreticulin protein which localises to the ER via a HDEL signal. HaCRT1 is hypothesised to modulate calcium levels within the ER lumen to suppress the cell death response (Liu et al, 2020). A calreticulin effector protein has also been identified within the root-knot nematode *Meloidogyne incognita*. This effector, Mi-CRT, is hypothesised to suppress ER stress pathways to prevent the triggering of downstream immune responses (Jing and Wang, 2020).

The ER is a key target of effectors from other plant pathogens to prevent the downstream induction of defence responses. For example, the oomycete *Phytophthora sojae* effector PsAvh262 interacts with soybean BiPs involved in UPR to prevent the downstream induction of cell death (Jing et al, 2016). Also, the PcAvr3a12 effector from *Phytophthora capsica* binds to the Arabidopsis PPIase protein involved in UPR (Fan et al, 2018). Moreover, effectors from bacteria and oomycete species target ER-localised NAC transcription factors, which are involved in the induction of plant defence signalling pathways (Breeze et al, 2020; Meisrimler et al, 2019; Block et al, 2014; Mclellan et al, 2013). Therefore, it is likely that additional unidentified cyst nematode effectors target various key components of the ER to enhance host susceptibility.

Several plant pathogen effectors which target the endoplasmic reticulum have been identified from oomycetes including *Phytophthora infestans* (Breeze et al, 2020). These contain a single C-terminal transmembrane domain (TMD). As proteins containing transmembrane domains have been discounted from previous cyst nematode effector screens (Thorpe et al, 2014; Gardner et al, 2018; Mitchum et al, 2013), the screening of proteins containing a single C-terminal TMD could identify novel cyst nematode effectors that target the ER.

1.5 Research gaps

1.5.1 The plant secretory pathway during syncytial formation

To further understand the role of the plant secretory pathway within syncytia, research gaps need to be addressed. The ER is suggested to play a key role within plant immune responses. Therefore, more research is required to understand the role of the ER within syncytia, especially the role of ER stress within defence responses, to support ultrastructural and transcriptional evidence. Also, more information on the trafficking between organelles of the secretory pathway is required. This includes transport between the ER and Golgi, and post-Golgi trafficking to support the role of exocytosis in defence, and to further elucidate vacuolar sorting mechanisms underlying replacement of the large central vacuole with smaller vacuoles. Currently, a large amount of evidence on subcellular trafficking within syncytia is based on the soybean major resistance QTL, *Rhg1*, within resistance to *H. glycines*. Thus, there is a need for further characterisation of the secretory pathways within other hosts, including the model host-cyst nematode system, *Arabidopsis*-*H. schachtii*. Additionally, more information is needed on the manipulation of the secretory pathway by cyst nematodes, with the need to identify effectors targeting the endomembrane system.

1.5.2 Cyst nematode effectors

Despite the characterisation of cyst nematode effectors targeting diverse subcellular processes (**Table 1.1**), there has been limited characterisation of effectors targeting the secretory pathway. Although evidence suggests that cyst nematodes target similar plant secretory pathway components to other biotrophic plant pathogens, such as fungi, oomycetes and bacteria, further research is needed to prove this hypothesis. Additionally, there have been no published cyst nematode effectors containing TMDs, despite increasing evidence to support the existence of transmembrane effector proteins from fungi and oomycetes (Breeze et al, 2020). As the majority of characterised transmembrane fungal and oomycete effectors target the endoplasmic reticulum, future cyst nematode effector screens that include transmembrane proteins could help to further unravel how the ER, an essential component of the secretory pathway, is manipulated by cyst nematodes.

1.6 Aims and objectives

Aim: To provide novel information on the plant secretory pathway during cyst nematode infection.

Objectives:

- Develop a set of novel dual fluorescence Arabidopsis lines that express plant secretory pathway markers.
- Image syncytia within dual fluorescence Arabidopsis lines that have been induced by the model cyst nematode species *H. schachtii*.

Aim: To identify novel cyst nematode transmembrane effector proteins that are hypothesised to target the ER, which is a key component of the plant secretory pathway.

Objectives:

- Design and conduct a bioinformatics pipeline on the *H. schachtii* and *G. pallida* proteomes to identify potential ER-targeting effectors containing a C-terminal transmembrane domain (TMD).
- Conduct subcellular localisation and in-situ hybridisation analyses of screened *H. schachtii* and *G. pallida* proteins.

Chapter 2 Materials and Methods

2.1 Nematode cyst collection and hatching

G. pallida cysts from the “Lindley” population, pathotype Pa2/3, were obtained from the soil of infected potato cv. Désirée) plants. *H. schachtii* cysts were collected from infected cabbage cv. Golden Acre plants. The soil was kept at 4 °C for a minimum of 3 months for diapause before cysts were collected. Cyst collection was conducted using the fenwick can method (Camacho et al, 2018; Fenwick, 1940). For sterilisation, cysts were placed in 0.5 mg/ml CTAB and 0.1 % v/v chlorhexidine digluconate for 30 min, then washed with sterile water. To stimulate J2 hatching, *G. pallida* cysts were exposed to potato root diffusate at 20 °C (Jones et al, 1996). To stimulate *H. schachtii* hatching, cysts were placed in 3 mM ZnCl₂ at 20 °C (Sijmons et al, 1991).

2.2 Arabidopsis infection with *H. schachtii* in tissue culture

Arabidopsis seeds were sterilised in 20 % bleach for 20 min. Following three washes, the seeds were placed at 4 °C in sterile water overnight. After stratification, Col-0 wildtype Arabidopsis seeds were plated onto square ½ MS10 plates, and grown vertically for 2 weeks before infection. Transgenic T₂ Arabidopsis seeds were plated onto ½ MS10 medium containing kanamycin (50 µg/ml) for approximately 2 weeks to allow for transgenic seed selection. Following this, seedlings were transferred onto square plates containing ½ MS10 media without kanamycin shortly before infection.

For infection, *H. schachtii* J2s were surface sterilised in a solution containing CTAB (0.5 mg/ml) and chlorhexidine digluconate (0.1 % v/v) for 30 min, followed by 3 washes in 0.1 % v/v Tween-20. The sterilised J2s were diluted to approximately 1 nematode per µl in the Tween solution, then 30 µl was used to infect each Arabidopsis plant, distributed across multiple sites on the roots. Plates were left to dry before being sealed with micropore tape and placed vertically. All plants were grown at 22 °C, with a 16 hr photoperiod.

2.3 Media

2.3.1 Luria-Bertani LB Growth Medium

10 g/l Tryptone

5 g/l NaCl

5 g/l Yeast extract

1 % bacteriological agar (w/v) was added for bacterial plate media

2.3.2 ½ MS 10 Media

2.15 g/l Murashige and Skoog medium with vitamins

10 g/l sucrose

5.75 g/l plant agar

pH 5.6

2.3.3 0.5 X TBE Buffer

0.54 g/l Tris

2.75 g/l boric acid

1 mM EDTA pH 8.0

2.3.4 Tobacco leaf infiltration buffer

50 mM MES

0.5 % glucose

2 mM Na₃PO₄

100 mM acetosyringone

pH 5.6

2.4 Molecular Cloning Techniques

2.4.1 Transformation of competent *Escherichia coli* cells

The *Escherichia coli* strain DH5α was used for *E. coli* transformations (Hanahan, 1985). For this, 1 μl of ~100 ng/μl DNA was added to 100 μl competent *E. coli* cells. These were placed on ice for 30 min, then placed at 42 °C for 2 min. After this, 1 ml of LB was added, followed by incubation at 37 °C for 1 hr. Cells were poured onto LB agar plates containing the relevant antibiotic selection and incubated at 37 °C overnight.

2.4.2 Transformation of competent *Agrobacterium tumefaciens* Gv3101 cells

DNA plasmids were transferred into the *Agrobacterium tumefaciens* strain Gv3101. This strain carries the helper plasmid pBBR1MCS5-VIRG-N54D, encoding the mutated virG gene, virGN54D (van der Fits et al, 2000). To transform the *Agrobacterium*, the freeze-thaw method was used (Xu and Qingshun, 2008). 1 μl ~100 ng/μl DNA was added to 45 μl competent *Agrobacterium* cells. This was placed at -80 °C for 15 min, followed by 37 °C for 4 min. 1 ml LB was then added to the transformed cells, with a 2-4-hour incubation at 28 °C with shaking at 200 rpm. Cells were poured onto LB plates then incubated at 28

°C for 2-3 days. LB liquid medium and agar for *Agrobacterium* growth contained rifampicin (100 µg/ml) in addition to the antibiotic selection relevant to the plasmid.

2.4.3 Colony PCRs

To screen *E. coli* and *A. tumefaciens* colonies for the presence of the desired gene, colony PCRs were conducted. For this, a single colony was suspended in 100 µl sterile distilled H₂O. 2 µl of this suspension was used as a template within the PCR. For the reaction, Mytaq (Bioline) was used according to the manufacturer's instructions. Reaction conditions are described in **section 2.4.10**, with an additional 5 minute 99 °C incubation step added prior to the initial denaturation step to lyse the bacterial cells.

2.4.4 DNA minipreps

Each construct was transformed into *E. coli* as described in **section 2.4.1**. A single colony was used to inoculate 5 ml LB containing the relevant antibiotic selection. The suspended colony was incubated at 37 °C overnight under constant agitation. Following this, minipreps were performed using the EZNA Plasmid DNA Mini Kit I (Omega Bio-tek), according to the manufacturer's instructions.

2.4.5 Preparative and qualitative restriction digests

Preparative restriction digests were conducted to cut DNA plasmids prior to ligations. Preparative restriction digests held a 50 µl total volume, containing 10-20 µl DNA, 1 µl restriction enzyme, 5 µl restriction buffer (10 X cutsmart or NEB buffer 3.1, supplied by NEB) and d.H₂O. This was incubated at 37 °C for 1 hr. For preparative digests, 1 µl samples were taken at 0 min, 20 min and 40 min, and ran on a 0.8 % agarose gel at 100 V to check that the samples had digested. Following this, DNA fragment isolations were performed as described in **section 2.4.8**.

Qualitative digests were conducted to check DNA preparations following minipreps. These held a 10 µl total volume, containing 1 µl DNA, 2 µl restriction enzyme, 1 µl restriction buffer (10 X cutsmart or NEB buffer 3.1, supplied by NEB), and d.H₂O. Samples were incubated at 37 °C for 1 hr, then ran on a 0.8 % agarose gel at 100 V.

2.4.6 Filling sticky ends

DNA polymerase I, large (Klenow) fragment (NEB) was used on digested DNA to remove the 3' overhang and fill in the 3' recessed end. Following a preparative digest, 33 µM of each dNTP was added to the tube, in addition to 1 unit of Klenow DNA polymerase I (NEB) per µg of DNA. This was incubated at 25 °C for 15 min. Following this, DNA was purified using the Wizard® SV Gel and PCR Clean-Up System (Promega) according to the manufacturer's instructions.

2.4.7 Dephosphorylation of 5' ends

The 5' end of digested DNA was dephosphorylated to prevent self-ligation. Following a preparative digest, 10 µl calf intestinal phosphatase (CIP) enzyme (NEB) was added, along with 10 µl 10 X CIP buffer (NEB), and the total volume was brought to 100 µl with d.H₂O. The reaction was incubated at 37 °C for 30 min. Column purification of the dephosphorylated DNA was conducted using the Wizard® SV Gel and PCR Clean-Up System (Promega) according to the manufacturer's instructions.

2.4.8 DNA fragment isolations

The isolation of fragments from constructs was performed using a preparative double restriction digest. Digested DNA was loaded onto a 1.2 % agarose gel containing 0.5 X TBE buffer, then ran at 50 V until the DNA fragments had separated. The DNA fragment was visualised and cut out of the agarose gel using the M-10 benchtop UV transilluminator (UVP). The isolated fragment was then purified from the gel using the Wizard® SV Gel and PCR Clean-Up System (Promega) according to the manufacturer's instructions.

2.4.9 Ligations

Isolated fragments were ligated into cut, dephosphorylated vectors using an approximate molar ratio of 2 : 1 cut vector. The ligation was set up in a total volume of 20 µl with 1 µl T4 DNA Ligase (NEB), 2 µl 10 X T4 DNA Ligase buffer (NEB), the appropriate amount of fragments and vector, and d.H₂O. Two controls were used, the first contained all reagents excluding T4 DNA ligase, to test for improperly cut vectors. The second control contained all reagents excluding the DNA fragment, to test for improperly dephosphorylated vectors. The ligation mix and the two controls were incubated at 25 °C for 1 hr, then 5 µl of this mixture was used to transform into *E. coli*. Transformed *E. coli* cells were poured onto LB agar plates containing the relevant antibiotic selection and incubated overnight at 37 °C. Several colonies from the plates were selected and inoculated in 5 ml LB medium to prepare for minipreps.

2.4.10 Polymerase Chain Reaction (PCR)

PCRs were conducted using the relevant primers, according to the manufacturer's instructions. For the cloning of effector genes, the proof-reading Phusion® DNA polymerase (ThermoFisher Scientific) was used. For colony PCRs and in-situ PCRs, Mytaq™ DNA polymerase (Bioline) was used. For in-situ single stranded probe synthesis PCRs, Onetaq® DNA polymerase (NEB) was used. All PCRs were conducted according to the manufacturer's instructions, with the conditions listed in **Table 2.1**.

Table 2. 1. The PCR conditions for each DNA polymerase enzyme used.

| DNA polymerase | Step | Temperature | Time | Cycles |
|-----------------------|----------------------|----------------------------|----------------|---------------|
| OneTaq® (NEB) | Initial denaturation | 94 °C | 30 s | 1 |
| | Denaturation | 94 °C | 15-30 s | |
| | Primer Annealing | 45-68°C (Primer specific) | 15-60 s | 30 |
| | Extension | 68 °C | 1 min per kb | |
| | Final Extension | 68 °C | 5 min | 1 |
| | Hold | 4-10 °C | ∞ | ∞ |
| MyTaq™ (Bioline) | Initial denaturation | 95 °C | 1 min | 1 |
| | Denaturation | 95 °C | 15 s | |
| | Primer Annealing | 55 °C | 15 s | 25-35 |
| | Extension | 72 °C | 10 s | |
| | Final Extension | 72 °C | 5-10min | 1 |
| | Hold | 4-10 °C | ∞ | ∞ |
| Phusion® (NEB) | Initial denaturation | 98 °C | 30 s | 1 |
| | Denaturation | 98 °C | 5-10 s | |
| | Primer Annealing | 45-72 °C (Primer specific) | 10-30 s | 25-35 |
| | Extension | 72 °C | 15-30 s per kb | |
| | Final Extension | 72 °C | 5-10 min | 1 |
| | Hold | 4-10 °C | ∞ | ∞ |

2.4.11 Sanger Sequencing

All DNA minipreps were verified using sanger sequencing, with samples sent to Genewiz for Azenta life sciences. Samples were prepared according to the company instructions.

2.5 Arabidopsis transformation by floral dip

Arabidopsis Col-0 plants were grown in pots of compost at 22 °C under a 16 hr photoperiod. 4-week-old plants were transformed using the floral dip method (Clough and Bent, 1998). For this, constructs were transformed into *A. tumefaciens* Gv3101 using the method as previously described. For this, a single *A. tumefaciens* colony was inoculated into 20 ml LB containing spectinomycin (100 µg/ml), streptomycin (300 µg/ml) and rifampicin (100 µg/ml), then incubated at 28 °C overnight under constant agitation. This culture was then added to 200 ml LB containing the same concentrations of antibiotics, and incubated at 28 °C under constant agitation, until an O.D.₆₀₀ of 0.5-0.8 was reached. The bacterial cells were pelleted by centrifugation at 2,500 g then resuspended in a 5 % sucrose solution containing 0.01 % Silwet L-77. Arabidopsis stems with multiple unopened flower buds were dipped into the solutions for 2 min, then plants were placed horizontally into trays with a propagator lid, at 22 °C with a 16 hr photoperiod to maintain high levels of humidity. After 24 hr, the propagator lid was removed and the plants were placed upright.

2.6 *Agrobacterium*-mediated transient gene expression within tobacco

4-week-old *Nicotiana tabacum* cv. Petit Havana plants, grown in a glasshouse at 21 °C, were used for *Agrobacterium*-mediated tobacco leaf infiltrations. Tobacco leaves were infiltrated with *A. tumefaciens* Gv.3101, which had been cultured overnight at 28 °C in Luria Bertani (LB) medium containing the relevant antibiotic selection.

Prior to infiltration, overnight *Agrobacterium* cultures were washed in infiltration buffer and resuspended to O.D.₆₀₀ 0.1. For co-infiltrations, a 1:1 ratio of each construct was used. The *Agrobacterium* resuspension inoculated the lower epidermis of tobacco leaves using a 1 ml syringe without a needle (Brandizzi et al, 2002; Sparkes et al, 2006). After 48 hr, infiltrated tobacco leaves were imaged using confocal microscopy (**section 2.6**). To prepare infiltrated tobacco leaf samples for confocal microscopy, leaf rectangles (approx. 1 cm X 0.5 cm) were mounted onto a microscope slide with tap water, with the lower epidermis facing the cover slip. For each construct imaged, leaves across a minimum of three plants were infiltrated. Over 100 cells across these plants were then viewed under the confocal microscope, to ensure the cells imaged gave a reliable representation of marker expression.

2.7 Confocal Laser Scanning Microscopy (CLSM)

Confocal microscopy was performed using the Zeiss LSM 880 laser scanning microscope (Zeiss). Excitation lines of an argon ion laser of 514 nm for YFP and GFP, and 594 nm for RFP and mCherry were used, with the pinhole set to 1 Airy unit. Zen black software version 2.3 (ZEISS) was used to capture images. For post-acquisition image processing, Zen blue lite version 2.4 (ZEISS) was used. Although laser power and detection gain were dependent on the fluorescence of the cells, a maximum laser power of 10 mW and detection gain of 1000 was used to ensure cells could be imaged without photobleaching occurring, and to avoid saturation and/or signal interference with background fluorescence.

Chapter 3 The development of dual fluorescence reporter constructs to monitor the plant secretory pathway

3.1 Introduction

Fluorescence live cell imaging is a useful approach for characterising cellular processes such as the plant secretory pathway. This approach involves the translational fusion of localisation tags to fluorescent proteins (Van de Meene et al, 2017; Hanton and Brandizzi, 2006). Fluorescence microscopy can provide information on organelle dynamics and protein interactions and also allows the subcellular localisation of novel proteins to be characterised (Hanton and Brandizzi, 2006; Dixit et al, 2006). Both transient and stable expression systems are used to express fluorescent markers within cells. Transient expression offers rapid and highly efficient expression, allowing for large-scale genetic analyses (Sparkes et al, 2006). However, this technique is limited to specific tissue types, such as tobacco leaf epidermal cells and protoplasts (Denecke et al, 2012).

Alternatively, stable plant transformation can be used to study whole plant tissues. Although this technique is more time consuming than transient expression, efficient transformation protocols have been developed for several model plant species including crops (Gelvin, 2003). Transient expression is often used to validate marker constructs prior to their use for plant stable transformation (Jelly et al, 2014). Conveniently, binary vectors containing fluorescent markers can be used for both stable and transient expression, using *Agrobacterium*-mediated techniques (Hwang et al, 2017). Therefore, sets of organelle marker constructs are a valuable resource for fluorescence imaging, useful for both transient and stable expression systems.

Although marker sets for the plant secretory pathway exist (Nelson et al, 2007; Geldner et al, 2009), no sets of double-fluorescent markers for these subcellular compartments are available. Double-fluorescent markers are advantageous, enabling combinatorial analysis (Geldner et al, 2009). Here, a set of dual fluorescence constructs have been developed using validated plant secretory pathway markers. Each construct contains the cis-Golgi marker ERD2b fused to yellow fluorescent protein (secYFP). secYFP consists of a signal peptide followed by a short sequence that harbours a glycosylation site (sec), added onto the N-terminus of the YFP protein for insertion into the ER (Foresti et al, 2006). ERD2b (ER retention defective 2b) is a H/KDEL binding receptor that associates with the cis-Golgi cisternae membranes via its transmembrane regions (Silva-Alvim et al, 2018).

Each construct also contains another plant secretory pathway marker fused to red fluorescent protein (RFP), to label the ER, TGN, PVCs, LPVCs, vacuoles and tonoplast. For this, two different ER markers were used: the conventional HDEL ligand fused to the C-terminus of RFP (Gomord et al, 1997), and p24 δ 5, which belongs to the p24 protein family. p24 δ 5 is involved in COPI and COPII cycling between the ER and Golgi. Secreted RFP (secRFP) was fused to the transmembrane region of the p24 δ 5 protein, which is solely responsible for the association of this protein with COPI and COPII components (Montesinos et al, 2012).

The post-Golgi organelle markers included RFP fused to the TGN marker syntaxin 61 (SYP61), a Q-SNARE involved in TGN to PM trafficking (Drakakaki et al, 2012) and the PVC marker BP80 (binding protein of 80 kD), a vacuolar sorting receptor that traffics between the Golgi and PVCs (daSilva et al, 2006). The LPVC marker used was Rha1, the Arabidopsis Rab5 homologue which is a C-terminally lipid anchored GTPase involved in PVC maturation (Bottanelli et al, 2012). For the vacuoles, a vacuole lumen marker, aleurain, and a tonoplast marker, CBL6 were used. Aleurain is a thiol protease obtained from barley, its localisation mediated by the vacuolar sorting receptor BP80 (daSilva et al, 2006). CBL6 (calcineurin B-like protein 6) is a calcium binding protein that localises to the tonoplast membrane via N-terminal S-acylation (Zhang et al, 2017a). Additionally, two BP80 mutants were used within the RFP fusions. These two mutations were of the YXX Φ motif in BP80's cytosolic tail that is responsible for vacuolar sorting. One of the mutants contained a substitution of the tyrosine for alanine, which re-directs BP80 to the TGN. The other mutant was the substitution of leucine in the cytosolic tail for alanine, which redirects BP80 to the LPVCs (Foresti et al, 2010; daSilva et al, 2006). Following the development of each construct, the subcellular localisation of each marker was validated using tobacco leaf *Agro*-infiltrations. Subsequently, these constructs have been transformed into the model plant species Arabidopsis. Segregating T₂ generation transgenic lines were then developed, with transgene expression screened within the root and cotyledon epidermal cells.

3.2 Methods

3.2.1 Organelle markers within the double fluorescent constructs

The dual fluorescent reporter constructs developed are listed in **Table 3.1**. Each construct expresses the cis-Golgi marker secYFP-ERD2b, plus an additional organelle marker fused to RFP. Each construct was developed from pTASH2, which is a modified version of a secYFP-ERD2b construct developed by F. Alvim (Silva-Alvim et al, 2018).

Table 3. 1. A list of the double fluorescence organelle marker constructs developed. pTASH2 expresses the cis-Golgi marker secYFP-ERD2b alone. The subcellular localisation of the markers within each construct is given, in addition to the promoters for each gene and the publication from which the marker fragment was developed. All marker fragments were obtained from the Denecke lab group.

| Name | Localisation | Marker co-expressed with TR2:secYFP-ERD2b | Marker fragment publication |
|---------|-----------------------|---|-----------------------------|
| pTASH2 | cis-Golgi | - | Silva-Alvim et al, 2018 |
| pTASH3 | cis-Golgi + LPVC | pNOS:RFP-Rha1 | Gershlick et al, 2014 |
| pTASH4 | cis-Golgi + PVC | 35S:RFP-BP80 | |
| pTASH5 | cis-Golgi + PVC | pNOS:RFP-BP80 | Foresti et al, 2010 |
| pTASH6 | cis-Golgi + PVC | TR2:RFP-BP80 | |
| pTASH7 | cis-Golgi + ER | 35S:RFP-HDEL | Gershlick et al, 2014 |
| pTASH8 | cis-Golgi + ER | 35S:secRFP-p24aTM | Alvim, 2018 |
| pTASH9 | cis-Golgi + TGN | 35S-RFP-BP80(Tyr) | Foresti et al, 2010 |
| pTASH10 | cis-Golgi + TGN | 35S:RFP-SYP61 | Bottanelli et al, 2011 |
| pTASH11 | cis-Golgi + LPVC | 35S:RFP-BP80(Leu) | Foresti et al, 2010 |
| pTASH12 | cis-Golgi + vacuole | 35S:Aleu-RFP | Foresti et al, 2010 |
| pTASH13 | cis-Golgi + tonoplast | 35S:CBL6-RFP | Bottanelli et al, 2011 |

3.2.2 Promoters used for marker expression

The promoters used to express the marker genes within each construct are listed in **Table 3.1**. The TR2 mannopine synthase promoter from *Agrobacterium tumefaciens* was used to express secYFP-ERD2b. This promoter has intermediate levels of expression, stronger than the nopaline synthase promoter, pNOS (Velten et al, 1984), but weaker than the strong constitutive cauliflower mosaic virus promoter, 35S (Sanger et al, 1990). The 35S promoter was used for the expression of most RFP-marker fusions. However, for the LPVC marker Rha1, the weak pNOS promoter was used to avoid merging of the PVCs with the LPVCs (Bottanelli et al, 2012). Also, for the PVC marker BP80, three constructs were developed, under the control of either 35S, TR2 or pNOS. Promoters with varying strengths were used to express RFP-BP80 due to evidence that high levels of overexpression is toxic within the plant (Foresti et al, 2010).

3.2.3 DNA plasmid construction

pTASH1 was developed as a precursor to pTASH2. This was created through filling in the EcoRI restriction site of the TR2:secYFP-ERD2b:3'NOS construct pTFLA25 (Silva-Alvim et al, 2018; **Figure 3.1**). To achieve this, a restriction digest was performed on pTFLA25 using the EcoRI restriction enzyme. After this, the sticky ends were filled using Klenow polymerase, then the vector was self-ligated.

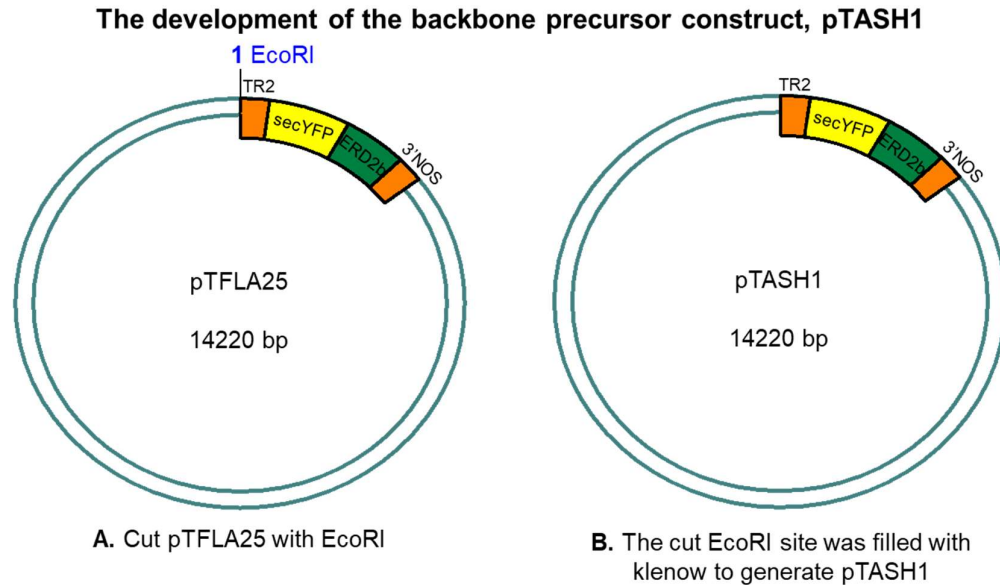


Figure 3. 1. The development of pTASH1, a precursor to pTASH2, which is the backbone for all dual reporter constructs made. The pTASH1 construct was developed by filling in the EcoRI restriction enzyme site of pTFLA25, expressing secYFP-ERD2b. For this, a two-step process was used: **A.** pTFLA25 was cut with EcoRI to generate sticky ends. **B.** The sticky ends were filled with Klenow to remove the EcoRI restriction site.

To create pTASH2, the 3'NOS terminator sequence of pTASH1 was removed and replaced by a 3'ADH terminator sequence followed by a polylinker sequence (**Figure 3.2**). The polylinker sequence that was introduced with the 3'ADH fragment contained several restriction sites, including EcoRI, BamHI and HindIII, which were unique to the plasmid (**Figure 3.3**). As the additional RFP-marker fragments to be added into pTASH2 to generate further constructs contained the 3'NOS sequence, the 3'ADH terminator sequence was used for secYFP-ERD2b to avoid homologous recombination of repeated sequences. The DNA fragment containing the 3'ADH terminator sequence was obtained from a construct developed by L. Adams, named pLA30. To isolate the 3'ADH sequence, pLA30 was cut at the BamHI and HindIII restriction sites. pTASH1 was also cut with

BamHI and HindIII to allow for the ligation of the 3'ADH fragment into the cut pTASH1 vector (**Figure 3.2**). The properties of pTASH2 are shown in **Figure 3.3**. This plant transformation vector contains ampicillin resistance for bacterial selection and kanamycin resistance for plant selection. pTASH2 also contains many unique restriction sites located throughout the plasmid, allowing for easy plasmid manipulation using restriction cloning (**Figure 3.3**).

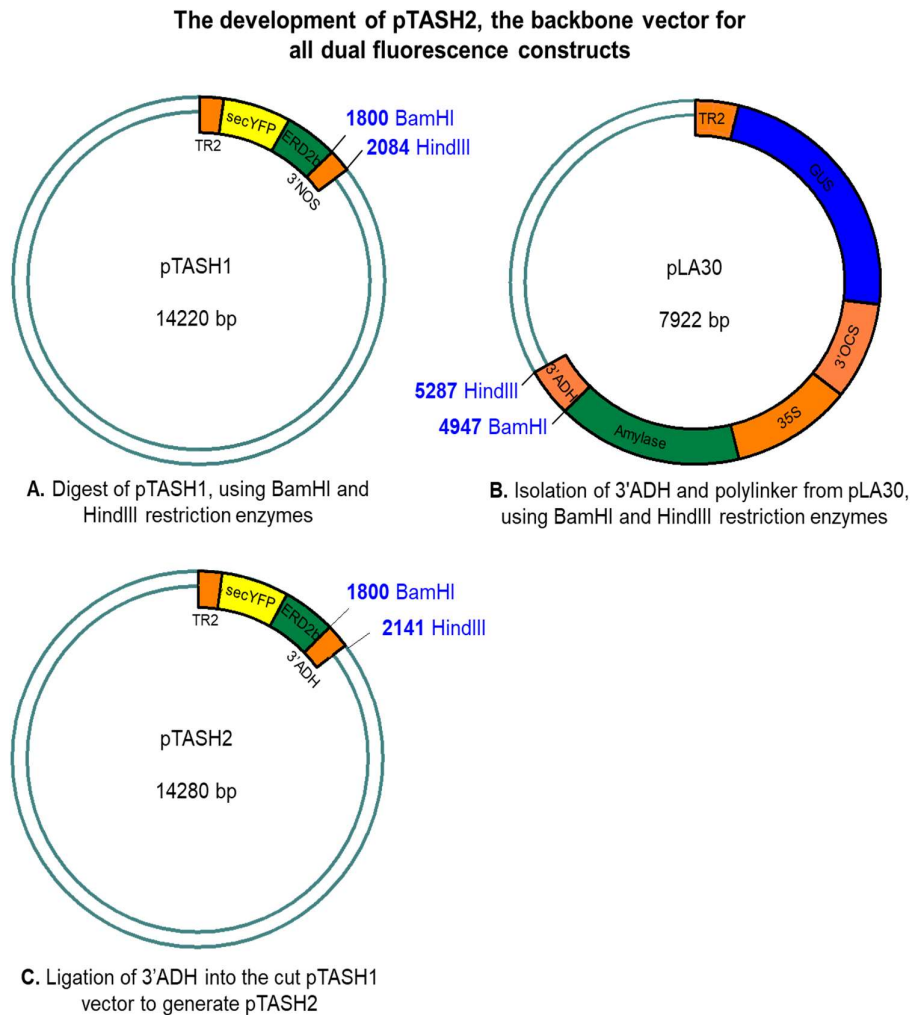


Figure 3. 2. The development of pTASH2, a backbone construct for all pTASH dual fluorescence constructs. For this, the terminator sequence of secYFP-ERD2b, 3'NOS, was replaced with 3'ADH. This was achieved using the BamHI and HindIII restriction enzymes, in the three following steps: **A.** pTASH1 was cut with the BamHI and HindIII restriction enzymes, with the restriction sites positioned at either side of the 3'NOS terminator sequence. **B.** The construct pLA30 was cut with BamHI and HindIII, which has restriction sites flanking the 3'ADH terminator sequence. **C.** The 3'ADH fragment from pLA30 was ligated into the cut pTASH1 vector to generate pTASH2.

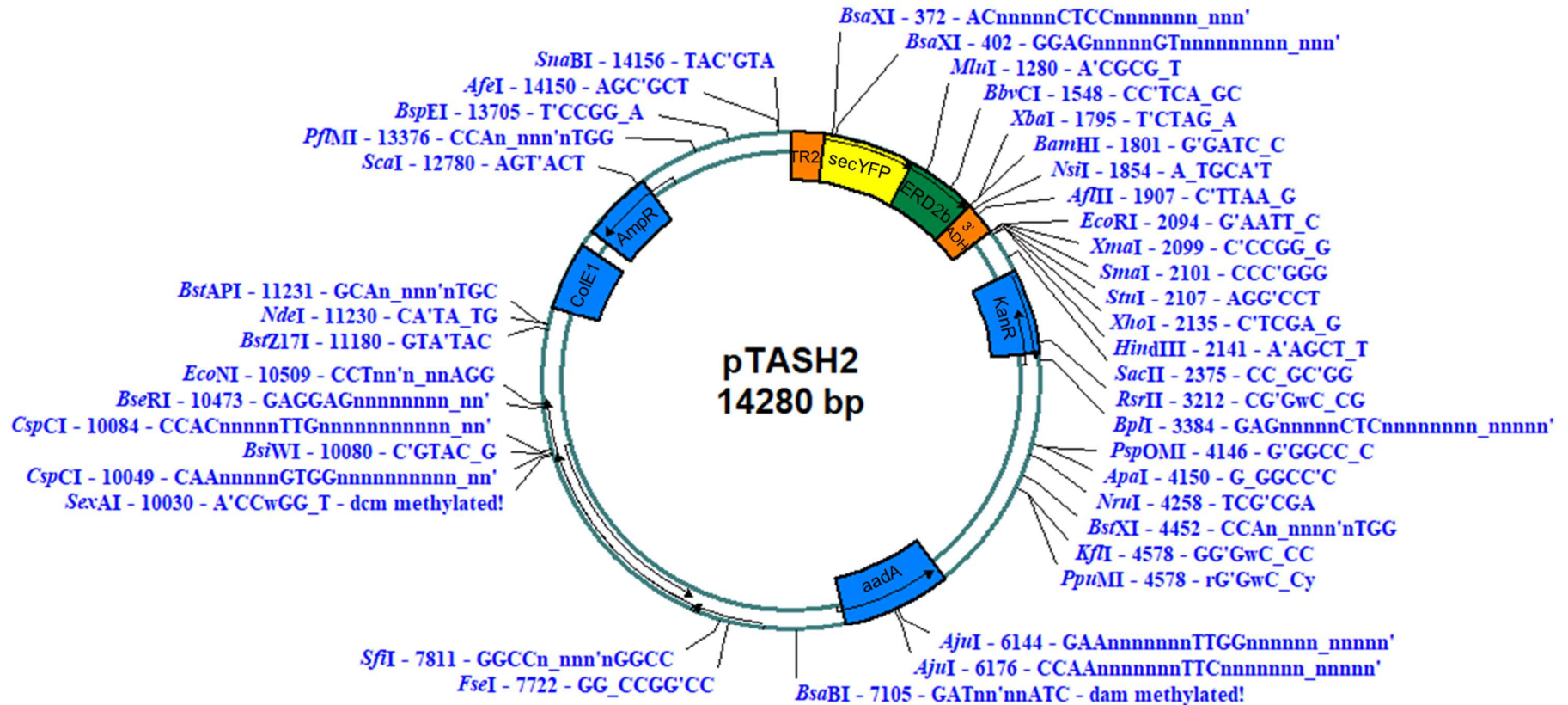


Figure 3. 3. pTASH2 plasmid features. In addition to TR2:secYFP-ERD2b:3'ADH, this plasmid contains a kanamycin resistance gene (KanR) as the plant selectable marker, an aadA gene (aadA) conferring spectinomycin and streptomycin resistance, a ColE1 origin of replication sequence (ColE1) and an ampicillin resistance gene (AmpR). Unique restriction sites in pTASH2 are labelled, showing their position and sequence. Restriction sites flank the TR2 promoter, secYFP, ERD2b and 3'ADH terminator sequences, allowing for plasmid modifications using restriction cloning.

To make each double fluorescent construct, a plant secretory pathway marker fused to RFP was inserted into the backbone vector pTASH2, containing secYFP-ERD2b. For this, pTASH2 was cut at the EcoRI and HindIII restriction sites (**Figure 3.4**). Constructs containing the RFP-marker were also cut with EcoRI and HindIII, to allow for ligation into the cut pTASH2 vector. All constructs containing the RFP-marker fusions were obtained from the Denecke lab (**Table 3.1**). Following the development of each construct, qualitative EcoRI-HindIII and NheI restriction digests were performed, in addition to sanger sequencing.

Dual fluorescence construct development, using pTASH3 as an example

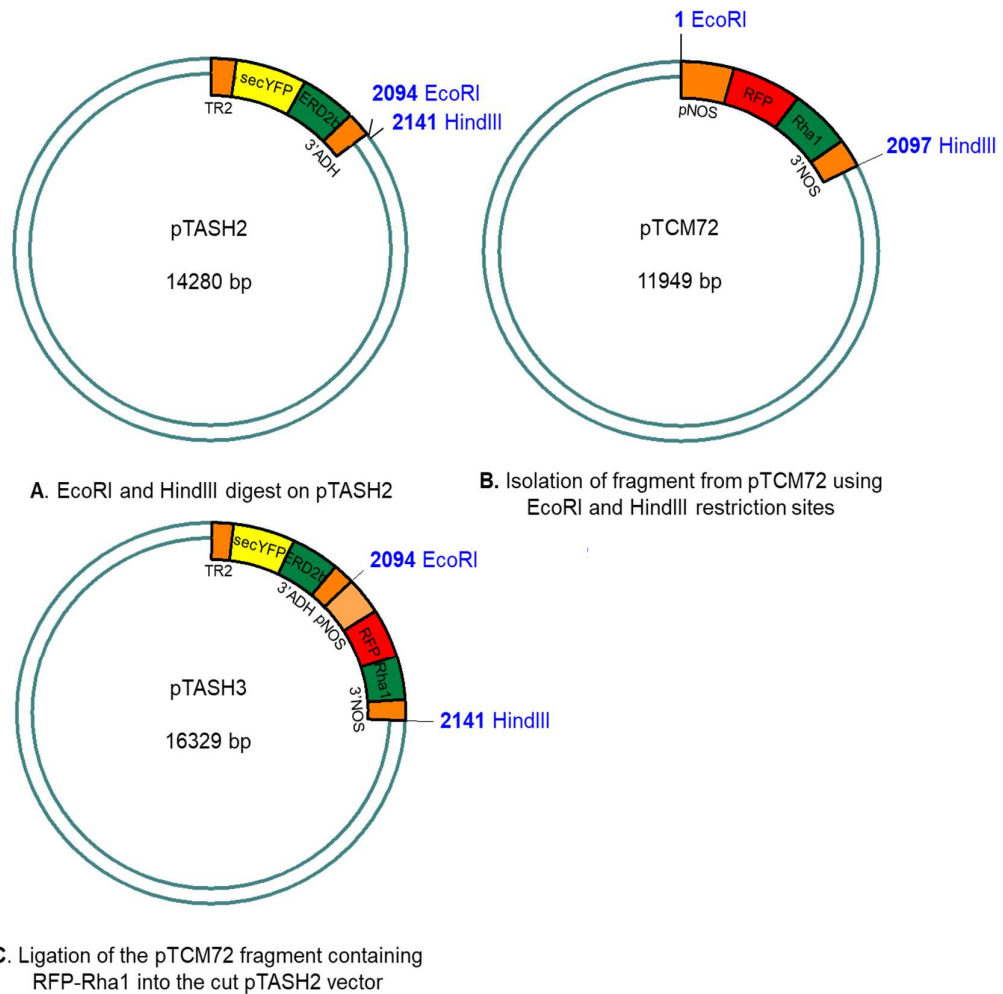


Figure 3. 4. The development of the dual reporter construct pTASH3, used to demonstrate how all dual fluorescence constructs were created. A. To create all constructs, pTASH2 was cut with EcoRI and HindIII restriction enzymes. This excised a small fragment following the TR2:secYFP-ERD2b:3'ADH sequence. **B.** Plasmids containing the RFP-marker fragment have EcoRI and HindIII restriction sites at either side of the promoter:RFP-fusion:terminator sequence. This includes pTCM72 containing the LPVC marker RFP-Rha1. **C.** pTASH3 was developed by ligating the pTCM72 fragment into the cut pTASH2 vector.

3.2.4 Primers for sequencing

A 100 ng/ μ l sample of each pTASH construct was sent to Genewiz for sanger sequencing, using primers listed in **Table 3.2**. When sequencing the plasmids, each of the primers were used singularly, in separate reactions. Together, this provided overlapping sequence reads of the promoter-FP-marker-terminator sequences and their flanking vector backbone regions.

Table 3. 2. Primer sequences used for the DNA sequencing of pTASH constructs. F and R represent forward and reverse respectively, and the primer name represents the region which the primer was specific to. All primer sequences were used to sequence the dual fluorescence constructs. However, for pTASH1 and pTASH2, vector-F, secYFP-F, ERD2b-F and vector-R were used.

| Primer Name | Primer Sequence (5' to 3') |
|-------------|----------------------------|
| backbone-F | TGGTCGATAAGAAAAGGCAAT |
| secYFP-F | GAACGGCATCAAGGTGAAC |
| ERD2b-F | GAGAGCAAGATACGTTTCGTCA |
| RFP-F | CCGAGGACGTCATCAAGG |
| RFP-R | CTTGGTCACCTTCAGCTTGG |
| 3'NOS-R | TGTTTGAACGATCTGCTTCG |
| backbone-R | TATCCGCTCACAATCCACA |

3.2.5 The selection of primary transformants

T₁ Arabidopsis seeds were sterilised in 20 % bleach for 20 min, washed with sterile water, then stratified at 4 °C overnight. Stratified seeds were grown on half strength Murashige and Skoog medium (1/2 MS10) agar plates containing cefotaxime (300 μ g/ml) and kanamycin (50 μ g/ml). Plates were grown under sterile conditions, at 22 °C under a 16 hr photoperiod. After 2 weeks, seedlings resistant to kanamycin were selected and transferred to compost. To screen transgene expression, T₂ seeds were collected from each T₁ plant. These were sterilised and placed onto 1/2 MS10 plates containing kanamycin, and placed under growth conditions as previously described.

3.2.6 Screening transgene expression using confocal microscopy

To select the best expressing transgenic lines, T₂ seedlings grown on 1/2 MS10 media containing kanamycin were selected after two weeks. The phenotypic traits of selected marker lines were qualitatively assessed, to ensure that there were no mutational consequences of genetic transformation that could affect marker localisation. Following this, whole seedlings were transferred onto a microscope slide containing water to

ensure live cell imaging was conducted. The root and cotyledon epidermal cells of each transgenic line was imaged using confocal microscopy, using settings as described in **Chapter 2.7**. For each construct, at least three T₂ lines showing strong transgene expression in both the roots and cotyledon epidermal cells were selected.

3.3 Results

3.3.1 Qualitative restriction digests

Following the development of each construct, qualitative restriction digests were performed to verify the sequence and quality of the plasmids. A double restriction digest for samples of each construct is shown, using the EcoRI and HindIII restriction enzymes (**Figure 3.5**). EcoRI-HindIII restriction digests produced two DNA fragments from each construct, with the presence of a single EcoRI restriction site following the 3' ADH sequence, and a single HindIII restriction site following the 3' NOS sequence. A second fragment was not observed for the digest of the positive pTASH2 sample, due to its small size of 47 base pairs. The positive pTASH13 sample failed to be cut with both enzymes on the occasion shown, yet displayed the correct band sizes when the digest was repeated for this sample (**Figure 3.5**).

Additional qualitative restriction digests, including a NheI restriction digest, were also performed to identify positive DNA preparations for each construct (**Figure 3.6**). NheI digestion of pTASH2 produced three fragments, as two NheI restriction sites are present within the vector backbone, and another is present within the 3'NOS sequence. The NheI restriction digest of the double expression constructs, excluding pTASH10, produced four fragments, due to an additional NheI restriction site within the RFP sequence. However, this NheI restriction site is not present within pTASH10, therefore only three DNA fragments were observed from the digest of this construct (**Figure 3.6**). Following the identification of positive samples using qualitative restriction digests, DNA sequencing was performed. Full sequences of the promoter- reporter- terminator regions within each construct have been obtained.

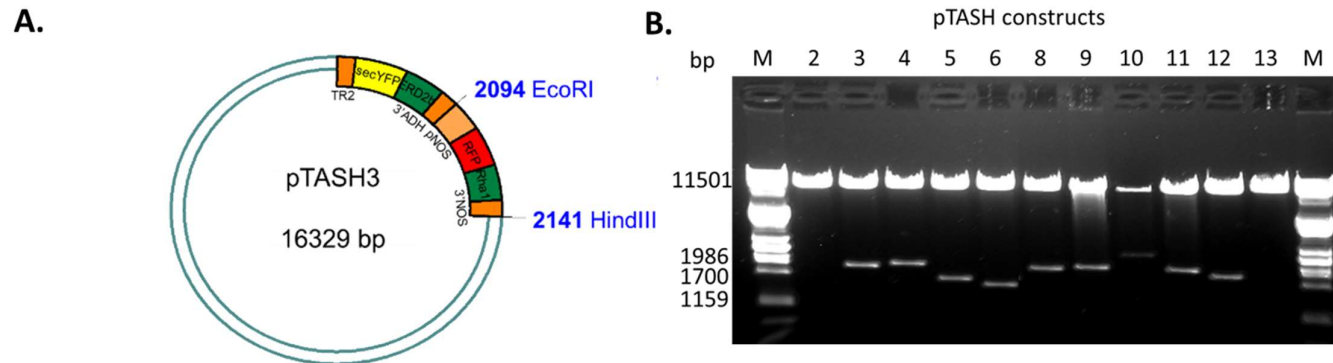


Figure 3. 5. Qualitative EcoRI-HindIII restriction digests performed on the pTASH constructs. **A.** The positions of the of the EcoRI and HindIII restriction sites within the double fluorescent constructs, using pTASH3 as an example. The expected band sizes (bp) from the EcoRI-HindIII digest of pTASH3 are 14,233 and 2096. **B.** A gel image of the restriction digest, with the lanes representing pTASH construct numbers. Fragments were separated on a 0.8 % agarose gel, using phage lambda DNA digested with PstI as the marker (M).

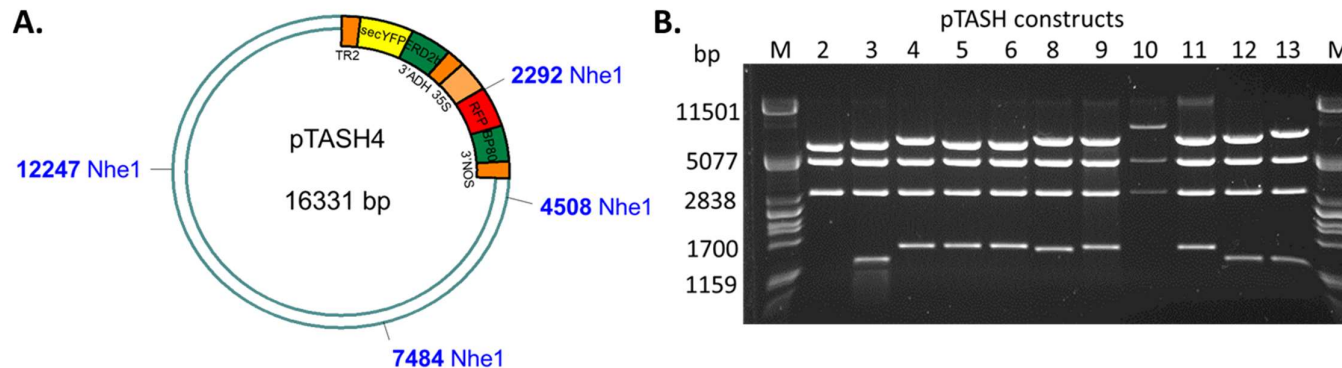


Figure 3. 6. Qualitative NheI restriction digest performed on the pTASH constructs. **A.** The positions of the NheI restriction sites within the double expression constructs, with pTASH4 used as an example. The expected fragment sizes (bp) from the NheI digest of pTASH4 are: 6376, 4763, 2976, 2216. **B.** A gel image of the restriction digest, with the lanes representing pTASH construct numbers. Fragments were separated on a 0.8 % agarose gel, using phage lambda DNA digested with PstI as the marker (M).

3.3.2 Subcellular localisation of the double fluorescent reporter constructs

pTASH2, the vector backbone expressing the Golgi marker secYFP-ERD2b

Each double expression construct contains the Golgi marker ERD2b fused to yellow fluorescent protein (secYFP) as a common marker, and an additional plant secretory pathway marker fused to red fluorescent protein (RFP). To verify that the subcellular localisation of each marker was as expected when co-expressed with secYFP-ERD2b, *Agrobacterium*-mediated tobacco leaf infiltrations were conducted. Confocal microscopy of infiltrated tobacco leaf epidermal cells showed that for pTASH2 expressing secYFP-ERD2b alone, punctate secYFP-ERD2b dots were observed within the cytosol (**Figure 3.7**). This supports secYFP-ERD2b localisation within the Golgi. Punctate secYFP-ERD2b dots were also consistently observed within tobacco leaf epidermis cells expressing each double expression construct (**Figures 3.8 to 3.18**).

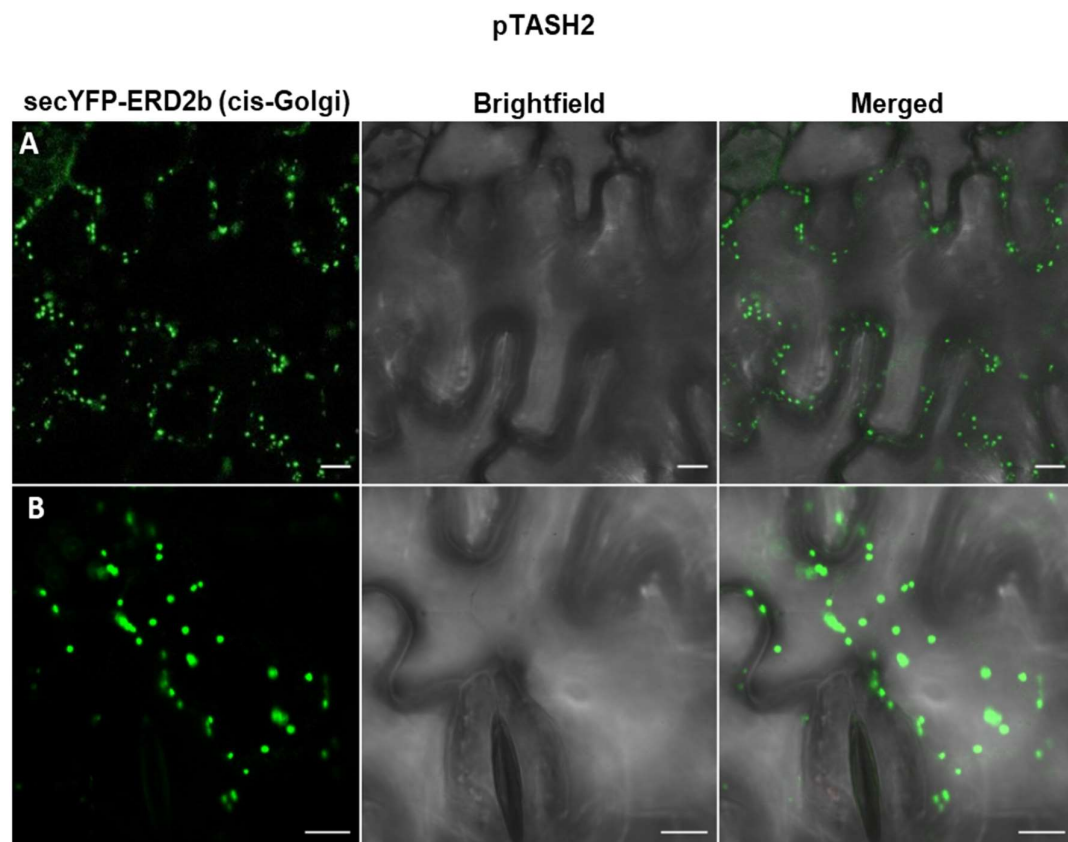


Figure 3. 7. Tobacco leaf epidermal cells infiltrated with pTASH2, expressing the Golgi marker secYFP-ERD2b alone. A. The central focal plane of an infiltrated cell, showing secYFP-ERD2b punctae within the cytoplasm. The large central vacuole takes up the majority of the space within the cell. **B.** A focused view of the cortical cytoplasm, showing punctate secYFP-ERD2b dispersed throughout the cytoplasm. Scale bars represent 10 μ m.

pTASH3 co-expressing the LPVC marker RFP-Rha1

The double expression construct pTASH3 co-expresses the Golgi marker secYFP-ERD2b with the LPVC marker RFP-Rha1. Within infiltrated tobacco leaf epidermis cells, punctate secYFP-ERD2b and RFP-Rha1 dots were observed, which did not co-localise (**Figure 3.8C**). This supports the localisation of secYFP-ERD2b within the Golgi, and RFP-Rha1 within the LPVCs. RFP-Rha1 leakage to the vacuole was also suggested within infiltrated cells, with labelling of the tonoplast observed (**Figure 3.8A&B**).

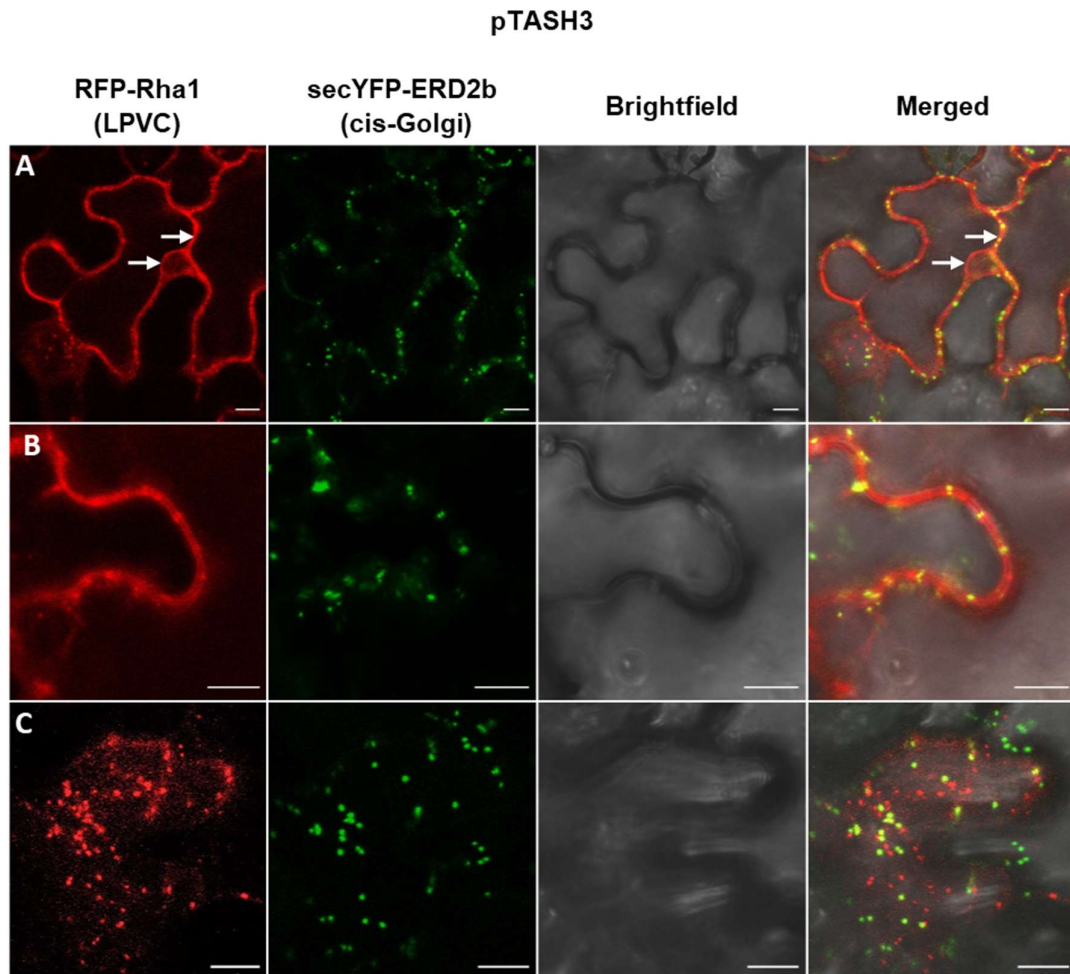


Figure 3. 8. pTASH3, co-expressing the Golgi marker secYFP-ERD2b and the LPVC marker RFP-Rha1, within infiltrated tobacco leaves. A. The central focal plane of a cell, demonstrating the partial localisation of RFP-Rha1 to the tonoplast. White arrows label transvacuolar strands. **B.** A magnified view of the central focal plane, showing RFP-Rha1 punctae and tonoplast localisation. **C.** The cortical cytoplasm of a cell, showing RFP-Rha1 and secYFP-ERD2b punctae which do not co-localise. Scale bars represent 10 μ m.

pTASH4, pTASH5 and pTASH6, co-expressing the PVC marker RFP-BP80 under the control of different promoters

The double expression constructs pTASH4, pTASH5 and pTASH6 express RFP-BP80 under the control of three promoters with varying strengths, due to reports of RFP-BP80 toxicity under high levels of overexpression (daSilva et al, 2005). pTASH4 expresses RFP-BP80 under the control of the 35S promoter, and pTASH5 and pTASH6 express RFP-BP80 under the control of the pNOS and TR2 promoters respectively. The pNOS and TR2 promoters drive weaker constitutive expression in comparison to the 35S promoter. When infiltrated into tobacco leaves, all three constructs co-expressed punctate secYFP-ERD2b and RFP-BP80 dots. Partial co-localisation was suggested between secYFP-ERD2b and RFP-BP80 for all three constructs (**Figures 3.9 to 3.11**). This supports that secYFP-ERD2b localises to the Golgi and RFP-BP80 localises to the PVC when the two markers are co-expressed. Partial co-localisation could reflect the transient localisation of RFP-BP80 within the Golgi. Within infiltrated tobacco leaf epidermis cells, 35S:RFP-BP80 (pTASH4) and pNOS:RFP-BP80 (pTASH5) also labelled the tonoplast and vacuoles (**Figures 3.9 and 3.10**). However, within pTASH6, expressing RFP-BP80 under the control of the TR2 promoter, no additional tonoplast or vacuole localisation was observed (**Figure 3.11**).

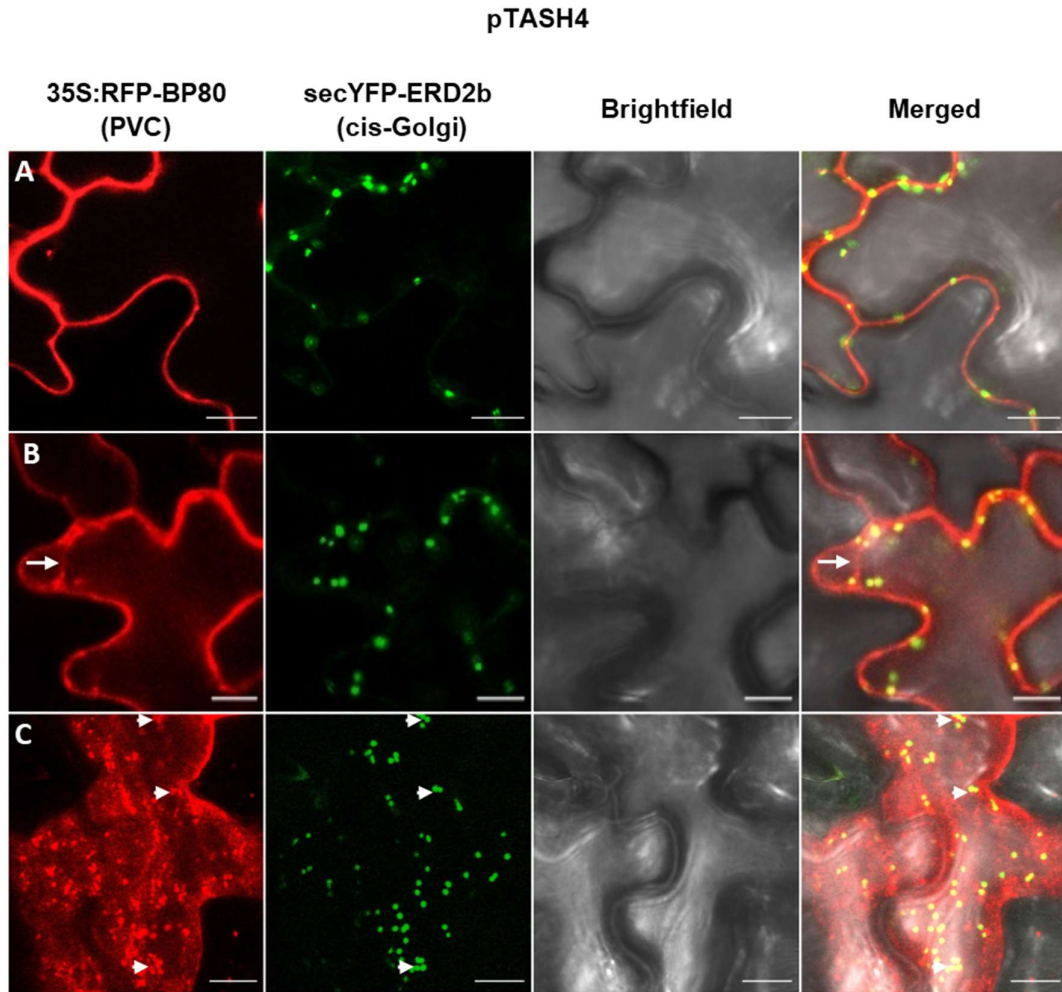


Figure 3. 9. pTASH4, co-expressing the Golgi marker secYFP-ERD2b and the PVC marker RFP-BP80 under the control of the 35S promoter, within infiltrated tobacco leaves. A. The central plane of tobacco leaf epidermal cells, showing the partial localisation of 35S:RFP-BP80 to the tonoplast. **B.** A magnified view of the centre of an infiltrated cell, showing 35S:RFP-BP80 in the tonoplast, evidenced by a transvacuolar strand which is labelled with a white arrow. **C.** The cortical cytoplasm of an infiltrated tobacco cell. Some secYFP-ERD2b punctae are closely associated with 35S:RFP-BP80 punctae (white arrowhead). Vacuolar localisation of 35S:RFP-BP80 is also observed. Scale bars represent 10 μ m.

pTASH5

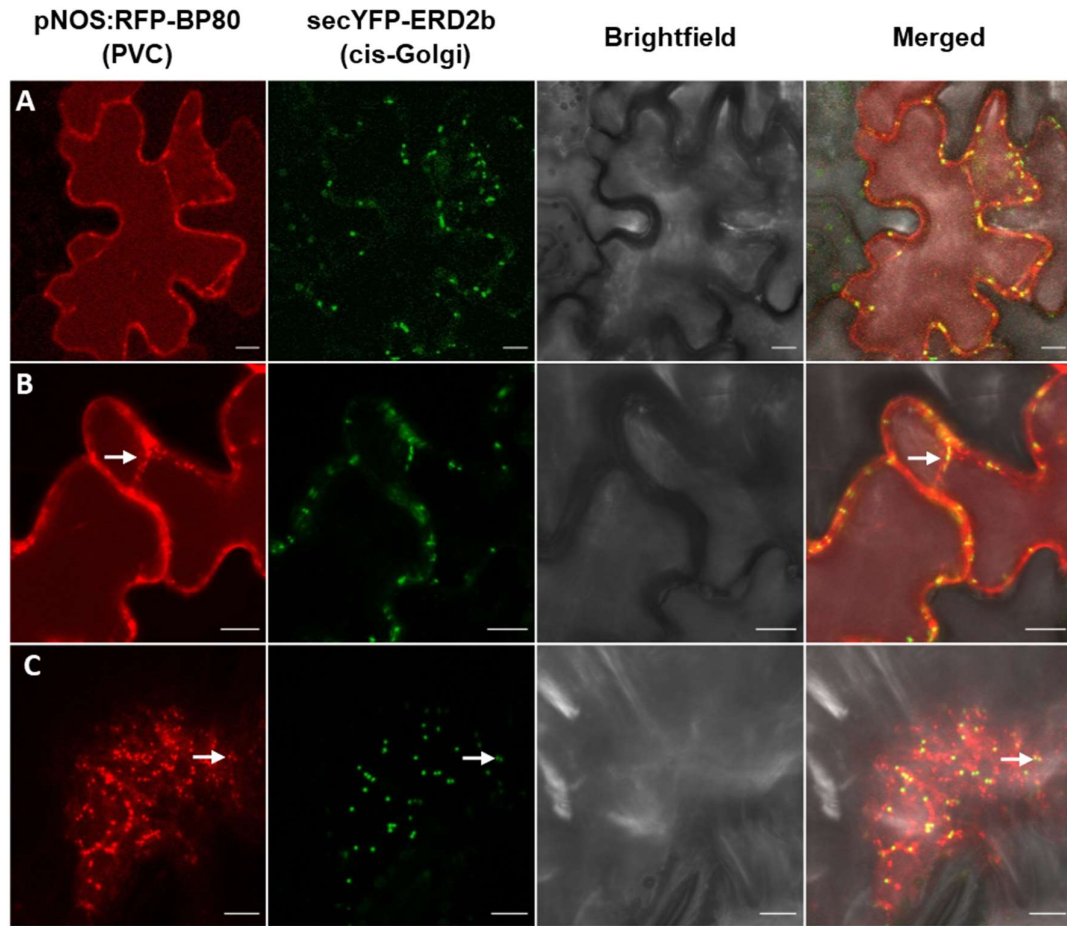


Figure 3. 10. Tobacco leaf epidermis cells infiltrated with pTASH5, co-expressing the Golgi marker secYFP-ERD2b and the PVC marker pNOS:RFP-BP80. A. The central focal plane of an infiltrated cell, showing the partial localisation of pNOS:RFP-BP80 to the tonoplast. **B.** A magnified view of an infiltrated cell, supporting pNOS:RFP-BP80 localisation within the tonoplast. A transvacuolar strand is labelled with a white arrow, containing punctate secYFP-ERD2b dots that are in transit through the transvacuolar strand. **C.** The cortical cytoplasm of an infiltrated tobacco leaf epidermal cell, showing the punctate secYFP-ERD2b and RFP-BP80 dots. Although most secYFP-ERD2b punctae don't colocalise with pNOS:RFP-BP80, some are closely associated (white arrow). Scale bars represent 10 μ m.

pTASH6

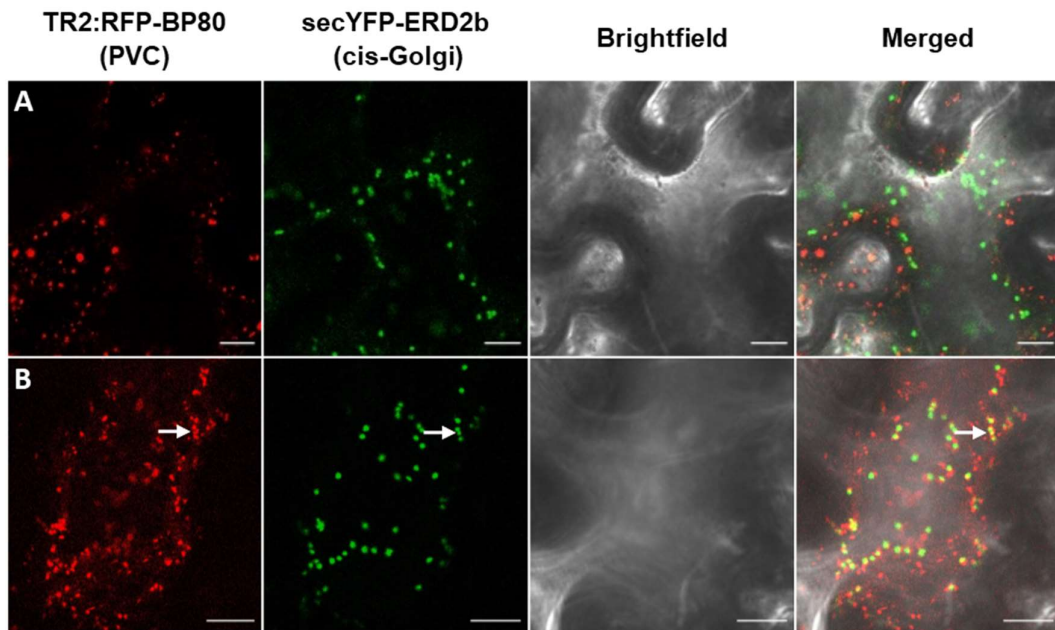


Figure 3. 11. pTASH6, co-expressing the cis-Golgi marker secYFP-ERD2b and the PVC marker TR2:RFP-BP80, within infiltrated tobacco leaves. A. The centre of an infiltrated cell, showing punctate TR2:RFP-BP80 and secYFP-ERD2b which do not co-localise. For TR2:RFP-BP80, no additional tonoplast or vacuole localisation is observed. **B.** The cortical cytoplasm of an infiltrated tobacco leaf cell, showing the punctate secYFP-ERD2b and RFP-BP80 dots which do not co-localise, although some punctae are closely associated (white arrow). Scale bars represent 10 μ m.

pTASH7, co-expressing the ER marker RFP-HDEL

When the ER marker RFP-HDEL was co-expressed with the cis-Golgi marker secYFP-ERD2b, ER localisation was not observed. Instead, RFP-HDEL punctae were shown, which completely co-localised with secYFP-ERD2b punctae (**Figure 3.12**). This suggests that co-expression with secYFP-ERD2b results in Golgi localisation of RFP-HDEL.

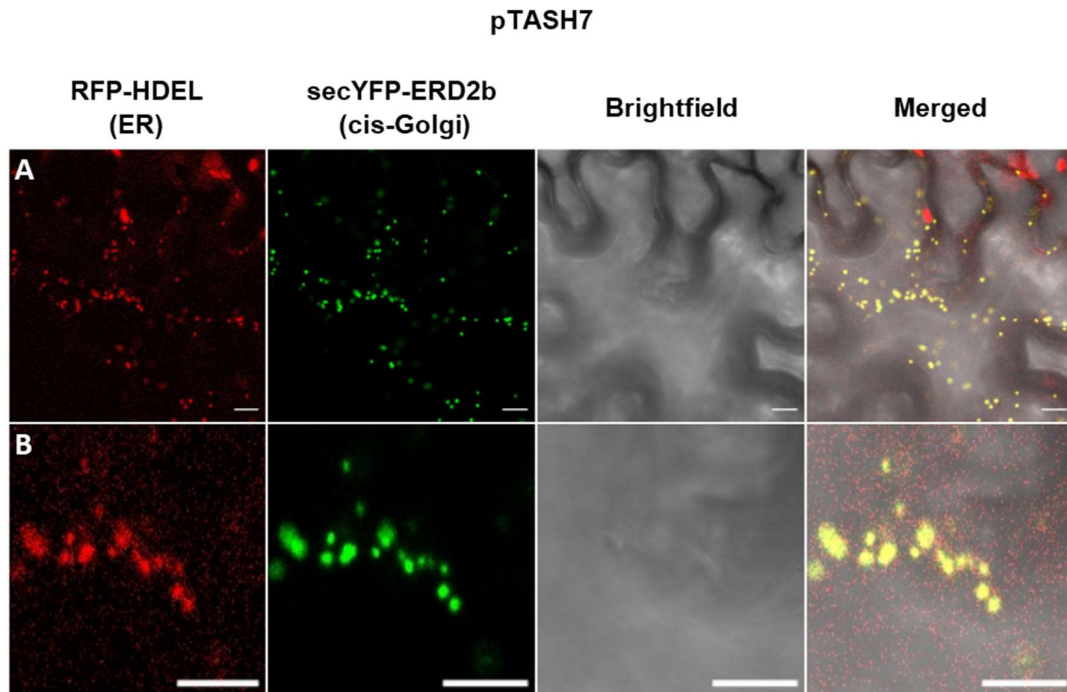


Figure 3. 12. pTASH7, co-expressing the Golgi marker secYFP-ERD2b and the ER marker RFP-HDEL within infiltrated tobacco leaf epidermis cells. A. The cortical cytoplasm of an infiltrated cell, showing RFP-HDEL punctae, rather than a network of cisternae and tubules typical of the ER. **B.** A magnified view of A., showing the co-localisation of secYFP-ERD2b with RFP-HDEL. Scale bars represent 10 μ m.

pTASH8, co-expressing the ER marker secRFP-p24aTM

The construct pTASH8 was developed to co-express the Golgi marker secYFP-ERD2b with the ER marker, secRFP-p24aTM. Within tobacco leaf epidermis cells infiltrated with pTASH8, secRFP-p24aTM labelled the ER network (**Figure 3.13**). secYFP-ERD2b punctate dots were also expressed, in close proximity to the labelled ER network.

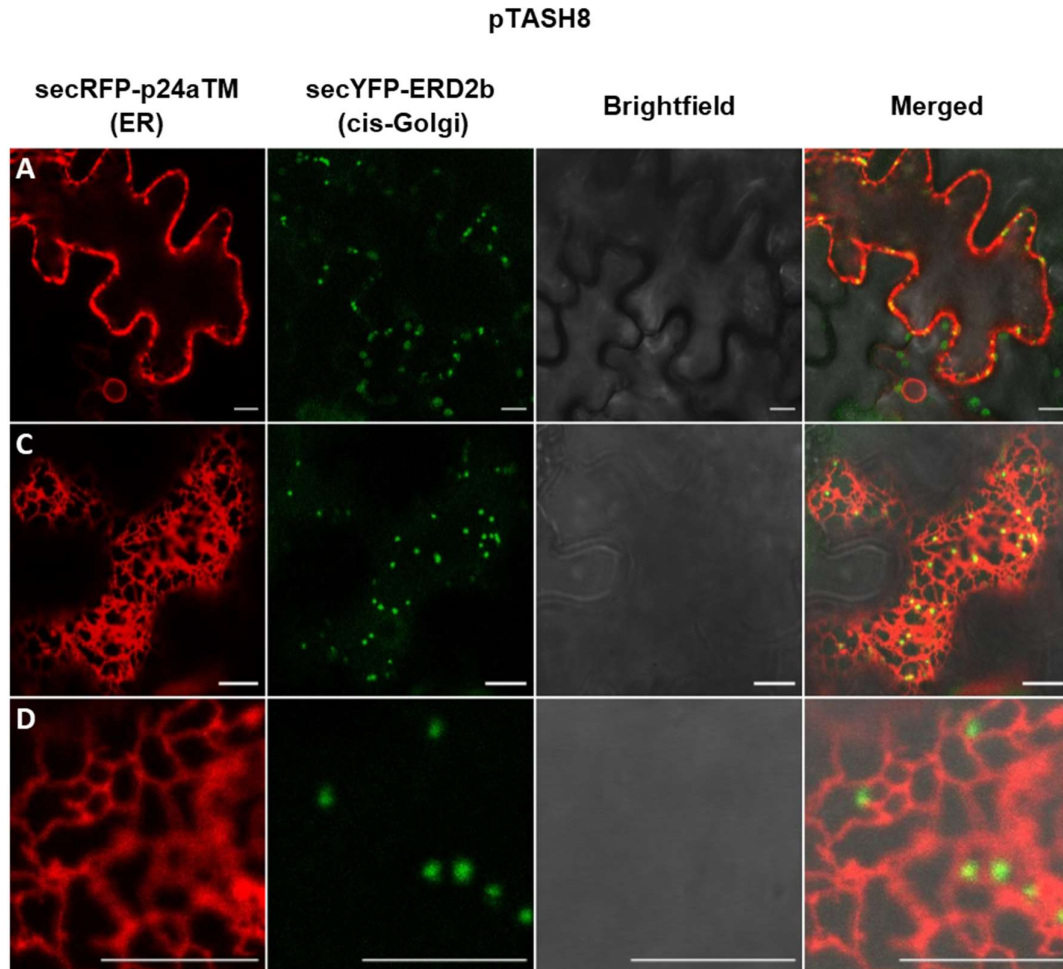


Figure 3. 13. pTASH8, co-expressing the Golgi marker secYFP-ERD2b and the ER marker secRFP-p24aTM within infiltrated tobacco leaf epidermis cells. A. The central focal plane of an infiltrated cell, showing secRFP-p24aTM localised within the cytoplasm, with the large central vacuole occupying the majority of the cell. **B.** The cell surface of an infiltrated tobacco leaf epidermis cell, showing secRFP-p24aTM labelling the ER network. Punctate secYFP-ERD2b dots are in close proximity to the labelled ER network. **C.** A magnified image of the infiltrated tobacco leaf epidermis cell shown within B, further illustrating the close proximity of the punctate secYFP-ERD2b dots to the labelled ER network. Scale bar represents 10 μ m.

pTASH10, co-expressing the TGN marker RFP-SYP61

The double expression construct pTASH10 co-expresses the Golgi marker secYFP-ERD2b with the TGN marker RFP-SYP61. pTASH10 expression within infiltrated tobacco leaf epidermis cells showed punctate secYFP-ERD2b and RFP-SYP61 dots within the cytosol (**Figure 3.14B&C**). secYFP-ERD2b and RFP-SYP61 dots localised to separate compartments, yet yellow merged dots were shown within some infiltration images. This indicates a close association with secYFP-ERD2b and RFP-SYP61, supporting secYFP-ERD2b localisation within the Golgi, and RFP-SYP61 expression within the closely located TGN. Leakage of RFP-SYP61 to the plasma membrane was also observed within infiltrated tobacco leaf epidermis cells (**Figure 3.14A**).

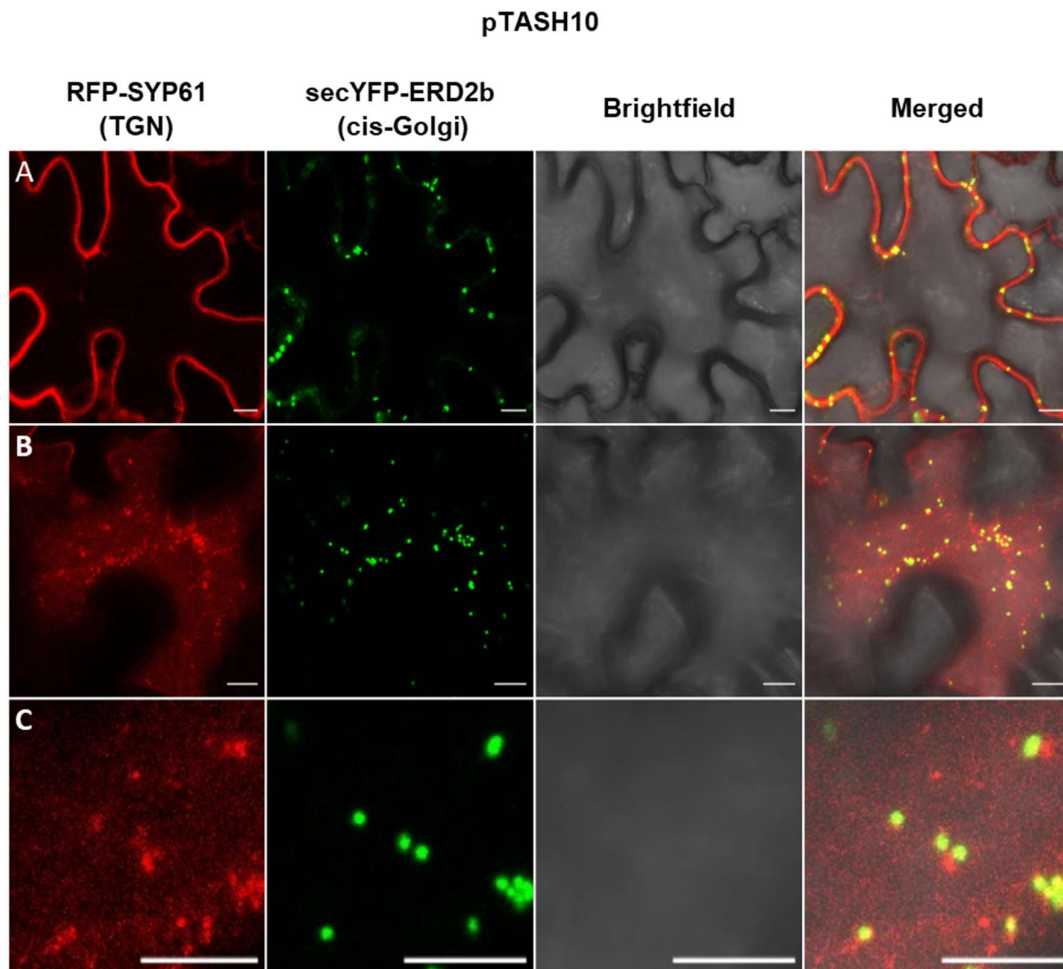


Figure 3. 14. pTASH10, co-expressing the Golgi marker secYFP-ERD2b and the TGN marker RFP-SYP61 within infiltrated tobacco leaves. A. The centre of an infiltrated cell, showing the partial localisation of RFP-SYP61 to the plasma membrane. **B.** The cortical cytoplasm of an infiltrated cell, showing punctate RFP-SYP61 dots which do not co-localise with secYFP-ERD2b. **C.** A magnified image of the cortical cytoplasm, further demonstrating no co-localisation between RFP-SYP61 and secYFP-ERD2b. Scale bars represent 10 μm .

pTASH9 and pTASH11, co-expressing the two BP80 mutants, RFP-BP80(Tyr) and RFP-BP80(Leu) respectively

The double expression constructs pTASH9 and pTASH11 were developed to co-express secYFP-ERD2b with two RFP-BP80 mutants, RFP-BP80(Tyr) and RFP-BP80(Leu) respectively. Both mutations are present within the YMPL motif of the cytosolic tail of BP80, which is responsible for vacuolar sorting (daSilva et al, 2006). However, the mutants have different subcellular localisations; the tyrosine mutant, RFP-BP80(Tyr), has previously been characterised to re-direct RFP-BP80 from the PVC to the TGN, with leakage to the plasma membrane also observed (Foresti et al, 2010). Tobacco leaf epidermis cells infiltrated with pTASH9 expressed punctate RFP-BP80(Tyr) dots which did not co-localise with the punctate secYFP-ERD2b dots (**Figure 3.15B&C**). This supports RFP-BP80(Tyr) localising to the TGN. RFP-BP80(Tyr) leakage to the plasma membrane was also observed within infiltrated tobacco leaf epidermis cells (**Figure 3.15A**). The other BP80 mutant construct, pTASH11, co-expresses secYFP-ERD2b with RFP-BP80(Leu). RFP-BP80(Leu) has previously been shown to localise to the LPVCs, with tonoplast localisation also observed (Foresti et al, 2010). This was validated by tobacco leaf epidermis cells infiltrated with pTASH11 (**Figure 3.16**).

pTASH9

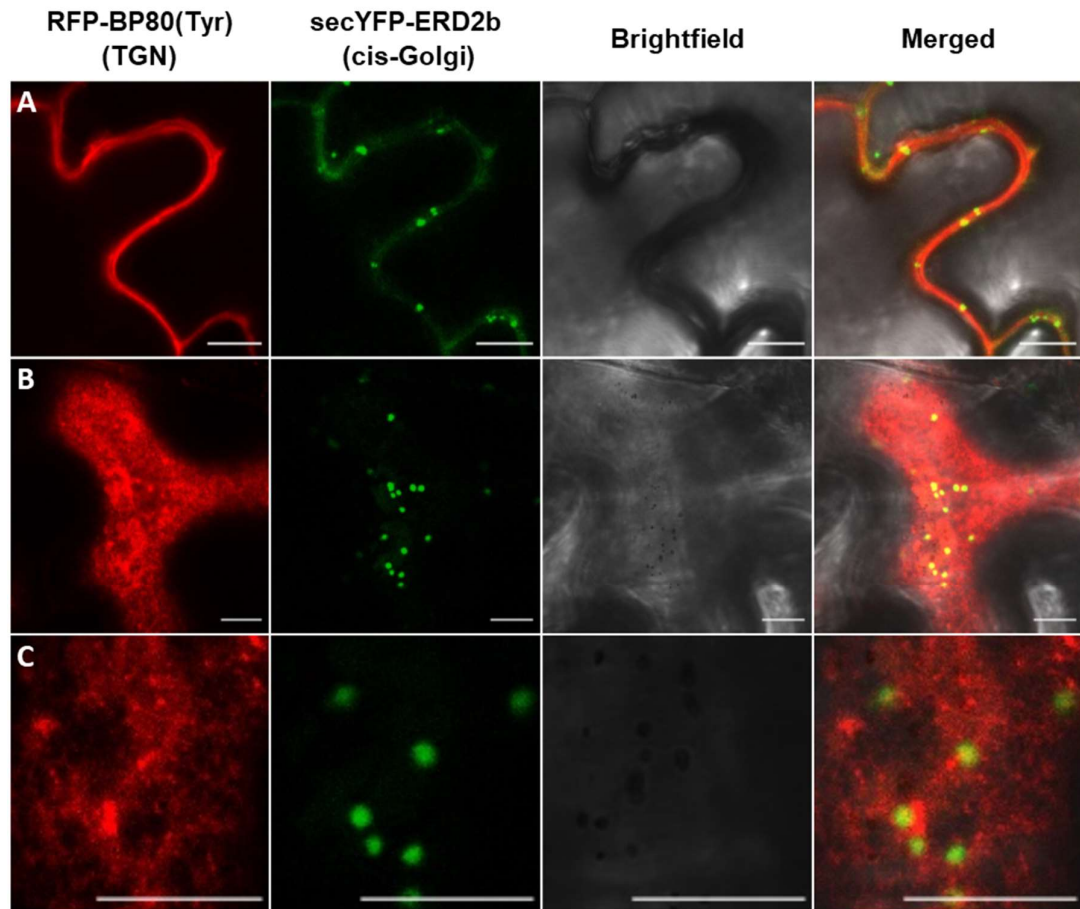


Figure 3. 15. pTASH9, co-expressing the Golgi marker secYFP-ERD2b with the TGN marker RFP-BP80(Tyr) within infiltrated tobacco leaf epidermis cells. A. A magnified image of the cell periphery, showing the partial localisation of RFP-BP80(Tyr) to the plasma membrane. **B.** The cortical cytoplasm of an infiltrated tobacco cell, showing RFP-BP80(Tyr) punctae which do not co-localise with secYFP-ERD2b. **C.** A magnified view of B, to further show that RFP-BP80(Tyr) and secYFP-ERD2b do not co-localise. Scale bars represent 10 μ m.

pTASH11

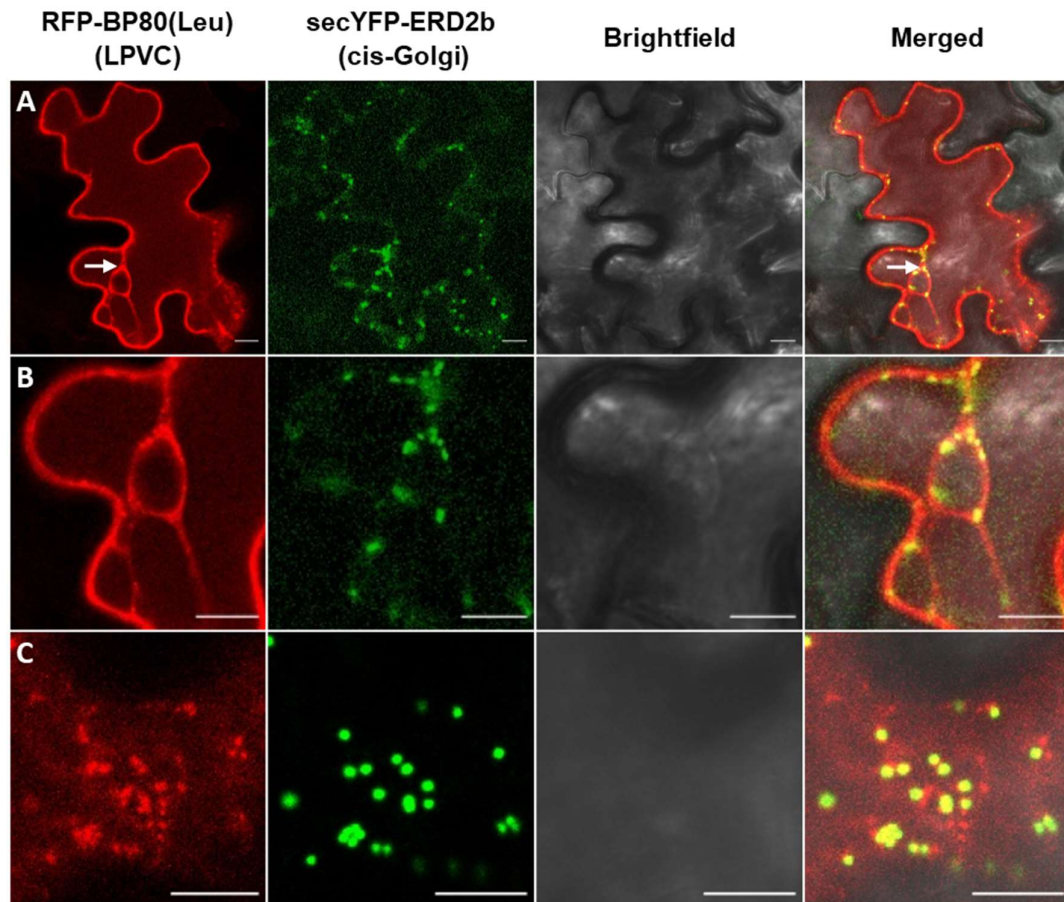


Figure 3. 16. pTASH11, co-expressing the Golgi marker secYFP-ERD2b with the LPVC marker RFP-BP80(Leu) within infiltrated tobacco leaf epidermis cells. A. The centre of an infiltrated cell, showing the partial localisation of RFP-BP80(Leu) to the tonoplast. Transvacuolar strands are shown, labelled with a white arrow. secYFP-ERD2b punctae are present within the cytoplasm, and through the transvacuolar strand. **B.** A magnified view of A, further showing the partial localisation of RFP-BP80(Leu) within the tonoplast. **C.** The cortical cytoplasm of an infiltrated tobacco leaf epidermis cell, expressing punctate secYFP-ERD2b dots which do not co-localise with the punctate RFP-BP80(Tyr) dots. Scale bars represent 10 μ m.

pTASH12, co-expressing the vacuole marker Aleu-RFP

The double expression construct pTASH12 was developed to co-express the Golgi marker secYFP-ERD2b with the vacuole marker Aleu-RFP. Within the central focal plane of infiltrated cells, negative Aleu-RFP staining of the nucleus was observed, supporting localisation to the large central vacuoles (**Figure 3.17A**). In addition to labelling the vacuole, punctate Aleu-RFP dots were also expressed within infiltrated tobacco leaf epidermis cells, which did not co-localise with the punctate secYFP-ERD2b dots (**Figure 3.17B&C**).

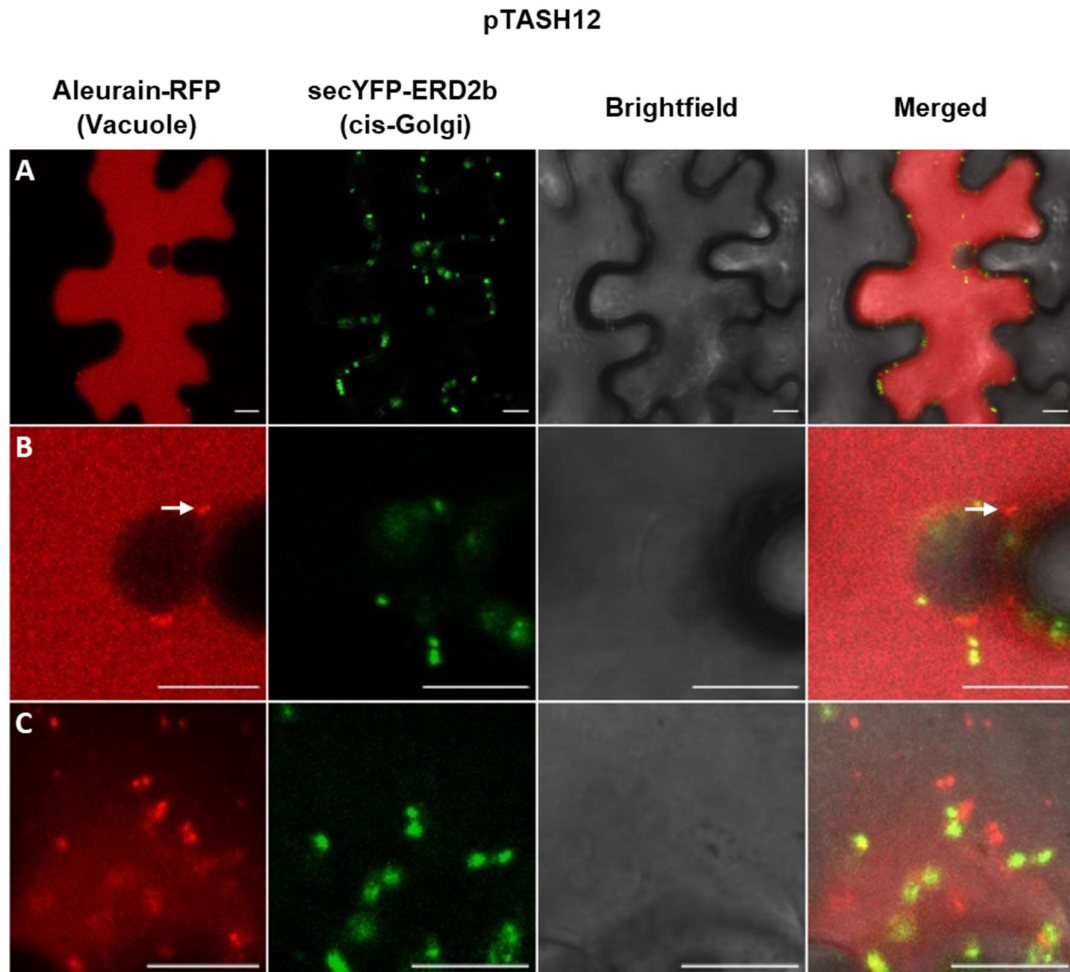


Figure 3. 17. pTASH12, co-expressing the Golgi marker secYFP-ERD2b with the vacuole marker Aleu-RFP within infiltrated tobacco leaf epidermis cells. A. The centre of an infiltrated cell, showing Aleu-RFP labelling the large central vacuole, which takes up most of the cell. **B.** A magnified view of A, with Aleu-RFP showing negative staining of the nucleus. Additional Aleu-RFP punctae are also observed (white arrow). **C.** The cortical cytoplasm of an infiltrated cell, showing Aleu-RFP punctae which do not co-localise with secYFP-ERD2b. Scale bars represent 10 μ m.

pTASH13, co-expressing the tonoplast marker CBL6-RFP

The double expression construct pTASH13 was developed to co-express the Golgi marker secYFP-ERD2b with the tonoplast marker CBL6-RFP. Infiltrated tobacco leaf epidermis cells supported the localisation of secYFP-ERD2b within the Golgi, and CBL6-RFP localisation within the tonoplast. Transvacuolar strands were suggested to be labelled by CBL6-RFP, with punctate secYFP-ERD2b dots located within these strands (**Figure 3.18A**). A corrugated tonoplast membrane was observed, illustrating where the tonoplast wraps around different organelles, including the nuclear envelope. CBL6-RFP punctate dots were also shown, suggesting CBL6-RFP localises to an additional subcellular compartment (**Figure 3.18B&C**). Most CBL6-RFP punctae did not co-localise with secYFP-ERD2b, however, some were closely associated.

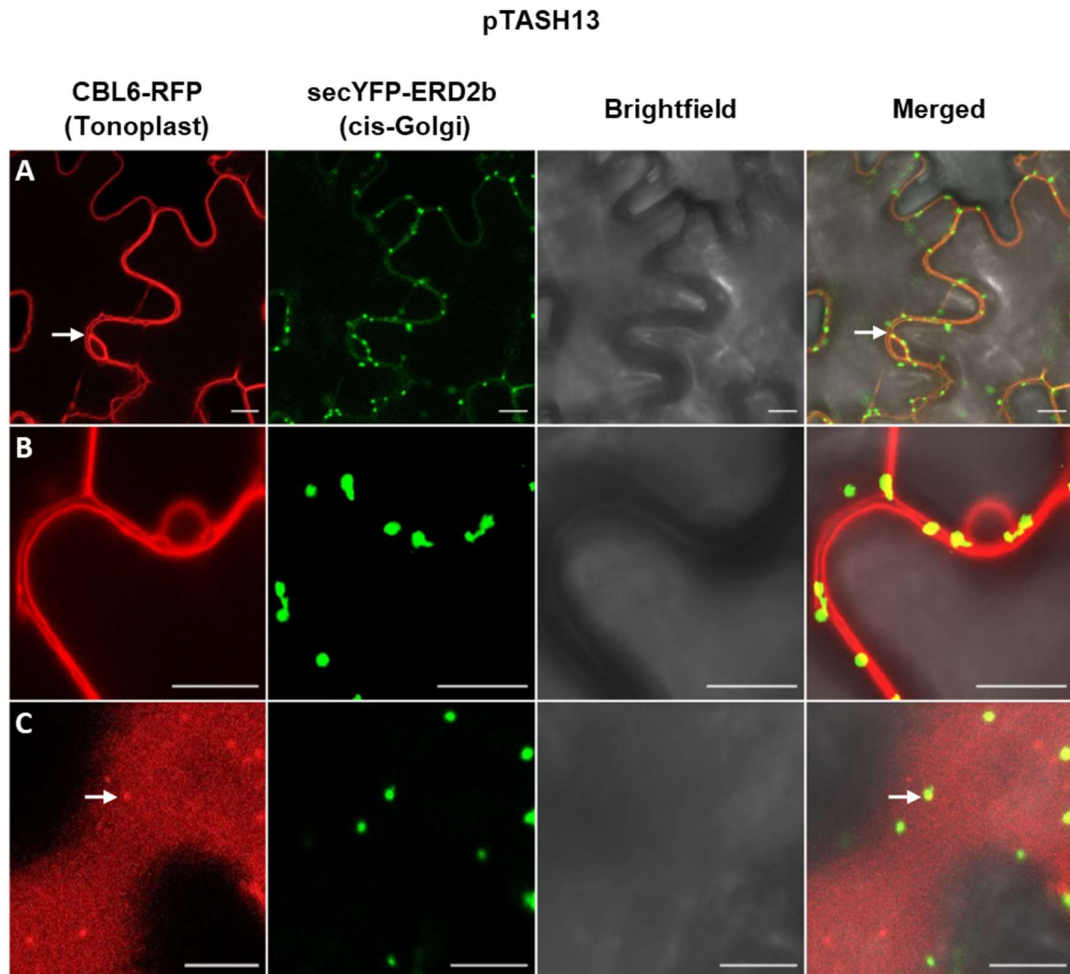


Figure 3. 18. pTASH13, co-expressing the Golgi marker secYFP-ERD2b and the tonoplast marker CBL6-RFP within infiltrated tobacco leaves. A. The central focal plane of an infiltrated tobacco cell, showing the labelling of CBL6-RFP to the tonoplast. A CBL6-RFP transvacuolar strand is shown (white arrow), which contains secYFP-ERD2b punctae. **B.** A magnified view of the cell periphery, showing the CBL6-RFP labelled tonoplast membrane of two adjacent cells. **C.** An infiltrated tobacco leaf epidermis cell expressing punctate secYFP-ERD2b and CBL6-RFP dots, some of which co-localise (white arrow). Scale bars represent 10 μ m.

6.3 Selection of primary transformants

Primary transformed (T_1) seeds were plated onto $\frac{1}{2}$ MS10 media containing cefotaxime and kanamycin. After two weeks, seedlings resistant to kanamycin were observed (**Figure 3.19**). Despite attempting selection of the seeds from approximately ten transformed plants, no transgenic seedlings were identified for pTASH4 lines expressing 35S:RFP-BP80 (**Figure 3.19**), and also for the constructs expressing the two BP80 mutants, RFP-BP80(Tyr) and RFP-BP80(Leu). Following the growth of transgenic seedlings, typically, 24 transgenic primary transformants for each construct were selected to be transferred to compost. To select the best expressing primary transformant lines, T_2 seeds were collected from each T_1 plant.

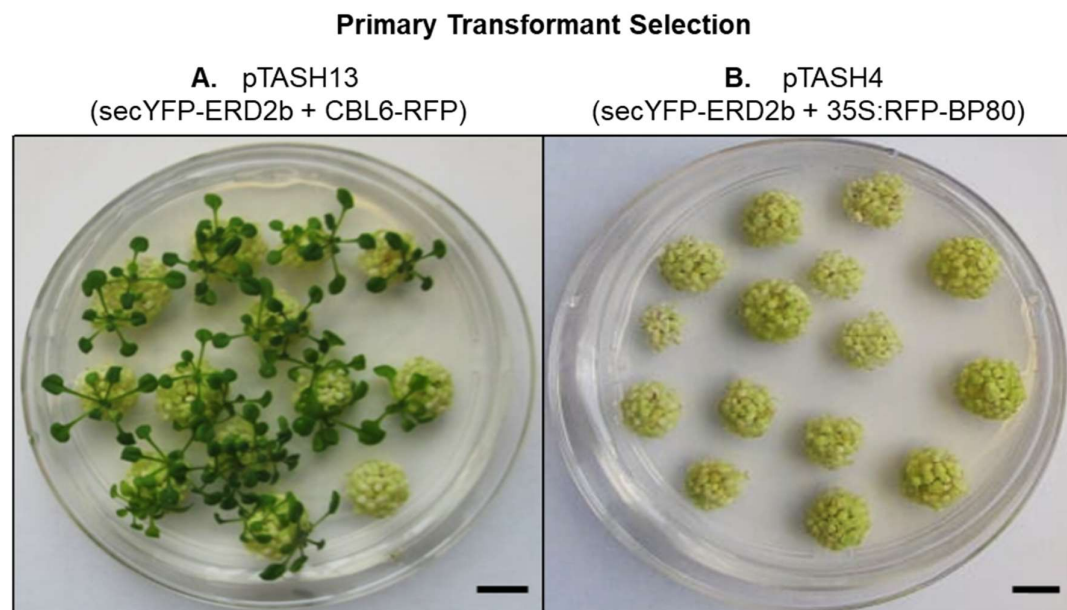


Figure 3. 19. Primary transformed, T_1 seedlings grown on $\frac{1}{2}$ MS10 plates containing kanamycin and cefotaxime, after two weeks of growth. A. T_1 seedlings collected from Arabidopsis transformed with pTASH13, which co-expresses the Golgi marker secYFP-ERD2b with the tonoplast marker, CBL6-RFP. Some T_1 seedlings are resistant to kanamycin. **B.** T_1 seedlings collected from Arabidopsis transformed with pTASH4, which co-expresses the Golgi marker secYFP-ERD2b with RFP-BP80, under the control of the 35S promoter. No T_1 seedlings are resistant to kanamycin. Scale bars represent 1 cm.

6.4 Screening the expression of primary Arabidopsis transformants

T_2 generation seeds collected from each T_1 plant were plated onto $\frac{1}{2}$ MS10 media containing kanamycin. T_2 seedlings resistant to kanamycin were transferred onto media without antibiotics and grown for two weeks before analysing transgene expression with confocal microscopy. The root and cotyledon tissues of T_2 seedlings were imaged to select three lines for each

construct. Confocal images of the best expressing line for each construct are shown, for the roots (Figures 3.20 and 3.21) and cotyledons (Figures 3.22 and 3.23).

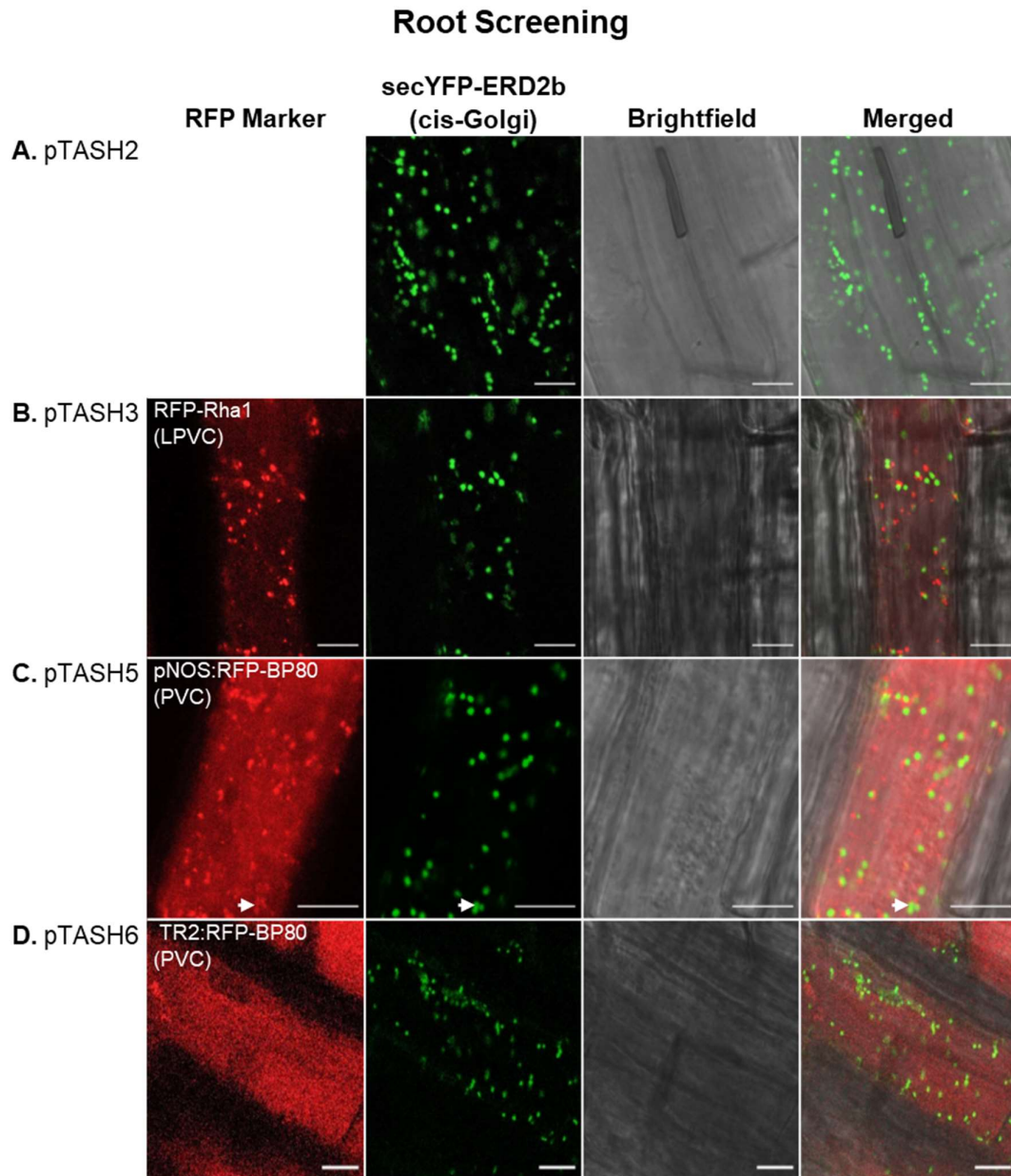


Figure 3. 20. Confocal images of the roots of selected T₂ transgenic lines. A. pTASH2 expresses the cis-Golgi marker secYFP-ERD2b alone. All other constructs express secYFP-ERD2b with an additional organelle marker fused to RFP. **B.** pTASH3 co-expressing the LPVC marker RFP-Rha1. RFP-Rha1 labelled punctate structures, with vacuole localisation also observed. **C and D.** pTASH5 and pTASH6 co-express the PVC marker RFP-BP80 under the control of different promoters. With pTASH5, expressing pNOS:RFP-BP80, more punctae are labelled, some of which are closely associated with secYFP-ERD2b (white arrow). pTASH6, expressing TR2:RFP-BP80, shows stronger leakage to the vacuoles, with less punctae visible. Scale bars represent 10 μ m.

Root Screening Continued

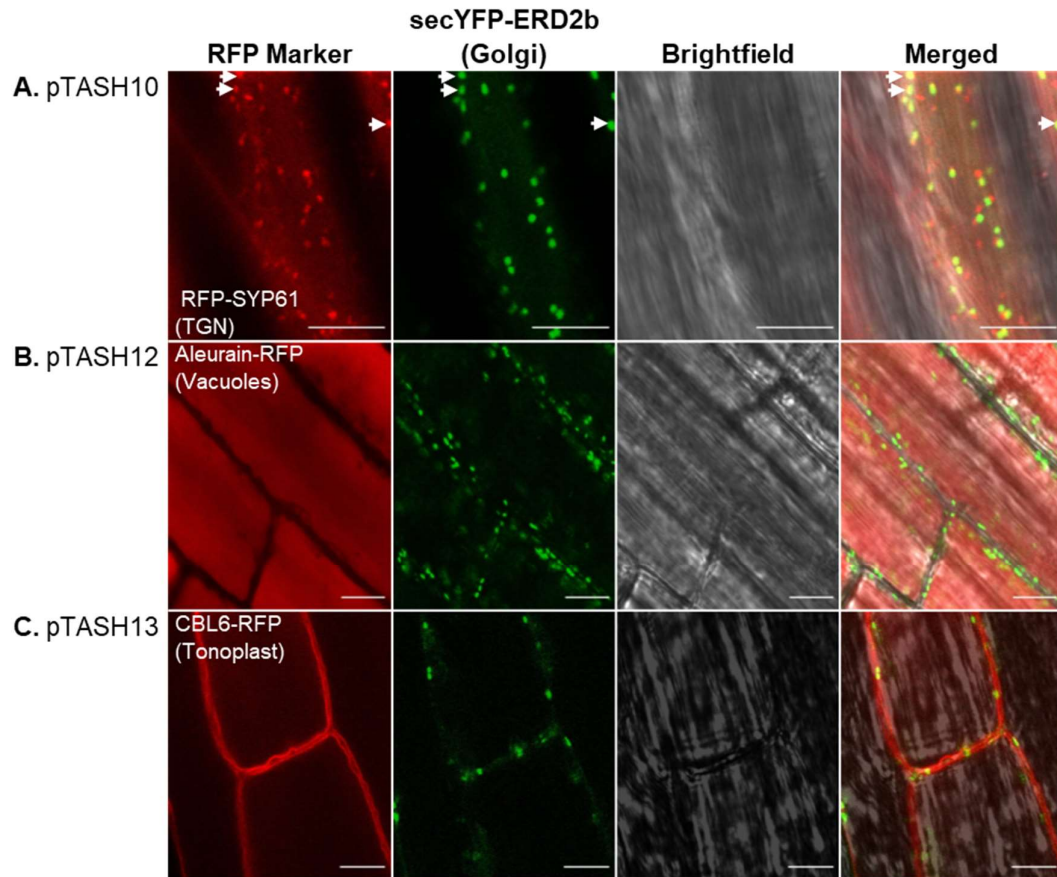


Figure 3. 21. Continued confocal images of root cells of the best expressing T₂ transgenic lines. **A.** pTASH10 expresses RFP-SYP61, which localises to the TGN, with additional plasma membrane localisation observed. Some RFP-SYP61 punctae are closely associated with secYFP-ERD2b punctae (white arrows). **B.** pTASH12 expresses Aleurain-RFP, which localises to the vacuoles, with no additional punctae shown. **C.** pTASH13 expresses CBL6-RFP, which localises to the tonoplast. Scale bars represent 10 μ m.

Cotyledon Screening

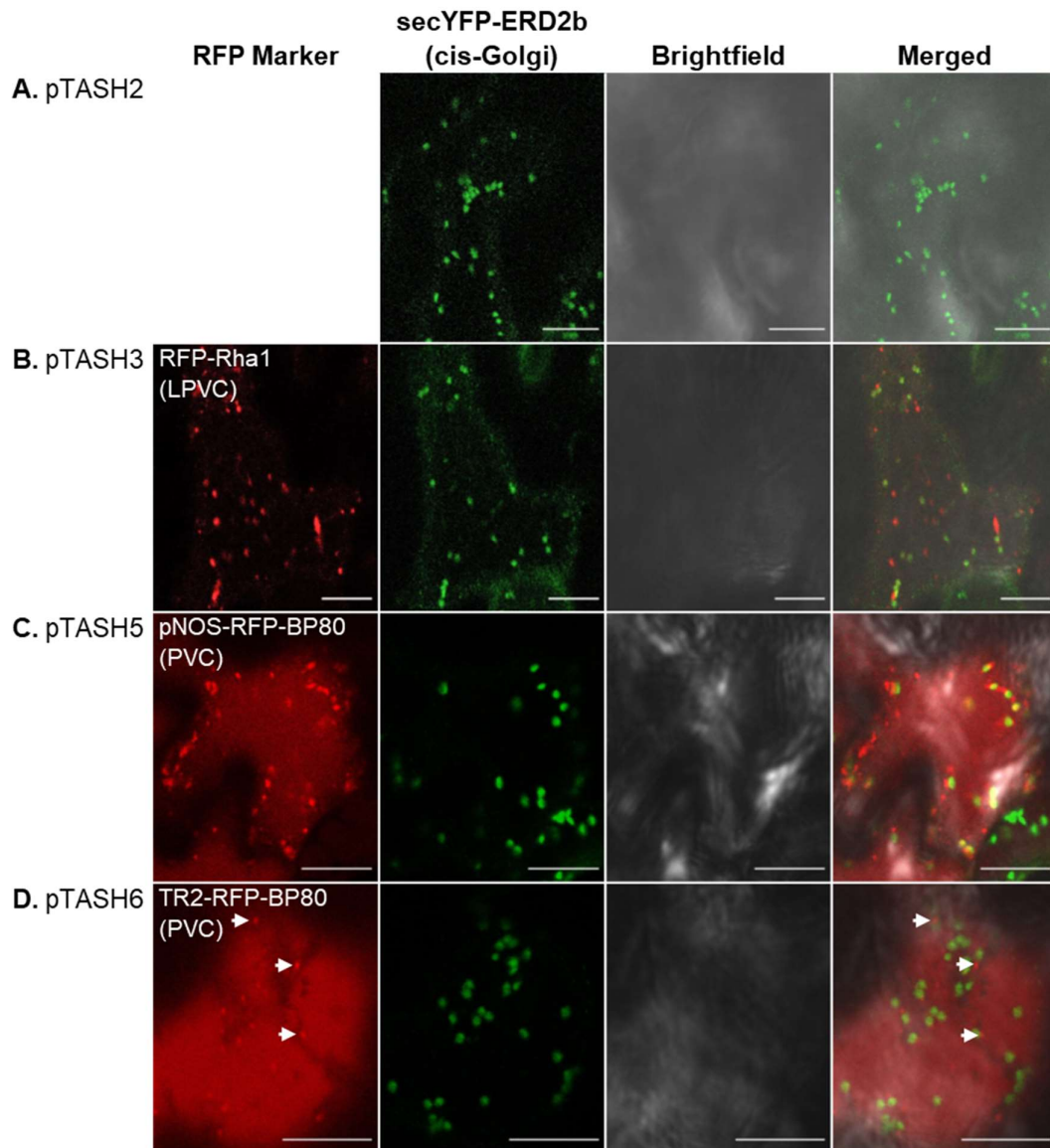


Figure 3. 22. Confocal images of the cotyledons of selected T₂ transgenic Arabidopsis lines. A. pTASH2 expresses punctae within the cytoplasm, as is characteristic of this marker. **B.** pTASH3 expresses the LPVC marker RFP-Rha1 as punctae, with no vacuole or tonoplast localisation observed. **C.** Within pTASH5, pNOS:RFP-BP80 is expressed as punctae, with strong vacuole leakage also observed. **D.** For pTASH6, TR2:RFP-BP80 shows strong vacuole localisation, with few punctae observed. Although, some punctae are labelled with a white arrow. Scale bars represent 10 μ m.

Coytledon Screening Continued

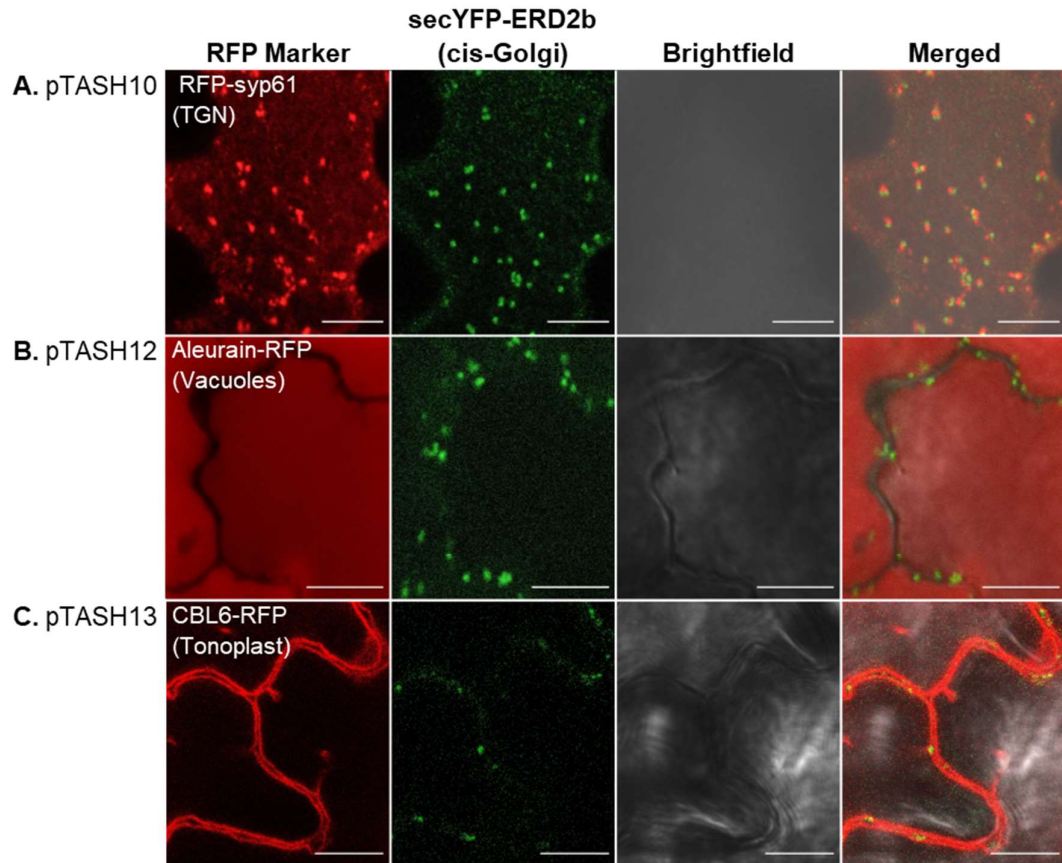


Figure 3. 23. Continued confocal images of the cotyledons of selected T₂ transgenic lines. A. pTASH10 expresses RFP-SYP61, with punctae which do not co-localise with secYFP-ERD2b. Partial plasma membrane localisation is also observed. **B.** pTASH12 expresses Aleurain-RFP, localising to the vacuoles. No punctae are observed. **C.** pTASH13 expresses CBL6-RFP, which localises to the tonoplast. The labelled tonoplast membrane is convoluted, with transvacuolar strands shown. Scale bars represent 10 μ m.

The cis-Golgi marker, secYFP-ERD2b, showed consistent subcellular localisation between the stable and transient expression systems. As shown in pTASH2, which expresses this marker alone, bright punctae were dispersed throughout the cytoplasm, as is characteristic of the Golgi (**Figures 3.20 and 3.22**). This was consistent for all of the dual fluorescence constructs developed. However, differences in the localisation of other markers were observed between the expression systems. This includes pTASH3, which expresses the LPVC marker RFP-Rha1. For this marker, weak vacuole localisation was observed within the roots of T₂ lines (**Figures 3.8 and 3.20**), but not the cotyledon tissue (**Figure 3.22**). Also, a unique feature of RFP-Rha1 expression within infiltrated tobacco leaf epidermal cells was the strong tonoplast localisation, rather than vacuole localisation (**Figure 3.8**).

pTASH5, expressing the PVC marker pNOS:RFP-BP80, showed different localisations in the stable and transient expression systems. For example, pNOS:RFP-BP80 partially localised to the vacuoles in Arabidopsis tissue, yet in tobacco leaf epidermal cells, also partially localised to the tonoplast (**Figures 3.10, 3.20 and 3.22**). Differences were also observed between the two types of Arabidopsis tissues. Within the roots of T₂ lines, close association of secYFP-ERD2b and pNOS:RFP-BP80 punctae were observed (**Figures 3.10 and 3.20**). However, this wasn't observed in cotyledon cells, which showed weaker expression of RFP-BP80 punctae (**Figure 3.22**).

Differences were also observed for the other RFP-BP80 construct, pTASH6, that expresses this marker under the control of the stronger TR2 promoter. pTASH6 showed stronger leakage to the vacuoles and had less PVC punctae within screened Arabidopsis tissue, compared to pNOS:RFP-BP80 (**Figures 3.20 and 3.22**). This supports that the higher expression of RFP-BP80 results in stronger leakage to the vacuoles. However, tobacco leaf infiltrations of pTASH5 and pTASH6 showed conflicting results, with hardly any vacuole localisation observed for TR2:RFP-BP80 (**Figure 3.11**).

Within pTASH10 T₂ lines co-expressing the TGN marker RFP-SYP61, expression was comparable between the different expression systems, showing partial plasma membrane localisation, plus punctae which closely associated with secYFP-ERD2b (**Figures 3.14, 3.21 and 3.23**). However, differential expression of the pTASH12 construct was observed, which expresses the vacuole marker Aleu-RFP. Within T₂ lines expressing this construct, the large central vacuole was labelled within root and cotyledon cells, with no Aleu-RFP punctae observed (**Figures 3.21 and 3.23**). This was in contrast to infiltrated tobacco leaf cells, which expressed Aleu-RFP punctae that localised to an unidentified subcellular compartment (**Figure 3.17**). Differential marker localisation was also observed for pTASH13, that expresses the tonoplast marker CBL6-RFP. In T₂ lines, the tonoplast was labelled, with no CBL6-RFP punctae observed

(**Figures 3.21 and 3.23**). This contrasted the transient expression of pTASH13 in tobacco leaf epidermal cells, showing CBL6-RFP punctae that did not co-localise with secYFP-ERD2b (**Figure 3.18**).

Perhaps the most notable difference in marker localisation between the expression systems was for pTASH8, which expresses the ER marker secRFP-p24aTM. Within the roots of pTASH8 T₂ lines, partial localisation of secRFP-p24aTM to the vacuoles was observed (**Figure 3.24**). However, this was not observed in the cotyledon cells of the same T₂ lines, or within tobacco leaf epidermal cells infiltrated with this construct (**Figure 3.13**). Additionally, within both the roots and cotyledon cells of pTASH8 T₂ lines, spindle-shaped ER bodies were labelled, which are a common feature of Arabidopsis epidermal cells (**Figure 3.24**).

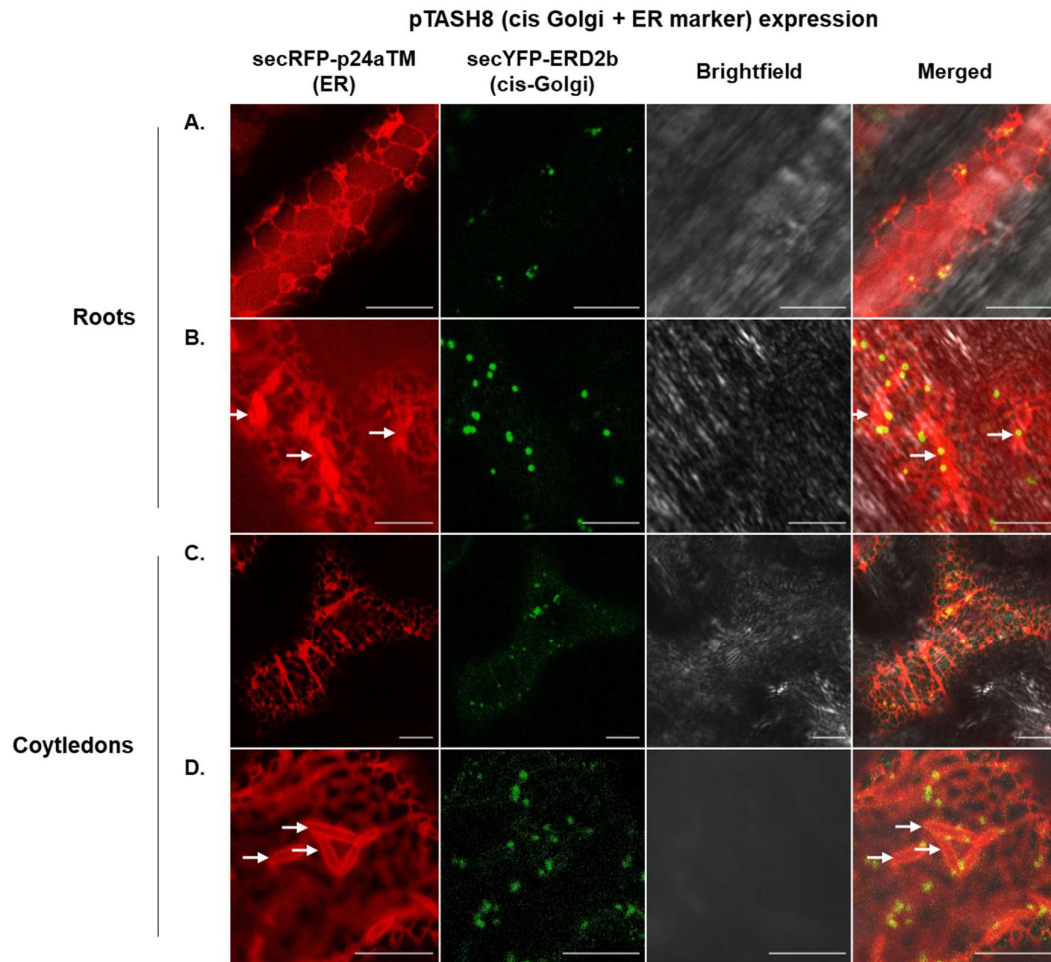


Figure 3. 24. Confocal images of the roots and cotyledons of selected T₂ generation transgenic lines expressing pTASH8. This construct expresses the cis-Golgi marker secYFP-ERD2b with the ER marker secRFP-p24aTM. **A.** A root cell expressing pTASH8, showing secRFP-p24aTM localisation within the ER network, with localisation in the vacuoles also observed. **B.** A magnified image of a root cell expressing pTASH8, showing spindle-shaped ER bodies (white arrows) that is typical within plants belonging to the *Brassicales* order. **C.** A cotyledon cell showing the localisation of secRFP-p24aTM within the ER only. **D.** A magnified view of secRFP-p24aTM expression within a cotyledon cell, showing the labelling of ER bodies (white arrows). Scale bars represent 10 μ m.

3.4 Discussion

3.4.1 Construct Design

This set of double fluorescent reporter constructs were developed to provide a novel and customisable resource to monitor the plant secretory pathway. The use of the cis-Golgi marker secYFP-ERD2b was an effective common marker across all constructs, apart from the construct co-expressing the ER marker RFP-HDEL. For strong and constitutive marker expression, most marker genes were expressed under the 35S promoter. However, some marker genes were expressed under weaker promoters, to avoid the toxic effects of overexpression and to reduce leakage to other subcellular compartments. For example, with the PVC marker BP80, RFP fusions under the control of three constitutive different promoters were developed, including 35S, TR2 and pNOS. BP80 expressed under the control of the 35S promoter produced toxic effects on Arabidopsis plants, with higher levels of BP80 expression also producing different subcellular localisations (**see section 3.4.2.3**). This supports that high levels of RFP-BP80 expression is toxic, causing strong inhibition of BP80-mediated vacuolar sorting through competition with wildtype BP80 (da Silva et al, 2005). The weak pNOS promoter was used for RFP-Rha1 expression to avoid defects in PVC maturation (Bottanelli et al, 2012). As no lethal effects of RFP-Rha1 stable expression were observed, with no defects in marker localisation, pNOS was a suitable promoter for RFP-Rha1.

3.4.2 *Agrobacterium*-mediated tobacco leaf infiltrations and transgenic Arabidopsis lines

Agrobacterium-mediated tobacco leaf infiltrations were conducted to rapidly observe the subcellular localisation and the marker expression levels prior to the stable transformation of Arabidopsis. Constructs transiently expressed in tobacco leaf epidermal cells generally showed higher levels of expression than when stably expressed in Arabidopsis T₂ root and cotyledon cells. This is supported by artefacts of overexpression observed within infiltrated tobacco cells, which were not observed in root or cotyledon cells of Arabidopsis lines. This includes the partial tonoplast localisation of RFP-Rha1 and RFP-BP80, and the punctate structures that were labelled by the vacuole marker Aleu-RFP and the tonoplast marker CBL6-RFP. Artefacts of overexpression have previously been shown for the markers secYFP-ERD2b, RFP-BP80 and RFP-Rha1 (Silva-Alvim et al, 2018; Foresti et al, 2010; Bottanelli et al, 2012). This suggests that these markers are inducing stress on the secretory pathway, by saturating trafficking machinery to interfere with the function of the endogenous versions of the Arabidopsis genes. Moreover, with the simultaneous expression of two fluorescent secretory pathway

markers, the stress induced on the secretory pathway could be expected to be greater than when expressing the markers alone. However, within the transgenic *Arabidopsis* lines, all markers — with the exception of the ER marker secRFP-p24aTM — localised to their intended subcellular compartment. This suggested that the co-expression of the markers did not cause major changes to the plant secretory pathway. However, to confirm this, phenotypic characterisation of the transgenic lines should be conducted, as phenotypic changes including altered plant growth and development would be expected with disruption to the secretory pathway (Bassham et al, 2008). This further phenotypic characterisation is required to help validate the use of these marker lines to study the secretory pathway during infection with cyst nematodes in **Chapter 4**.

The method of transformation that was used to develop the *Arabidopsis* lines could also cause disruption to marker localisation. The floral dip method results in random T-DNA insertion into the *Arabidopsis* genome, with the inability to control the number of transgene copies and the site of insertion. Consequently, transgenes are often inserted into or near functional gene sequences (Dinh et al, 2014). This could result in unwanted genetic mutations that could affect cellular processes including the secretory pathway, which would reduce the validity of the use of these *Arabidopsis* lines in future research. Therefore, future work could be conducted to sequence the selected *Arabidopsis* lines, to verify that the sites of T-DNA insertions aren't causing mutations to functional genes. Future work could also include the use of methods for targeted DNA insertion to develop fluorescent *Arabidopsis* lines (Dong and Ronald, 2021).

3.4.2.1 pTASH2, expressing only the cis-Golgi marker secYFP-ERD2b

Confocal laser scanning microscopy (CLSM) supports that secYFP-ERD2b localises to the Golgi, with punctae observed throughout the cytoplasm (Silva-Alvim et al, 2018). This confirms that the fusion of secYFP to the N-terminus of ERD2b does not localise to the ER, in contrast to C-terminal fluorescent protein ERD2b fusions (Silva-Alvim et al, 2018). Also, importantly, the localisation of secYFP-ERD2b was consistent when co-expressed with all RFP-marker fusions developed, supporting its use as common marker in this set of constructs.

3.4.2.2 pTASH3, co-expressing the LPVC marker RFP-Rha1

When pTASH3 was transiently and stably expressed, RFP-Rha1 punctae did not co-localise with secYFP-ERD2b, supporting LPVC localisation (Foresti et al, 2010). This also supports that even under high levels of expression, Rha1 does not partially localise to the Golgi (Bottanelli et al, 2012). However, differences in expression across the *Arabidopsis* tissues was observed, with leakage to the vacuoles in root cells of T₂ lines, yet not cotyledon cells. Cotyledon expression appeared to be lower than root expression,

which could result in less leakage of RFP-Rha1 to the vacuoles, below the RFP detection threshold.

Contrastingly, strong labelling of the tonoplast was observed in tobacco leaf epidermal cells infiltrated with pTASH3. Tonoplast localisation hasn't previously been documented for fluorescent Rha1 fusions (Bottanelli et al, 2012; Foresti et al, 2010). However, this could reflect a saturation of Rha1 recycling machinery, with Rha1 present in LPVCs which fuse with the tonoplast (Lee et al, 2004). This is likely an artefact of RFP-Rha1 overexpression, as this was not observed within the roots or cotyledons of T_2 Arabidopsis lines showing lower levels of expression. However, previous FP-Rha1 fusions such as Venus-Rha1, are expressed under the control of the stronger TR2 promoter, which show no tonoplast localisation when infiltrated into tobacco leaf epidermal cells (Bottanelli et al, 2012; Foresti et al, 2010).

3.4.2.3 pTASH4, 5 and 6, co-expressing the PVC marker RFP-BP80

pTASH 4, 5 and 6, expressing RFP-BP80 under the control of different strength promoters, all support the predominant localisation of RFP-BP80 to the PVCs when expressed transiently (Foresti et al, 2010). Of the three promoters, 35S provided the strongest expression, followed by pNOS, with TR2 showing the weakest expression. This was evidenced by leakage to the vacuoles observed for infiltrations with the 35S and pNOS constructs, compared to TR2, which showed little to no vacuole localisation. This could reflect saturation of the receptors which mediate BP80 recycling under higher levels of expression (da Silva et al, 2005). However, the weakest expression of BP80 observed for the TR2 promoter was unexpected, as pNOS is generally considered to be the weakest promoter of the three (Angenon et al, 1989).

Partial tonoplast localisation was also observed in infiltrations using the 35S and pNOS promoters. Although no tonoplast localisation has previously been shown for fluorescent BP80 fusions (da Silva et al, 2006; Paris et al, 1997), this may result from the presence of BP80 within LPVCs which fuse with the tonoplast, due to saturation of BP80 recycling machinery. This was not observed for infiltrations with the lower expression provided by TR2, suggesting that partial tonoplast localisation of RFP-BP80 is an artefact of overexpression. A commonality between infiltrated tobacco cells for all three RFP-BP80 constructs was the close association of punctae with secYFP-ERD2b. Although co-localisation of fluorescent BP80 fusions with a Golgi marker has not been observed in transfected protoplasts (da Silva et al, 2005), BP80 has been detected in the Golgi using immunogold electron microscopy (Paris et al, 1997). This supports the cycling of BP80 from the Golgi to the PVCs (da Silva et al, 2006).

The reported toxic effects of RFP-BP80 overexpression (da Silva et al, 2005) were confirmed in this work as it was not possible to generate transgenic Arabidopsis lines expressing 35S:RFP-BP80. However, transgenic lines expressing RFP-BP80 under the weaker promoters, pNOS and TR2, were able to grow. In contrast to the infiltrations, no tonoplast localisation was observed for pNOS-directed expression of RFP-BP80 in Arabidopsis root or cotyledons. This supports the hypothesis that the partial tonoplast localisation in infiltrated leaves was an artefact of overexpression. Also contrary to the infiltrations, TR2:RFP-BP80 Arabidopsis lines showed stronger vacuole leakage in root and cotyledon cells than those expressing pNOS:RFP-BP80. This is consistent with previous observations that the TR2 promoter is stronger than the pNOS promoter. Also importantly, hardly any RFP-BP80 punctae were imaged for TR2:RFP-BP80 Arabidopsis lines. This indicates that the stable expression of RFP-BP80 induced by the TR2 promoter is too high, resulting in almost complete leakage to the vacuoles. The pNOS promoter still induced high leakage of RFP-BP80 to the vacuoles, but there was also abundant punctae in the cytoplasm of the cells, supporting that these lines can still be used as a PVC marker.

3.4.2.4 pTASH7 and pTASH8, co-expressing ER markers

For pTASH7, which co-expresses the ER marker RFP-HDEL, co-localisation with secYFP-ERD2b at the Golgi was observed. This is despite FP-HDEL proteins, when expressed alone, localising to the ER (Pain et al, 2019). The co-localisation at the Golgi may be due to secYFP-ERD2 competing with endogenous ERD2. When transiently expressed in *N. benthamiana* protoplasts, secYFP-ERD2 is a non-functional form of ERD2, unable to recycle HDEL ligands back to the ER (Silva-Alvim et al, 2018). Therefore, secYFP-ERD2b prevent the recycling of HDEL ligands, resulting in the Golgi localisation of RFP-HDEL. As RFP-HDEL expressed in pTASH7 didn't localise to its predicted compartment, Arabidopsis lines expressing this construct were not developed. Dual fluorescent constructs expressing HDEL could still be developed in the future, with the use of an alternative Golgi marker that doesn't disrupt the function of ERD2-mediated recycling. For example, GFP-HDEL maintains ER localisation when co-expressed with the trans-Golgi marker ST-mRFP (Osterrieder et al, 2017).

The other ER marker used, secRFP-p24aTM, localised to the ER network as expected within tobacco leaf infiltrations (Langhans et al, 2008). No co-localisation with secYFP-ERD2b was observed, despite the hypothesis that p24 proteins traffic between the ER and Golgi within COPI and COPII vesicles (Langhans et al, 2008). However, secRFP-p24aTM also localised to the vacuoles within Arabidopsis T₂ lines. This may be an artefact of overexpression specific to root cells. As p24 cycles between the ER and Golgi (Montesinos et al, 2012), saturation of the COPI-mediated recycling to the ER may

result in the transport of this protein to the vacuoles for degradation. In both the roots and cotyledons of the screened Arabidopsis lines, secRFP-p24aTM localised to spindle-shaped ER bodies. These are common within Arabidopsis and other plants of the *Brassicales* order. ER bodies contain abundant β -glucosidases, therefore are suggested to have a role in pathogen attack and herbivory (Nakano et al, 2014).

3.4.2.5 pTASH10, co-expressing the TGN marker RFP-SYP61

For pTASH10 expressing the TGN marker RFP-SYP61, punctae and partial plasma membrane localisation was observed in both transient and stable expression systems. Partial plasma membrane localisation has previously been shown under high levels of RFP-SYP61 expression within infiltrated tobacco leaves (de Marcos Lousa et al, 2016). SYP61 is a vesicle-associated Q-SNARE, hypothesised to cycle between the TGN and plasma membrane (Drakakaki et al, 2012). This supports the partial plasma membrane localisation of RFP-SYP61 and enables the use of this construct also as a plasma membrane marker.

Additionally, some RFP-SYP61 punctae were closely associated with secYFP-ERD2b within tobacco leaves infiltrated with pTASH10. This likely reflects the close proximity of the TGN and Golgi compartments, rather than partial localisation of RFP-SYP61 to the Golgi. Previously, YFP-SYP61 was not shown to co-localise with RFP-TM-ERD2, yet partial overlap between the two fluorescence signals has been observed due to transient close encounters between the two subcellular compartments (Silva-Alvim et al, 2018).

3.4.2.6 pTASH9 and 11, co-expressing the two BP80 mutants, RFP-BP80(Tyr) and RFP-BP80(Leu)

The two RFP-BP80 mutants, RFP-BP80(Tyr) and RFP-BP80(Leu) localise to the expected subcellular compartments when infiltrated into tobacco leaves. For example, RFP-BP80(Tyr) localised to the TGN, with leakage to the plasma membrane. RFP-BP80(Tyr) punctae did not co-localise with secYFP-ERD2b, consistent with previous observations that GFP-BP80(Tyr) does not co-localise with the Golgi marker ST-RFP in tobacco leaf infiltrations (Foresti et al, 2010). Weak vacuole localisation of RFP-BP80(Tyr) was also observed, which could be due to the cleavage and subsequent vacuolar processing of RFP (da Silva et al, 2006). Weaker vacuole localisation was observed within the RFP-BP80(Tyr), compared to the pTASH constructs (pTASH4, 5 and 6) expressing RFP-BP80. This is supported by less GFP-core fragment detected in the vacuoles of tobacco leaf protoplasts expressing GFP-BP80(Tyr) compared to GFP-BP80 (daSilva et al, 2005). The weaker vacuole localisation of RFP-BP80(Tyr) compared to RFP-BP80 could reflect impaired trafficking from the Golgi to the PVC.

The other BP80 mutant used, RFP-BP80(Leu), accumulated in punctae which did not co-localise with secYFP-ERD2b, supporting LPVC localisation. Leakage of RFP-BP80(Leu) to the vacuoles was also observed, as previously has been shown (Foresti et al, 2010). This could reflect the more efficient transport of RFP-BP80(Leu) from the Golgi to the PVC, or defective recycling. Increased vacuole leakage is expected for RFP-BP80(Leu) compared to RFP-BP80(Tyr) and RFP-BP80 (da Silva et al, 2006). However, this was not visible within infiltrated cells, which could be due to the lack of sensitivity of confocal microscopy. Moreover, tonoplast localisation of RFP-BP80(Leu) when expressed from pTASH11 was observed, which hasn't previously been documented. This could be due to the presence of RFP-BP80(Leu) in LPVCs which fuse with the tonoplast. Some RFP-BP80(Leu) punctae overlap with secYFP-ERD2b punctae, although previous co-localisation of GFP-BP80(Leu) with the Golgi marker ST-RFP has not been shown (Foresti et al, 2010). This could reflect the transit of RFP-BP80(Leu) through the Golgi, or the close proximity of the labelled Golgi and LPVCs.

No transgenic lines Arabidopsis lines could be generated for either of the BP80 mutant constructs. This may be due to the toxicity of RFP-BP80(Tyr) and RFP-BP80(Leu). This contrasts with both mutants displaying reduced competition for wildtype BP80, therefore the toxicity of these mutants was expected to be reduced (Foresti et al, 2010). However, the defects of RFP-BP80(Tyr) on vacuolar sorting and the defects of RFP-BP80(Leu) on receptor recycling between the Golgi and PVCs, could be causing of the lethal effect of transgene expression. To overcome this, constructs expressing these markers under the control of weaker promoters, such as pNOS and TR2, could be developed.

3.4.2.7 pTASH12, co-expressing the vacuole marker Aleu-RFP

pTASH12 co-expresses Aleu-RFP, which labelled the large central vacuole of infiltrated tobacco leaf epidermal cells, as expected from previous observations (Flückiger et al, 2003). However, punctae were also observed, which did not co-localise with secYFP-ERD2b. These may represent the LPVCs, which has previously been observed under high levels of Aleu-RFP overexpression (Foresti et al, 2010). Aleu-RFP punctae were not observed in the transgenic Arabidopsis lines, which show lower levels of expression, to support that LPVC localisation is an artefact of overexpression. Aleurain is a thiol protease, suggested to be trafficked to the lytic vacuoles via the PVCs. This is evidenced by the localisation of Aleu-GFP to the PVCs under the treatment of tobacco BY-2 cells with wortmannin (Miao et al, 2008). Therefore, it is plausible for Aleu-RFP to transiently localise to the LPVCs.

3.4.2.8 pTASH13, co-expressing the tonoplast marker CBL6-RFP

CBL6-RFP, expressed within pTASH13, localised to the tonoplast as previously characterised (Bottanelli et al, 2012). However, CBL6-RFP punctae were also observed within pTASH13 tobacco leaf infiltrations. Some punctae co-localised with secYFP-ERD2b, and some localised to separate subcellular compartments. This localisation may reflect the trafficking of CBL6-RFP through the Golgi and post-Golgi organelles to the tonoplast. However, CBL6 was previously suggested to reach the vacuole via a COPII-independent pathway, being insensitive to sec12 overexpression (Bottanelli et al, 2011), which inhibits COPII transport (Hanton et al, 2007). CBL6 is also suggested to bypass the Golgi and post-Golgi compartments, its localisation insensitive to the Rab mutants Rha1, ara6, and Rab7 (Bottanelli et al, 2011). Instead, CBL6 is suggested to be synthesised in the cytosol, then targeted to the vacuoles via an N-terminal tonoplast targeting signal (Zhang et al, 2017a). Therefore, CBL6-RFP punctae which occur under high levels of expression localise to an unidentified compartment, which may not be the post-Golgi organelles. CBL6-RFP punctae were not observed in pTASH13 Arabidopsis lines which have lower levels of expression than the infiltrated tobacco leaves. Thus, expressing CBL6-RFP under the control of a weaker promoter, such as TR2 or pNOS, within transient expression assays could prevent the occurrence of punctae within transient expression systems.

Table 3. 3. A summary of the localisation of each marker gene across the transient and stable expression systems. The predicted localisation for each marker is given, in addition to the observed localisation within infiltrated tobacco leaves compared to the cotyledon and root tissue of stable Arabidopsis T₂ lines.

| Gene | Predicted localisation | Tobacco leaves | Arabidopsis coytedons | Arabidopsis roots |
|---------------|-------------------------------|-----------------------------|------------------------------|--------------------------|
| secYFP-ERD2b | Golgi | Golgi | Golgi | Golgi |
| secRFP-p24aTM | ER | ER | ER | ER and vacuoles |
| RFP-SYP61 | TGN | TGN and PM | TGN and PM | TGN and PM |
| pNOS:RFP-BP80 | PVC | PVC, vacuole and tonoplast | PVC and vacuole | PVC and vacuole |
| TR2:RFP-BP80 | PVC | PVC | Vacuole | Vacuole |
| RFP-Rha1 | LPVC | LPVC, vacuole and tonoplast | LPVC | LPVC and vacuole |
| Aleu-RFP | Vacuole | Vacuole and punctae | Vacuole | Vacuole |
| CBL6-RFP | Tonoplast | Tonoplast and punctae | Tonoplast | Tonoplast |

3.4.3 Conclusions

In conclusion, the set of dual fluorescence constructs and Arabidopsis lines has successfully been developed. The subcellular localisations of each marker across the expression systems and tissue types are listed in **Table 3.3**.

The development of dual fluorescence secretory pathway markers, across transient and stable expression systems has shown:

- Consistent marker expression of the Golgi marker secYFP-ERD2b and the TGN marker RFP-SYP61 across the expression systems and tissue types
- Altered localisation of the ER marker RFP-HDEL when co-expressed with the Golgi marker secYFP-ERD2b
- Variable localisation of the ER marker secRFP-p24aTM between different Arabidopsis tissues
- Variable marker localisation of the PVC marker RFP-BP80, the LPVC marker RFP-Rha1, the vacuole marker Aleu-RFP and the tonoplast marker CBL6-RFP when transiently or stably expressed
- Possible lethal effects of the PVC marker 35S:RFP-BP80, in addition to the two RFP-BP80 mutants, RFP-BP80(Tyr) and RFP-BP80(Leu) in Arabidopsis

In summary:

- The dual fluorescence Arabidopsis lines developed, when used as a set, monitor all major compartments of the secretory pathway, including the ER, Golgi, TGN, PVCs, LPVCs, vacuoles, tonoplast and plasma membrane
- However, the discrepancies between marker localisation in transient and stable expression systems, and the different types of plant tissues, highlights the need for the characterisation of the plant secretory pathway within more varied experimental systems
- A summary of the most suitable dual fluorescence constructs to be used to study the secretory pathway in Arabidopsis roots is given in **Table 3.4**

Table 3. 4. A summary of the stable transgenic lines that were selected for use in Chapter 4.

| Construct | RFP marker | Localisation | Additional RFP-marker localisation in Arabidopsis roots |
|------------------|-------------------|-----------------------|--|
| pTASH2 | - | cis-Golgi | - |
| pTASH3 | RFP-Rha1 | cis-Golgi + LPVC | Vacuoles |
| pTASH5 | pNOS:RFP-BP80 | cis-Golgi + PVC | Vacuoles |
| pTASH8 | secRFP-p24aTM | cis-Golgi + ER | Vacuoles |
| pTASH10 | RFP-SYP61 | cis-Golgi + TGN | Plasma membrane |
| pTASH12 | Aleu-RFP | cis-Golgi + vacuole | - |
| pTASH13 | CBL6-RFP | cis-Golgi + tonoplast | - |

Chapter 4 Imaging syncytia within fluorescent Arabidopsis marker lines

4.1 Introduction

Large changes to the plant secretory pathway are described during cyst nematode infection, including the proliferation of the ER and Golgi, fusion of the PVCs with the plasma membrane and the fragmentation of the large central vacuole (Sobczak et al, 1997). So far, this knowledge has largely been provided by 2D electron microscopy (EM) techniques, such as transmission EM (Grundler et al, 1998; Kim et al, 2010; Sobczak et al, 1997) and scanning EM (Jones and Dropkin, 1975). Although more advanced EM techniques could provide 3D images of syncytia, such as serial block-face (SBF) and focused ion beam (FIB) milling scanning EM, these require fixed and inanimate cell samples, which limits the information that could be provided on subcellular trafficking (van Weering et al, 2010). Additionally, these techniques are expensive and labour intensive (Reigoto et al, 2021; de Jonge and Peckys, 2016).

Therefore, alternative techniques focused on live-cell imaging, such as fluorescence microscopy, may be better suited to characterise the plant secretory pathway within syncytia. Despite this, there has been limited use of fluorescence microscopy to study these feeding sites. Thus far, examples in syncytia include the imaging of fluorescent proteins fused to markers for sugar transport (Juergensen et al, 2003), the actin cytoskeleton (de Almeida Engler et al, 2004) and cytokinin signalling pathway (Siddique et al, 2015). Therefore, the use of fluorescent organelle markers within syncytia is a relatively unused technique which could provide novel insight into the cell biology of host-cyst nematode interactions.

Here, fluorescent organelle markers are used to further characterise the plant secretory pathway within syncytia. The set of dual fluorescence Arabidopsis lines developed in **Chapter 3** were infected with the beet cyst nematode *Heterodera schachtii* to provide a model plant-cyst nematode interaction (Sijmons et al, 1991). The Arabidopsis marker lines infected with *H. schachtii* collectively label key compartments of the plant secretory pathway. For example, syncytia were imaged in transgenic roots co-expressing the cis-Golgi marker secYFP-ERD2b with either a ER, TGN, PVC, LPVC, vacuole or tonoplast marker fused to RFP. Syncytia were also examined within a GFP-HDEL Arabidopsis marker line due to the partial vacuole localisation of secRFP-p24aTM observed within the roots.

Syncytia induced by J3 and J4 stage female *H. schachtii* were imaged. At these life stages, previously characterised changes to the secretory pathway during syncytial

formation are predicted to have already occurred. This includes the replacement of the large central vacuole, formation of PVCs and proliferation of the ER, which have been documented within the first 48 hours of syncytial formation (Golinowski et al, 1996). The imaging of syncytia within *Arabidopsis* marker lines could validate previous descriptions of organelle ultrastructure within syncytia, such as ER proliferation and vacuole fragmentation (Golinowski et al, 1996). Imaging the expression of these constructs within syncytia could also provide further information on post-Golgi trafficking, such as secretion via the TGN and unconventional secretion via the PVCs. Additionally, novel information could be provided on vacuolar sorting, including PVC maturation and LPVC fusion with the tonoplast.

To complement the confocal microscopy of syncytia in fluorescent *Arabidopsis* marker lines, a bioinformatics approach was taken to understand the dynamics of plant secretory pathway gene expression during syncytial development. This used previously published gene expression data from *Arabidopsis* syncytia induced by *H. schachtii* (Siddique et al, 2021). Genes selected for analysis were obtained from a previously published list of plant secretory pathway genes (Rojo and Denecke, 2008). This was hypothesised to provide novel information on the secretory pathway, including mechanisms of ER-Golgi trafficking, vacuolar sorting and secretion.

In addition to this set of genes, those involved in ER stress were selected for analysis, to support previous EM observations of swollen and proliferated ER in syncytia (Kim et al, 2012). For the Golgi, COG complex genes were chosen, due to evidence that this complex is involved in soybean resistance to *H. glycines* (Klink et al, 2021). Genes relating to vacuole function were also selected, including vacuolar processing enzymes, due to evidence that *H. schachtii* may suppress vacuole-mediated cell death in *Arabidopsis* (Pogorelko et al, 2019). Also, tonoplast intrinsic proteins were selected, as these have previously been shown to be downregulated in *Arabidopsis* syncytia to support cyst nematode parasitism (Baranowski et al, 2019). In addition to these genes, the marker genes used for fluorescence microscopy, p2455, ERD2, SYP61, Rha1, BP80, aleurain and CBL6 were selected, to support the confocal microscopy observations within syncytia.

4.2 Methods

4.2.1 *Arabidopsis* marker lines infected with *H. schachtii*

To image syncytia, several transgenic T₂*Arabidopsis* lines developed in **Chapter 3** were used. This included pTASH12, co-expressing the vacuole marker Aleu-RFP, pTASH13 co-expressing the tonoplast marker CBL6-RFP, pTASH10 co-expressing the TGN

marker RFP-SYP61, pTASH3, co-expressing the LPVC marker RFP-Rha1, and pTASH5 co-expressing the PVC marker RFP-BP80 under the control of the pNOS promoter. Additionally, an Arabidopsis line expressing the ER marker GFP-HDEL was imaged, which was obtained from the Nottingham Arabidopsis Stock Centre (NASC; Nelson et al, 2007). This was to provide additional information on the ER within syncytia, due to the ER marker secRFP-p24aTM partially localising to the vacuoles of Arabidopsis roots (see **section 3.3.2**).

4.2.2 Confocal microscopy of Arabidopsis syncytia

To prepare samples for confocal microscopy, root sections containing syncytia were cut from the plants, then transferred from the growth media onto a microscope slide containing water. Uninfected Arabidopsis lines of a similar age were imaged as controls. Both uninfected and infected roots were imaged at varying focal planes, including the epidermis, cortex and vascular cylinder. At the syncytium, tile scans at a X 20 magnification were taken. Tile scans were stitched together to provide an overview of the infected root; showing syncytia in addition to the adjacent uninfected root cells. Following this, the tile scans were cropped to provide enlarged images of the centre of the syncytium and the adjacent cells.

For each marker line, multiple syncytia at varying time points between 8 and 18 dpi were imaged. At least five syncytia from different plants were imaged, with no visible difference between those induced across the different timepoints, or those induced by male or female cyst nematodes. Therefore, the images processed into figures are representative of all syncytia imaged.

4.2.3 The analysis of secretory pathway related genes in Arabidopsis syncytia

To analyse gene expression in syncytia, previously published RNA-seq data for Arabidopsis syncytia induced by *H. schachtii* was used (Siddique et al, 2021). This published dataset contained normalised expression values for each gene, with three biological replicates for control and infected roots at each time point: 10 hpi, 48 hpi, 12 dpi female, 12 dpi male and 24 dpi female. In this obtained data set, the differentially expressed (DE) genes were also listed (\log_2 fold change > 0.5 , adjusted p-value ≤ 0.01). To analyse the expression of the plant secretory pathway genes in this chapter, the \log_2 fold change (\log_2 FC) was calculated for each gene, using the published normalised expression values for control and infected samples.

Plant secretory pathway-related genes of interest were chosen from the available gene expression data (Siddique et al, 2021) based on Arabidopsis genes with characterised roles in secretory pathway trafficking (Rojo and Denecke, 2008), and genes that are relevant to secretory pathway-mediated immune responses (**Table 4.1**). This included

key genes involved in the ER stress response, such as heat shock 70 proteins and calreticulins, and genes involved in downstream UPR signalling, including *IRE1a* and *IRE1b*, and the bZIP genes *bZIP17*, *bZIP28* and *bZIP60* (Howell, 2021), and genes involved in trafficking between the ER and Golgi. For the Golgi, genes comprising subunits of the conserved oligomeric Golgi (COG) complex were selected, in addition to genes involved in post-Golgi trafficking to both the plasma membrane and vacuoles. For the vacuoles, vacuolar processing enzymes and tonoplast membrane proteins were chosen. To further the gene expression analysis in this chapter, these genes selected for analysis were manually grouped into clusters based on similar expression profiles. A summary of the names of the plant secretory pathway genes chosen for expression analysis are listed in **Table 4.1**.

Table 4. 1. The names of the plant secretory pathway genes selected for expression analysis, and the reason why they were selected.

| Reason for gene selection | Gene name |
|---|---|
| Listed as a plant secretory pathway gene in Rojo and Denecke (2008) | STL2P, RHD3, SARA1A, SAR1B, SYP31, SEC22, AGD7, MEMB11, BS14A, SYP71, SYP121, SYP132, ADL6, VTI1b, EPS1, VPS35, VPS35, GRV2, VPS9a, MAG1, VPS35, BP80, Ara7, SYP21, SGR4, VCL1, VAM3, VAMP711 |
| Plant secretory pathway genes characterised since Rojo and Denecke (2008) | p2455, ARF1, ERD2, α 1-COP, α 2-COP, γ 1-COP, ERD2b, HAP13, RABA1a, RABA1b, RABA1c, RABA1d, RABA1e, RABA1f, RABA1g, RABA1h, RABA1i, SYP32, SYP61, SYP122, Ara6, EXT-like, Rha1, Aleurain, CBL6 |
| Role in the ER stress response | bZIP60, bZIP17, bZIP28, IRE1a, IRE1b, BIP2, BIP3, HSP70T-2, HPS70, HSP70-4, HSP70-3, HSP70-16, ERD2, HSP70b, CRT1, CRT2, CRT3, EBS1 |
| Role in the Golgi COG complex | COG1, COG2, COG3, COG5, COG6, COG7, COG8 |
| Tonoplast intrinsic proteins | α TIP3;1, δ -TIP2;1, δ -TIP2;2, δ -TIP2;3, γ TIP1;1, ϵ TIP4;1 |
| Role in vacuole mediated immune responses | α -VPE, β -VPE, δ -VPE, γ -VPE |

4.3 Results

4.3.1 Expression analysis of secretory pathway related genes in *Arabidopsis syncytia*

To complement the confocal microscopy of syncytia in fluorescent *Arabidopsis* marker lines, the gene expression of 98 secretory pathway-related genes was analysed using available transcript abundance data (Siddique et al, 2021). Genes selected for analysis were manually separated into clusters based on their expression over the various parasitic life stages measured. From this, five clusters were identified, incorporating 48 out of the 98 genes (**Figure 4.1**). All genes that were significantly differentially expressed between uninfected and infected samples ($\log_2FC > 0.02$, adjusted p-value > 0.05) were present in these clusters, and genes that weren't selected had low levels of expression across the parasitic life stages.

The first cluster in **Figure 4.1** was labelled 'Early Infection'. This included genes that were only upregulated at the early infection time points, 10 hpi and 48 hpi, then were downregulated at all further timepoints, being the most downregulated at the 12 dpi female life stage (**Figure 4.1A**). Contrastingly, the next two clusters described genes that were only upregulated during later stages of infection. However, the 'Late Infection 1' cluster described genes that were most upregulated at the 12 dpi male and female life stages (**Figure 4.1B**), whereas the 'Late Infection 2' cluster described genes that were most upregulated at the 12 dpi female and 24 dpi female life stages (**Figure 4.1C**). The fourth expression cluster included genes that had \log_2FC values peaking at 10 hpi, 12 dpi female and 24 dpi (**Figure 4.1D**), and the fifth expression cluster described genes that were downregulated across all life stages ('Downregulated'; **Figure 4.1E**). Genes in this category were most downregulated at 12 dpi female. To complement **Figure 4.1**, the expression of all genes studied is shown in **Tables 4.2 to 4.7**.

4.3.1.1 ER stress related genes

ER stress response genes were analysed to support previous claims of ER stress in *Arabidopsis syncytia* and to further elucidate the function of the ER in plant-cyst nematode interactions. Nine out of the 18 ER stress response genes were assigned to expression clusters. This includes *bZIP17*, *EBS1*, *IRE1a* and *HSP70T-2*, which were assigned to the two 'Late Infection' clusters (**Figure 4.1B and C**). Although none of these were significantly differentially expressed, all genes were downregulated at 10 hpi and also 48 hpi, then upregulated at all other life stages, with upregulation peaking at 12 dpi female. Other ER stress response genes were assigned to the early infection cluster, including *bZIP60*, *BIP2*, *CRT1*, *CRT2* and *HSP70* (**Figure 4.1A**), all of which apart from *HSP70* were significantly differentially expressed. These five ER stress response genes in the 'Early Infection' cluster were upregulated during early infection and downregulated

at 12 dpi female. Of the ER stress response genes not included in the graphs, most were downregulated at 10 hpi and 48 hpi (**Table 4.2**).

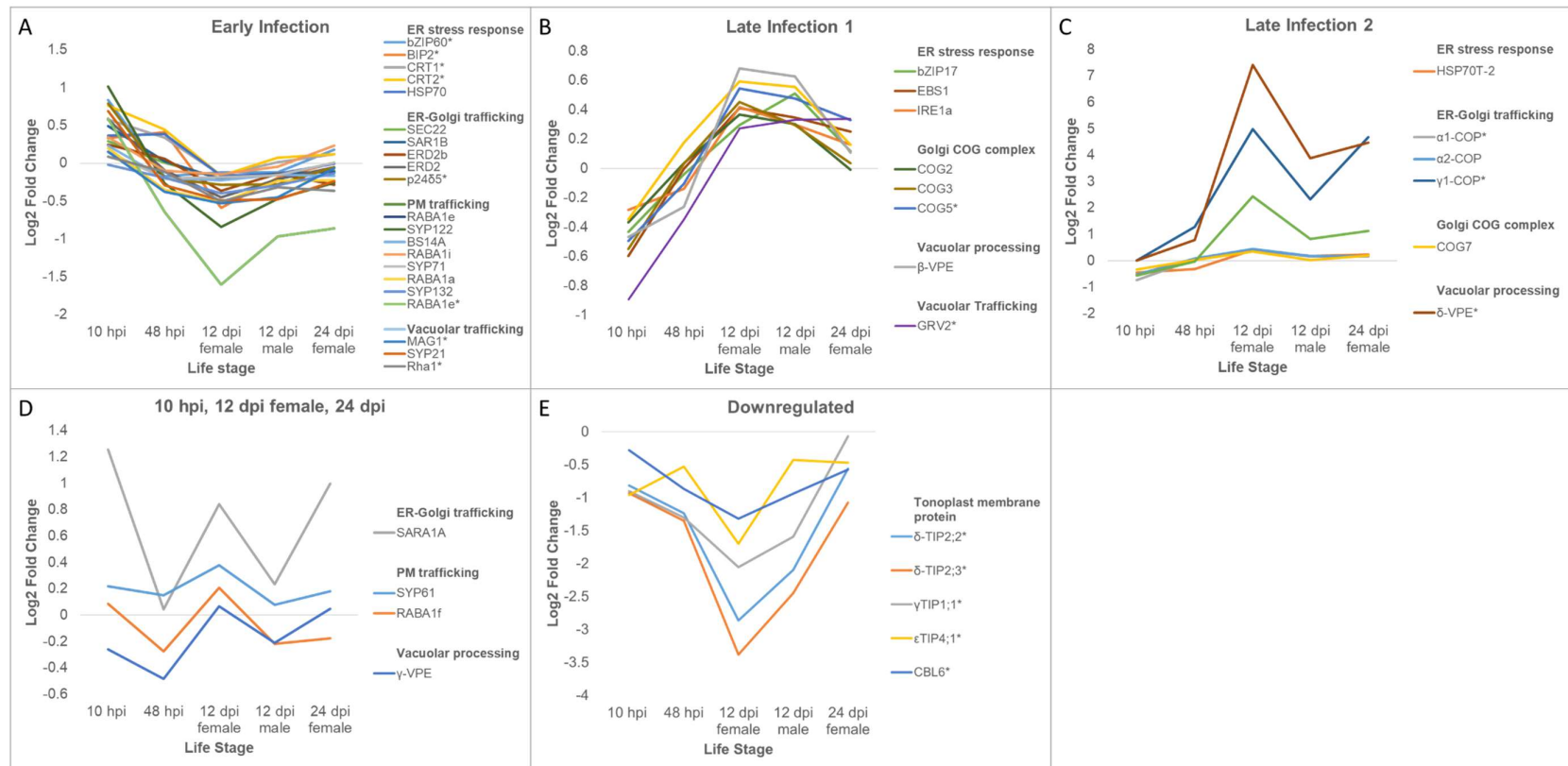


Figure 4. 1. The expression clusters of plant secretory pathway genes in *Arabidopsis* syncytia induced by *H. schachtii*, across various parasitic life stages. Of the 98 genes analysed, 48 were manually assigned to five expression clusters. **A.** The ‘Early Infection’ cluster, describing genes upregulated during early infection, at 10 hpi and 48 hpi. **B.** The ‘Late Infection’ cluster, describing genes only upregulated from later on during infection, peaking at the 12 dpi life stages. **C.** The ‘Late Infection 2’ cluster. This differs from B. in that the 12 dpi male log₂FC values are lower than the female 12 dpi and 24 dpi life stages. Log₂ fold change (log₂FC) values were calculated from previously published normalised expression values (Siddique et al, 2021). Differentially expressed genes (log₂FC > 0.2; adjusted p-value > 0.05) are indicated with an asterisk (*) in the figure legends.

4.3.1.2 ER-Golgi and COG trafficking genes

Genes involved in trafficking between the ER and Golgi were analysed to support the fluorescence microscopy of these two organelles in syncytia. The three COPI coatomer subunits analysed, $\alpha 1$ -COP, $\alpha 2$ -COP, $\gamma 1$ -COP, were assigned to the 'Late Infection 2' cluster (**Figure 4.1C**). $\alpha 1$ -COP and $\gamma 1$ -COP were significantly differentially expressed. Although $\alpha 2$ -COP wasn't, this gene had a similar expression profile to the other two COPI subunits analysed: upregulated the most at 12 dpi female ($\alpha 1$ -COP: 0.41, $\alpha 2$ -COP: 0.44, $\gamma 1$ -COP: 4.99). Additionally, all three COPI subunit genes were upregulated at 48 hpi, 12 dpi male and 24 dpi. However, $\alpha 1$ -COP and $\alpha 2$ -COP were downregulated at 10 hpi ($\alpha 1$ -COP: -0.73, $\alpha 2$ -COP: -0.52), but $\gamma 1$ -COP had no expression in either the control or infected roots at this time point (**Figure 4.1C**).

Five genes involved in trafficking between the ER and the Golgi were assigned to the 'Early Infection' cluster (**Figure 4.1A**): *SEC22*, *SAR1B*, *ERD2*, *ERD2b* and *p2465*. Although, *p2465* was the only ER-Golgi trafficking gene significantly differentially expressed in this cluster. These five genes were upregulated at 10 hpi (0.24-0.79), with low log₂FC values at 48 hpi (-0.09 to 0.06), and were downregulated at all further life stages, with downregulation peaking at 12 dpi female (-0.50 to -0.20; **Figure 4.1A**). However, the ER-Golgi trafficking gene *SARA1A* was assigned to the '10 hpi, 12 dpi female and 24 dpi' cluster, with the highest upregulation at the 10 hpi time point (1.26; **Figure 4.1C**).

Seven COG subunit genes were chosen due to previous evidence that COG subunit genes are involved in soybean resistance to the cyst nematode *H. glycines* (Lawaju et al, 2020). Of the seven COG genes analysed, only one, *COG5* was significantly differentially expressed. However, *COG2*, *COG3* and *COG7* followed similar expression patterns, downregulated at 10 hpi (< -0.03), and upregulated the most at 12 dpi female (0.18-0.54), with *COG5* the having the highest log₂FC at this time point. The other two COG genes, *COG1* and *COG8* followed different expression patterns (**Table 4.4**).

4.3.1.3 Post-Golgi trafficking genes

Genes involved in post-Golgi trafficking to the plasma membrane were assigned to several clusters (**Figure 4.1**). Of these genes, *RABA1e* was significantly differentially expressed, assigned to the 'Early Infection' cluster (**Figure 4.1A**). *RABA1e* was upregulated at 10 hpi (0.59), then downregulated at all subsequent time points, with downregulation peaking at 12 dpi female (-1.61). Additionally, six genes involved in post-Golgi trafficking to the PM were assigned to the early infection cluster (**Figure 4.1A**). However, none of these genes were significantly differentially expressed. Additionally, *SYP61* and *RABA1f* were assigned to the '10 hpi, 12 dpi female and 24 dpi' expression

cluster, although SYP61 was upregulated across all time points, and RABA1f was only upregulated at 10 hpi and 12 dpi female (**Figure 4.1D**).

4.3.1.4 Vacuolar trafficking genes and other vacuole-related genes

Genes related to vacuolar trafficking, or other vacuole-related functions, were the most differentially regulated out of all of the gene categories studied (**Figure 4.1E; Tables 4.6 and 4.7**). All tonoplast membrane proteins studied apart from α -TIP3;1 and δ -TIP2;1 had similar expression profiles, assigned to the 'Downregulated' cluster (**Figure 4.1E**). These genes were downregulated at all life stages, with downregulation peaking at 12 dpi female (-1.32 to -3.38). *CBL6* was the least downregulated of these genes at 12 dpi female, and was the only gene out of all tonoplast membrane genes in the 'Downregulated' category that wasn't significantly differentially expressed.

Of the vacuolar trafficking genes analysed, *GRV2* was significantly differentially regulated and assigned to the 'Late Infection 1' expression cluster (**Figure 4.1B**). *GRV2* was the most downregulated gene in the whole cluster at 10 hpi (-0.89) and 48 hpi (-0.34). This gene was then upregulated at all further life stages, gradually increasing from 12 dpi female to 12 dpi male and 24 dpi female (0.27-0.34). Three other vacuolar trafficking genes were assigned to another cluster, 'Early Infection' (**Figure 4.1A**). These were *MAG1*, *Rha1* and *SYP21*. Although only *MAG1* and *Rha1* were significantly differentially expressed, *SYP21* had a similar expression profile, upregulated at 10 hpi (*MAG1*: 0.15, *Rha1*: 0.08, *SYP21*: 0.69), and downregulated at all other time points, with downregulation peaking at 12 dpi female (*MAG1*: -0.53, *Rha1*: -0.50, *SYP21*: -0.49).

For the vacuolar processing enzymes (VPEs), three genes were assigned to different expression clusters: β -VPE to the 'Late Infection 1', δ -VPE to 'Late Infection 2', and γ -VPE to '10 hpi, 12 dpi female and 24 dpi' (**Figures 4.1B to D**). At 10 hpi, δ -VPE had no expression, and the other two VPEs assigned to clusters were downregulated at this time point (β -VPE: -0.47, γ -VPE: -0.26). Although the three VPEs had differing expression profiles, assigned to different expression clusters, all genes were also upregulated at 12 dpi female. However, δ -VPE was the only significantly expressed VPE, much higher upregulated at 12 dpi female (7.42), compared to β -VPE (0.68) and γ -VPE (0.07). The only VPE analysed that wasn't assigned to an expression cluster, α -VPE, was downregulated at all time points other than 10 hpi (**Table 4.7**).

Tables 4. 2 to 4. 7- The expression of secretory pathway-related genes in syncytia formed in Arabidopsis roots. The log2 fold changes (log2FCs) for each gene are given across the various time points: 10 hours post infection (hpi), 48 hpi, 12 days post infection (dpi) female and male, and 24 dpi female. The log2FC for each gene was calculated using previously published RNA-seq data (Siddique et al, 2021). Asterisks (*) represent genes which were significantly differentially expressed between the control and infected samples at any of the time points. A heat map is presented for the log2FC values, with red representing positive values and blue representing negative values.

Table 4. 2. The expression of ER-related genes in Arabidopsis syncytia.

| Gene | Name | Localisation | Process | 10 hpi | 48 hpi | 12 dpi female | 12 dpi male | 24 dpi female |
|-----------|--|--------------|--------------------|--------|--------|---------------|-------------|---------------|
| AT1G42990 | *bZIP60 basic region/leucine zipper motif 60 | ER | ER stress response | 0.84 | -0.17 | -0.12 | -0.12 | 0.18 |
| AT2G40950 | bZIP17 Basic-leucine zipper (bZIP) transcription factor family protein | ER | ER stress response | -0.43 | -0.04 | 0.30 | 0.51 | 0.12 |
| AT3G10800 | bZIP28 Basic-leucine zipper (bZIP) transcription factor family protein | ER | ER stress response | -0.21 | -0.26 | -0.09 | 0.04 | 0.10 |
| AT2G17520 | IRE1a Endoribonuclease/protein kinase IRE1-like | ER | ER stress response | -0.28 | -0.14 | 0.42 | 0.30 | 0.16 |
| AT5G24360 | IRE1b | ER | ER stress response | -0.45 | -0.21 | 0.03 | 0.01 | -0.02 |
| AT5G42020 | *BIP2 Heat shock protein 70 (Hsp 70) family protein | ER | ER stress response | 0.33 | 0.41 | -0.59 | -0.19 | 0.01 |
| AT1G09080 | BIP3 Heat shock protein 70 (Hsp 70) family protein | ER | ER stress response | 2.50 | 1.59 | 1.46 | 2.06 | 3.58 |
| AT2G32120 | HSP70T-2 Heat shock protein 70 (Hsp 70) family protein | ER | ER stress response | -0.45 | -0.31 | 0.40 | 0.18 | 0.23 |
| AT4G16660 | HPS70 Heat shock protein 70 (Hsp 70) family protein | ER | ER stress response | 0.36 | 0.38 | -0.17 | -0.14 | -0.01 |
| AT3G12580 | HSP70-4 Heat shock protein 70 (Hsp 70) family protein | ER | ER stress response | -0.38 | -0.29 | -0.60 | -0.24 | -0.03 |
| AT3G09440 | HSP70-3 Heat shock protein 70 (Hsp 70) family protein | ER | ER stress response | 0.02 | 0.32 | -0.60 | -0.02 | -0.21 |
| AT1G11660 | HSP70-16 Heat shock protein 70 (Hsp 70) family protein | ER | ER stress response | -0.49 | -0.06 | 0.06 | -0.11 | 0.07 |
| AT1G56410 | ERD2 Heat shock protein 70 (Hsp 70) family protein | ER | ER stress response | 0.84 | 1.48 | 0.06 | 1.17 | 1.83 |
| AT1G16030 | HSP70b Heat shock protein 70 (Hsp 70) family protein | ER | ER stress response | 0.47 | 0.32 | 0.07 | 0.11 | -0.01 |
| AT1G56340 | *CRT1 Calreticulin 1 | ER | ER stress response | 0.58 | 0.34 | -0.16 | 0.02 | 0.12 |
| AT1G09210 | *CRT2 Calreticulin 2 | ER | ER stress response | 0.77 | 0.45 | -0.17 | 0.07 | 0.12 |
| AT1G08450 | CRT3 Calreticulin 3 | ER | ER stress response | 0.08 | 0.13 | 0.21 | 0.16 | 0.08 |
| AT1G71220 | EBS1 UDP-glucose:glycoprotein glucosyltransferases | ER | ER stress response | -0.60 | 0.00 | 0.41 | 0.35 | 0.25 |

Table 4. 3. The expression of ER and Golgi trafficking components in Arabidopsis syncytia.

| Gene | Name | Localisation | Process | 10 hpi | 48 hpi | 12 dpi female | 12 dpi male | 24 dpi female |
|-----------|--|---------------|---------------------------|--------|--------|---------------|-------------|---------------|
| AT2G01470 | STL2P SEC12P-like 2 protein | ER | ER to Golgi | 0.16 | 0.02 | 0.18 | -0.05 | 0.12 |
| AT3G13870 | RHD3 Root hair defective 3 GTP-binding protein | ER | ER to Golgi | -0.17 | -0.02 | 0.20 | -0.07 | 0.19 |
| AT1G09180 | SARA1A secretion-associated RAS super family 1 | Cytosol, ERES | ER to Golgi | 1.26 | 0.04 | 0.84 | 0.23 | 1.00 |
| AT1G56330 | SAR1B secretion-associated RAS 1B | Cytosol, ERES | ER to Golgi | 0.49 | 0.03 | -0.21 | -0.14 | -0.11 |
| AT5G05760 | SYP31 syntaxin of plants 31 | Golgi | ER to Golgi | 0.01 | -0.12 | 0.07 | -0.02 | 0.04 |
| AT1G11890 | SEC22 Synaptobrevin family protein | ER, ERES | ER to Golgi & Golgi to ER | 0.29 | 0.01 | -0.20 | -0.15 | -0.10 |
| AT1G21900 | *p24&5 marker emp24/gp25L/p24 family/GOLD family protein | ER | Golgi to ER | 0.79 | -0.20 | -0.29 | -0.28 | -0.05 |
| AT1G23490 | ARF1 ADP-ribosylation factor 1 | Golgi | Golgi to ER | 0.27 | 0.03 | -0.01 | -0.14 | -0.09 |
| AT1G29330 | ERD2 ER lumen protein retaining receptor family protein | Golgi | Golgi to ER | 0.58 | -0.09 | -0.45 | -0.21 | -0.06 |
| AT2G37550 | AGD7 ARF-GAP domain 7 | Golgi | Golgi to ER | 0.04 | 0.14 | -0.10 | -0.05 | -0.17 |
| AT1G62020 | *α1-COP coatomer protein complex, subunit alpha1 | Golgi | Golgi to ER | -0.74 | 0.05 | 0.41 | 0.16 | 0.16 |
| AT2G21390 | α2-COP coatomer protein complex, subunit alpha 2 | Golgi | Golgi to ER | -0.52 | 0.08 | 0.44 | 0.17 | 0.19 |
| AT2G16200 | *γ1-COP coatomer protein complex, subunit gamma 1 | Golgi | Golgi to ER | 0.00 | 1.28 | 4.99 | 2.32 | 4.69 |
| AT3G25040 | ERD2b Marker | Golgi | Golgi to ER | 0.24 | 0.06 | -0.36 | -0.14 | -0.29 |

Table 4. 4. The expression of Golgi-related trafficking genes in Arabidopsis syncytia.

| Gene | Name | Localisation | Process | 10 hpi | 48 hpi | 12 dpi female | 12 dpi male | 24 dpi female |
|-----------|---|--------------|-------------------|--------|--------|---------------|-------------|---------------|
| AT3G24350 | SYP32 syntaxin of plants 32 | Golgi | Golgi maintenance | 0.23 | -0.02 | -0.18 | -0.21 | -0.13 |
| AT2G36900 | MEMB11 membrin 11 | Golgi | Golgi to TGN | -0.04 | -0.19 | -0.02 | 0.12 | 0.03 |
| AT1G29160 | COG1 Component of oligomeric golgi complex 1 | Golgi | Golgi COG complex | 0.46 | -0.05 | -0.31 | 0.03 | -0.15 |
| AT4G24840 | COG2 Component of oligomeric golgi complex 2 | Golgi | Golgi COG complex | -0.37 | 0.04 | 0.37 | 0.30 | -0.01 |
| AT1G73430 | COG3 Component of oligomeric golgi complex 3 | Golgi | Golgi COG complex | -0.55 | 0.03 | 0.45 | 0.30 | 0.03 |
| AT1G67930 | *COG5 Component of oligomeric golgi complex 5 | Golgi | Golgi COG complex | -0.49 | -0.10 | 0.55 | 0.48 | 0.33 |
| AT1G31780 | COG6 Component of oligomeric golgi complex 6 | Golgi | Golgi COG complex | -0.34 | 0.06 | 0.18 | 0.14 | 0.18 |
| AT5G51430 | COG7 Component of oligomeric golgi complex 7 | Golgi | Golgi COG complex | -0.32 | 0.03 | 0.35 | 0.03 | 0.20 |
| AT5G11980 | COG8 Component of oligomeric golgi complex 8 | Golgi | Golgi COG complex | -0.13 | 0.14 | 0.11 | 0.13 | 0.01 |

Table 4. 5. The expression of genes related to post-Golgi trafficking to the plasma membrane (PM) in Arabidopsis syncytia.

| Gene | Name | Localisation | Process | 10 hpi | 48 hpi | 12 dpi female | 12 dpi male | 24 dpi female |
|-----------|--|--------------|----------------|--------|--------|---------------|-------------|---------------|
| AT3G58170 | BS14A BET1P/SFT1P-like protein 14A | Golgi | PM trafficking | 0.23 | -0.20 | -0.23 | -0.15 | -0.17 |
| AT1G60780 | HAP13 Clathrin adaptor complexes medium subunit family protein | TGN | PM trafficking | -0.02 | 0.14 | -0.15 | -0.18 | -0.16 |
| AT1G06400 | RABA1a Ras-related small GTP-binding family protein | TGN | PM trafficking | 0.20 | -0.35 | -0.52 | -0.23 | -0.23 |
| AT1G16920 | RABA1b RAB GTPase homolog A1B | TGN | PM trafficking | -0.22 | 0.28 | -0.27 | 0.23 | -0.29 |
| AT5G45750 | RABA1c RAB GTPase homolog A1C | TGN | PM trafficking | 0.30 | 0.36 | 0.04 | 0.13 | -0.09 |
| AT4G18800 | RABA1d RAB GTPase homolog A1D | TGN | PM trafficking | 0.19 | -0.18 | -0.07 | -0.08 | -0.24 |
| AT4G18430 | *RABA1e RAB GTPase homolog A1E | TGN | PM trafficking | 0.59 | -0.65 | -1.61 | -0.97 | -0.86 |
| AT5G60860 | RABA1f RAB GTPase homolog A1F | TGN | PM trafficking | 0.08 | -0.27 | 0.21 | -0.22 | -0.17 |
| AT3G15060 | RABA1g RAB GTPase homolog A1G | TGN | PM trafficking | 0.83 | 0.32 | 0.53 | 0.34 | 0.12 |
| AT2G33870 | RABA1h RAB GTPase homolog A1H | TGN | PM trafficking | 0.00 | 0.00 | 0.00 | 0.00 | 0.00 |
| AT1G28550 | RABA1i RAB GTPase homolog A1I | TGN | PM trafficking | 0.34 | -0.10 | -0.15 | -0.05 | 0.23 |
| AT1G28490 | SYP61 Marker syntaxin of plants 61 | TGN | PM trafficking | 0.22 | 0.15 | 0.38 | 0.08 | 0.18 |
| AT3G09740 | SYP71 syntaxin of plants 71 | PM | PM trafficking | 0.15 | -0.20 | -0.19 | -0.16 | 0.01 |
| AT3G11820 | SYP121 syntaxin of plants 121 | PM | PM trafficking | 0.36 | -0.28 | -0.12 | -0.14 | -0.16 |
| AT3G52400 | SYP122 syntaxin of plants 122 | PM | PM trafficking | 1.02 | -0.27 | -0.85 | -0.47 | -0.26 |
| AT5G08080 | SYP132 syntaxin of plants 132 | PM | PM trafficking | -0.02 | -0.19 | -0.40 | -0.29 | -0.13 |

Table 4. 6. The expression of vacuolar trafficking genes in *Arabidopsis* syncytia. Collectively, these genes are involved in trafficking between the Golgi, trans-Golgi network (TGN), prevacuolar compartment (PVC), late prevacuolar compartment (LPVC) and the vacuoles.

| Gene | Name | Localisation | Process | 10 hpi | 48 hpi | 12 dpi female | 12 dpi male | 24 dpi female |
|-----------|--|--------------|----------------------|--------|--------|------------------|----------------|------------------|
| AT1G10290 | ADL6 dynamin-like protein 6 | Golgi | Vacuolar trafficking | -0.61 | -0.14 | 0.30 | 0.37 | 0.27 |
| AT3G54840 | Ara6 Rab-like GTPase | TGN | Vacuolar trafficking | 0.31 | -0.28 | -0.07 | -0.13 | 0.01 |
| AT1G26670 | VTI1b Vesicle transport v-SNARE family protein | TGN | Vacuolar trafficking | 0.08 | -0.42 | -0.19 | -0.15 | -0.11 |
| AT5G11710 | EPS1 ENTH/VHS family protein | TGN | Vacuolar trafficking | 0.21 | -0.05 | -0.01 | -0.21 | -0.04 |
| AT4G26750 | EXT-like hydroxyproline-rich glycoprotein family protein | PVC | Vacuolar trafficking | -0.26 | -0.48 | 0.27 | 0.52 | 0.61 |
| AT1G75850 | VPS35 homolog B | PVC | Vacuolar trafficking | -0.17 | -0.14 | 0.12 | -0.10 | 0.11 |
| AT2G17790 | VPS35 homolog A | PVC | Vacuolar trafficking | -0.23 | 0.01 | 0.05 | 0.05 | 0.06 |
| AT2G26890 | *GRV2 DNAJ heat shock N-terminal domain-containing protein | PVC | Vacuolar trafficking | -0.89 | -0.34 | 0.27 | 0.33 | 0.34 |
| AT3G19770 | VPS9a Vacuolar sorting protein 9 (VPS9) domain | PVC | Vacuolar trafficking | -0.05 | -0.04 | -0.05 | -0.08 | 0.01 |
| AT3G47810 | *MAG1 Calcineurin-like metallo-phosphoesterase superfamily protein | PVC | Vacuolar trafficking | 0.15 | -0.38 | -0.53 | -0.45 | -0.06 |
| AT3G51310 | VPS35 homolog C | PVC | Vacuolar trafficking | -0.01 | 0.15 | 0.35 | 0.16 | -0.06 |
| AT3G52850 | BP80 marker; vacuolar sorting receptor homolog 1 | PVC | Vacuolar trafficking | 0.47 | 0.02 | 0.42 | 0.07 | 0.20 |
| AT4G19640 | Ara7 Ras-related small GTP-binding family protein | PVC | Vacuolar trafficking | 0.36 | -0.31 | -0.26 | -0.29 | -0.09 |
| AT5G16830 | SYP21 syntaxin of plants 21 | PVC | Vacuolar trafficking | 0.69 | -0.29 | -0.49 | -0.48 | -0.24 |
| AT5G39510 | SGR4 Vesicle transport v-SNARE family protein | PVC | Vacuolar trafficking | 0.19 | -0.37 | -0.37 | -0.31 | 0.05 |
| AT2G38020 | VCL1 vacuoleless1 | PVC | Vacuolar trafficking | -0.05 | -0.16 | -0.11 | -0.21 | 0.12 |
| AT5G45710 | *Rha1 marker; Rab GTPase | LPVC | Vacuolar trafficking | 0.08 | -0.11 | -0.50 | -0.32 | -0.36 |
| AT5G46860 | VAM3 Syntaxin/t-SNARE family protein | Tonoplast | Vacuolar trafficking | 0.07 | -0.29 | -0.24 | -0.25 | -0.16 |
| AT4G32150 | VAMP711 vesicle-associated membrane protein 711 | Vacuoles | Vacuolar trafficking | -0.07 | -0.40 | -0.17 | -0.02 | -0.05 |

Table 4. 7. The expression of vacuolar processing genes and tonoplast membrane proteins in Arabidopsis syncytia.

| Gene | | Localisation | Process | 10 hpi | 48 hpi | 12 dpi female | 12 dpi male | 24 dpi female |
|-----------|--|---|---------------------|--------|--------|------------------|----------------|------------------|
| AT5G60360 | Homolog of aleurain marker | Vacuole | Vacuolar protease | 0.06 | -0.50 | -0.26 | -0.43 | 0.00 |
| AT2G25940 | α -VPE | Vacuole | Vacuolar processing | 0.31 | -0.09 | -0.34 | -0.43 | -0.36 |
| AT1G62710 | β -VPE | Vacuole | Vacuolar processing | -0.47 | -0.26 | 0.68 | 0.63 | 0.11 |
| AT3G20210 | * δ -VPE | Vacuole | Vacuolar processing | 0.00 | 0.79 | 7.42 | 3.89 | 4.47 |
| AT4G32940 | γ -VPE | Vacuole | Vacuolar processing | -0.26 | -0.48 | 0.07 | -0.21 | 0.05 |
| AT4G16350 | *CBL6 Marker; calcineurin B-like protein 6 | Tonoplast | Tonoplast membrane | -0.28 | -0.87 | -1.32 | -0.94 | -0.58 |
| AT1G73190 | α TIP3;1 alpha tonoplast integral protein 1 | Tonoplast (mostly protein storage vacuoles) | Tonoplast membrane | -0.35 | 1.76 | -0.02 | -0.49 | 0.17 |
| AT3G16240 | δ -TIP2;1 delta tonoplast integral protein 1 | Tonoplast (mostly protein storage vacuoles) | Tonoplast membrane | -0.69 | -0.17 | -0.03 | -0.24 | 0.21 |
| AT4G17340 | * δ -TIP2;2 delta tonoplast intrinsic protein 2 | Tonoplast (mostly protein storage vacuoles) | Tonoplast membrane | -0.82 | -1.24 | -2.86 | -2.10 | -0.56 |
| AT5G47450 | * δ -TIP2;3 delta tonoplast intrinsic protein 3 | Tonoplast (mostly protein storage vacuoles) | Tonoplast membrane | -0.93 | -1.35 | -3.38 | -2.45 | -1.07 |
| AT2G36830 | * γ TIP1;1 gamma tonoplast intrinsic protein 1 | Tonoplast (mostly lytic vacuoles) | Tonoplast membrane | -0.90 | -1.30 | -2.05 | -1.59 | -0.07 |
| AT2G25810 | * ϵ TIP4;1 epsilon tonoplast integral protein 1 | Tonoplast (mostly lytic vacuoles) | Tonoplast membrane | -0.96 | -0.53 | -1.70 | -0.43 | -0.47 |

4.3.2 Confocal imaging of syncytia in fluorescent Arabidopsis lines

Images of one representative syncytium for each Arabidopsis marker line are presented below. For each line, the pattern of expression was consistent regardless of the age of the syncytium, from 8 dpi to 18 dpi. Each figure shows a single syncytium and its surrounding root cells, with an overview image of the infected root, in addition to magnified images of the syncytium and its adjacent cells. The boundaries of the syncytium are marked on the brightfield channels of each image, the demarcations the same within each figure, regardless of image magnification. As a control, the epidermal, cortical and vascular cells of uninfected roots from the same line are also presented.

4.3.2.1 General limitations associated with the imaging of fluorescent Arabidopsis lines

Certain features associated with the confocal imaging of Arabidopsis syncytia were observed. This includes limitations of the confocal microscope, with marker resolution reduced with increased tissue depth, from the epidermis to the vascular region. Examples of this are shown in uninfected control cells for the common cis-Golgi marker (**Figure 4.8**), the ER marker GFP-HDEL (**Figure 4.4**) and the tonoplast marker (**Figure 4.8**). As syncytia were typically beneath the epidermis, within the cortical and vascular region, this limited the resolution of the syncytial cells imaged. Variable marker expression also impeded imaging for all marker lines, with inconsistent fluorescence in cells of the same root. For example, secYFP-ERD2b expression was inconsistent within uninfected roots, with regions of no expression or autofluorescence in cells at the same focal plane (**Figure 4.2**). Therefore, obtaining syncytia with optimal marker expression was not always possible. Consequently, some of the infected roots imaged showed poor expression of the common cis-Golgi marker secYFP-ERD2b, in cells within and surrounding the syncytium (**Figures 4.7 and 4.9**).

Root structure also impeded imaging. For instance, due to the cylindrical shape of roots, imaging the cortical cytoplasm within cells beneath the epidermis was challenging. This impeded marker visualisation of the ER network in GFP-HDEL lines, which extends throughout the cortical cytoplasm (**Figure 4.4**). Moreover, the presence of the large central vacuole in uninfected roots often impeded marker visualisation. Strong leakage of fluorescent protein to the large central vacuoles was observed in several of the Arabidopsis marker lines, including the ER marker secRFP-p24aTM (**Figure 4.2**), the PVC marker RFP-BP80 (**Figure 4.14**) and the LPVC marker RFP-Rha1 (**Figure 4.12**). Consequently, the intended subcellular compartment for each marker could not be imaged with clarity.

4.3.2.2 Expression of the cis-Golgi marker secYFP-ERD2b in all dual fluorescence Arabidopsis lines

Common features of the cis-Golgi marker secYFP-ERD2b expression were observed across the Arabidopsis marker lines imaged. In uninfected roots of all lines, the cis-Golgi marker secYFP-ERD2b labelled punctate structures as expected. Within infected roots, punctate secYFP-ERD2b structures were also observed in cells directly surrounding the syncytium (**Figures 4.3, 4.11, 4.13**). However, in all marker lines imaged, no secYFP-ERD2b expression was detected in the syncytium, even at increased laser power and detection gain (**Figures 4.3 and 4.11**).

4.3.2.3 pTASH8, co-expressing the ER marker secRFP-p24aTM

Within uninfected pTASH8 Arabidopsis roots, secRFP-p24aTM partially localised to the large central vacuoles, as previously shown during T₂ line screening (**Figure 3.24**). secRFP-p24aTM expression was mostly vacuolar in cells directly bordering the syncytium (**Figure 4.3B**). In some of these cells, secRFP-p24aTM punctae were visible (**Figure 4.3B**), which could indicate vacuolar fragmentation. Within the syncytium, the expression of secRFP-p24aTM was hardly detected (**Figure 4.3A**), even under increased laser power and detection gain (**Figure 4.3C**). Consequently, syncytia within another Arabidopsis ER marker line, GFP-HDEL, were also imaged.

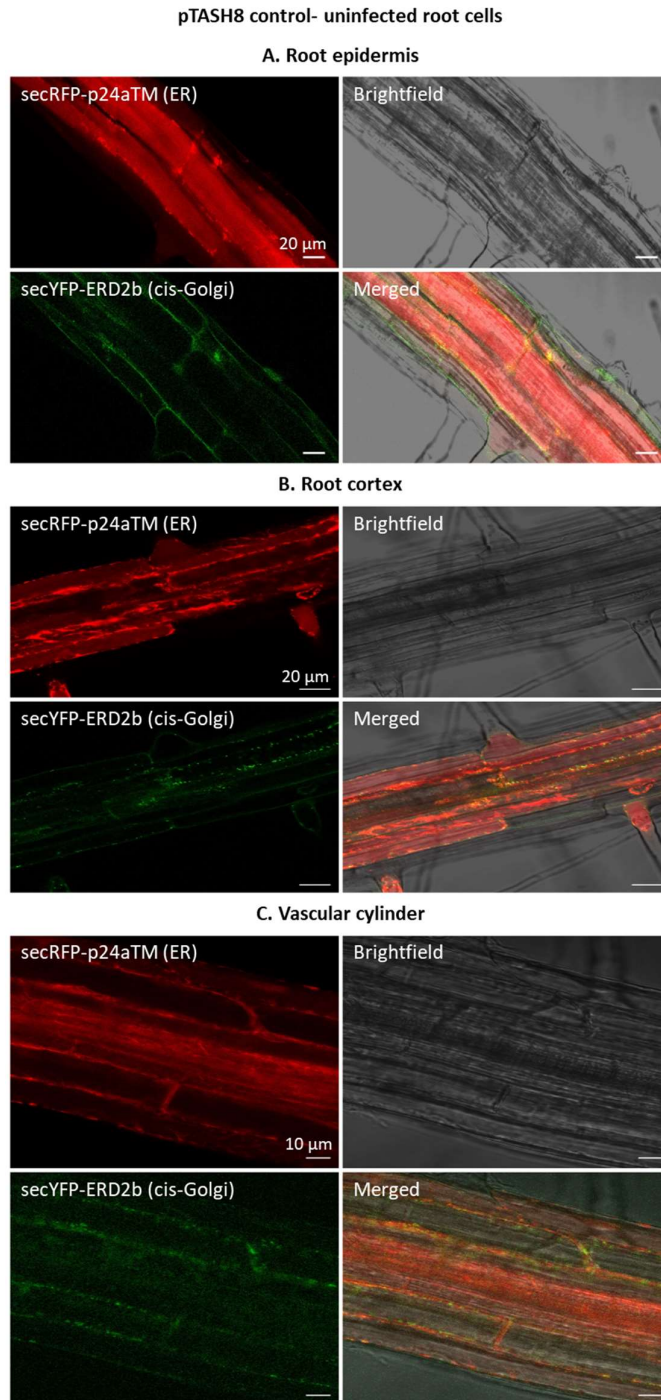


Figure 4. 2. The uninfected control roots of pTASH8 *Arabidopsis* lines, expressing the ER marker secRFP-p24aTM with secYFP-ERD2b. **A.** The root epidermis, showing secRFP-p24aTM expression mostly within the vacuoles, with some ER network labelled. secYFP-ERD2b expression is poor. **B.** Root cells just beneath the root epidermis, showing labelling of the ER network and weak vacuole localisation. secYFP-ERD2b punctae are present in some cells towards the centre of the root. **C.** The focal plane of the vascular cylinder, showing secRFP-p24aTM expression within the vacuoles of cells, with little ER detected. secYFP-ERD2b punctae are not present in the vascular cylinder cells.

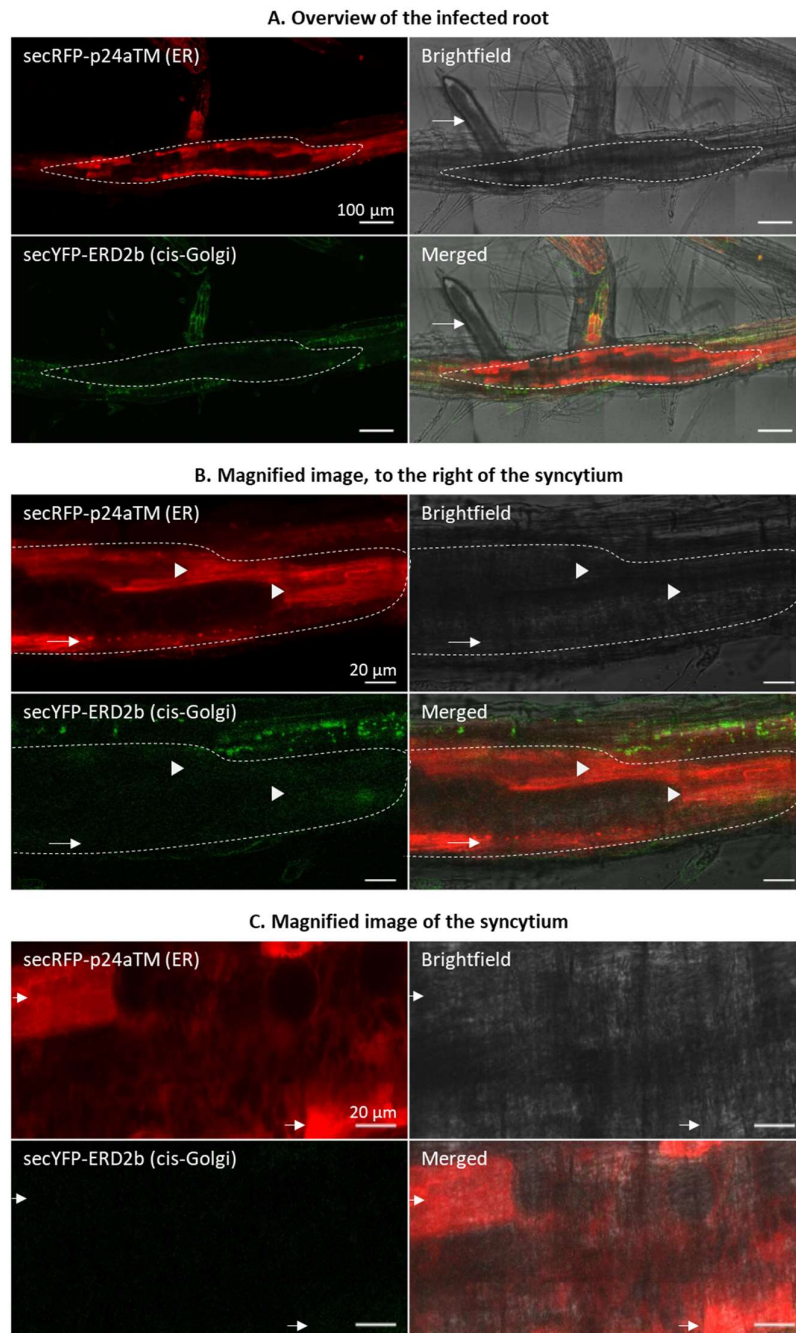
8 dpi syncytia within *Arabidopsis* expressing pTASH8

Figure 4.3. 8 days post infection (dpi) syncytia induced by *H. schachtii* within *Arabidopsis* roots expressing pTASH8. **A.** A tile scan of the whole section of infected root, showing the syncytium to the right of the feeding *H. schachtii* (white arrow). No secRFP-p24aTM or secYFP-ERD2b expression is observed in the syncytium. **B.** A magnified image of the region to the right of the syncytium, showing secRFP-p24aTM expression in the vacuoles (white arrow heads) and the presence of secRFP-p24aTM punctae (white arrow) in cells directly bordering the syncytium. **C.** A magnified image of syncytial cells, with a higher laser power and detection gain. Poor marker resolution is observed, with no definite subcellular compartment labelled by secRFP-p24aTM. However, cells directly bordering the syncytium still show secRFP-p24aTM within the vacuoles (white arrows). In each image, the dashed lines demarcate the syncytium.

4.3.2.4 The ER marker GFP-HDEL expression within syncytia

In contrast to secRFP-p24aTM, no leakage of GFP-HDEL to the vacuoles was observed in uninfected roots (**Figure 4.4**). Additionally, spindle-shaped structures were observed which may represent ER bodies (**Figure 4.4A and B**). Also contrasting to secRFP-p24aTM, GFP-HDEL was expressed in syncytial cells (**Figure 4.5**). As the large central vacuole was not present in syncytia, GFP-HDEL occupied a large volume in syncytial cells, also appearing to be continuous across the syncytium, which is likely due to the partial cell wall dissolution and protoplast fusion of syncytial cells (**Figure 4.5C**). Additionally, GFP-HDEL expression appeared to be brighter in certain regions of the syncytium (**Figure 4.5B**), which could indicate region-specific increased abundance of ER in syncytia. Also, importantly, no movement of GFP-HDEL could be observed in syncytial cells.

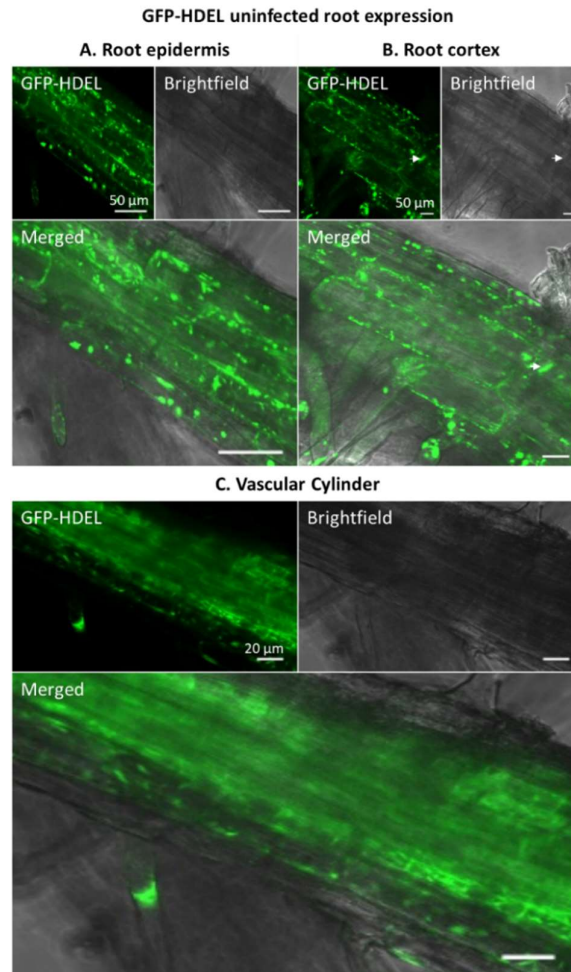


Figure 4. 4. Uninfected Arabidopsis roots expressing the ER marker GFP-HDEL. A. and B. Cells at the root epidermis and root cortex respectively, showing GFP-HDEL expression in the ER, although no tubular or cisternal ER network is observed, due to the large central vacuoles occupying most of the space within the cell. Vesicle shaped GFP-HDEL structures are observed, which may be ER bodies (white arrows). **C.** GFP-HDEL expression within vascular cells, showing a diffused GFP signal throughout the vascular region.

13 dpi syncytia within *Arabidopsis* expressing GFP-HDEL

A. Overview of the infected root

B. A magnified view of the syncytium

C. A magnified view of cells to the left of the nematode

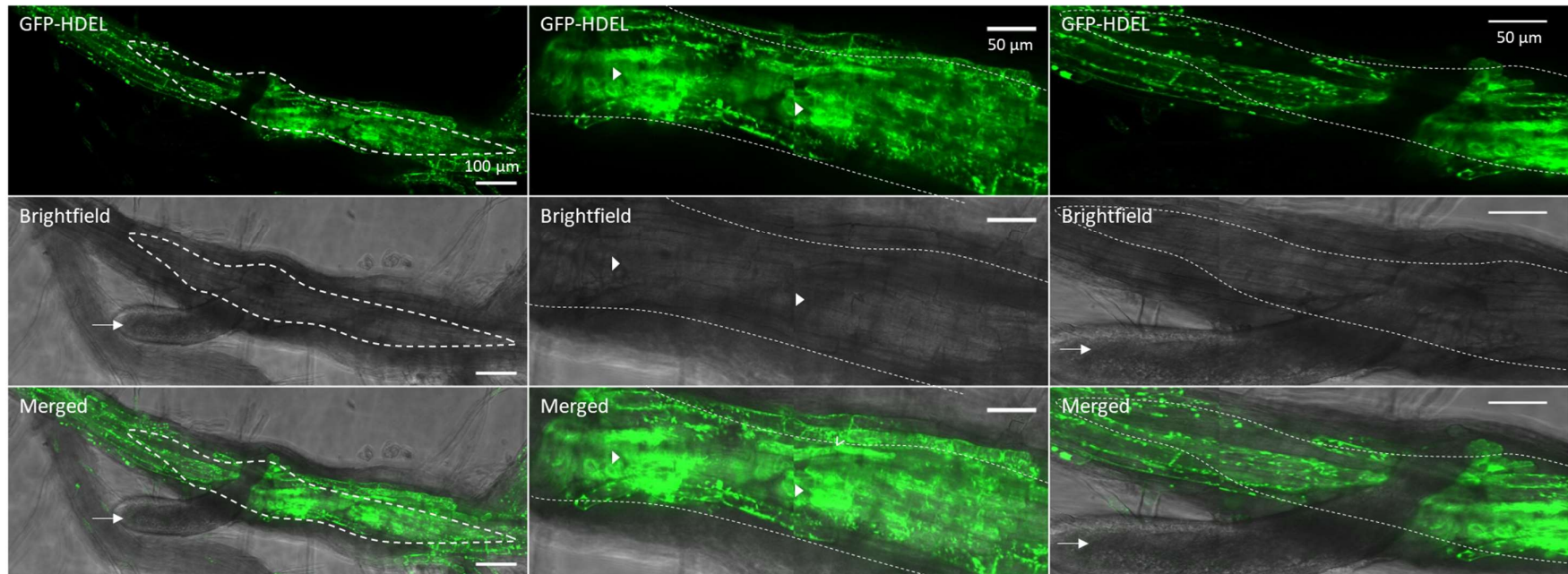


Figure 4.5. 13 dpi syncytia induced by *H. schachtii* in *Arabidopsis* lines expressing GFP-HDEL. **A.** An overview of the syncytium, showing the female *H. schachtii* (white arrow), with the syncytium to the right of the worm. GFP-HDEL expression is present in syncytial cells, with expression appearing to be brighter and more abundant compared to non-syncytial cells to the left of the worm. **B.** A magnified view of the syncytium. The large central vacuole is not present in syncytial cells, instead the labelled ER network occupies most of the cell. Two brighter regions of GFP-HDEL are observed in the syncytium (white arrowheads). **C.** Cells to the left of the nematode (white arrow). GFP-HDEL occupies the majority of the syncytial cells, due to the lack of a large central vacuole. In each image, the dashed lines demarcate the syncytium.

4.3.2.5 pTASH12, co-expressing the vacuole marker Aleu-RFP

High Aleu-RFP expression was observed in the epidermis, cortex and vascular cylinder of uninfected cells, with bright labelling of the large central vacuoles (**Figure 4.6**). Additionally, in some cells at all tissue depths imaged, autofluorescence was also observed as thin 'stripes' running across cells. Within infected roots, several small Aleu-RFP labelled vacuoles were present in the syncytium (**Figure 4.7**). Interestingly, vacuoles appeared larger towards the outer edges of the syncytium. In cells directly bordering the syncytium, large central vacuoles were present (**Figure 4.7B and C**). However, some cells bordering the syncytium also contained small vacuoles (**Figure 4.7C**).

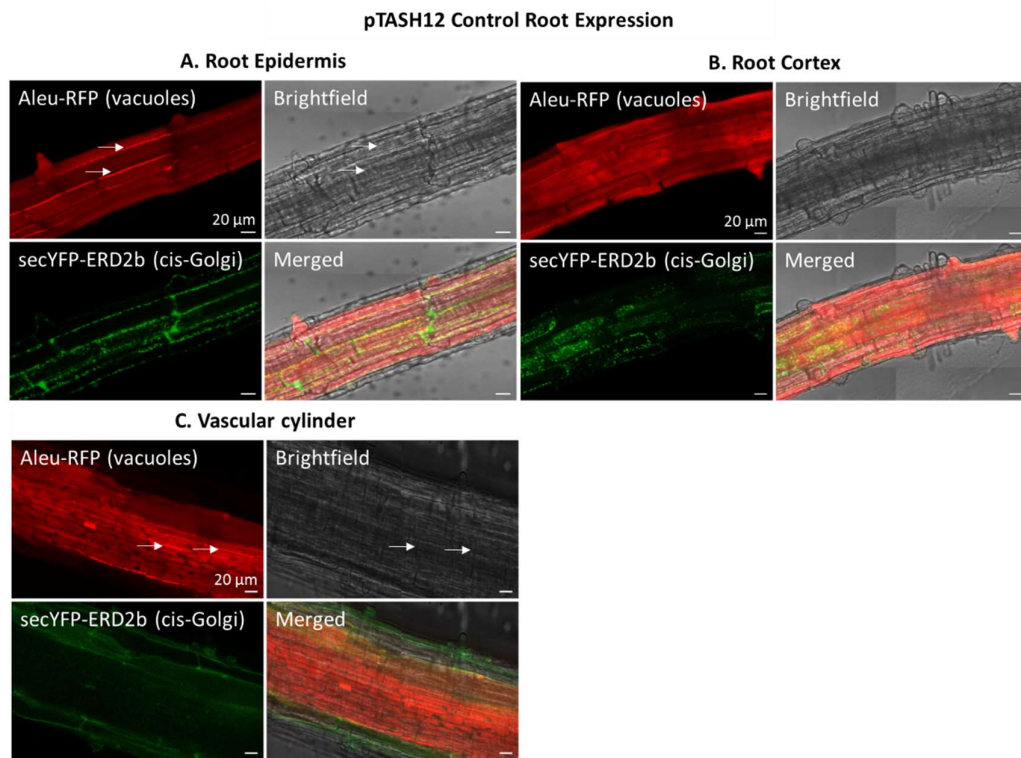
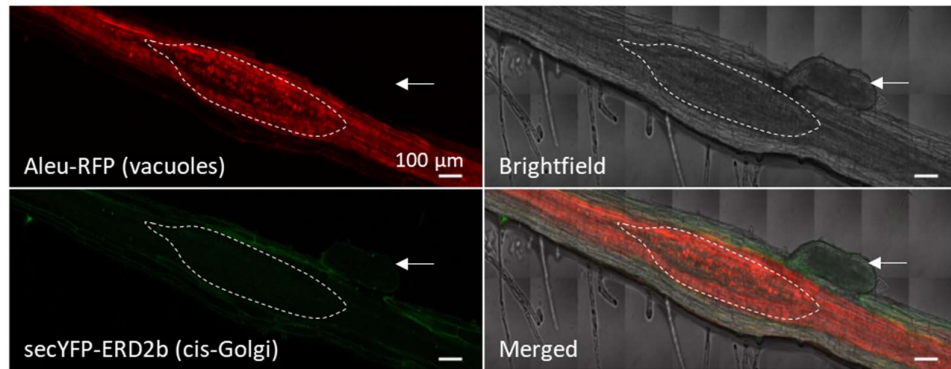


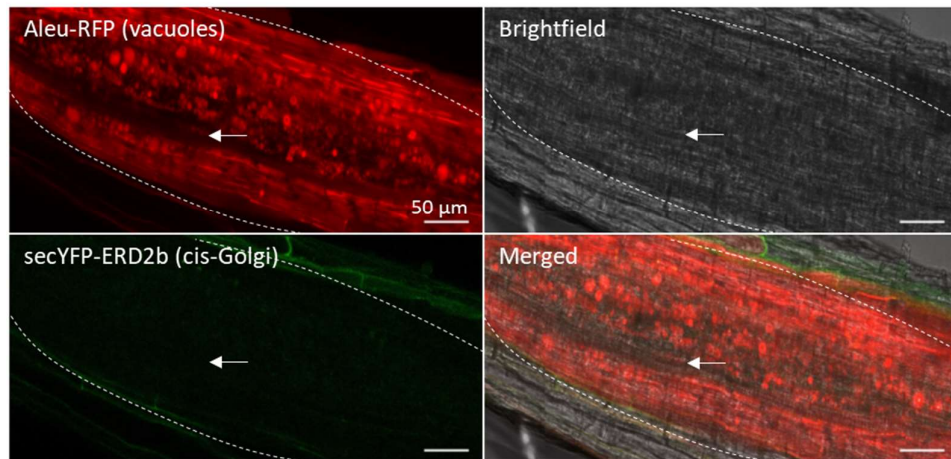
Figure 4. 6. pTASH12 expression within uninfected Arabidopsis root cells. A. Expression of pTASH12 in the epidermis, showing the presence of Aleu-RFP in the large central vacuoles. Linear stripes of Aleu-RFP expression across root cells are observed (arrows), which may be artefacts of overexpression, or autofluorescence. secYFP-ERD2b is expressed as bright punctae within the cytoplasm of the cells. **B.** pTASH12 expression in the root cortex. Although Aleu-RFP expression varies, consistent labelling of the vacuoles is observed. secYFP-ERD2b expression also varies across the cells, with some cells expressing very weak punctae, and some cells expressing punctae with additional cytoplasm localisation, which may be autofluorescence. **C.** The expression of pTASH12 in the vascular cylinder. Aleu-RFP is brighter in the vascular region than surrounding cells and Aleu-RFP stripes are also observed across the cells (white arrows). Negative staining of the nucleus is observed for Aleu-RFP, supporting vacuole localisation. There is poor secYFP-ERD2b expression, with only autofluorescence detected in the cytoplasm of cells.

10 dpi syncytia within Arabidopsis expressing pTASH12

A. Overview of the infected root



B. Magnified image of the centre of the syncytium



C. Magnified image of cells to the right of the syncytium

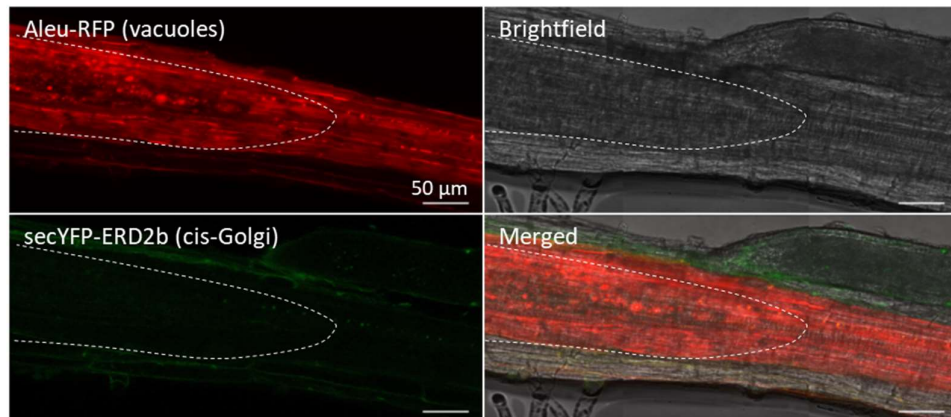


Figure 4. 7. 10 dpi syncytia in pTASH12 Arabidopsis roots. **A.** An overview of the syncytium induced by a female J3 *H. schachtii* (white arrow), showing the presence of small vacuoles and the absence of the large central vacuole within syncytial cells. No secYFP-ERD2b expression is visible in the syncytium or the surrounding cells, only autofluorescence is detected. **B.** A magnified view of the syncytium, showing Aleu-RFP vacuoles of varying sizes in the syncytium. A region in the syncytium containing no vacuoles was present (white arrow). **C.** An image of cells to the right of the syncytium, showing Aleu-RFP within the large central vacuoles of non-syncytial cells. In each image, the dashed lines demarcate the syncytium.

4.3.2.6 pTASH13, co-expressing the tonoplast marker CBL6-RFP

CBL6-RFP consistently labelled the tonoplasts of uninfected roots (**Figure 4.8**). Within infected roots, there was strong CBL6-RFP expression in cells surrounding the syncytium (**Figure 4.9A and C**). This appeared as a strong diffused signal across the whole of the cell resembling an out of focus tonoplast. This was also observed in uninfected roots (**Figure 4.8**), and supports the presence of the large central vacuoles in cells surrounding the syncytium. In syncytial cells, no CBL6-RFP expression was observed, even with higher laser power (**Figure 4.9B**). However, in cells at the periphery of the syncytium, fragmented CBL6-RFP labelled vacuoles were imaged (**Figure 4.9B and C**).

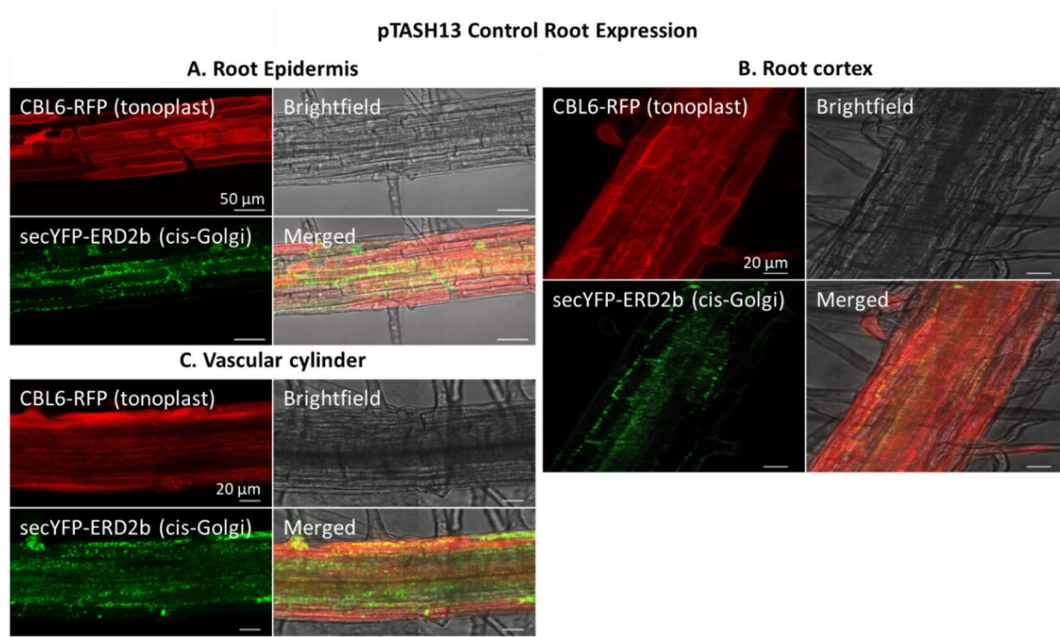
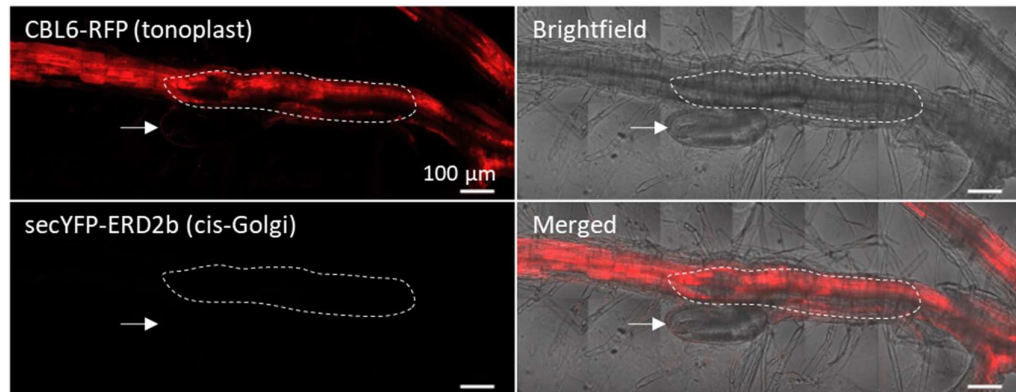


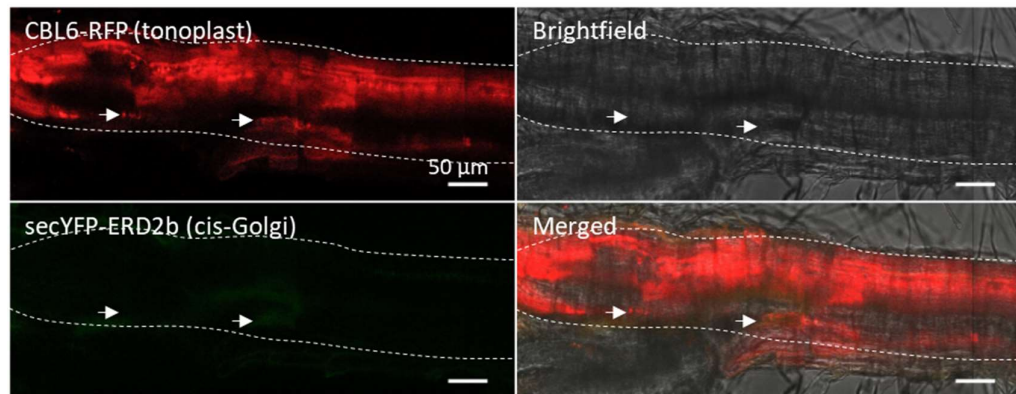
Figure 4. 8. pTASH13 expression in uninfected Arabidopsis root cells. A. Expression in the epidermis, with CBL6-RFP labelling the tonoplasts and secYFP-ERD2b expressed as punctae in the cytoplasm. Strong levels of expression of CBL6-RFP and secYFP-ERD2b are shown. **B.** pTASH13 expression in the root cortex, showing lower levels of CBL6-RFP and secYFP-ERD2b expression. CBL6-RFP can appear diffused in the cells depending on the focal plane. secYFP-ERD2b expression is undetectable in some cells. **C.** The expression in the vascular cylinder, showing reduced clarity of both markers.

17 dpi syncytia within *Arabidopsis* expressing pTASH13

A. Overview of the infected root



B. Magnified image of the centre of the syncytium



C. Magnified image of cells to the left of the syncytium

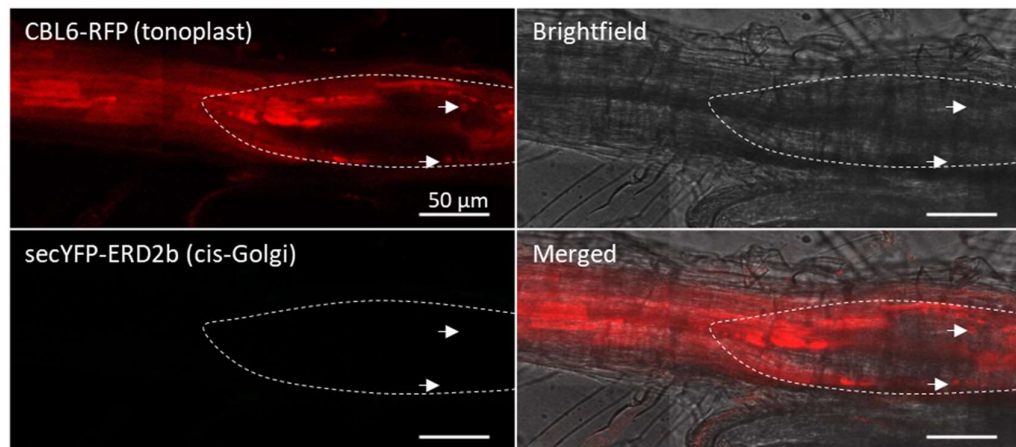


Figure 4. 9. The expression of pTASH13 within *Arabidopsis* syncytia induced by *H. schachtii*, at 17 dpi. A. An overview of the syncytium, showing CBL6-RFP expression in the tonoplast of uninfected roots to the left of the syncytium and no CBL6-RFP expression in the syncytium. secYFP-ERD2b expression is undetectable in the root, in both uninfected and infected regions. The nematode is labelled with a white arrow. **B.** A magnified image of the syncytium. In cells at the periphery of the syncytium, some fragmented CBL6-RFP labelled vacuoles are observed (white arrows). **C.** A magnified image of cells to the left of the syncytium, further showing the small CBL6-RFP vacuoles (white arrows) at the syncytium's periphery. In each image, the dashed lines demarcate the syncytium.

4.3.2.7 pTASH10, co-expressing the TGN marker RFP-SYP61

The expression of the TGN marker RFP-SYP61 was comparable in uninfected cells of infected and control roots: only weak punctae were visible, and RFP-SYP61 also partially localised to the plasma membrane (**Figures 4.10 and 4.11**), which appeared as a diffused RFP signal when imaging the cell surface (**Figure 4.10A and C**). However, no RFP-SYP61 punctae were visible in cells directly bordering the syncytium, with only plasma membrane fluorescence observed (**Figure 4.11A and C**). In contrast to uninfected cells, no RFP-SYP61 expression was detected in the syncytium (**Figure 4.11B**).

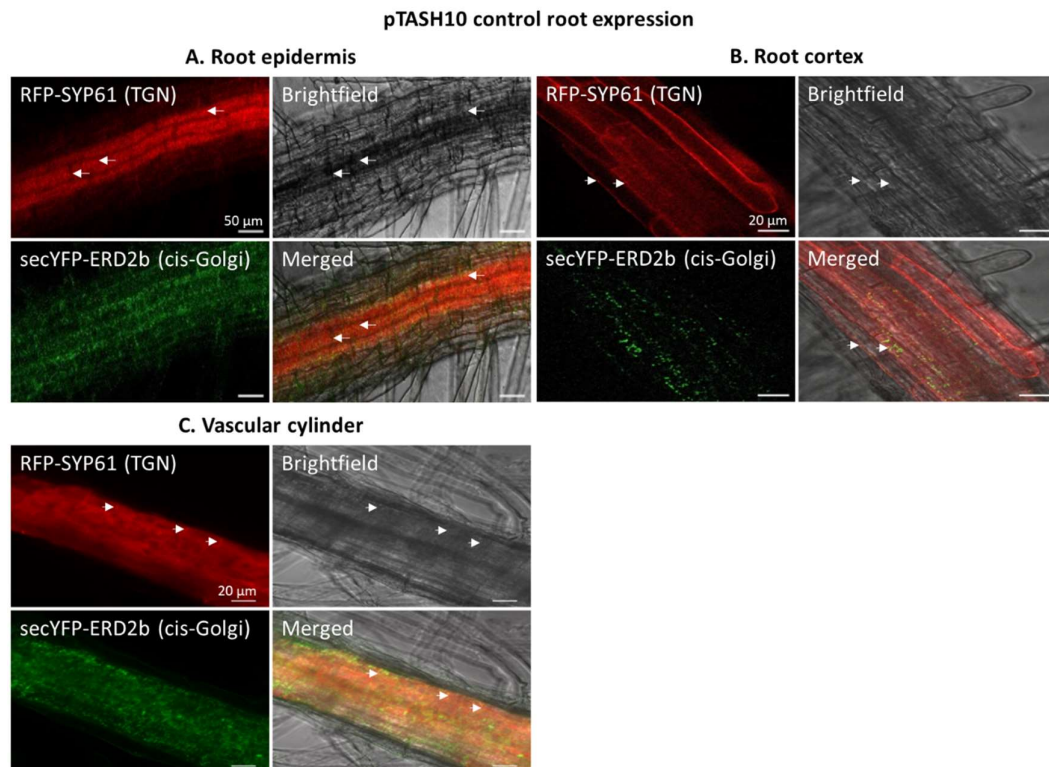
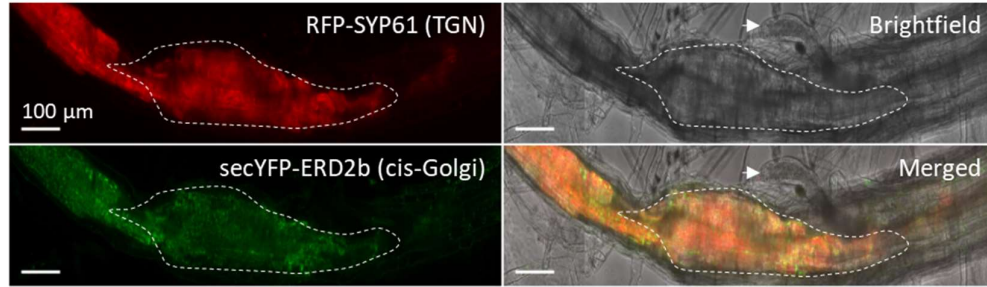


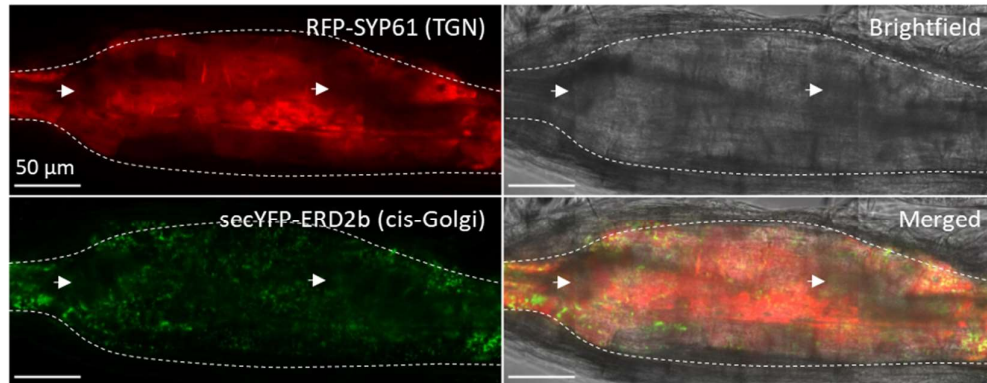
Figure 4. 10. The expression of pTASH10 in uninfected Arabidopsis root cells. A. Expression in the epidermis. For RFP-SYP61, although some weak punctae are visible (white arrows), a strong RFP signal is diffused throughout cells. For secYFP-ERD2b, weak expression is observed, with auto fluorescence in the cytoplasm due to high laser power. **B.** Expression in the root cortex. For RFP-SYP61, punctae are weak (white arrows), with partial localisation to the plasma membrane. **C.** Expression at the centre of the root. For RFP-SYP61, strong plasma membrane localisation of is observed (white arrows). secYFP-ERD2b punctae are expressed, with YFP auto fluorescence observed due to high laser power. Punctae are less visible at the centre of the root, compared to cortical and epidermal cells.

12 dpi syncytia within *Arabidopsis* expressing pTASH10

A. Overview of the infected root



B. Magnified image of the syncytium



C. Magnified image of cells to the left of the syncytium

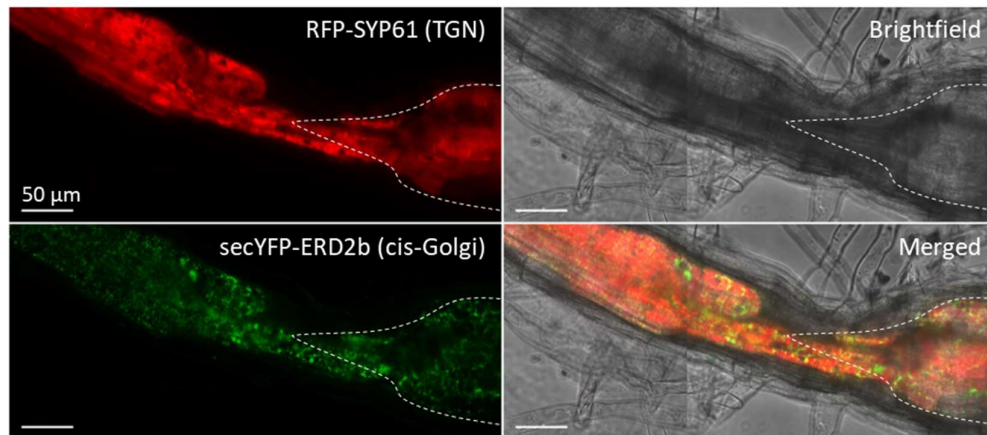


Figure 4. 11. The expression of pTASH10 within *Arabidopsis* syncytia induced by *H. schachtii*, at 12 dpi. **A.** An overview of the syncytium, showing the nematode to the right of the root (white arrow). **B.** A magnified image of the syncytium, showing two regions containing no marker expression (white arrows). In cells surrounding these marker-free regions, marker expression is typical of uninfected cells, with secYFP-ERD2b localising to punctae and RFP-SYP61 diffused across the whole cell, indicating plasma membrane localisation. **C.** A magnified image of cells to the left of the syncytium, with marker expression typical of uninfected cells. In each image, the dashed lines demarcate the syncytium.

4.3.2.8 pTASH3, co-expressing the LPVC marker RFP-Rha1

The expression of RFP-Rha1 was variable in uninfected pTASH3 roots. For example, in epidermal and cortical cells, RFP-Rha1 labelled punctate structures, in addition to the large central vacuoles and tonoplasts (**Figure 4.12A and B**). Within infected roots, cells surrounding syncytia had RFP-Rha1 expression comparable to that of uninfected cells, with large central vacuoles and punctate structures labelled (**Figure 4.13A and B**). Within the syncytium itself, no RFP-Rha1 expression was imaged, apart from punctae at the periphery of the syncytium which resembled fragmented vacuoles (**Figure 4.13C**).

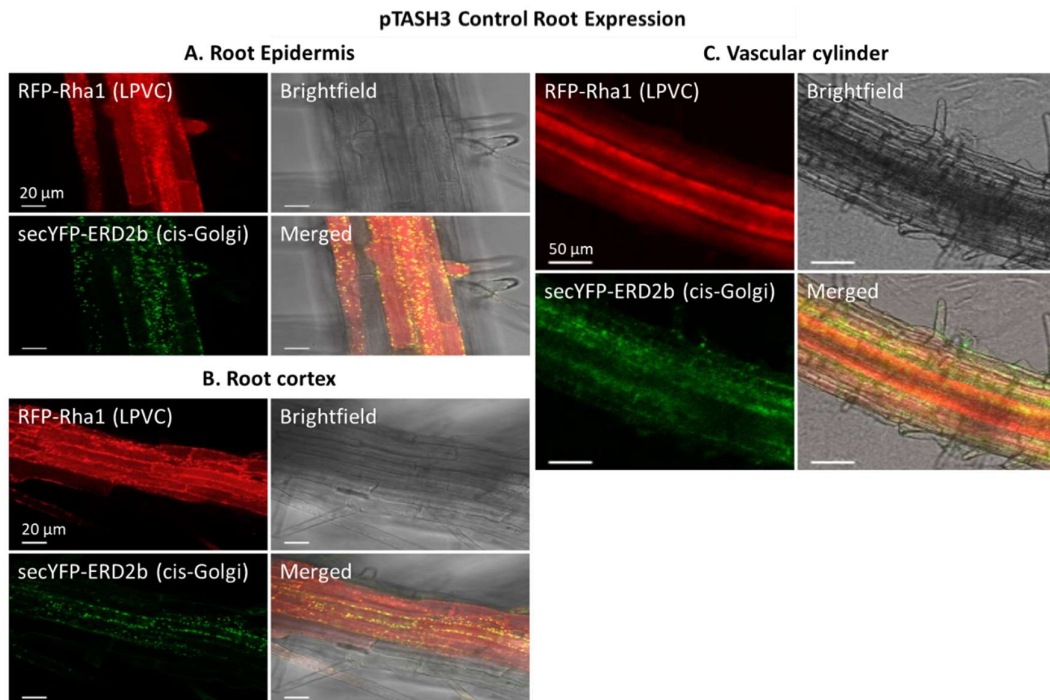
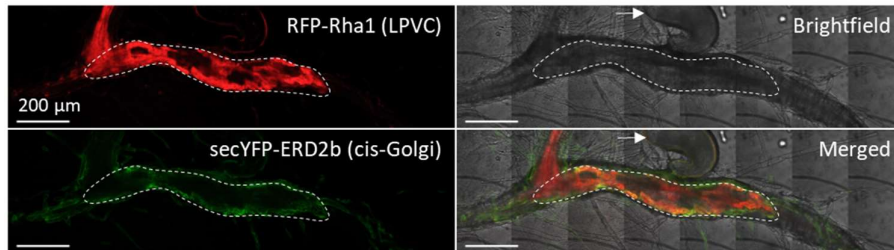


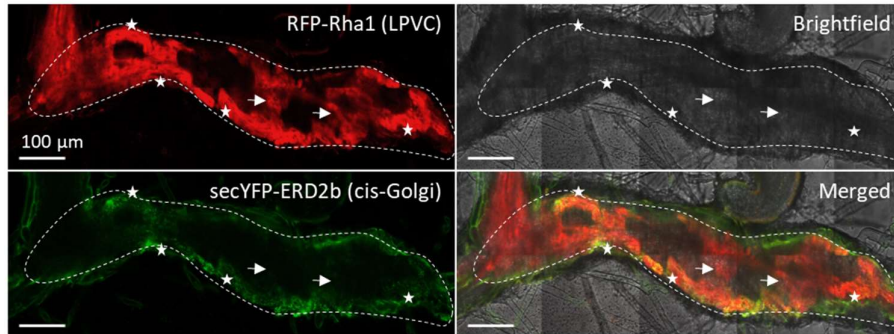
Figure 4. 12. The expression of pTASH3 in uninfected Arabidopsis root cells. A. Expression in the epidermis. For RFP-Rha1, LPVC punctae are present in the cytosol, with also strong vacuolar leakage and weak tonoplast localisation observed. There is consistent secYFP-ERD2b expression across the cells, with abundant punctae in the cytoplasm. **B.** Expression in the root cortex. For both markers, expression is similar to that in the epidermis. RFP-Rha1 punctae are visible, with additional vacuole and tonoplast localisation, and abundant secYFP-ERD2b punctae. **C.** Expression at the centre of the root. For RFP-Rha1, only a diffused RFP signal in the vacuoles is imaged, with no punctae visible. For secYFP-ERD2b, expression is weaker compared to the cortex and the epidermis. Although some punctae are visible, there is a diffused YFP signal present in the cytoplasm of cells.

18 dpi syncytia within *Arabidopsis* expressing pTASH3

A. Overview of the infected root



B. Magnified image of the centre of the syncytium



C. Magnified image of cells bordering the syncytium

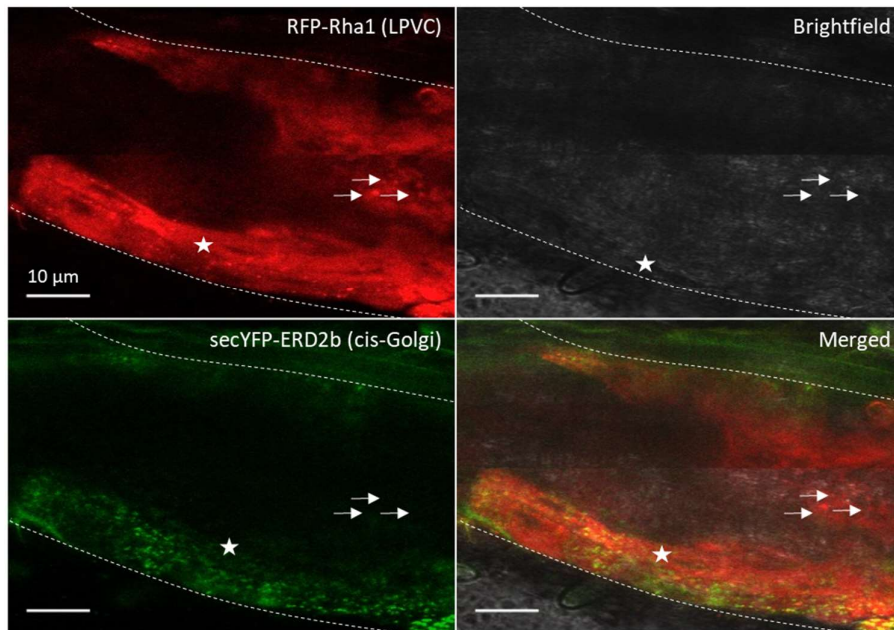


Figure 4. 13. The expression of pTASH3 within *Arabidopsis* syncytia induced by *H. schachtii*, at 18 dpi. **A.** An overview of the syncytium induced by a female J4 worm (white arrow). Due to the difference in focal planes, marker expression in the root cells next to the syncytium is unable to be visualised. **B.** A magnified image of the syncytium, showing no marker expression in syncytial cells. In some cells directly bordering the syncytium, there are punctate secYFP-ERD2b (stars). In cells at the periphery of the syncytium, RFP-Rha1 punctae are present, and there are no secYFP-ERD2b punctae (arrows). **C.** A magnified image of cells surrounding the syncytium, further showing marker expression typical of uninfected cells directly bordering the syncytium (star). At the syncytium's periphery, cells with fragmented RFP-Rha1 but no secYFP-ERD2b expression are shown (arrows). In each image, the dashed lines demarcate the syncytium.

4.3.2.9 pTASH5, co-expressing the PVC marker RFP-BP80

In the uninfected roots of pTASH5 lines, RFP-BP80 was only visualised in the vacuoles. No punctate structures, typical of PVC localisation, were visualised at the three tissue depths (Figure 4.14). This was also true for non-syncytial cells in infected roots, including those directly next to the syncytium (Figure 4.15A and C). Despite the vacuole localisation of RFP-BP80 in uninfected roots, no punctate structures resembling fragmented vacuoles were observed in the syncytium (Figure 4.15B).

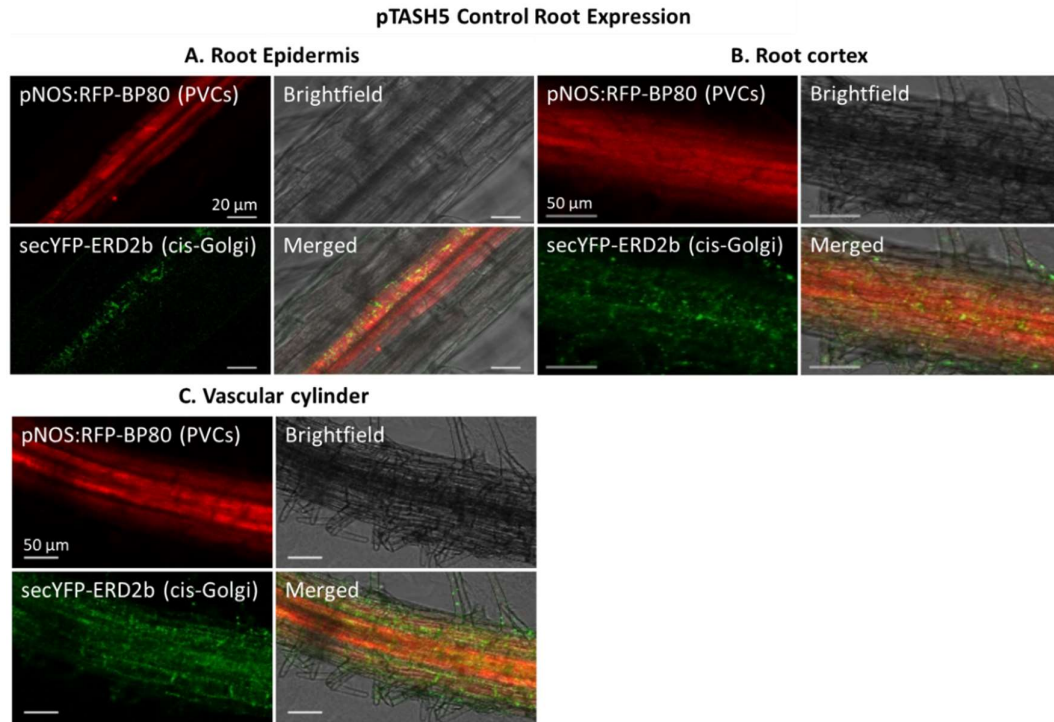
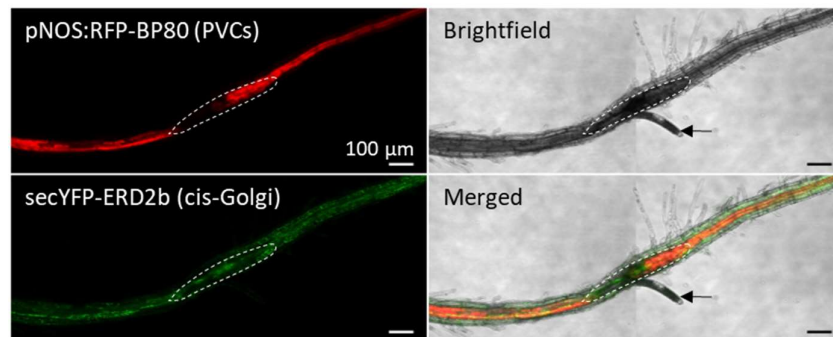


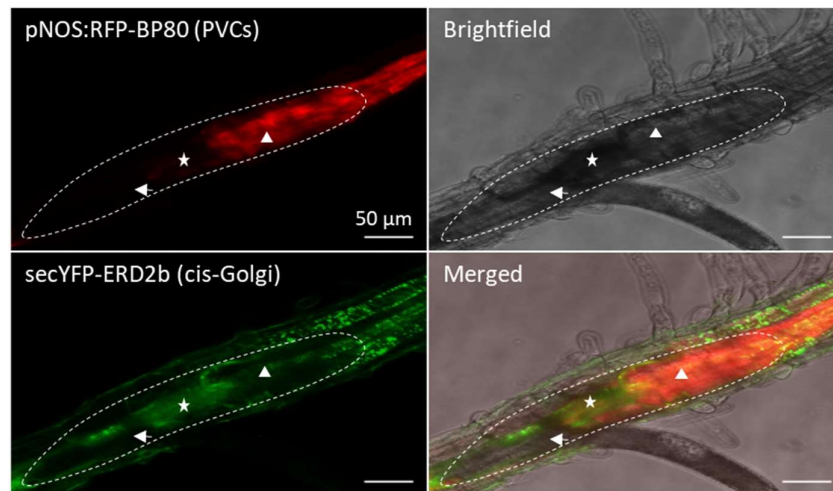
Figure 4. 14. The expression of pTASH5 in the roots of uninfected Arabidopsis. **A.** Expression in the epidermis. RFP-BP80 is expressed in the vacuoles, with no PVC punctae observed. secYFP-ERD2b expression appears as normal, with punctae in the cytoplasm. **B.** Expression in the root cortex. RFP-BP80 is consistently expressed in the vacuoles of the cells. secYFP-ERD2b is weak, with autofluorescence visible in the cytoplasm of cells. **C.** Expression at the centre of the root. RFP-BP80, expressed in the vacuoles, shows brighter expression at the vascular cylinder. secYFP-ERD2b expression was similar to the cortical cells, showing weak expression of punctae and autofluorescence in the cytoplasm.

13 dpi syncytia within *Arabidopsis* expressing pTASH5

A. Overview of the infected root



B. Magnified image of the centre of the syncytium



C. Magnified image of cells to the right of the syncytium

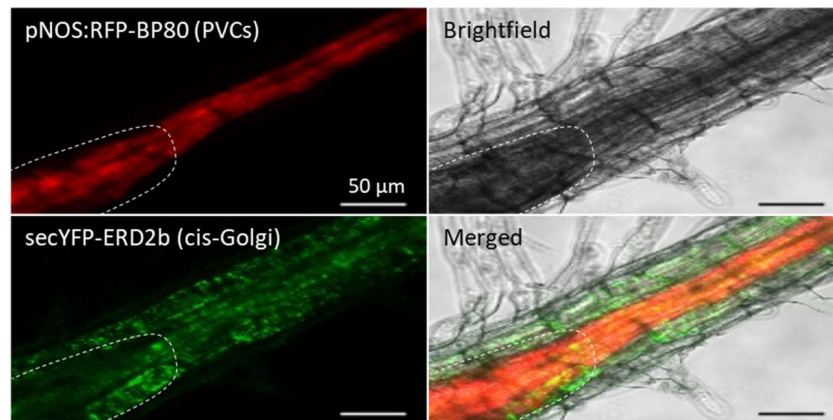


Figure 4. 15. The expression of pTASH5 within *Arabidopsis* syncytia induced by *H. schachtii*, at 13 dpi. A. An overview of the syncytium induced by a J3 worm (arrow). RFP-BP80 is only expressed in the vacuoles of uninfected root cells at either side of the syncytium. **B.** A magnified image of the syncytium. RFP-BP80 is expressed in the vacuoles of cells to the right of the worm (triangle), although there are no secYFP-ERD2b punctae visible. Within the syncytium, there is no expression of RFP-BP80, although there is secYFP-ERD2b autofluorescence (star). The worm lies on top of the root (arrow), blocking marker visualisation in some syncytial cells. **C.** A magnified image of cells to the right of the syncytium, to further show marker expression in uninfected cells. RFP-BP80 is expressed in the vacuoles, and secYFP-ERD2b punctae are present. In each image, the dashed lines demarcate the syncytium.

4.4 Discussion

4.4.1 General observations using fluorescence microscopy in *Arabidopsis* syncytia

General observations could be made for the confocal microscopy of *Arabidopsis* syncytia, including weaker marker resolution in deeper tissues such as the vascular region, compared to cortex and epidermal cells, which are discussed below.

4.4.1.1 Poor marker resolution at increased tissue depths

In contrast to the preliminary T₂ line screening in **Chapter 3**, this chapter aimed to obtain a more accurate depiction of the marker expression within the roots of each marker line. Decreased image resolution was observed in the cortical and vascular regions of the roots compared to the epidermis. This was a limitation of the confocal microscopy techniques used. To overcome this, tissue clearing and other fluorescent microscopy techniques such as two-photon excitation microscopy could be attempted (Musielak et al, 2016). For example, the tissue clearing solution ClearSee and two-photon microscopy have previously been used to image the cell walls in soybean syncytia induced by *H. glycines* (Ohtsu et al, 2017). Imaging transverse sections of the root could be another method to increase marker resolution in the vascular region. This has been used for the fluorescence microscopy of syncytia using cell wall antibodies, with high resolution observed throughout the syncytium (Levin et al, 2020; Zhang et al, 2017c). Therefore, the sectioning and clearing of infected root tissue within pTASH *Arabidopsis* lines should be conducted in future experiments to improve the resolution of the secretory pathway markers.

4.4.1.2 Regions of no marker expression in the syncytia

For all marker lines imaged apart from the ER marker line GFP-HDEL and the vacuole marker line Aleu-RFP, there was undetectable expression within the syncytium. This was a significant result, suggesting that key aspects of subcellular trafficking, such as COPI and COPII cycling, secretion and vacuolar sorting were altered within syncytia. However, for some lines, weak marker expression was detected not only in syncytia but in the whole root system of the plant. This reflects the variability in marker expression within plants of the same T₂ line and could be solved with imaging syncytia across a larger number of plants, as syncytia from only five plants was used in the analysis. However, the sample size was limited due to issues with contamination of the *H. schachtii* J2s in tissue culture. Not only did microbial contamination limit sample sizes, but it could also influence the secretory pathway of *Arabidopsis* roots. Therefore, to improve the sample

size and increase the validity of marker expression, aseptic culturing of *H. schachtii* should be conducted in future experiments.

Regions of no marker expression observed only in syncytia, with normal expression throughout the rest of the root, was unlikely to be due to decreased promoter activity in syncytial cells compared to uninfected root tissue. The CaMV35S promoter is the best studied of those used here in relation to syncytial expression. There is conflicting information on the activity of this promoter in syncytia. Although several studies report detectable expression of genes controlled by 35S in syncytia induced by J3 and J4 stage *H. schachtii* (Siddique et al, 2015), there are also reports of downregulation within syncytial cells at these time stages. For example, 35S:GFP in Arabidopsis syncytia induced by *H. schachtii* showed a significant decrease in fluorescence between 7 and 25 dpi (Urwin et al, 1997). Furthermore, undetectable expression of 35S:gusA was observed after 10 dpi in Arabidopsis syncytia induced by *H. schachtii* (Goddijn et al, 1993). However, the CaMV35S promoter controlled the expression of several markers that were imaged, including Aleu-RFP and GFP-HDEL, which showed detectable expression in the syncytium. This disproves the hypothesis that downregulation of the 35S promoter inherently caused a lack of fluorescence in syncytia.

There is less information on the syncytial activity of the two other promoters used within the marker lines, TR2 and pNOS. The TR2 promoter controlled the expression of the common cis-Golgi marker secYFP-ERD2b, and the pNOS promoter controlled the expression of the PVC marker RFP-BP80. However, the expression of TR2:GFP was observed in potato roots infected with *G. rostochiensis* at up to 13 dpi (Goverse et al, 1998), and pNOS:GUS expression was detectable in Arabidopsis syncytia induced by *H. schachtii* at 6 dpi (Barthels et al, 1997). Nevertheless, alternative promoters to the TR2 and pNOS promoters could be used to generate further fluorescent Arabidopsis lines. For instance, the promoter regions of the Arabidopsis genes *AtSUC2* (Juergensen et al, 2003; Hofmann and Grundler, 2006) and *Pdf2.1* (Siddique et al, 2011) have shown high levels of expression in syncytia.

4.4.2 The ER and Golgi in syncytia

4.4.2.1 The expression of the ER marker GFP-HDEL

GFP-HDEL was expressed in syncytia, supporting the high abundance of ER observed using EM (Golinowski et al, 1996). A potentially significant result was the inability to image the movement of GFP-HDEL in syncytial cells. The ER is a highly dynamic organelle, with the remodelling of tubules and cisternae essential to many cellular processes, including immune responses to fungi and oomycetes (Hardham et al, 2008). Therefore, cyst nematodes may disrupt ER remodelling in syncytia to suppress immune

responses. This may occur via disruption to rapid bulk streaming along the actin cytoskeleton (Lichtscheidl and Url, 1990), with disorganisation of the actin network previously documented in syncytia (de Almeida Engler et al, 2010). To confirm and further characterise changes to the ER dynamics in syncytia, the imaging software AnalyzER (Pain et al, 2019) could be used on Arabidopsis GFP-HDEL lines over the time course of syncytial formation.

Additionally, ER bodies were observed in both syncytial and uninfected cells. ER bodies are induced upon wounding and contain high levels of β -glucosidases that are involved in plant defence (Yamada et al, 2020). *PYK10*, the gene encoding the most abundant β -glucosidase in Arabidopsis ER bodies, is highly upregulated at 10 hpi and 48 hpi in syncytia induced by *H. schachtii* (Siddique et al, 2021). This suggests that these structures may increase in abundance during early infection as a response to wounding caused by nematode migration. These structures have not been described by previous EM studies of Arabidopsis syncytia induced by *H. schachtii*. However, most ultrastructural studies of Arabidopsis syncytia were carried out before the first reports of ER bodies in plant cells (Grundler et al, 1998; Golinowski et al, 1996; Sobczak et al, 1997; Gunning, 1998; Matsushima et al, 2003). Nevertheless, more recent 2D EM studies of Arabidopsis syncytia have identified dilated regions of ER within syncytia, which could represent ER bodies (Baranowski et al, 2019).

To confirm the presence of ER bodies in syncytia, fluorescence microscopy techniques that can image increased tissue depths, such as two-photon microscopy are required. Not only would this technique identify ER bodies, it would confirm previous EM observations of the ER including proliferated ER membranes and the wrapping of the ER around the nematode's stylet. The proliferation of the ER is hypothesised to be a mechanism of ER stress during plant defence responses (Eichmann and Schäfer, 2012), and the aggregation of the ER around the stylet is hypothesised to be a feature of pathogenicity to directly provide the nematode with essential proteins and lipids (Grundler and Böckenhoff, 1997). Therefore, further microscopy would provide more information on the ultrastructure and dynamics of the ER, to help to uncover the complex role of this organelle within plant-cyst nematode interactions.

4.4.2.2 secRFP-p24aTM expression in syncytia

As discussed in the previous chapter, the ER marker secRFP-p24aTM labelled both the ER and the vacuoles in the roots of Arabidopsis lines. As the large central vacuole occupied the majority of space in non-syncytial imaged cells, this hindered the ability to visualise the ER network. However, even in the absence of a central vacuole, there was no distinct labelled ER network in the syncytium, which could be caused by a defect in

the trafficking of p24 δ 5. This protein is a cargo receptor that traffics between the ER and Golgi within COPI and COPII vesicles (Montesinos et al, 2014). Therefore, defects in COPI and COPII cycling may occur in syncytia.

4.4.2.3 secYFP-ERD2b expression in syncytia

EM studies of syncytial cells have described the presence of abundant Golgi which have ultrastructural evidence of high biosynthetic activity (Fudali et al, 2007; Endo, 1991; Melillo et al, 1990). This may reflect increased synthesis of cell wall components and antimicrobial compounds within infected cells. However, in all marker lines imaged, there was no secYFP-ERD2b expression within syncytia. Therefore, this fluorescent marker was unable to support previous EM evidence of increased Golgi bodies. In some cases, a lack of secYFP-ERD2b expression was also detected in cells bordering the syncytium. In these cells, the large central vacuoles were labelled. This could suggest that alterations in subcellular trafficking, such as COPI and COPII cycling, occur in cells bordering the syncytium, despite no changes to vacuole morphology yet occurring. Other changes such as mitosis are suggested to occur in cells prior to their incorporation into the syncytium (de Almeida Engler et al. 1999). Therefore, it is plausible that subcellular changes altering the trafficking or functioning ERD2b could also occur outside the syncytium.

4.4.2.4 The expression of ER and Golgi related genes in syncytia

ER stress

ER stress has been hypothesised in syncytia from the increased expression of protein synthesis genes and observations of dilated ER cisternae (Kim et al, 2012; Endo, 1991; Vitale and Boston, 2008). ER stress related genes, *BIP2*, *CRT1* and *CRT2* were significantly differentially expressed in syncytia and followed a similar expression pattern; upregulated only during early infection. These three genes encode ER-resident protein folding chaperones. This suggests that ER stress may be an early response during infection, which coincides with previous ultrastructural evidence of ER proliferation at 24 hpi (Golinowski et al, 1996). Furthermore, the downregulation of calreticulins *CRT2* and *CRT3* as syncytia develop could be a feature of pathogen manipulation, with these two genes also having a role in Ca²⁺ homeostasis, and subsequent plant defence responses associated with calcium signalling (Michalak et al, 1999). Calreticulin function is modulated by another cyst nematode species, *H. avenae*. This species secretes a calreticulin effector protein, HaCRT1, that is hypothesised to modulate calcium levels within the host ER lumen to suppress the cell death response (Liu et al, 2020). Therefore, *H. schachtii* effectors may act similarly to HaCRT1 to suppress ER-induced plant cell death.

Other ER stress response genes showed varied expression patterns within syncytia, including those that were downregulated during early infection then upregulated during later stages of infection. This includes *EBS1*, which is involved in the sensing of misfolded proteins (Deng et al, 2013), and *bZIP17* and *IRE1a*, which are components of UPR signalling (Kim et al, 2018). This could suggest that the induction of UPR occurs during syncytial development, as a result of increased protein synthesis.

Although the marker lines used in this chapter were unable to quantify ER stress, the fluorescent dye Proteostat® could be used in future experiments. Proteostat® has previously been used to detect ER stress in *Arabidopsis* roots, with the dye intercalating with mis-folded or polyubiquitinated proteins to emit fluorescence (Cho and Kanehara, 2017). Additionally, chemical treatments could be used to test the role of ER stress in syncytia. For example, tunicamycin could be used, which is a N-glycosylation inhibitor that induces ER stress, resulting in PCD and the production of reactive oxygen species including H₂O₂ (Yang et al, 2014; Watanabe and Lam, 2008). Although tunicamycin has mostly been used to study the role of the ER in abiotic stress, such as photooxidative stress (Beaugelin et al, 2020) and salt stress (Aydemir et al, 2020), it has been used to elucidate the role of ER stress in response to several plant pathogens, including the fungal pathogen *Colletotrichum lagenarium* (Sticher and Metraux, 2000). Therefore, tunicamycin could be used to study role of ER stress related defence responses in resistance to cyst nematodes.

ER-Golgi trafficking

As previously mentioned, the lack of secRFP-p24aTM and secYFP-ERD2b expression in *Arabidopsis* syncytia could reflect altered COPI and COPII vesicle trafficking between the ER and Golgi. This is supported by the gene expression analysis of several COPI and COPII trafficking components. For example, the COPI coatomer subunits $\alpha 1$ -COP and $\gamma 1$ -COP were significantly differentially expressed, with these two genes and the other COPI coatomer subunit, $\alpha 2$ -COP, having a similar expression pattern. These genes were upregulated the most during late infection, with log₂FC values peaking at 12 dpi female. A second cluster of ER-Golgi trafficking genes followed a different expression pattern, upregulated at 10 hpi, with downregulation at all further life stages, the most downregulated at 12 dpi female. Genes within this cluster include p2465 and ERD2b, supporting altered regulation of COPI and COPII cycling in syncytia, which could explain the lack of secRFP-p24aTM and secYFP-ERD2b expression. However, the contrasting expression patterns of COPI coatomer subunits and other ER-Golgi trafficking genes requires further investigation, to more thoroughly understand the role of the early secretory pathway during cyst nematode infection.

COG genes

To further elucidate the role of Golgi-mediated trafficking in syncytia, the expression of COG subunits were studied. The COG has several roles in plant cells, involved in glycosylation (Smith and Lupashin, 2009), Golgi structure (Rui et al, 2020), and retrograde trafficking (Tan et al, 2016). Although the COG complex is involved in soybean resistance to *H. glycines* (Klink et al, 2022; Klink et al, 2021; Lawaju et al, 2020), the role of the COG is yet to be investigated in susceptible plant-cyst nematode interactions such as Arabidopsis- *H. schachtii*. Therefore, the eight COG subunits were chosen for gene expression analysis.

Of the COG subunit genes analyzed, *COG5* was significantly differentially expressed, and *COG2*, *COG3* and *COG7* followed a similar expression pattern to this gene. These four COG subunits were downregulated during early infection then upregulated at the 12 dpi female and male life stages. This supports the role of the COG within late stages of syncytial development in Arabidopsis, and provides temporal expression of these genes throughout syncytial development, which hasn't before been analysed.

4.4.3 Post-Golgi organelles in syncytia: the TGN, PVCs and LPVCs

4.4.3.1 The expression of the TGN marker RFP-SYP61

No RFP-SYP61 expression was detected in syncytia, despite expression observed in surrounding cells. Consequently, no characterisation of the structure or abundance of the TGN in syncytia could be provided. This organelle has previously been unable to be characterised using EM (Baranowski et al, 2019). Nevertheless, the lack of RFP-SYP61 within the syncytium could indicate altered subcellular trafficking. Similar observations have also been made for cyst nematode resistance genes in soybean. For instance, the localisation of Syp61-mCherry was shown to become diffused when co-infiltrated with the soybean α -SNAP protein GmSNAP18, which confers resistance to *H. glycines* (Bayless et al, 2016). GmSNAP18 has been hypothesised to disrupt vesicle trafficking in the host to promote resistance (Bekal et al, 2015). Similarly, an Arabidopsis SNAP protein has been identified, AtSNAP2, which is the target of a *H. schachtii* effector, HsSNARE1 (Zhao and Liu, 2022). This supports that altered vesicle trafficking may occur within Arabidopsis infected with *H. schachtii*, which could account for the disruption to the localisation of RFP-SYP61 in the syncytium.

4.4.3.2 The PVC and LPVC markers in Arabidopsis syncytia

Roots imaged in this chapter showed complete vacuole localisation of the PVC marker RFP-BP80. This was in contrast to the roots imaged for the transgenic line screening in **Chapter 3**, with PVC punctae in addition to vacuole localisation observed. The roots

imaged in this chapter were several weeks older than those imaged in **Chapter 3**, therefore the complete vacuole localisation of RFP-BP80 could be due to increased cell stress as the plants matured. As RFP-BP80 is synthesised in the ER (Niemes et al, 2010), overexpression of this marker, in addition to environmental stress, may induce ER-phagy and subsequently result in vacuole localisation of the fluorescent marker.

No RFP-BP80 labelled vacuoles were observed in the syncytium. As RFP-BP80 is trafficked through the conventional ER-Golgi-TGN-PVC vacuolar trafficking route (Niemes et al, 2010), alterations to the trafficking between any of these compartments could prevent RFP-BP80 from localising to the vacuoles. This could support previous evidence of unconventional fusion of the PVCs with the plasma membrane in syncytia within EM studies; indicated from the presence of paramural bodies (Golinowski et al, 1996). PVC fusion with the plasma membrane is a common plant immune response against biotrophic pathogens to secrete defence-related compounds (Wang et al, 2014a; An et al, 2006b). Therefore, in syncytial cells, PVC markers may be trafficked to the plasma membrane rather than the vacuoles, preventing their recycling back to the Golgi (daSilva et al, 2006). This could be tested further with the use of alternative PVC markers such as ARA7 and SYP22 (Cui et al, 2016; Nodzyński et al, 2013). Additionally, alternative imaging techniques such as 3D electron tomography or immunogold EM could be used to complement the fluorescence microscopy.

4.4.3.3 The expression of the LPVC marker RFP-Rha1 in syncytia

In uninfected roots, RFP-Rha1 localised to punctae, in addition to the tonoplast and vacuoles. However, within the syncytium, RFP-Rha1 labelled structures which resembled small vacuoles that were present only at the periphery. As RFP-Rha1 is hypothesised to traffic between PVCs and the tonoplast (Lee et al, 2004), lack of RFP-Rha1 expression in the syncytium could indicate altered vacuolar trafficking, which could be due to the unconventional fusion of the PVCs with the plasma membrane.

4.4.3.4 The expression of post-Golgi trafficking components in syncytia

Golgi-PM trafficking

Trafficking between the Golgi and PM may function in syncytia to increase the secretion of defence related or cell wall related compounds. To test this hypothesis, the expression of several Golgi-PM trafficking components was analysed, including syntaxins, RABA1 GTPases and adaptin proteins. Syntaxins in particular have a previously characterised role in plant defence (Robatzek, 2007), with *SYP121* upregulated in a resistant soybean line infected with *H. glycines* (Kandoth et al, 2011). Similarly, *SYP61* was upregulated at 12 dpi female, which could support a role of syntaxins in a defence response to *H.*

schachtii. However, all other Golgi-PM trafficking genes assigned to clusters were upregulated during early infection, then subsequently downregulated. This included the significantly differentially expressed *RABA1e* and non-significant genes such as *RABA1a*, *BS14A*, the syntaxins, *SYP71*, *SYP122* and *SYP132*, and *SYP121*. This contrasts the upregulation of *SYP121* in soybean resistance to *H. glycines* (Kandath et al, 2011), and could suggest the initiation of defence responses during early infection that are subsequently suppressed by the pathogen as infection progresses.

Vacuolar sorting components

With the loss of the large central vacuole in syncytial cells, it was hypothesised that subcellular components involved in vacuolar sorting would be differentially expressed in syncytia. *MAG1* and *Rha1* were significantly differentially expressed, although *SYP21* also had a similar expression pattern to these two genes; upregulated at 10 hpi then downregulated at all other life stages. This suggests that vacuolar sorting decreases as syncytia develop, which is in line with loss of the large central vacuole in syncytial cells. However, *GRV2* was a significantly differentially expressed gene with an opposing expression profile to the other vacuolar sorting genes, downregulated during early infection then upregulated from 12 dpi onwards. *GRV2* contributes towards vacuolar morphology, with mutants displaying enlarged vacuoles (Silady et al, 2008). Therefore, this gene may function in syncytia to support vacuole fragmentation.

4.4.4 The vacuoles in syncytia

4.4.4.1 The expression of the vacuole marker Aleu-RFP

Aleu-RFP labelled abundant small vacuoles within syncytia, supporting several ultrastructural studies using EM (Baranowski et al, 2019; Golinowski et al, 1996). Although lytic vacuoles have been identified in syncytia using immunogold EM (Baranowski et al, 2019), further investigation is required to understand the abundance of lytic vacuoles in comparison to protein storage vacuoles (PSVs) in syncytia. As PSVs are a nutrient storage compartment for the cell, their characterisation would provide more insight into the metabolic state and subcellular trafficking processes within syncytia. Additionally, further investigation into vacuole morphology during early syncytial development is required. Although fragmented vacuoles have been observed in syncytia as early as 24 hpi (Golinowski et al, 1996), the dynamics of vacuolar changes during early syncytial development are yet to be characterised, with changes potentially occurring prior to incorporation of cells into the syncytium.

This is supported by the observation of small vacuole-like structures at the periphery of the syncytium in several of the marker lines. Additionally, the confocal images suggested that larger vacuoles were present on the periphery of the syncytium, with smaller

vacuoles closer to the centre. Such spatial cellular differences have not previously been documented within syncytia and should be investigated further. This could suggest that a gradual reduction in vacuole size occurs as syncytial cells mature, with younger, newly incorporated syncytial cells present on the periphery.

4.4.4.2 The expression of the tonoplast marker CBL6-RFP

Within the syncytia, CBL6-RFP labelled small vacuoles, only at the periphery of the syncytium. These were a similar size to the Aleu-RFP labelled vacuoles. The lack of CBL6-RFP expression throughout the syncytium, in contrast to Aleu-RFP expression, could reflect the smaller surface area that the tonoplast occupies compared to the vacuole lumen. Other fluorescent tonoplast markers, such as the lytic vacuole marker γ TIP1 and the general vacuole marker V-ATPase subunit E have been used for immunogold transmission EM in syncytia (Baranowski et al, 2019). These have evidenced the presence of tonoplast membranes throughout the syncytium.

4.4.4.3 The expression of vacuole-related genes in syncytia

From the fragmentation of the large central vacuole, it was hypothesised that vacuole and tonoplast related genes would be differentially regulated in Arabidopsis syncytia. For this, the expression of various vacuole-related genes was analysed, including vacuolar processing enzymes and tonoplast intrinsic proteins (TIPs). Two vacuolar processing genes were upregulated during later stages of infection, β -VPE and δ -VPE, which were significantly differentially expressed. β -VPE is involved in the maturation of PSVs (Shimada et al, 2003), supporting the presence of this type of vacuole within the syncytia. δ -VPE is associated with cell death (Hatsugai et al, 2015), which could indicate the activation of this defence response in syncytia.

Several TIPs were significantly differentially expressed in syncytial cells, downregulated across all timepoints. This includes δ -TIP2;2, δ -TIP2;3, γ TIP1;1 and ϵ TIP4;1. As γ TIPs mostly localise to lytic vacuoles (Ma et al, 2004) and δ -TIPs mostly localise to PSVs (Jauh et al, 1998), it can be hypothesised that the downregulation of TIPs affects both types of vacuoles. The downregulation of these proteins in syncytia may be a feature of pathogen manipulation, as the mutation of γ -TIP;1 in Arabidopsis increased susceptibility to *H. schachtii* (Baranowski et al, 2019). The downregulation of TIPs in Arabidopsis syncytia is hypothesised to restrict the water loss in syncytial cells, increasing turgor pressure and possibly increasing the osmosis of sugars from the phloem into the syncytium (Baranowski et al, 2019). Additionally, another tonoplast membrane protein, the calcium sensor CBL6, was downregulated in Arabidopsis across all life stages. As the vacuole is the largest subcellular storage compartment for Ca^{2+} , alterations in CBL6 expression could affect calcium signalling to potentially alter plant defence responses.

This is supported by the role of other CBL proteins, including CBL10, in plant resistance (Sardar et al, 2017). Therefore, the downregulation of CBL6 in Arabidopsis may be induced by the pathogen to suppress calcium-mediated defence responses.

4.4.5 Conclusions

The fluorescence microscopy of Arabidopsis syncytia across the marker lines, combined with the expression analysis of secretory pathway genes has provided novel insight into the endomembrane system during cyst nematode infection.

The key findings of this chapter include:

- No fluorescent Golgi, TGN, PVCs or LPVCs were detected in Arabidopsis syncytia, which could reflect altered subcellular trafficking
- The fragmented vacuoles labelled by Aleu-RFP support previous EM observations of vacuole morphology
- Gene expression analysis supports altered COPI and COPII cycling, altered post-Golgi trafficking to the plasma membrane and altered vacuolar sorting in syncytia
- Gene expression analysis has also identified novel genes and pathways which could be further studied in Arabidopsis syncytia, including ER stress and vacuole-mediated cell death

Chapter 5 Identifying novel cyst nematode effectors containing C-terminal transmembrane domains

5.1 Introduction

5.1.1 ER-targeting pathogen effectors containing a C-terminal TMD

The endoplasmic reticulum (ER) is the gateway of the secretory pathway (Hawes et al, 2015; Vitale and Denecke, 1999); a dynamic and pleomorphic network of tubules and cisternae. This organelle has several critical functions in the cell, including the production, folding and quality control of proteins, lipid biosynthesis, carbohydrate metabolism and calcium signalling (Hawes et al, 2015; Jacquemyn et al, 2017; Brandizzi et al, 2003). The ER is in close contact with several organelles including the nucleus, Golgi, endosomes, mitochondria and the plasma membrane, and extends into adjacent cells via plasmodesmata (Friedman and Voeltz, 2011; Levine and Loewen, 2006; Barton et al, 2011). Thus, the ER is essential for cellular homeostasis.

Unsurprisingly, the ER is critical for the response to plant abiotic and biotic stresses (Park and Park, 2019). Several ER-targeting plant pathogen effectors have been identified, each containing a C-terminal transmembrane domain (TMD). Tail-anchored (TA) proteins containing a single C-terminal TMD are a diverse and functionally important group of proteins (Lee et al, 2020). The C-terminal TMD of TA proteins has features that are responsible for its localisation to the target membrane. For example, the length and hydrophobicity of the TMD has been shown to distinguish transmembrane proteins targeting the ER, Golgi, plasma membrane and nucleus (Singh and Mittal, 2016). This has allowed the prediction of ER-targeting plant pathogen effectors containing a C-terminal TMD.

Screening plant pathogen effector proteins containing C-terminal TMDs with certain characteristics has successfully identified effectors that target the ER. For example, 9 out of 15 screened *Phytophthora infestans* RxLR effectors containing a single C-terminal TMD localised to the ER, with the rest localising to the Golgi or the mitochondria (Breeze et al, 2020). So far, the only identified binding partners of ER-targeting tail-anchored effectors are NAC transcription factors (TFs). NAC TFs relocalise from the ER to the nucleus during plant pathogen responses, to induce the transcription of defence-related signalling pathways (Bian et al, 2021). Currently, the set of identified C-terminal TMD effectors from *Phytophthora* spp. target NAC TFs within the ER, preventing their relocalisation to the nucleus. One example is the Pi03192 effector from *Phytophthora infestans*, which interacts with the potato NAC TFs NTP1 and NTP2 (McLellan et al, 2013). Similarly, the BLR05 and BLR09 effectors from the oomycete *Bremia lactucae*

bind to the potato NAC transcription factor LsNAC069 and prevent its nuclear localisation (Meisrimler et al, 2019). However, in addition to their interaction with NAC TFs, tail-anchored effectors may have other functions within the ER. For example, many ER-localised tail-anchored effectors from the oomycete species *Phytophthora infestans*, *Plasmopara halstedii* and *Hyaloperonospora arabidopsidis* did not bind to any of the studied Arabidopsis NAC TFs (Breeze et al, 2020).

5.1.2 Evidence of ER-targeting effectors in cyst nematodes

The ER is likely to be crucial for the plant response to cyst nematodes, with evidence of increased ER activity in syncytia (Kim et al, 2012; Kandoth et al, 2011). This could reflect the increased synthesis of defence-related compounds, or the increased metabolic activity in syncytia. Increased ER activity in the syncytial cells is hypothesised to induce ER stress, which is supported by the observation of proliferated ER membranes, and transcriptomic evidence (Kim et al, 2012; Sobczak et al, 2009; Magnusson et al, 1991). ER stress leads to the induction of plant immune responses including plant cell death (Kørner et al, 2015), which has been shown to contribute towards resistance to *H. glycines* in soybean (Wang et al, 2020b).

There is evidence that cyst nematodes secrete ER-targeting effectors to suppress ER-mediated immune responses. For example, the *Heterodera avenae* effector HaCRT1 is a calreticulin protein that localises to the ER via a HDEL signal. HaCRT1 is hypothesised to modulate calcium levels within the host ER lumen to suppress the cell death response (Liu et al, 2020). However, it is currently unknown how nematode proteins containing ER retention signals could exit the ER of the gland cell to be secreted into the host.

A feature of other ER-localised cyst nematode effectors may be the presence of a C-terminal transmembrane domain (TMD), as is characteristic of *Phytophthora* spp. effectors targeting this organelle (Breeze et al, 2020; McLellan et al, 2013; Meisrimler et al, 2019). However, proteins containing TMDs are discounted from cyst nematode effector predictions that use the typical bioinformatic pipelines (Thorpe et al, 2014; Gardner et al, 2018; Mitchum et al, 2013). This is likely because less is known about the secretion of transmembrane proteins (Gee et al, 2018). However, as transmembrane proteins are still trafficked through the TGN (Packdel and von Blume, 2018), cyst nematode transmembrane proteins may be packaged into secretory granules at the TGN, as is typical of effector proteins (Mitchum et al, 2013; Hussey and Mims, 1990). Therefore, the bioinformatic analysis of nematode proteins containing TMDs could identify novel effectors. As the length of TMDs has been shown to be unique to the target subcellular compartment (Singh and Mittal, 2016), screening TMDs of a specific length could identify cyst nematode proteins that target the ER.

Therefore, work described in this chapter aimed to identify novel ER-localised cyst nematode effectors, based on the presence of a predicted signal peptide and C-terminal TMD (Breeze et al, 2020). The list of putative effectors were narrowed based on expression data. Genes of interest were then studied further using in-situ hybridisation to test for gland cell expression, with tobacco leaf infiltrations also conducted for the analysis of *in planta* subcellular localisation.

5.2 Materials and Methods

5.2.1 Effector screen pipeline

A schematic overview of the effector screen pipeline is shown in **Figure 5.3**

5.2.1.1 Identification of secreted proteins with C-terminal TMDs

The predicted proteomes of *G. pallida* and *H. schachtii* were obtained from previously published genome and transcriptome data (Cotton et al, 2014; Siddique et al, 2021). The proteins from both sets of species were screened for the presence of a predicted signal peptide, using SignalP v5.0 software, that uses a deep neural network-based prediction method (Armenteros et al, 2019). The resulting proteins were screened for the presence of a C-terminal TMD. This was performed using the TMHMM v2.0 prediction software, which uses the Hidden Markov Model to predict TMDs (Krogh et al, 2001). To identify potential ER-localised transmembrane proteins, TMDs with a length of 17-22 residues and a maximum C-terminal tail of 30 residues after the predicted TMD were selected, based on Breeze et al. (2020).

5.2.1.2 Gene expression analysis

To identify putative effectors, gene expression cluster analysis was conducted on *H. schachtii* and *G. pallida* proteins containing a signal peptide and a C-terminal TMD. For this, normalised expression data for *H. schachtii* was obtained from Siddique et al, (2021), and the normalised expression data for *G. pallida* was obtained from Cotton et al, (2014). Genes with mean normalised expression values below 10 across all life stages were not assigned to a cluster. For *H. schachtii*, genes were separated into six clusters: J2, J2 and male, early infection (J2 to 48 hpi), female (12 dpi female and 24 dpi), late infection (12 to 24 dpi) and constant expression. Clusters most likely to contain effector proteins were J2, early infection and J2 and male.

For *G. pallida*, genes were separated into eight clusters: J2, early infection (J2 to 7 dpi), egg, egg/J2 and male, late infection (21 to 35 dpi), and adult male. Clusters which were deemed most likely to contain putative effector genes were early, egg/J2 and Male, and J2. The cluster expression graphs were created using R-studio, plotting the normalised

expression of each gene across the life stages. To visualise the trend in expression for each cluster, the locally weighted smoothing (LOESS) method was performed using the `geom_smooth` function from the R studio package `ggplot2`.

5.2.1.3 Additional analysis to identify putative *H. schachtii* and *G. pallida* effectors

Following gene expression analysis, several other parameters were used to narrow the effector screen (**Figure 5.3**). This includes the analysis of gene annotations, *H. schachtii* gland cell expression data, *G. pallida* DOG box analysis, and use of the subcellular localisation prediction software, WoLF PSORT. Genes within suitable expression clusters, in addition to fitting within one of these parameters, were selected for further analysis.

For the gene annotations of *G. pallida* and *H. schachtii* genes, those which were annotated as a 'putative effector', a 'esophageal gland secretory protein' or an effector homologue were selected for further analysis. For the *H. schachtii* gland cell expression data, genes upregulated in the gland cells at 10 hpi were identified. For this, 10 hpi gland cell expression data was obtained from Dr Sebastian Eves-van den Akker. This data was compared to the *H. schachtii* expression data collected from the whole worm tissue (Siddique et al, 2021), to identify genes that were highly upregulated in the gland cells during early parasitism. For *G. pallida*, the number of dorsal gland (DOG) promoter element motifs present in the gene promoter sequences were analysed, using previously published data (Eves-van den Akker et al, 2016). From this, many genes predicted to have dorsal gland expression had two or more DOG box motifs, 'ATGCCA', within 500 bp upstream of the gene's start codon (Eves-van den Akker et al, 2016). As a final parameter, a subcellular localisation prediction software, WoLF PSORT, was used to analyse the predicted subcellular localisations of the screened genes (Horton et al, 2007). This was to identify genes with predicted ER localisation.

Following selection of the genes, conserved features of each protein sequence were analysed using the protein domain structure visualisation software, DOG version 2.0 (Ren et al, 2009). Additionally, BLAST searches were performed to identify similar sequences from other organisms using the NCBI database, and the WormBase ParaSite database (Howe et al, 2017), as this is a more comprehensive resource for nematode genomics.

5.2.2 Gene cloning

Following the identification of putative effectors containing C-terminal TMDs, gene models were visualised using the genome browsers JBrowse (<https://jbrowse.org/>) or Apollo (<http://genomearchitect.github.io/>) to validate the gene sequence predictions against the mapped RNA-seq data. Gene model predictions were also compared against those of existing homologues and orthologues for further validation. To clone putative effectors, total RNAs were extracted from J2s using an RNeasy Mini Kit (Qiagen). This was converted to cDNA using Superscript II reverse transcriptase (Life Technologies) according to the manufacturer's instructions. The full-length coding sequences of the selected genes were amplified using primers listed within **Table 5.1**, using the proofreading DNA polymerase enzyme Phusion™ (Thermo Fisher Scientific). These genes were cloned into pGEM®-T Easy vectors after the addition of 'A-tails' (Promega), following the manufacturer's instructions. A map of the pGEM®-T Easy vector is shown in **Figure 5.1**. For GPLIN_000854400, the full length gene sequence cloned into the pGEM®-T Easy vector was provided by M. Coke within the P.E. Urwin lab. Following cloning, the construct sequences were validated with qualitative restriction digests and Sanger sequencing.

Table 5. 1. The forward (F) and reverse (R) primers used to amplify each gene from the cDNA.

| Gene ID | Sequence (5' to 3') |
|-----------------|--------------------------------|
| GPLIN_001269700 | F- ATGCTTCGTCGGCTCAAT |
| | R- TCATCGGCCCTCCCTATTA |
| GPLIN_000933000 | F- ATGAGGGACTTCGTCTGCTT |
| | R- TTAATGGATGACACGGACAA |
| Hsc_gene_10206 | F- ATGCTTTGTTTCGTGCTTTTC |
| | R- TCACTGTCGCAACGTTTTCT |
| Hsc_gene_19059 | F- ATGGCTTTCGGTTTCGTTAAT |
| | R- TCTTTATGCAATAGCACAGCACTG |
| Hsc_gene_2739 | F- CAAATCATTGCCTTTTCTTTGC |
| | R- ATCGCTATCCTTCGGCACT |
| Hsc_gene_19069 | F- ATGAAAGTTGGCACTCTTTGG |
| | R- TCTCTCAGTCCCTCTCTATCTCTCTC |
| Hsc_gene_15040 | F- TCGACTCATTCAATCAATCTTT |
| | R- CGGTATACCGATAATTTACAGACTCTC |
| Hsc_gene_14672 | F- ATGAGTGCTCCTCTGCTGCT |
| | R-TCAATTAGCGCCGAAATGG |

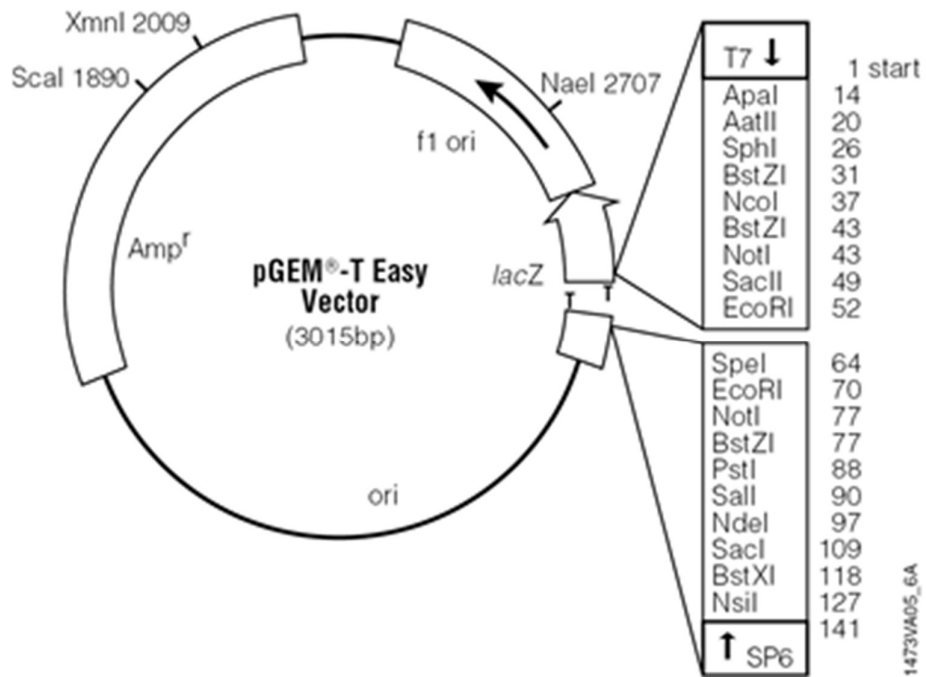


Figure 5. 1. A plasmid map of the pGEM®-T Easy vector. *H. schachtii* and *G. pallida* genes amplified from the cDNA were cloned into this vector. The map was obtained from Promega.

5.2.3 In-situ hybridisation

5.2.3.1 Probe Synthesis

In-situ hybridisation was conducted to confirm oesophageal gland expression of the selected genes, using labelled single-stranded DNA probes to bind to the mRNA of interest. To generate the probe, firstly a short double-stranded template of 200-250 bp was amplified, towards the 3' end of each gene from the corresponding pGEM®-T Easy clone. This PCR was conducted using Mytaq, as described in **section 2.3.10**, using primers listed in **Table 5.3**. Prior to primer design, gene sequences were BLAST searched against other *G. pallida* or *H. schachtii* genes to ensure that probes were specific to the gene of interest.

To generate the single-stranded in-situ probes, asymmetric PCR was conducted on the double-stranded probe template using Onetaq (New England Biolabs). This reaction was carried out according to the manufacturer's instructions, although DIG DNA labelling Mix (Roche) was added to incorporate Digoxigenin-11-dUTP, to label the probe. The reaction conditions are described in **Table 5.2**. As this was an asymmetrical PCR reaction to generate a single-strand probe, each reaction contained only a forward or reverse primer, the same used to generate the probe template (**Table 5.3**). The reverse primer generated a single-strand probe that was complementary in sequence to the mRNA of interest. Contrastingly, the forward primer was used as a negative control, generating a single-stranded probe unable to bind to the target mRNA. Following synthesis, probes were checked using agarose gel electrophoresis, with an increase in band size of the probe compared to the probe template verifying the incorporation of DIG dUTP.

Table 5. 2. In-situ probe synthesis reaction conditions using the Onetaq polymerase enzyme (New England Biolabs).

| Step | Temperature | Time | Cycles |
|----------------------|------------------------------|--------|--------|
| Initial Denaturation | 94 °C | 2 min | 1 |
| Denaturation | 94 °C | 15 s | |
| Primer Annealing | 45 - 68 °C (primer specific) | 30 s | 30 |
| Extension | 72 °C | 90 s | |
| Final Extension | 72 °C | 10 min | 1 |
| Hold | 4 °C | ∞ | ∞ |

Table 5. 3. The forward (F) and reverse (R) primers used to generate in-situ probes.

| Gene ID | Sequence (5' to 3') |
|-----------------|-------------------------------|
| GPLIN_001269700 | F- CCATGCTACTGTAACCAAGTGTATG |
| | R- TCATCGGCCCTCCCTATTA |
| GPLIN_000933000 | F- CTTTGTGTTCTTTTGTTCATTTTGG |
| | R- TTAATGGATGACACGGACAA |
| GPLIN_000854400 | F- TATCCGAGTCCTTCACTACTG |
| | R- AAGATGATCATCCAGTCCAAG |
| Hsc_gene_10206 | F- GAGCCCGGAACAGTATTGTCA |
| | R- TCACTGTGCGAACGTTTTCTC |
| Hsc_gene_19069 | F- ATCGGCATTTATTTGGTCTGC |
| | R- TCTCTCAGTCCCTCTCTATCTCTCTC |
| Hsc_gene_14672 | F- GTCCACTCTTTCGACTTGTTCC |
| | R- TCAATTAGCGCCGAAATGG |
| Hsc_gene_2739 | F- AAGCAATGGTCGATCAGTTG |
| | R- TAATACCGAAAAGCACCAAATG |
| Hsc_gene_19059 | F- CATTGGTGGCACTTTTAAAGG |
| | R- GGCGATCACCAACAATCCT |
| Hsc_gene_15040 | F- AGGCAGCGGAGCATTG |
| | R- CCGCATCATTGCCAAC |

5.2.3.2 Fixation, cutting, permeabilisation and hybridisation

For the J2 in-situ hybridisations, a previously published protocol was used for fixation of the worms (de Boer et al, 1998). However, for later parasitic stage in-situ hybridisations, which were performed by Mirela Coke, cabbage roots at 15 days post infection with *H. schachtii* were thoroughly cleaned, then cut into approximately 2 cm lengths before being briefly blended in water to facilitate efficient fixation. For fixation, blended roots were placed in 10 % formaldehyde for 3 days at room temperature. To collect the parasitic stage worms, the fixed root mixture was rinsed through 63 and 150 µm mesh sieves. The roots were blended again to help release fixed nematodes, which were collected on sieves of the same size. Following this, sucrose gradient centrifugation was performed on the collected worms, for the removal of root debris (40 % w/v; Acedo and Dropkin, 1982). In-situ hybridisation for both J2 and parasitic stage worms were then conducted according to de Boer et al. (1998).

After fixation, the worms were cut to allow for probe entry. For this, the worms were placed in a 10 % fixative solution and cut using a razor blade. For permeabilisation, proteinase K (0.5 mg/ml for J2s, 2 mg/ml for parasitic stages; Roche) diluted in M9 buffer (Sigma-Aldrich) was used, having an incubation of 30 min at room temperature. Following this, worms were washed in M9 buffer and pelleted on deep frozen ice for 15 min, before being re-suspended in -20 °C methanol for 30 secs. Subsequently, worms were suspended in -20 °C acetone for 1 min on deep frozen ice, before being rehydrated with RNase free water. The next steps were three washes in the hybridisation buffer (de Boer et al, 1998). After this, for pre-hybridisation, worms were placed in fresh hybridisation buffer and incubated at 50 °C for 15 min. For hybridisation, probes were denatured at 99 °C for 10 min, then added to the pre-hybridised worms, with an overnight incubation at 50 °C.

5.2.3.3 Detection and image acquisition

After probe hybridisation, several wash steps were conducted. This included 3 X 15 min washes in 4 x SSC buffer, followed by 3 X 20 min washes with 200 µl 0.1 X SSC / 0.1 % SDS buffer, at 50 °C. Worms were then washed with maleic acid buffer (Roche), before incubation in 1 % blocking reagent (Roche) in maleic acid buffer for 30 min at room temperature. Following the wash steps, worms were incubated in alkaline-phosphatase conjugated anti-digoxigenin antibody (Sigma-Aldrich), diluted 1:1000 in 1 % blocking reagent (Roche) in maleic acid buffer (Roche) for 2 hours at room temperature. To remove the anti-digoxigenin antibody, 3 X 15 min washes in maleic acid buffer with 0.01 % Tween-20 were conducted, followed by a brief wash in alkaline-phosphatase detection buffer (Roche). For staining, worms were incubated in NBT (337 µg/ml; Sigma-Aldrich)

and X-phosphate BCIP (175 µg/ml; Sigma-Aldrich) in alkaline phosphatase detection buffer (Roche) at 4 °C overnight. To stop the staining reaction, worms were washed twice in 0.01 % Tween-20, diluted in sterile H₂O.

To image worms after in-situ hybridisation, stained worms were washed three times with sterile water then mounted onto a microscope slide, the coverslip sealed with clear nail polish. Images were taken using the Zeiss Axio Scope A1 microscope, with the 20 X or 40 X objective lens. Images were processed using the Zen Blue software, version 2.3 (Zeiss). To verify gland cell expression, the distance from the stained gland cell to the base of the nematode's stylet was measured using the ImageJ software (Java; <https://imagej.nih.gov/>).

5.2.4 Subcellular localisation analysis

5.2.4.1 eGFP-fusion construct development

For subcellular localisation analysis, gateway cloning was used to generate N- and C-terminal GFP fusion constructs of putative effectors. Effector coding regions, without their signal peptides, were amplified from their respective pGEM®-T Easy plasmid using Phusion™ polymerase (Thermo Fisher Scientific), according to the manufacturer's instructions. The primers for these PCR reactions are listed in **Table 5.4**. For the C-terminal fusion constructs, the forward primer sequences were designed to add a Kozak sequence with a start codon, 'AAACAATG', onto the 5' end of the amplified gene product to initiate translation. Also, the reverse primer sequences for the C-terminal GFP constructs were designed to omit amplification of the stop codon at the end of the gene sequence.

Amplified putative effector gene fragments were inserted into the pCR™8/GW/TOPO™ Gateway entry vector by TA cloning, according to the manufacturer's instructions (Invitrogen). To generate GFP fusion constructs, the binary expression vectors pK7WGF2 (N-terminal GFP) and pK7FWG2 (C-terminal GFP) were used as destination vectors, expressing enhanced green fluorescent protein (eGFP; Karimi et al, 2002). Recombination of the entry and destination vectors was achieved using LR clonase™ (Invitrogen) following the manufacturer's instructions. The integrity of all clones were checked by Sanger sequencing using primers listed in **Table 5.4**. Plasmid maps for the pGEM®-T Easy vector, the entry pCR™8/GW/TOPO™ vector and the destination vectors, pK7WGF2 (N-terminal GFP) and pK7FWG2 (C-terminal GFP), are given in **Figure 5.2**.

Table 5. 4. The sequences of the forward (F) and reverse (R) primers used to clone each gene into the pCR™8/GW/TOPO™ gateway entry vector. Different PCR™8/GW/TOPO™ constructs, requiring different primers, were generated for the gateway reaction, for recombination with either N- or C- terminal eGFP destination constructs.

| Gene ID | N/C terminal eGFP | Sequence (5' to 3') |
|-----------------|-------------------|---|
| GPLIN_001269700 | N | F- CAACCGCCACACAGTACG R- TCATCGGCCCTCCCTATTA |
| | C | F- AAACAATGCAACCGCCAC R- TCGGCCCTCCCTATTAACAT |
| GPLIN_000933000 | N | F- CAGCTTCTTTCACTTGAGCG R- TTAATGGATGACACGGACAATG |
| | C | F- AAACAATGCAGCTTCTTTCACTT R- ATGGATGACACGGACAATGA |
| Hsc_gene_10206 | N | F- GATCTGTCAAATCAGATAAAGAATTG R- TCACTGTGCGAACGTTTTTCT |
| | C | F- AAACAATGGATCTGTCAAATCA R- CTGTGCGAACGTTTTTCTCG |
| Hsc_gene_19059 | N | F- GGTGAGCCACTTGGAAATGA R- TTAATAAGCAGCTTTCCCCC |
| | C | F- AAACAATGGGTCAGACCACTT R- AAAAGCAGCTTTCCCCCAT |
| Hsc_gene_2739 | N | F- ACCGCTGATCAGCAGAAGAG R- CTATCCTTCGGCACTGCCT |
| | C | F- AAACAATGACCGCTGATCAG R- TCCTTCGGCACTGCCTT |
| Hsc_gene_19069 | N | F- TCTTTCTGCCATTCTTCTCATT R- TCAGTGCCTCGGCGC |
| | C | F- AAACATGTCTTTCTGCCATT R- GTGCCTCGGCGCTTTT |
| Hsc_gene_14672 | N | F- CAGTTCCTTTGGCGG R- TCAATTAGCGCCGAAATGG |
| | C | F- AAACAATGCAGTTCCTTTGG R- ATTAGCGCCGAAATGGAG |
| Hsc_gene_15040 | N | F- TTTGACTCTGCCCAAAGTGTC R- TTACAGACTCTCGCTCTCTCCC |
| | C | F- AAACAATGTTTGACTCTGCC R- CAGACTCTCGCTCTCTCCC |
| GPLIN_000854400 | N | F- CAATTACAATCGAAGAGCATCG R- TCACAAAAGGCGAAAGCAC |
| | C | F- AAACAATGCAATTACAATCGAAGA R- CAAAAGGCGAAAGCACCG |

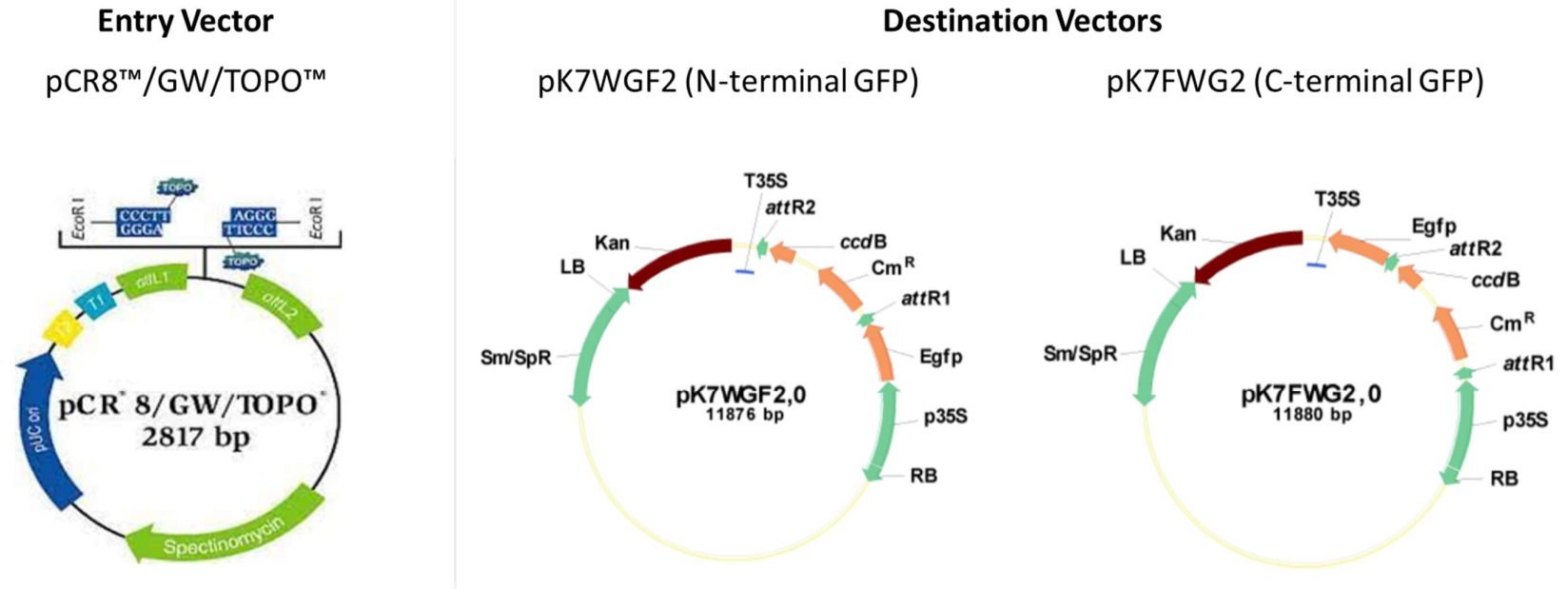


Figure 5. 2. Plasmid maps for the entry and destination gateway constructs, which were used to develop the N- and C- terminal GFP fusions. The map for the entry vector, pCR™8/GW/TOPO™, was obtained from ThermoFisher. The maps for the two destination vectors, pK7WGF2 and pK7FWG2, were obtained from the Heven Sze lab.

5.2.4.2 Tobacco leaf infiltration of GFP constructs

Tobacco leaf infiltrations were conducted as previously described (**section 2.4**). To predict the subcellular localisation of each gene, each construct was infiltrated alone. To help decide which organelle markers to co-infiltrate with each GFP construct, subcellular prediction software was used, including PSORTII (Horton and Nakai, 1997), MultiLoc2 (Blum et al, 2009) and MULocDeep (Jiang et al, 2021). These different prediction software were used in tandem to enhance the predictability.

5.2.4.3 Additional marker constructs used

To test the subcellular localisation of the putative effector genes, the GFP fusion constructs were co-infiltrated into tobacco leaf epidermal cells with the relevant organelle marker. This included markers for the cytoplasm, ER, Golgi, nucleus, peroxisome, mitochondria and plasmodesmata. The nucleus, peroxisome and mitochondria markers used for co-infiltrations were obtained from Addgene, developed in Ivanov and Harrison (2014). This includes the peroxisome marker mCherry-SKL. For this, the peroxisomal targeting sequence SKL was fused to the C-terminus of mCherry. For the mitochondria marker, ScCox4-mCherry was used, containing the signal peptide (the first 29 amino acids) of the yeast *Saccharomyces cerevisiae* Cytochrome C Oxidase Subunit 4 gene (ScCox4) fused to the N-terminus of mCherry. For the nucleus marker, the first 15 amino acids of the tobacco C2 polypeptide were fused to the N-terminus of mCherry. All constructs from Addgene were expressed under the control of the strong constitutive Arabidopsis AtUBQ10 promoter (Grefen et al, 2010). For the plasmodesmata marker, p35S::mCherry-PDCB1 was used (Benitez-Alfonso et al, 2013). Free GFP, 35S::GFP, was used as a control. This was obtained from the P. E. Urwin group.

5.3 Results

5.3.1 Overview of the effector screen pipeline

To identify putative novel cyst nematode effectors containing C-terminal TMDs, the predicted proteomes for *H. schachtii* and *G. pallida* were obtained from previously published data. The *H. schachtii* proteome contained 26,739 predicted proteins (Siddique et al, 2021), and the *G. pallida* proteome contained 16,403 predicted proteins (Cotton et al, 2014). Protein sequences from these two species were screened for the presence of a signal peptide using the SignalP software, and the presence of a C-terminal TMD using the TMHMM software. The length of the C-terminal TMD and C-terminal tail was also screened, consistent with previous a effector screen that identified ER-targeting plant-pathogen effectors (Breeze et al, 2020). From the effector screen in this chapter, 271 *H. schachtii* and 140 *G. pallida* proteins were identified (**Figure 5.3**).

From the set of *H. schachtii* and *G. pallida* proteins containing a predicted signal peptide and C-terminal TMD, an effector homologue search was conducted using known effector sequences from all cyst nematode species. This identified just two *H. schachtii* and three *G. pallida* proteins. These low numbers were not surprising, as effector-finding pipelines have typically discarded any proteins with TMDs. To identify further putative effectors, cluster analysis was performed on the expression profiles of the genes to identify those with temporal expression indicative of effector activity. This identified 68 *H. schachtii* and 56 *G. pallida* genes. Additional screening steps were conducted to narrow this list of putative effectors for further analysis. For example, the annotation of the proteins was analysed, in addition to the presence of DOG box sequences upstream of *G. pallida* genes, the predicted ER localisation, and enrichment in the gland cell transcriptome of *H. schachtii* at 10 hpi. This further reduced the list to fifteen *H. schachtii* and nine *G. pallida* genes of interest. The gene models for these were analysed to validate the sequences. From this, six *H. schachtii* and three *G. pallida* genes were cloned and used for further analysis (**Figure 5.3**).

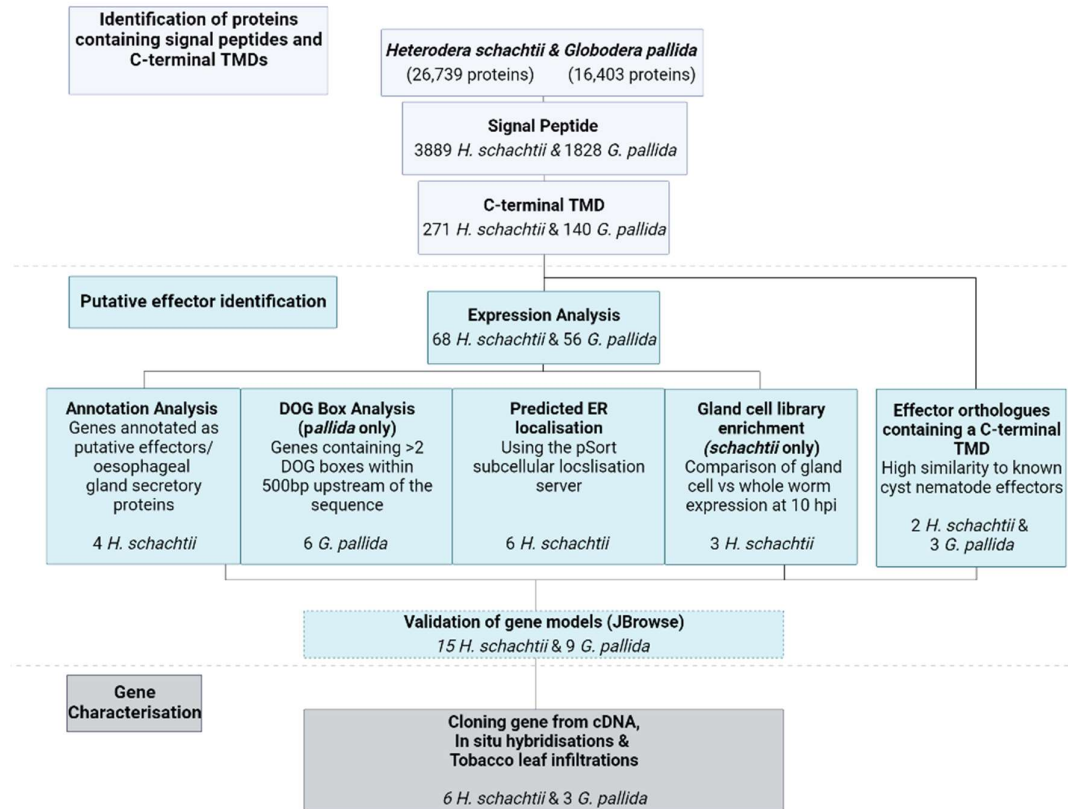


Figure 5. 3. A schematic of the effector screen pipeline. For this screen, the *H. schachtii* proteome, containing 26,739 predicted proteins, and the *G. pallida* ‘Lindley’ proteome, containing 16,403 proteins, were used. **The identification of proteins containing signal peptides and C-terminal TMDs:** from the predicted *H. schachtii* and *G. pallida* proteomes, proteins with predicted signal peptides and a C-terminal TMD were identified. **Putative effector identification:** Following this, several parameters were used to identify putative nematode effectors, including the analysis of gene expression, gene annotations, *G. pallida* DOG box promoter motifs, prediction of subcellular localisation, *H. schachtii* gland cell expression, and the analysis of similar sequences from other cyst nematode species. Gene model validation was conducted on the 15 *H. schachtii* and 9 *G. pallida* genes identified from this analysis. Of these genes, 7 *H. schachtii* and 5 *G. pallida* genes failed the gene model validation step. **Gene characterisation:** Gene cloning was performed, with two *H. schachtii* and one *G. pallida* cDNAs failing to be cloned. Consequently, a set of 6 *H. schachtii* and 3 *G. pallida* genes was used for analysis, with in-situ hybridisations and tobacco leaf infiltrations conducted.

5.3.2 Cluster analysis for the expression of tail-anchored cyst nematode proteins containing signal peptides

From the list of 271 *H. schachtii* and 140 *G. pallida* proteins containing a signal peptide and C-terminal TMD, gene expression cluster analysis was performed to identify genes with temporal expression resembling that of effector proteins. This was achieved using available transcriptome datasets (Siddique et al, 2021; Cotton et al, 2014). For *H. schachtii*, 238 out of 271 screened genes were assigned to eight clusters based on differential expression across the parasitism time course (**Figure 5.4**). The other 33 screened *H. schachtii* genes were not assigned to clusters due to low levels of expression. A large portion of the genes were assigned to the 'Male' cluster (104 genes), peaking at the adult male life stage. Genes expressed highest during early parasitism (Early; 44 genes) formed the second largest cluster, followed by genes expressed during late parasitism (Late; 25 genes). The 'Female' cluster (22 genes) was similar in size, with genes peaking in expression at the 12 dpi and 24 dpi female life stages. Interestingly, 15 genes peaked at both the J2 and male stages (J2 + Male). The three smallest clusters included genes that were exclusively expressed in the parasitic stages (Parasitic; 10 genes), genes with constant expression (Constant; 9 genes), and genes with expression that peaked at the J2 stage (J2; 9 genes). To identify putative effector proteins, gene clusters that were predicted to have likely functions in early parasitism were identified. These were the 'J2 + Male', 'J2' and the 'Early' clusters (**Figure 5.4**).

For the set of screened *G. pallida* proteins, 105 of 140 *G. pallida* genes had adequate levels of expression, and were assigned to six expression clusters (**Figure 5.5**). Similar to the *H. schachtii* cluster analysis, *G. pallida* genes expressed highest at the male life stage formed the largest cluster (Male; 33 genes). This was followed by genes expressed most highly in the egg/J2 and the male stage (Egg/J2 and Male; 25 genes), then genes most highly expressed in early parasitism (Early; 20 genes), genes peaking at the J2 stage (J2; 11 genes), genes expressed most highly in late parasitism (Late; 10 genes), and genes that peaked at the egg life stage (Egg; 6 genes). Gene clusters which were selected to most likely contain putative effector proteins were the 'J2', 'Early', 'Egg/J2 and Male' clusters (**Figure 5.5**).

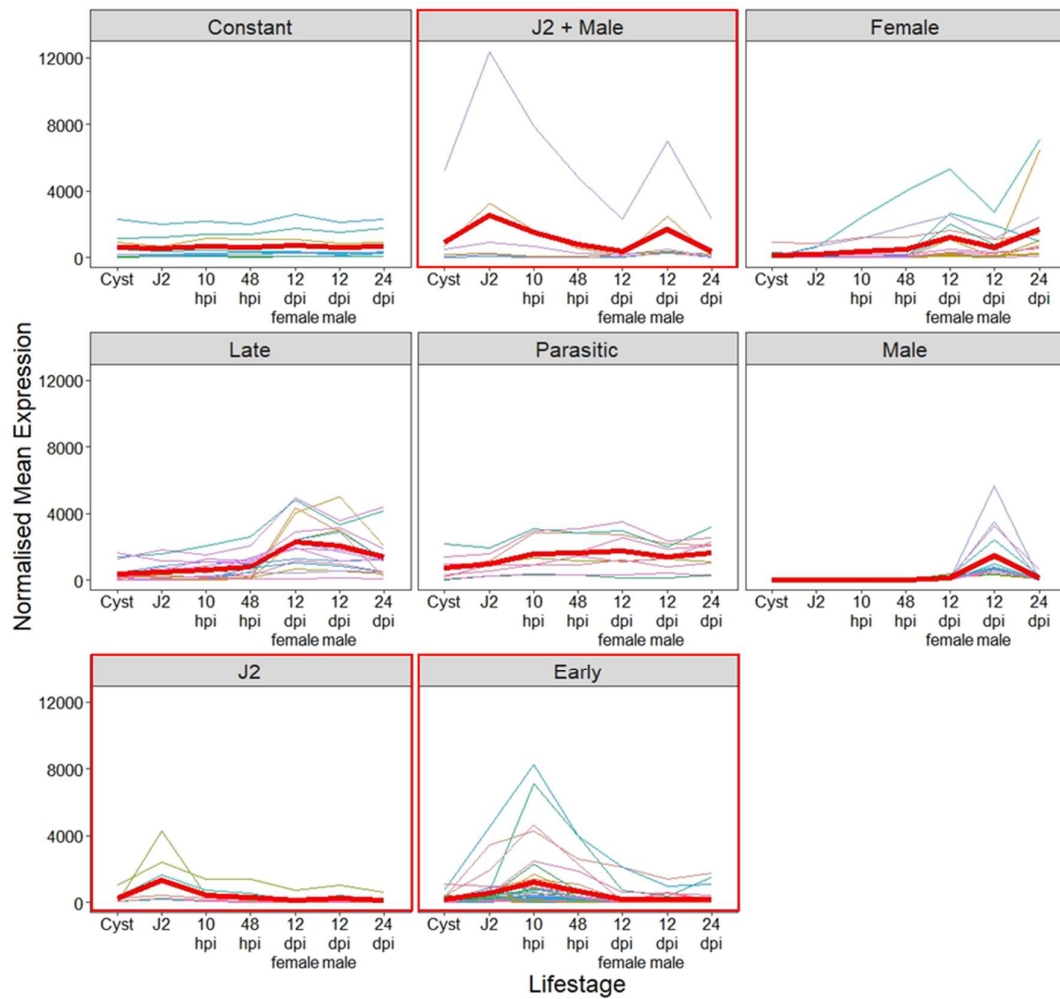


Figure 5. 4. The gene expression clusters of *H. schachtii* genes containing a signal peptide and a C-terminal TMD. In total, 271 genes were used for this analysis, manually assigned into eight different clusters, which included: genes with constant expression (9 genes), J2 and male (15 genes), Female (12 dpi female and 24 dpi; 22 genes), Late (12 - 24 dpi; 25 genes), Parasitic (10 hpi onwards; 10 genes), Male (12 dpi male; 104 genes) J2 (9 genes) and Early (J2 - 48 hpi; 44 genes). Clusters that are most likely to contain candidate effectors are outlined in red, including J2 and Male, J2 and Early. The mean normalised expression of each gene in each cluster is presented across the life stages. Each plot contains a red trendline that was fitted using the LOESS smoothing method.

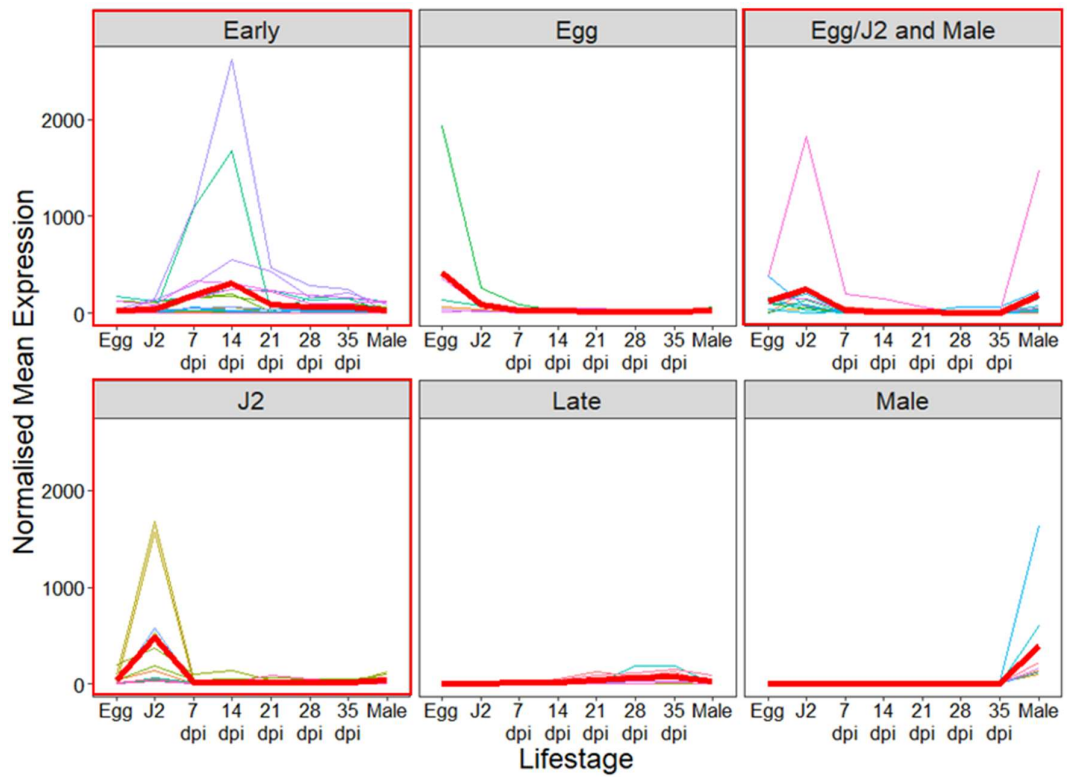


Figure 5. 5. The gene expression clusters of *G. pallida* genes containing a signal peptide and a C-terminal TMD. In total, 140 genes were used for this analysis, manually assigned into six clusters, that included: Early (J2 - 7 dpi; 20 genes), Egg (6 genes), Egg/J2 and Male (25 genes), J2 (11 genes), Late (21 dpi - male; 10 genes), and Male (33 genes). Clusters that are most likely to contain putative effector genes are outlined in red, including Early, Egg/J2 and Male, and J2. The mean normalised expression of each gene in each cluster is presented across the life stages. The red line in each cluster represents a trendline that was fitted using the LOESS smoothing method.

5.3.3 Genes chosen for further analysis

Genes either annotated as effectors, or belonging to the expression clusters indicative of effector function were chosen for further analysis. Those genes identified as having a temporal expression pattern of interest were further triaged to narrow the list as shown in **Figure 5.3**. An effector homologue search was conducted on screened *H. schachtii* and *G. pallida* proteins, using known effector sequences across all cyst nematode species. From this, three effector homologues were identified; the *H. schachtii* gene Hsc_gene_10206, a homologue of the *H. avenae* effector *Ha-acp1*, the *H. schachtii* gene Hsc_gene_14672, a homologue of *G. rostochiensis* and *G. pallida* SPRY-SEC effectors, and the *G. pallida* gene GPLIN_000933000, a homologue of the *H. glycines* effector G17G01 (**Table 5.5**).

In addition to effector homologues, several other parameters were used to identify putative effector genes (**Figure 5.3**). This included the analysis of protein annotations, *H. schachtii* gland cell expression data, *G. pallida* DOG box analysis, and the prediction of ER localisation. From this, four *H. schachtii* and one *G. pallida* genes were identified (**Table 5.6**). This included Hsc_gene_19069, annotated as 'putative oesophageal gland cell secretory protein 28', Hsc_gene_15040, suggested to be upregulated in the gland cells at 10 hpi, Hsc_gene_19059 and Hsc_gene_2739, two proteins with predicted ER localisation, and GPLIN_001269700, containing two DOG promoter element motifs within 500 bp upstream of the gene.

After gene model validation, this led to the cloning of six *H. schachtii* and three *G. pallida* genes from cDNA. Protein domain prediction and BLAST searches were conducted for each of the nine genes (**Tables 5.5 and 5.6**). In-situ hybridisations were then conducted to test for gland cell expression, and the *in-planta* subcellular localisation was inferred from the fusion of coding regions with GFP, and subsequent tobacco leaf infiltrations.

Table 5. 5. The selection of *H. schachtii* and *G. pallida* genes containing a signal peptide and C-terminal TMD, identified as homologues of cyst nematode effectors.

The gene name is listed, in addition to the name of the homologous effector gene under the 'Selection Criterion' column. Additionally, the gene's expression cluster, its predicted conserved domains, and its top NCBI BLAST hit are listed. The two *G. pallida* genes, GPLIN_000854400 and GPLIN_000933000, contain multiple TMDs including a C-terminal TMD, although all other proteins chosen for further analysis contain a single C-terminal TMD.

| Gene | Selection Criterion | Expression Cluster | Predicted Domains | Top BLAST hit |
|-----------------|--|--------------------|----------------------------|---|
| Hsc_gene_10206 | Putative <i>H. avenae</i> Ha-acp1 effector homologue | Early | Histidine Acid Phosphatase | <i>H. avenae</i> acid phosphatase (84.52% identity, e-value 0.0) |
| Hsc_gene_14672 | Putative SPRY-SEC effector | Male | B30.2/SPRY | <i>G. pallida</i> Ran-binding protein 10 (42.54% identity, e-value 5e-32) |
| GPLIN_000854400 | Putative <i>H. glycines</i> 16H02 effector homologue* | Egg + J2 + male | | <i>H. glycines</i> 16H02 (74.59% identity, e-value 1e-52) |
| GPLIN_000933000 | Putative <i>H. glycines</i> G17G01 effector homologue* | Male | | <i>H. glycines</i> G17G01 (33.18% identity, e-value 2e-16) |

*contains multiple TMDs

Table 5. 6. The selection of *H. schachtii* and *G. pallida* genes containing a signal peptide and C-terminal TMD. Multiple parameters were used to select these genes, which are listed under the 'Selection Criterion' column. Additional information about each gene is also presented, including the expression cluster that the gene was assigned to, its predicted conserved domains, and its top NCBI BLAST hit.

| Gene | Selection Criterion | Expression Cluster | Predicted domains | Top BLAST hit |
|-----------------|---|--------------------|-------------------|--|
| Hsc_gene_19069 | "Putative esophageal gland cell secretory protein 28" | J2/late | EGF-like | <i>M. enterolobii</i> unnamed protein product (64.74% identity, e-value 4e-69) |
| Hsc_gene_15040 | Upregulated in the gland cells at 10 hpi | Early | Coiled-coil | |
| Hsc_gene_19059 | Predicted ER localised protein (Wolf pSORT) | Early | | |
| Hsc_gene_2739 | Predicted ER localised protein (Wolf pSORT) | Early | | |
| GPLIN_001269700 | 2 DOG boxes | Egg + J2 + male | | |

5.3.4 Subcellular localisation prediction for each gene

Subcellular localisation prediction of the nine *H. schachtii* and *G. pallida* proteins was conducted, to help select organelle markers for co-infiltrations. For this, the sequences without their signal peptides were used, as this is predicted to be cleaved in the nematode gland cells prior to secretion into the plant. Following the tobacco leaf infiltrations of each putative effector gene-GFP construct, labelled structures such as the cytoplasm, ER and nucleus were readily identifiable prior to co-infiltration with organelle markers. However, punctate structures were observed in tobacco leaf epidermal cells infiltrated with several different constructs. These punctae could represent endosome, Golgi, mitochondria or peroxisome localisation. Therefore, the results from three different sub-cellular prediction tools (PSORTII, MultiLoc2 and MULocDeep) were combined to select the most appropriate organelle marker(s) to be co-infiltrated with each GFP construct. However, the localisation predictions of each server widely varied (**Table 5.7**), challenging the prediction of subcellular localisation.

Table 5. 7. The subcellular localisation prediction of each protein, using the three servers PSORTII, MultiLoc2 and MULocDeep. % likelihood of localisation is given for each predicted compartment. Highlighted in red are the subcellular markers that were used for co-infiltrations, based on the infiltration of the GFP constructs alone.

| Gene | PSORTII | MultiLoc2 | MULocDeep |
|--|---|--|--|
| GPLIN_000854400 <i>16H02 homologue</i> | Plasma membrane 35% Apoplast 35% Endoplasmic reticulum 17% Golgi 13% | Apoplast 79% Plasma membrane 10% Endoplasmic reticulum 5% Vacuole 2% Golgi 2% Cytoplasm 1% | Endoplasmic reticulum 61% Nucleus 4% Vacuole 3% Golgi 1.6% Mitochondria 1% |
| GPLIN_000933000 <i>G17G01 homologue</i> | Endoplasmic reticulum 67% Mitochondria 11% Plasma Membrane 11% Vacuole 11% | Golgi 66% Cytoplasm 12% Apoplast 9% Peroxisome 4% Chloroplast 4% | Endoplasmic reticulum 38% Nucleus 19% Membrane 11% Golgi 8% Vacuole 5% |
| GPLIN_001269700 <i>No annotation</i> | Endoplasmic reticulum 22% Nucleus 22% Cytoskeleton 11% Apoplast 11% Plasma membrane 11% Golgi 11% Endosome 11% | Cytoplasm 77% Nucleus 15% Peroxisome 5% Golgi 1% Mitochondria 1% | Nucleus 14% Endoplasmic reticulum 11% Apoplast 10% Golgi 3% Mitochondria 2% |
| Hsc_gene_10206 <i>Putative effector</i> | Cytoplasm 26% Endosome 22% Mitochondria 13% Nucleus 13% Plasma Membrane 9% Cytoskeleton 4% Golgi 4% Vacuole 4% Endoplasmic reticulum 4% | Cytoplasm 60% Nucleus 26% Peroxisome 9% Mitochondria 2% Golgi 1% Chloroplast 1% | Vacuole 19% Membrane 13% Apoplast 12% Mitochondria 3% Nucleus 2% |
| Hsc_gene_14672 <i>RBP-1 Effector</i> | Cytoplasm 26% Peroxisome 22% Nucleus 13% Mitochondria 13% Plasma membrane 9% | Cytoplasm 73% Peroxisome 17% Nucleus 6% Golgi 1% Mitochondria 1% Chloroplast 1% | Nucleus 29% Apoplast 7% Cytoplasm 7% |
| Hsc_gene_15040 <i>No annotation</i> | Cytoplasm 35% Nucleus 26% Mitochondria 17% Endoplasmic reticulum 9% | Cytoplasm 84% Nucleus 8% Peroxisome 4% Apoplast 2% Mitochondria 2% Plasma Membrane 1% | Membrane 32% Endoplasmic reticulum 20% Cytoplasm 12% Golgi 11% |
| Hsc_gene_19059 <i>No annotation</i> | Peroxisome 22% Nucleus 17% Cytoplasm 17% Plasma Membrane 13% Endoplasmic reticulum 9% Vacuole 4% Mitochondria 4% Golgi 4% Cytoskeleton 4% Apoplast 4% | Nucleus 80% Peroxisome 15% Mitochondria 3% Golgi 1% | Endoplasmic reticulum 24% Membrane 21% Cytoplasm 7% Apoplast 5% Vacuole 5% Golgi 4% |

| | | | |
|--|--------------------------|----------------------|--------------------------|
| Hsc_gene_19069 <i>Putative esophageal gland cell secretory protein 28</i> | Nucleus 65% | Cytoplasm 64% | Membrane 87% |
| | Plasma membrane 13% | Nucleus 13% | Cytoplasm 4% |
| | Mitochondria 13% | Apoplast 8% | Nucleus 2% |
| | Cytoplasm 4% | Peroxisome 7% | Plastid 1% |
| | | Mitochondria 2% | Apoplast 1% |
| <hr/> | | | |
| Hsc_gene_2739 <i>No annotation</i> | Nucleus 26% | Nucleus 47% | Cytoplasm 12% |
| | Cytoplasm 17% | Cytoplasm 34% | Membrane 4% |
| | Endosome 17% | Peroxisome 10% | Nucleus 2% |
| | Plasma membrane 13% | Mitochondria 5% | Mitochondria 2% |
| | Endoplasmic reticulum 9% | | Endoplasmic reticulum 2% |
| | Apoplast 4% | | |
| | Golgi 4% | | |
| | Cytoskeleton 4% | | |
| | Vacuole 4% | | |
| | | | |
| | | | |

5.3.5 The positive control gene GPLIN_000854400

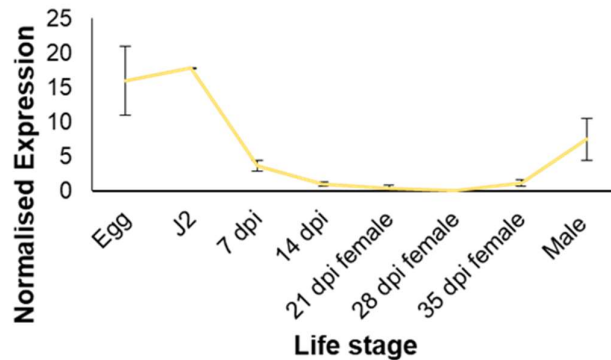
GPLIN_000854400 contains multiple TMDs in addition to a predicted signal peptide (**Figure 5.6C**). Although this gene did not fit the prerequisite of a single TMD at the C-terminus, it was chosen as a positive control as it is a previously characterised effector, that localises to the ER (unpublished) and contains a C-terminal TMD. This gene is a predicted homologue of the *H. glycines* 16H02 effector.

J2 in-situ hybridisations for GPLIN_000854400 suggested dorsal gland cell expression (**Figure 5.6B**), which has previously been observed (Thorpe et al, 2014). For the subcellular localisation analysis, both N- and C- terminal GFP fusions with GPLIN_000854400 showed strong ER localisation; labelling the nuclear envelope at the central focal plane of the cell, and the ER network in the cortical cytoplasm (**Figures 5.7 and 5.9**). ER localisation was validated by the complete co-localisation of both GFP fusions of GPLIN_000854400 with the ER marker secRFP-p24aTM (**Figures 5.8 and 5.10**).

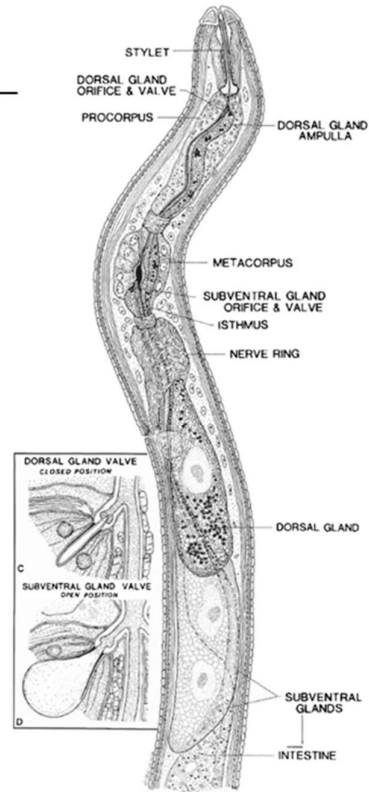
Although the subcellular localisation prediction server MULocDeep predicted the ER (61 %) as the most likely localisation, the other two servers, PSORTII and MultiLoc2, predicted the ER to be the third most likely localisation of this gene, reporting 17 % and 5 % likelihood of ER localisation, respectively (**Table 5.7**).

GPLIN_000854400 (16H02 effector)

A. Expression

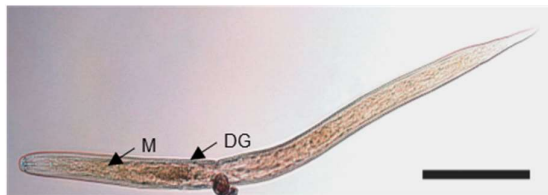


B. In-situ reference



C. J2 In-situ hybridisation

Antisense Probe



Sense Probe (negative control)



D. Protein domain structure prediction

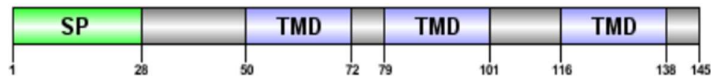


Figure 5. 6. The analysis of GPLIN_000854400, the ER-localised 16H02 effector used as a positive control. **A.** The expression of GPLIN_000854400 across the various life stages. For each life stage, the mean expression is shown, with error bars representing the standard deviation. Expression was highest at the egg and J2 stage, with a small peak also in the males. **B.** A longitudinal drawing of a *H. glycines* J2, to show the relative positioning of the dorsal and subventral esophageal glands below the metacarpal bulb (metacarpus). Image to be used as a reference for in-situ hybridisations, taken from Ali et al. (2017). **C.** J2 in-situ hybridisation, showing potential dorsal gland expression (DG). Scale bars represent 100 μ m. The metacarpal bulb (M) is labelled. **D.** Protein domain structure prediction, with a signal peptide (SP) and three transmembrane domains (TMDs).

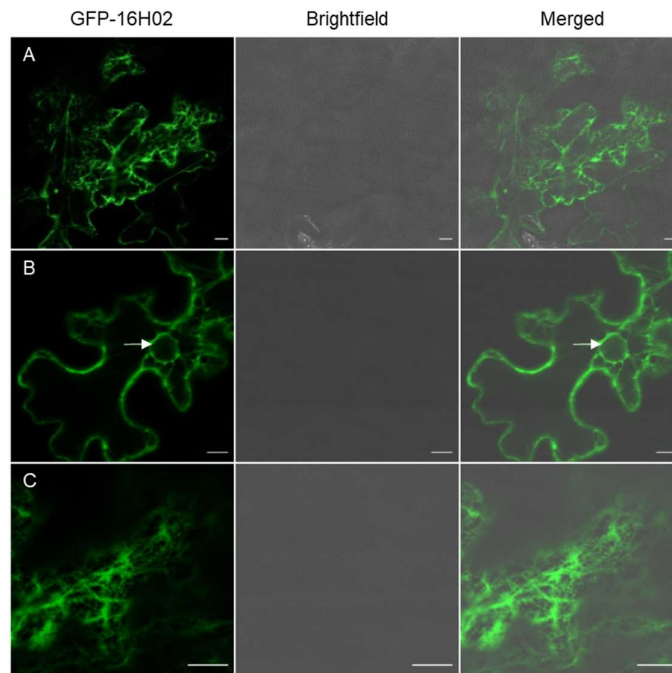


Figure 5. 7. Tobacco leaf epidermal cells *Agro*-infiltrated with GFP-16H02. A. An overview of infiltrated cells, showing GFP-16H02 labelling the ER network. **B.** A view of the centre of an infiltrated cell, showing the GFP-16H02 labelled ER in close association with the nuclear envelope (white arrow). **C.** GFP-16H02 labelled ER is dispersed throughout the cortical cytoplasm. Scale bars represent 10 μm .

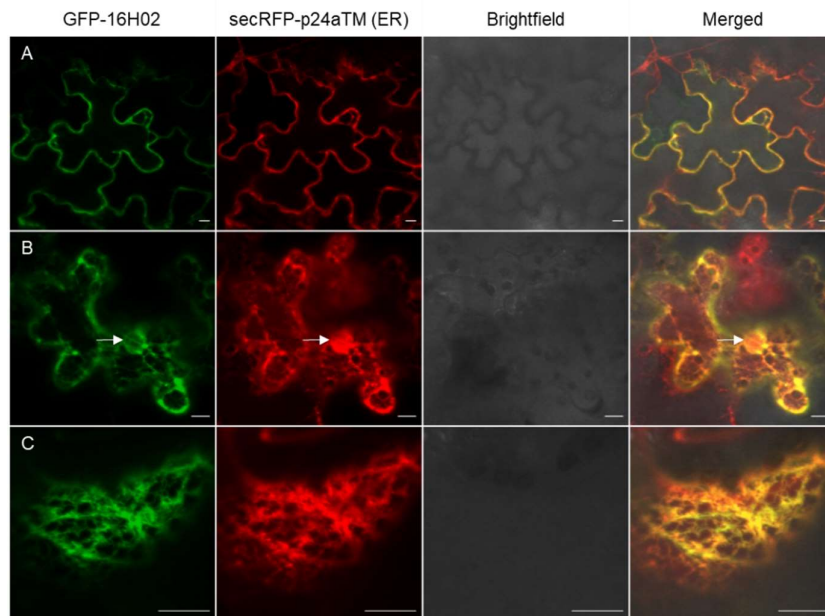


Figure 5. 8. Tobacco leaf epidermal cells co-infiltrated with GFP-16H02 and the ER marker secRFP-24aTM. A. An overview of infiltrated cells, showing the co-localisation of GFP-16H02 and secRFP-p24aTM. **B.** A view of the centre of an infiltrated cell, showing the labelling of both fluorescent protein fusions around the nuclear envelope (white arrow), as is expected with ER localisation. secRFP-p24aTM also is present in the nucleoplasm, but not the nucleolus. **C.** A view of the cortical cytoplasm, showing GFP-16H02 and secRFP-p24aTM labelled ER. Scale bars represent 10 μm .

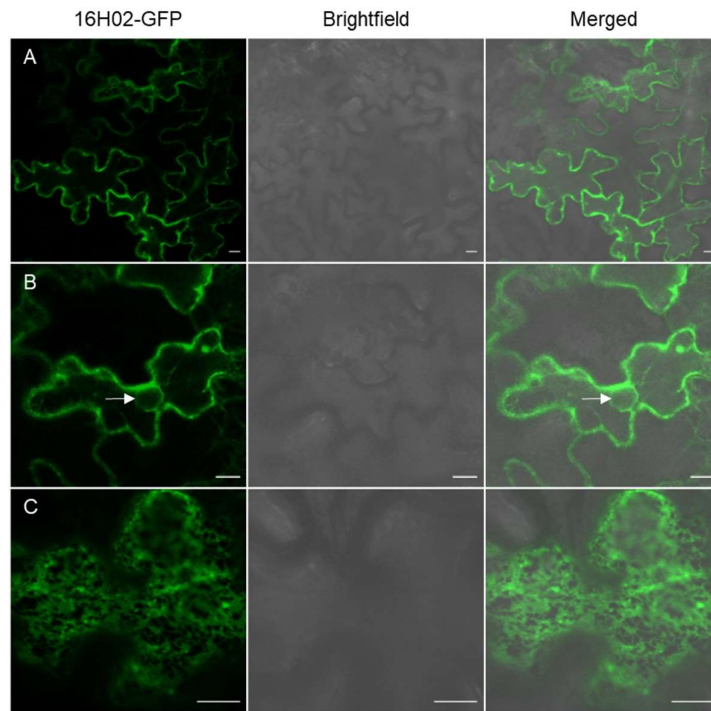


Figure 5. 9. Tobacco leaf epidermal cells *Agro*-infiltrated with 16H02-GFP. Expression was lower than that of GFP-16H02, however, the C-terminal 16H02 GFP fusion still localised to the ER network. **A.** An overview of infiltrated cells. **B.** A view of the centre of an infiltrated cell, showing the nuclear envelope (white arrow). **C.** A view of the cortical cytoplasm to show the labelled ER network. Scale bars represent 10 μm .

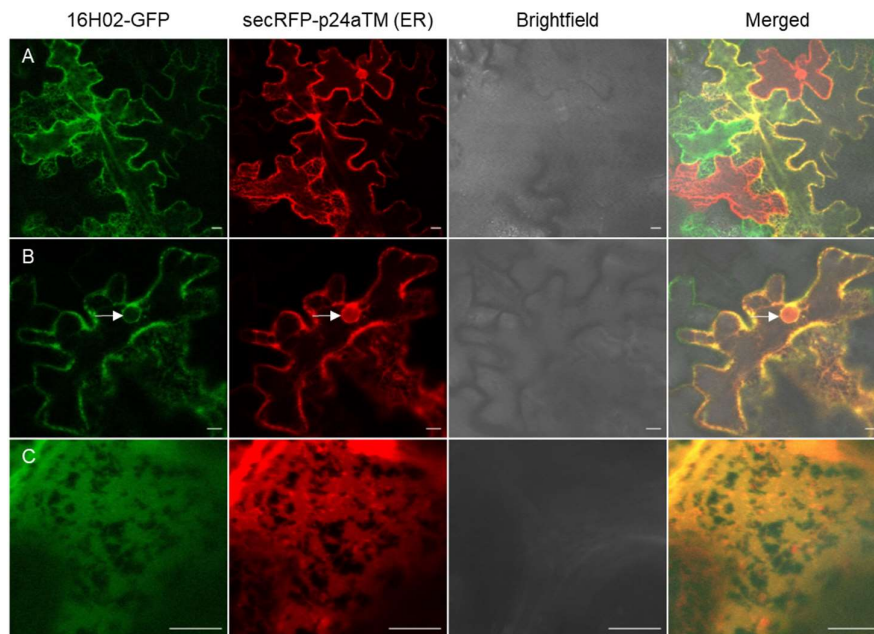


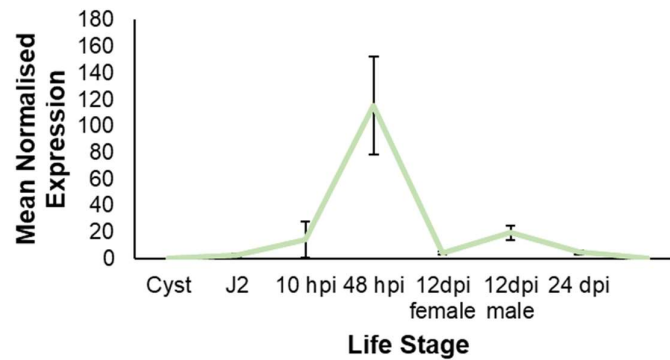
Figure 5. 10. Tobacco leaf epidermal cells co-infiltrated with 16H02-GFP and the ER marker secRFP-p24aTM. 16H02-GFP co-localises with secRFP-p24aTM. **A.** An overview of infiltrated cells. **B.** A view of the centre of an infiltrated cell, showing the nuclear envelope labelled by both fluorescent protein fusions (white arrow). secRFP-p24aTM also labelled the nucleoplasm, although 16H02-GFP did not. **C.** A view of the cortical cytoplasm. Scale bars represent 10 μm .

5.3.6 Hsc_gene_15040

Although Hsc_gene_15040 has no annotation, this gene was chosen due to its higher expression in the gland cells compared to other worm tissues at 10 hpi. This gene has a predicted coiled coil domain, and a KKXX-like motif KGVV in the C-terminal tail, which are likely responsible for ER localisation (**Figure 5.11D**). No similar proteins to Hsc_gene_15040 were identified with the NCBI BLAST search. However, with the WormBase BLAST search, two hits were found, the *H. schachtii* gene Hsc_gene_24973 (73.7 % amino acid identity, e-value 9.1e-30) and the *H. glycines* gene Hetgly10582 (70.1 % identity, e-value 0.0002). Hsc_gene_24973 and Hetgly10582 also had a signal peptide and a single, C-terminal TMD. Additionally, Hsc_gene_24973 had a similar expression profile to Hsc_gene_15040, peaking at 48 hpi. This gene was expressed in the gland cells (361 ± 95.6) at similar levels to Hsc_gene_15040 (321 ± 60.7). However, due to similarity in sequence and expression, Hsc_gene_24973 was not selected for further analysis.

The expression of Hsc_gene_15040 was indicative of effector activity, peaking at 48 hpi (115.5 ± 36.9), with a small second peak at 12 dpi male (19.4 ± 5.5). The mean normalised expression at all other life stages was below 4.5 (**Figure 5.11A**). This gene had moderate expression in the gland cells at 10 hpi (321 ± 60.7), compared to low expression for the RNA collected from the whole worm at this time point (14.3 ± 13.7). Despite this, the J2 in-situ hybridisation was unsuccessful, with no staining detected in the worm (**Figure 5.11B**). Parasitic stage in-situ hybridisations were subsequently conducted due to low J2 expression. These in-situs showed staining of the dorsal gland (**Figure 5.11C**).

For both N- and C- terminal GFP fusions, Hsc_gene_15040 ER localisation was suggested; with labelling of the nuclear envelope observed at the central focal plane of the cell, in addition to the tubular ER network being labelled in the cortical cytoplasm. The ER marker secRFP-p24aTM was co-infiltrated with both the N- and C- terminal Hsc_gene_15040 GFP constructs, with co-localisation observed (**Figures 5.13 and 5.15**). However, as the nucleoplasm was also labelled by both GFP fusions with Hsc_gene_15040, cytoplasm localisation was also hypothesised (**Figures 5.12 and 5.14**).

Hsc_gene_15040 (no annotation)**A. Expression****B. J2 In-situ hybridisation**

Antisense Probe

Sense Probe (negative control)

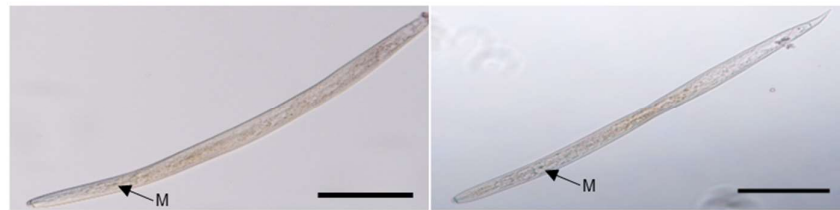
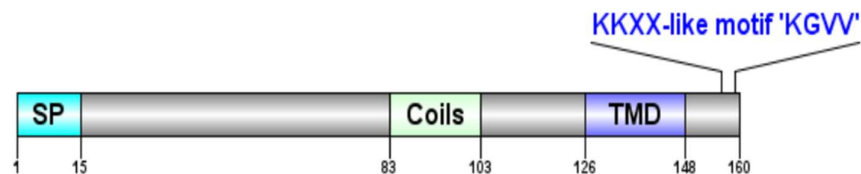
**C. Parasitic stage in-situ hybridization****D. Protein domain structure prediction**

Figure 5. 11. The analysis of Hsc_gene_15040, a *H. schachtii* gene with no annotation. A. The normalised expression of Hsc_gene_15040 across the various life stages. For each life stage, the mean expression is shown, with error bars representing the standard deviation. Expression peaked at 48 hpi, with little expression at the other life stages. **B.** J2 in-situ hybridisation, showing no staining in the worms for the antisense or sense probe. Scale bars represent 100 μm . The metacarpal bulb is labelled (M). **C.** Parasitic stage in-situ hybridization, with staining of the dorsal glands shown (DG). Scale bars represent 10 μm . **D.** Protein domain structure prediction, with a coiled coil domain (Coils) present before the transmembrane domain (TMD) and a KKXX-like motif, 'KGVV' in the C-terminal tail. SP= signal peptide.

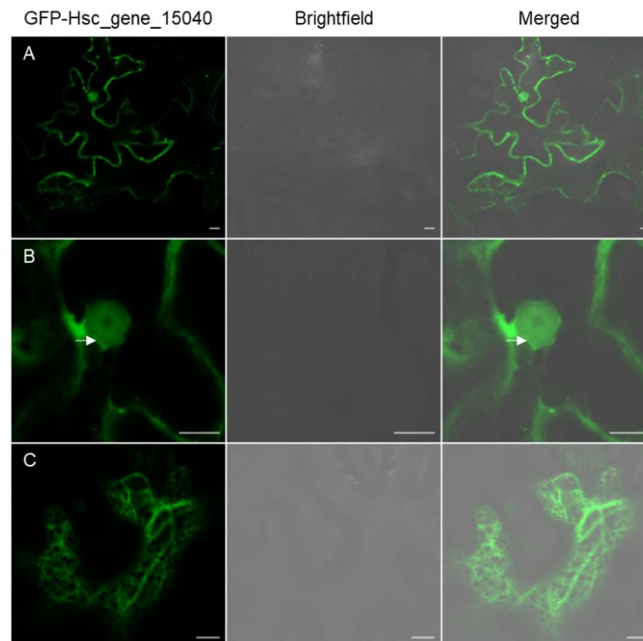


Figure 5. 12. Tobacco leaf epidermal cells *Agro*-infiltrated with the N-terminal GFP fusion for *Hsc_gene_15040*. From these images, this gene was predicted to localise to the ER. **A.** An overview of infiltrated cells. **B.** A view of the centre of an infiltrated cell, showing nucleoplasm and faint nuclear envelope localisation (white arrow). **C.** A view of the cortical cytoplasm to show the labelled ER network. Scale bars represent 10 μm .

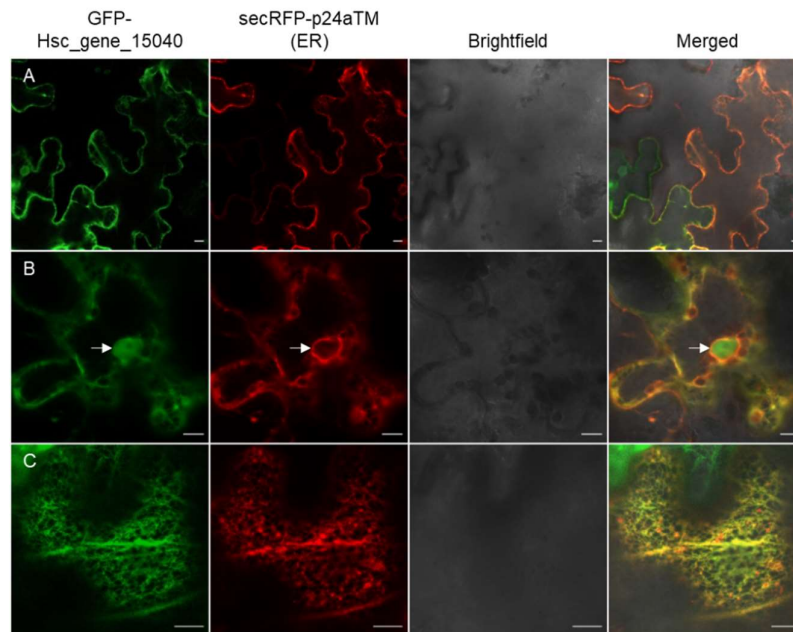


Figure 5. 13. Tobacco leaf epidermal cells co-infiltrated with GFP-*Hsc_gene_15040* and the ER marker *secRFP-p24aTM*. **A.** An overview of infiltrated cells. **B.** A view of the centre of an infiltrated cell. The nuclear envelope was labelled by both constructs, with localisation also in the nucleoplasm for GFP-*Hsc_gene_15040* (white arrow). **C.** A view of the cortical cytoplasm to show GFP-*Hsc_gene_15040* and *secRFP-p24aTM* labelling the ER network. Scale bars represent 10 μm .

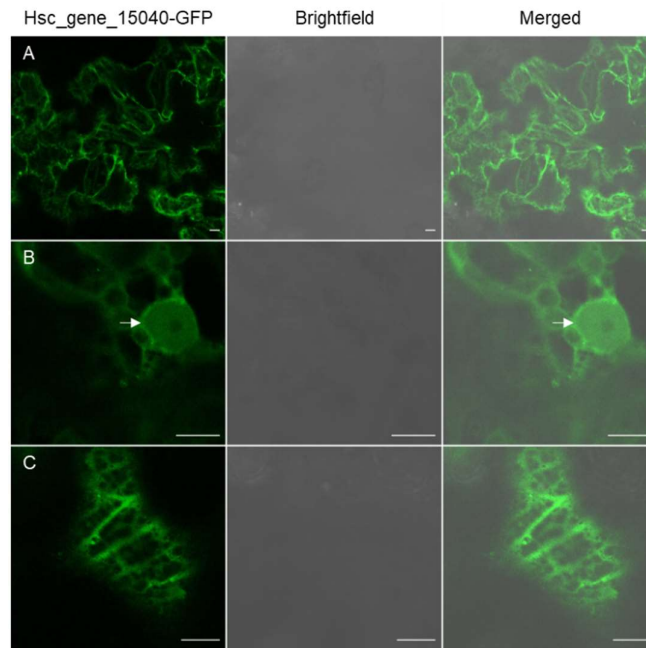


Figure 5. 14. Tobacco leaf epidermal cells *Agro*-infiltrated with the C-terminal GFP fusion of *Hsc_gene_15040*. Both the N- and C- terminal GFP fusions for *Hsc_gene_15040* were predicted to localise to the ER. **A.** An overview of infiltrated cells. **B.** A view of the centre of an infiltrated cell, showing localisation to the nucleoplasm and nuclear envelope (white arrow). **C.** A view of the cortical cytoplasm to show the ER labelled network. Scale bars represent 10 µm.

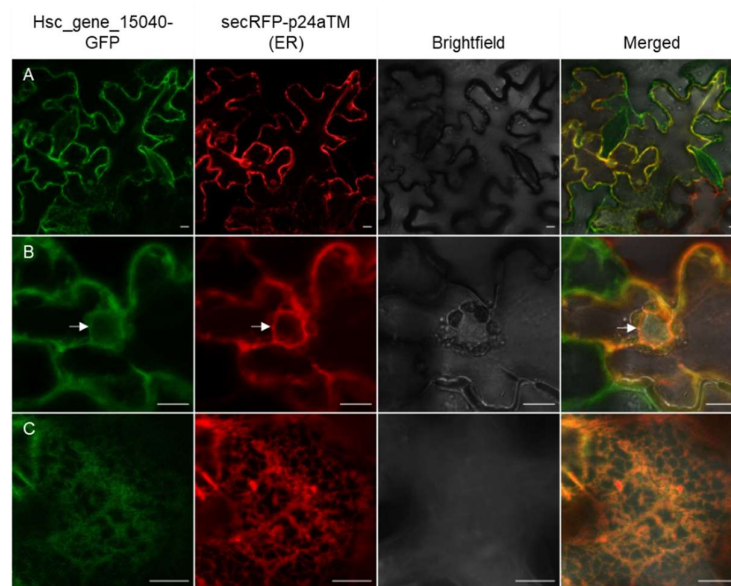


Figure 5. 15. Tobacco leaf epidermal cells co-infiltrated with *Hsc_gene_15040*-GFP and the ER marker *secRFP-p24aTM*. **A.** An overview of infiltrated cells. **B.** A view of the centre of an infiltrated cell. Both constructs label the nuclear envelope (white arrow). **C.** A view of the cortical cytoplasm to show *Hsc_gene_15040*-GFP and *secRFP-p24aTM* labelling the ER network. Scale bars represent 10 µm.

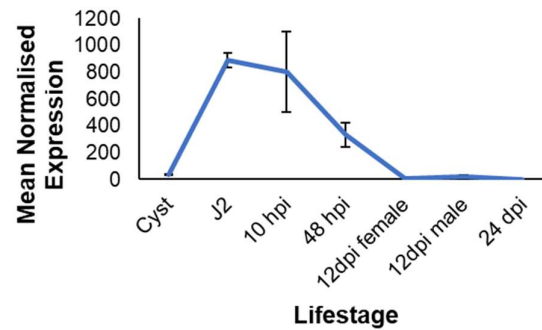
5.3.7 Hsc_gene_2739

Although Hsc_gene_2739 has no annotation, this gene was chosen as it had predicted ER localisation using the WoLF p-SORT subcellular localisation software. In addition to the predicted signal peptide and C-terminal TMD of Hsc_gene_2739, this gene had a predicted 4 residue pattern 'pat4' nuclear localisation signal present at the C-terminus (**Figure 5.16C**). With the NCBI BLAST search, no matches were identified. However, with the WormBase BLAST search, 40 hits were found. All hits were for genes belonging to cyst nematode species, *H. schachtii*, *H. glycines* and *G. rostochiensis* and *G. pallida*.

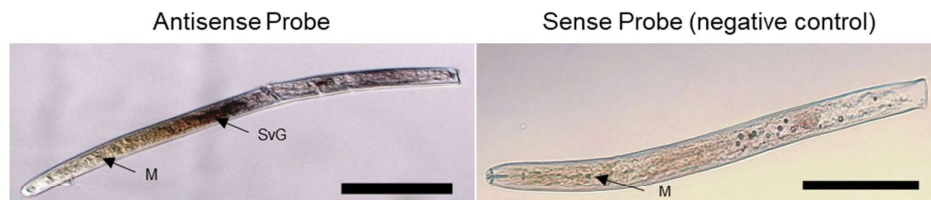
Hsc_gene_2739 was expressed highest in the early parasitic stages, from the J2 life stage through to 48 hpi (**Figure 5.16A**). The mean normalised expression was highest at the J2 (888.9 ± 52.1) and 10 hpi stages (801.6 ± 297.9), decreasing at 48 hpi (331.9 ± 89.8). Also indicating effector activity, Hsc_gene_15040 J2 in-situ hybridisations showed staining of the subventral glands (**Figure 5.16B**). The presence of the predicted nuclear localisation signal was consistent with localisation of the N- and C- terminal Hsc_gene_2739 constructs to the nucleus (**Figures 5.17 and 5.19**). The nucleoplasm and the nucleolus were labelled in tobacco leaf infiltrations of both N- and C- terminal constructs. However, the nucleolus had brighter fluorescence than the surrounding nucleoplasm. No fluorescence was observed in any other subcellular compartment. Co-localisation of both the N- and C- terminal Hsc_gene_2739 constructs with the nucleus marker NLS-mCherry was observed, although the nucleus marker only labelled the nucleoplasm, with no labelling of the nucleolus (**Figures 5.18 and 5.20**).

Hsc_gene_2739 (no annotation)

A. Expression



B. J2 In-situ hybridisation



C. Protein domain structure prediction



Figure 5. 16. The analysis of Hsc_gene_2739, a *H. schachtii* protein with no annotation. **A.** The normalised expression of Hsc_gene_2739 across the various life stages. For each life stage, the mean expression is shown, with error bars representing the standard deviation. Expression peaked at the J2 life stage, although expression remained considerable at 10 hpi, to decrease at 48 hpi. Expression at all other life stages was 0. **B.** J2 in-situ hybridisation, showing dark staining around the subventral glands (SvG), with the metacarpal bulb (M) also labelled. Scale bars represent 100 µm. **C.** Protein domain structure prediction, with the presence of a 4 residue pattern nuclear localisation signal (pat4 NLS). SP= signal peptide, TMD= transmembrane domain.

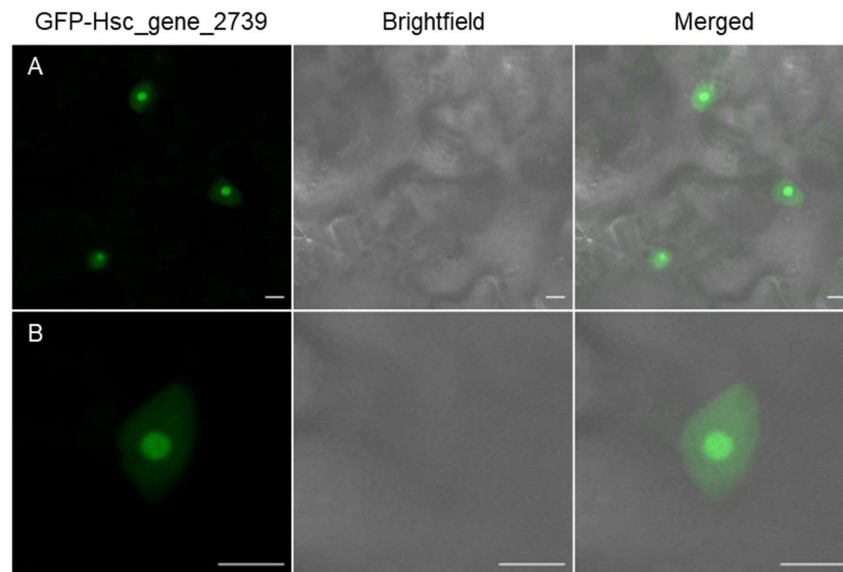


Figure 5. 17. Tobacco leaf epidermal cells *Agro*-infiltrated with GFP-Hsc_gene_2739. Nucleus localisation was observed, with stronger fluorescence in the nucleolus compared to the nucleoplasm. **A.** An overview of infiltrated cells. **B.** A view of the centre of an infiltrated cell, showing the nucleus at greater detail. Scale bars represent 10 μm .

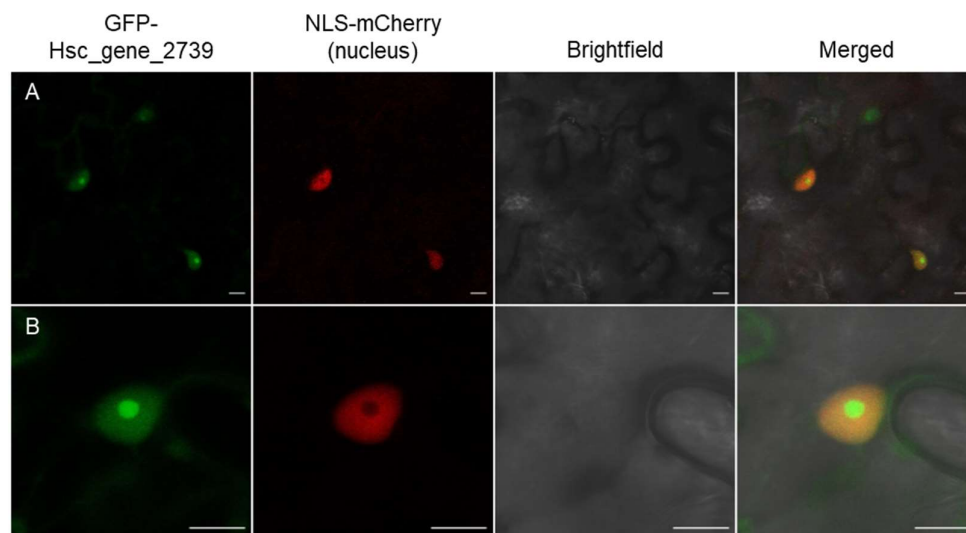


Figure 5. 18. Tobacco leaf epidermal cells co-infiltrated with GFP-Hsc_gene_2739 and the nucleus marker NLS-mCherry. Co-localisation of the two markers was observed. **A.** An overview of infiltrated cells. **B.** A view of the centre of an infiltrated cell, showing the nucleus in greater detail. GFP-Hsc_gene_2739 showed stronger fluorescence in the nucleolus, although NLS-mCherry only localised to the nucleoplasm. Scale bars represent 10 μm .

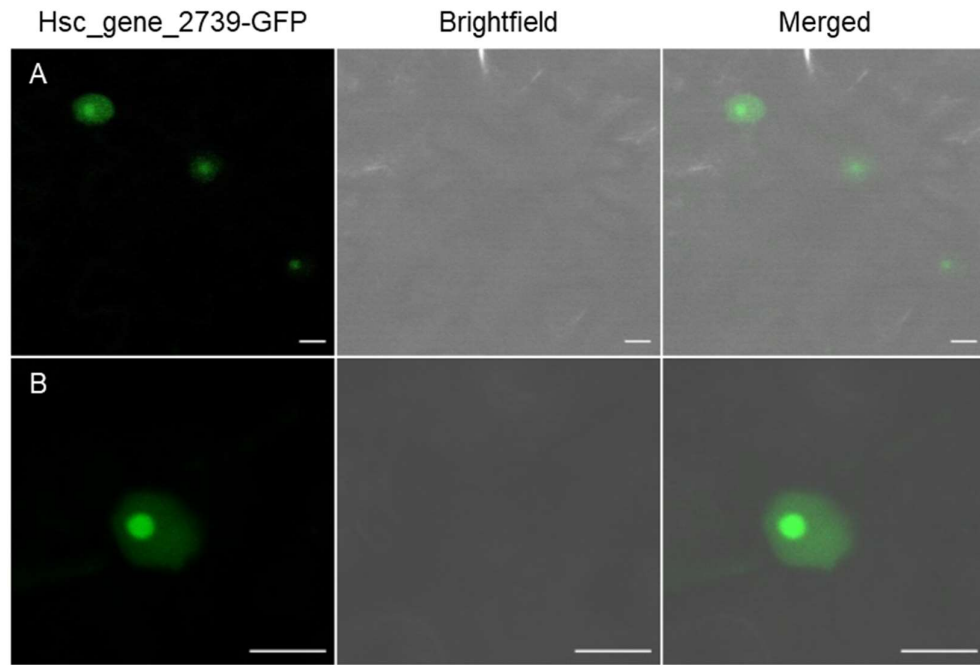


Figure 5. 19. Tobacco leaf epidermal cells *Agro*-infiltrated with Hsc_gene_2739-GFP. Nucleus localisation was observed in both the N- and C- terminal fusions of this gene. **A.** An overview of infiltrated cells. **B.** A view of the centre of an infiltrated cell, showing the nucleus in greater detail. As was observed for the N-terminal GFP fusion, fluorescence was stronger in the nucleolus than the nucleoplasm. Scale bars represent 10 μm .

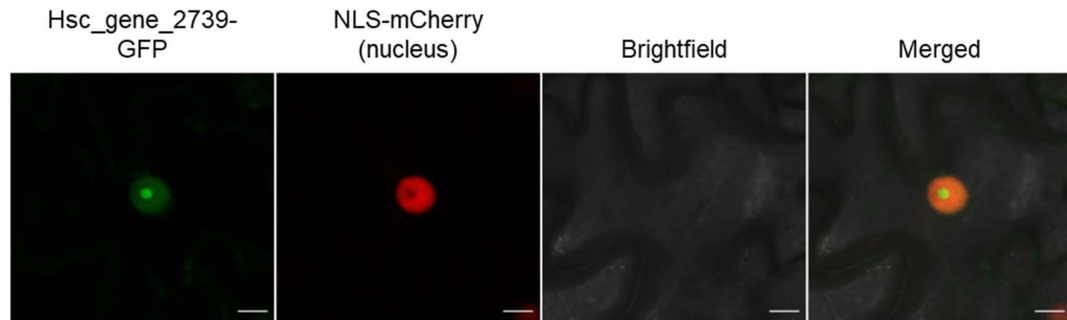


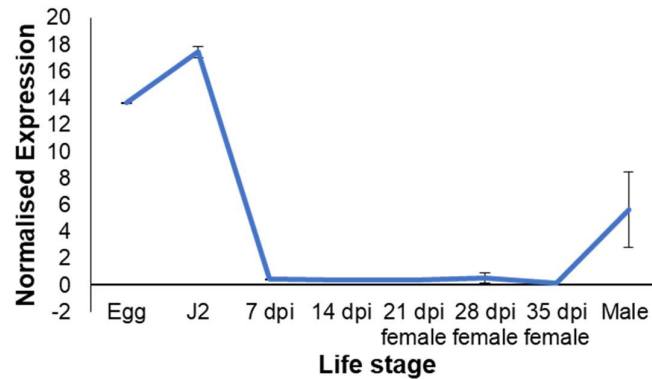
Figure 5. 20. Tobacco leaf epidermal cells co-infiltrated with Hsc_gene_2739-GFP and the nucleus marker NLS-mCherry. The images show the centre of an infiltrated cell, focusing on the nucleus. Both markers co-localise, although NLS-mCherry fluorescence was not present in the nucleolus. Scale bars represent 10 μm .

5.3.8 GPLIN_001269700

GPLIN_001269700 was an unannotated gene, chosen due to the presence of two DOG box promoter element motifs within 500 bp upstream of the gene. This protein had no predicted domains, other than the prerequisite signal peptide, C-terminal TMD and two localisation signals present in the signal peptide (**Figure 5.21C**). Despite this, 48 NCBI BLAST hits were found to match GPLIN_001269700. The most similar were two unnamed protein products from the root-knot nematode *Meloidogyne enterolobii*, sharing 47 % sequence identity (e-values 4e-99 and 5e-99). Other hits included genes from other cyst nematode species, including *H. glycines*, several root-knot nematode *Meloidogyne* spp., in addition to genes from mycophagous and animal parasitic nematode species.

The expression of GPLIN_001269700 could indicate effector activity (**Figure 5.21A**). For instance, expression peaked at the J2 stage (17.4 ± 0.4), although expression was also high at the egg stage (13.6 ± 0.005), and had a small peak at the male stage (5.6 ± 2.8). However, this gene had low levels of expression relative to other *G. pallida* genes of the same dataset, with expression being no higher than 17 throughout all life stages measured. J2 in-situ hybridisation of this gene showed dorsal gland localisation (**Figure 5.21B**).

The N-terminal GFP construct, GFP-GPLIN_001269700, likely had cytoplasm localisation. This was indicated through labelling of the nucleoplasm but not the nucleolus. Weak ER localisation was also suggested from images of the cortical cytoplasm of cells infiltrated with GFP-GPLIN_001269700 (**Figure 5.22**). When co-infiltrated with the ER marker secRFP-p24aTM, co-localisation was observed (**Figure 5.23**). The C-terminal GFP fusion for GPLIN_001269700 also showed weak cytoplasm localisation, with faint staining of the nucleoplasm (**Figure 5.24**). Possible ER localisation may also have been observed, with partial co-localisation with the ER marker secRFP-p24aTM (**Figure 5.25**). However, as the expression of GPLIN_001269700-GFP was very weak, this was not confirmed. Additionally, in contrast to the N-terminal GFP construct for GPLIN_001269700, the C-terminal GFP fusion localised to punctae within infiltrated tobacco leaf cells (**Figure 5.25**). No additional organelle marker was co-infiltrated with this gene. Although, from the subcellular localisation prediction servers, markers for the Golgi, endosomes, peroxisomes and mitochondria could be used for future infiltrations (**Table 5.7**).

GPLIN_001269700 (No annotation)**A. Expression****B. J2 In-situ hybridisation**

Antisense Probe

Sense Probe (negative control)

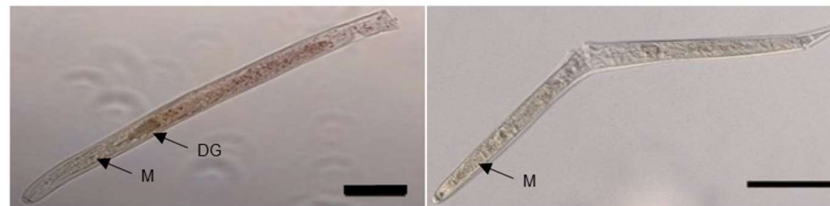
**C. Protein domain structure prediction**

Figure 5. 21. The analysis of GPLIN_001269700, a *G. pallida* gene with no annotation. A. Expression of GPLIN_001269700 across the various life stages. For each life stage, the mean expression is shown, with error bars representing the standard deviation. Expression is highest at the egg and J2 life stages, with a smaller peak present in adult males. There is very little expression at all other life stages. **B.** J2 in-situ hybridisation, showing staining in the dorsal gland (DG). The metacorporeal bulb is also labelled (M). Scale bars represent 100 μ m. **C.** Protein domain structure prediction, with a predicted XXRR-like motif, LRRL, and a predicted mitochondrial presequence cleavage site, RRL|NV, at the N-terminus prior to the predicted signal peptide. SP= signal peptide. TMD= transmembrane domain.

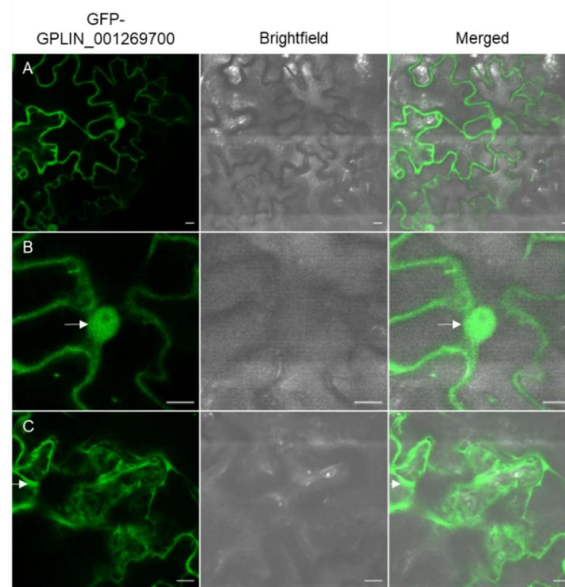


Figure 5. 22. Tobacco leaf epidermal cells *Agro*-infiltrated with GFP-GPLIN_001269700. Cytoplasm and possible weak ER localisation was observed. **A.** An overview of infiltrated cells. **B.** A view of the centre of an infiltrated cell, showing GFP-GPLIN_001269700 labelling the nucleoplasm (white arrow), with no nuclear envelope localisation observed. **C.** The cortical cytoplasm of a cell, showing cytoplasmic localisation, with possible localisation in some ER tubules (white arrow), although these might be cytoplasmic strands. Scale bars represent 10 µm.

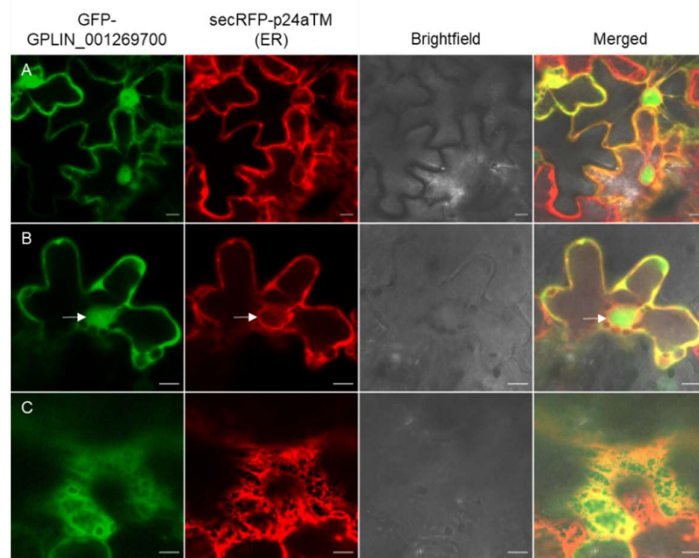


Figure 5. 23. Tobacco leaf epidermal cells co-infiltrated with GFP-GPLIN_001269700 and the ER marker secRFP-p24aTM. GPLIN_001269700 appeared to localise to the cytoplasm rather than the ER. **A.** An overview of infiltrated cells. **B.** A view of the centre of an infiltrated cell, showing GFP-GPLIN_001269700 labelling the nucleoplasm (white arrow), while secRFP-p24aTM labelled the nuclear envelope. **C.** The cortical cytoplasm of a cell. For secRFP-p24aTM, a distinct ER pattern was observed. However, for GFP-GPLIN_001269700, a much more diffused signal was visualised. Scale bars represent 10 µm.

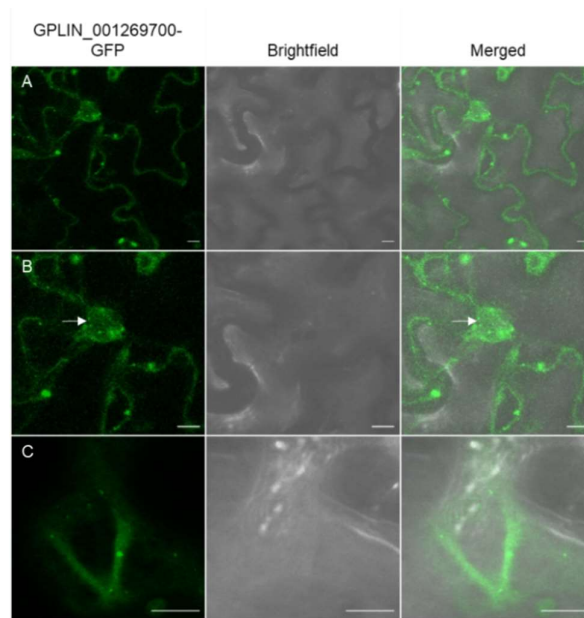


Figure 5. 24. Tobacco leaf epidermal cells *Agro*-infiltrated with GPLIN_001269700-GFP. Weak cytoplasm localisation was observed, in addition to punctate structures and possible weak ER localisation. **A.** An overview of infiltrated cells. **B.** A view of the centre of an infiltrated cell, showing GPLIN_001269700-GFP labelling the nucleoplasm and nuclear envelope (white arrow). **C.** The cortical cytoplasm of a cell, showing ER or cytoplasmic strands, with punctae. Scale bars represent 10 μ m.

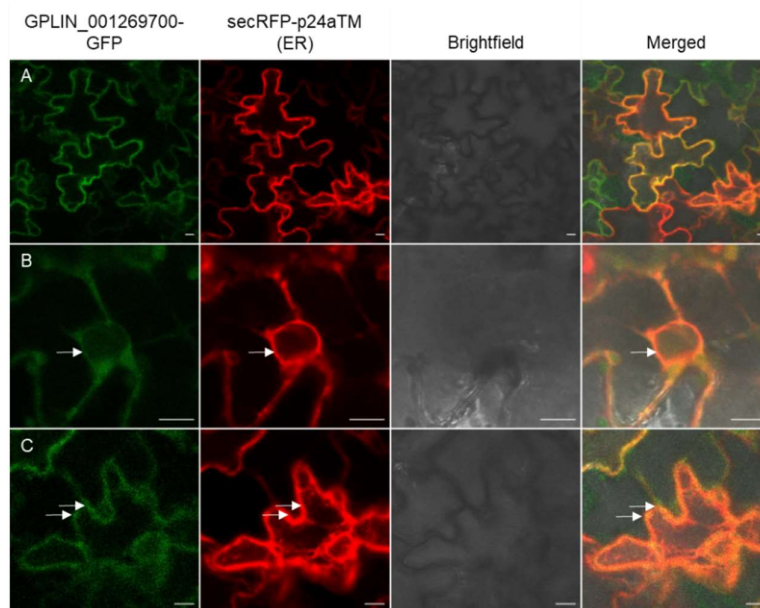


Figure 5. 25. Tobacco leaf epidermal cells co-infiltrated with GPLIN_001269700-GFP and the ER marker secRFP-p24aTM. Although GPLIN_001269700-GFP expression was much weaker than secRFP-p24aTM expression, co-localisation between the two constructs was observed. **A.** An overview of infiltrated cells. **B.** A view of the centre of an infiltrated cell, showing GPLIN_001269700-GFP and secRFP-p24aTM labelling the nuclear envelope (white arrow). **C.** A cell showing GPLIN_001269700 labelling very weak punctae (white arrows). Scale bars represent 10 μ m.

5.3.9 Hsc_gene_19069

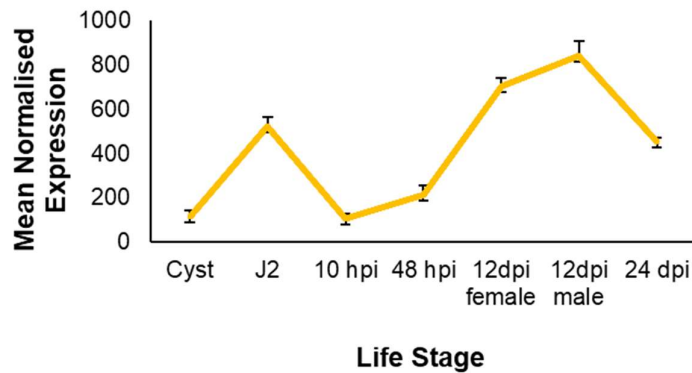
Hsc_gene_19069 was chosen due to its annotation “putative esophageal gland cell secretory protein 28”. In addition to the prerequisite signal peptide and C-terminal TMD, Hsc_gene_19069 contained a predicted EGF-like (epidermal growth factor-like) domain. Also, subcellular localisation motifs were identified in the sequence, including a C-terminal KKXX-like motif KAPR (**Figure 5.26C**).

Several BLAST hits for Hsc_gene_19069 were identified. For the WormBase BLAST search, this included the *H. schachtii* protein, Hsc_gene_1528, which had the same annotation to Hsc_gene_19069, and shared 96.8 % identity (e-value 1.9e-123). This gene also has a similar expression profile to Hsc_gene_19069, although the expression at the J2 stage (453.7 ± 57.1) was lower than that for Hsc_gene_19069 (520 ± 44.1). In addition to this paralogue, 53 other WormBase BLAST hits were identified, which only included genes belonging to cyst nematode and root-knot nematode species. The most similar *G. pallida* gene was GPLIN_000231600, which has the same structure as Hsc_gene_19069, containing a predicted signal peptide and C-terminal TMD. With GPLIN_000231600, expression also peaked at the J2 stage. Other NCBI BLAST hits included the tenascin-R gene from the migratory plant root nematode *Ditylenchus destructor* (46.9 % identity; e-value 3e-57) and the *Acp-5* gene from the leaf nematode *Aphelenchoides besseyi* (43.8% sequence similarity; e-value 1e-42) that has predicted phosphatase activity.

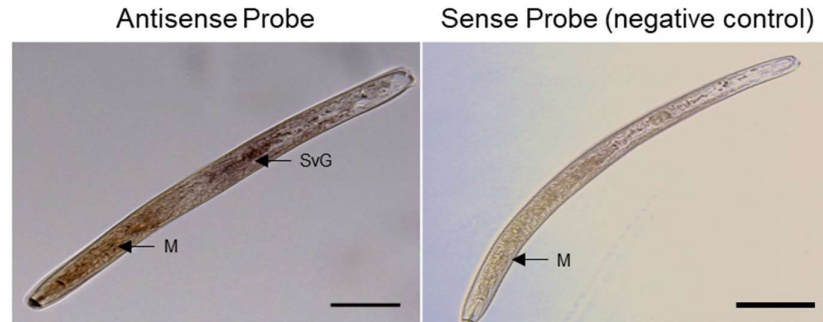
The expression of Hsc_gene_19069 could potentially indicate a role in parasitism. This gene peaked at the J2 (520.1 ± 44.1), 12 dpi female (702.8 ± 37.1), 12 dpi male (841.5 ± 63.1) and 24 dpi female life stages (453.1 ± 16.6). The mean normalised expression was below 250 for all other life stages. Additionally, J2 in-situ hybridisations suggested that this gene was expressed in the subventral glands (**Figure 5.26B**). The subcellular localisation of the N- and C- terminal Hsc_gene_19069-GFP constructs appeared to be the same, labelling the cytoplasm and punctate structures (**Figures 5.27 and 5.29**). Both GFP fusion constructs were co-infiltrated with the mitochondria marker ScCOX4sp-mCherry, as mitochondria was the best predicted localisation of the punctate structures (**Table 5.7**). However, no co-localisation was observed between ScCOX4sp-mCherry and the N- and C- terminal Hsc_gene_19069 GFP constructs (**Figures 5.28 and 5.30**).

Hsc_gene_19069
(putative esophageal gland cell secretory protein 28)

A. Expression



B. J2 In-situ hybridisation



C. Protein domain structure prediction

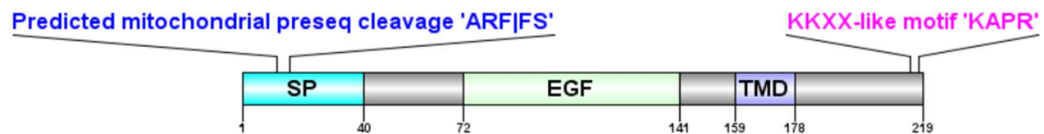


Figure 5. 26. The analysis of Hsc_gene_19069 (putative esophageal gland cell secretory protein 28). **A.** The expression of Hsc_gene_19069 across various time points. Expression peaked at J2, 12 dpi female, 12 dpi male and 24 dpi. hpi= hours post infection, dpi = days post infection. **B.** J2 in-situ hybridisations, showing staining where the subventral glands (SvG) were expected to be. The metacarpal bulb (M) is also labelled. Scale bars represent 100 µm. **C.** Protein domain structure prediction of Hsc_gene_19069. A predicted mitochondrial presequence cleavage site (ARF|FS) was located in the signal peptide. This protein also contained a predicted epidermal growth factor (EGF) domain, which was followed by a C-terminal transmembrane domain (TMD) and a KKXX-like motif 'KAPR' in the C-terminal tail. SP= signal peptide.

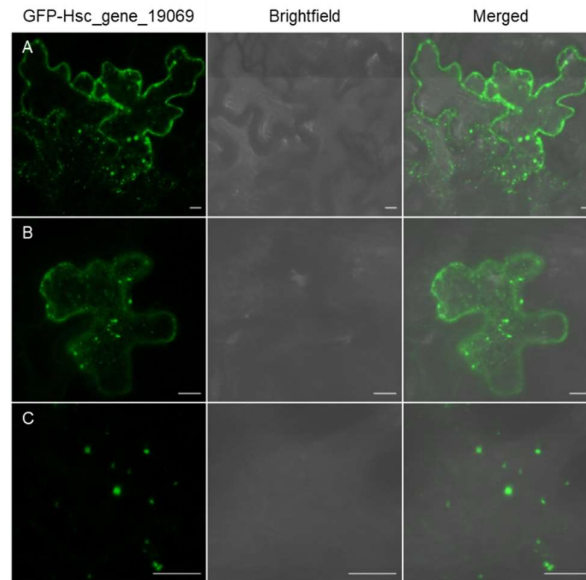


Figure 5. 27. Tobacco leaf epidermal cells *Agro*-infiltrated with GFP-Hsc_gene_19069. Cytoplasm and punctae localisation was observed. **A.** An overview of infiltrated cells. **B.** A view of the centre of an infiltrated cell, showing GFP-Hsc_gene_19069 label numerous punctate structures and the cytoplasm. **C.** The cortical cytoplasm of a cell, showing the labelled punctae in more detail. Scale bars represent 10 μ m.

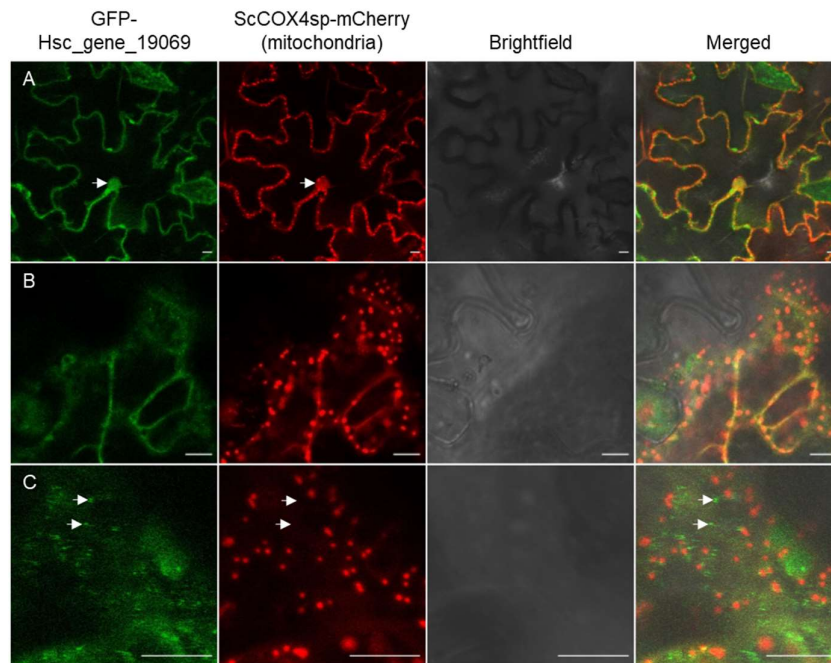


Figure 5. 28. Tobacco leaf epidermal cells co-infiltrated with GFP-Hsc_gene_19069 and the mitochondria marker ScCOX4sp-mCherry. No co-localisation between the two markers was observed. **A.** An overview of infiltrated cells, with both constructs showing fluorescence in the nucleoplasm (white arrow). **B.** A view of the centre of an infiltrated cell. Due to weak expression, no punctae are observed for GFP-Hsc_gene_19069. **C.** The cortical cytoplasm of a cell, showing labelled GFP-Hsc_gene_19069 punctae which do not co-localise with ScCOX4sp-mCherry (white arrows). Scale bars represent 10 μ m.

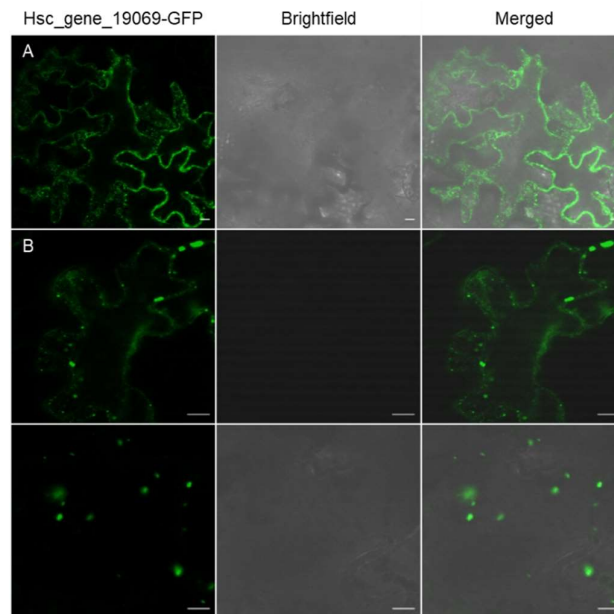


Figure 5. 29. Tobacco leaf epidermal cells *Agro*-infiltrated with Hsc_gene_19069-GFP. Cytoplasm and punctae localisation was observed, similar to the N-terminal fusion. **A.** An overview of infiltrated cells. **B.** A view of the centre of an infiltrated cell, showing Hsc_gene_19069-GFP within the cytoplasm and punctae. **C.** The cortical cytoplasm of a cell, showing the labelled punctae in more detail. Scale bars represent 10 μm .

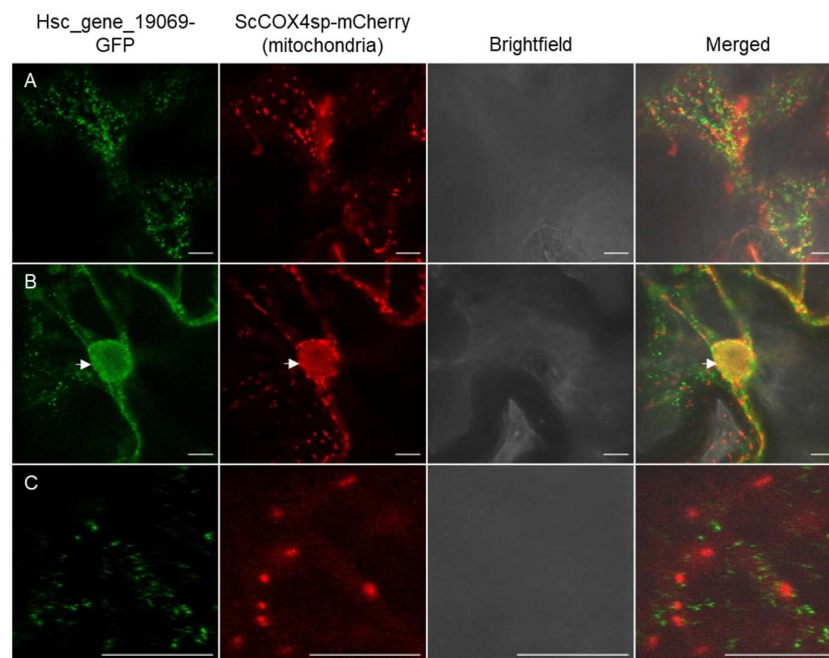


Figure 5. 30. Tobacco leaf epidermal cells co-infiltrated with Hsc_gene_19069-GFP and the mitochondria marker ScCOX4sp-mCherry. No co-localisation between the two FP-gene fusions was observed. **A.** An overview of an infiltrated cell, showing punctae labelled by both constructs, which do not co-localise. **B.** A view of the centre of an infiltrated cell, showing both FP-gene fusions labelling the nucleoplasm (white arrow). **C.** The cortical cytoplasm of a cell, showing the labelled punctae in more detail. Scale bars represent 10 μm .

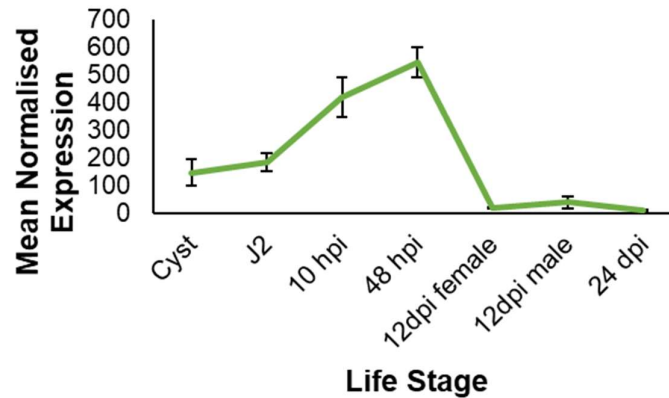
5.3.10 Hsc_gene_19059

Although Hsc_gene_19059 had no annotation, it had predicted ER localisation using the subcellular localisation prediction software WoLF pSORT. No NCBI BLAST hits were found for this gene, and the WormBase BLAST hits were only uncharacterised genes from other cyst nematode species, *H. glycines*, *G. rostochiensis* and *G. pallida*. Hsc_gene_19059 was expressed at the cyst stage (145.8 ± 47.8), yet was the highest at the J2 (184.1 ± 32.8), 10 hpi (418.9 ± 71.8) and 48 hpi (546.1 ± 55.6) life stages. The mean normalised expression was below 40 for all other life stages (**Figure 5.31A**). The J2 in-situ hybridisations for Hsc_gene_19059 were unsuccessful, with no staining detected in any region of the worms (**Figure 5.31C**). As the expression of Hsc_gene_19059 was almost three times higher at 48 hpi compared to the J2 life stage, early parasitic stage in-situ hybridisations would be useful to test for gland cell expression.

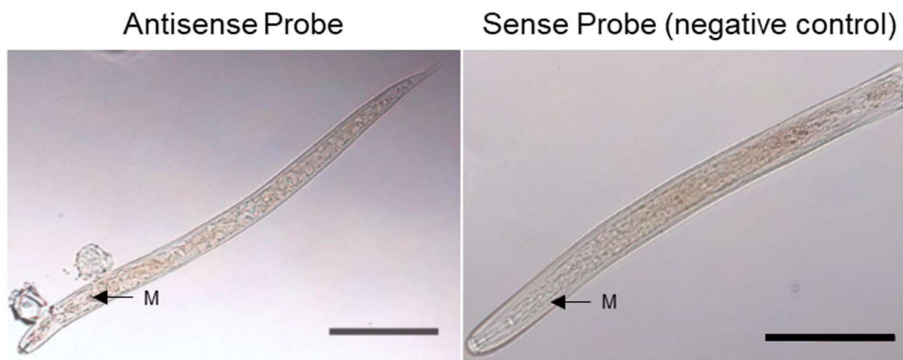
This gene had two predicted subcellular localisation signals, a bipartite nuclear localisation signal prior to the C-terminal TMD, and a KKXX-like motif, GKAA, in the C-terminal tail, which is associated with ER retention (**Figure 5.31C**). Both the N- and C-terminal GFP fusions for Hsc_gene_19059 showed localisation to the nucleus and punctate structures of tobacco leaf cells, with brighter labelling of the nucleolus compared to the nucleoplasm (**Figures 5.32 and 5.34**). As the peroxisome was predicted to be the most likely subcellular localisation of the punctate structures, the peroxisome marker mCherry-SKL was co-infiltrated with both N- and C-terminal GFP fusion constructs for Hsc_gene_19059. Interestingly, for GFP-Hsc_gene_19059, the punctae completely co-localised with the peroxisome marker (**Figure 5.33**). However for the C-terminal GFP fusion some, but not all, of the abundant punctae present in the cytoplasm co-localised with the peroxisome marker (**Figure 5.35**). As the subcellular prediction servers also predicted mitochondria and Golgi localisation (**Table 5.7**), markers for these organelles could be co-infiltrated with Hsc_gene_19059 to help identify the localisation of the additional punctate structures. Moreover, as C-terminal TMDs are features of both peroxisome and mitochondria targeting proteins (Costello et al, 2017), the mitochondria may be a likely localisation of the punctate structures.

Hsc_gene_19059 (No annotation)

A. Expression



B. J2 In-situ hybridisation



C. Protein domain structure prediction

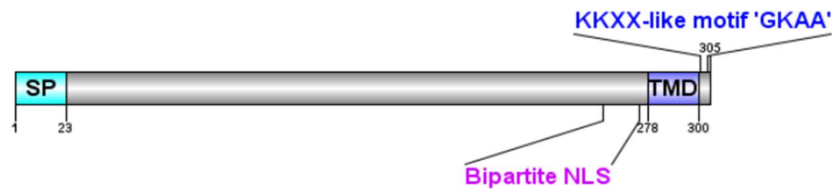


Figure 5. 31. The analysis of Hsc_gene_19059 (no annotation). **A.** The normalised expression of Hsc_gene_19059 across various time points. Expression peaked at 10 and 48 hours post infection (hpi) for this gene. Low expression was observed at the cyst and J2 life stages, and from 12 days post infection (12 dpi) onwards. For each life stage, the mean expression is shown, with error bars representing the standard deviation. **B.** J2 in-situ hybridisation of Hsc_gene_19059. There was no visible staining of any structures. The metacarpal bulb is labelled (M). Scale bars represent 100 μ m. **C.** Protein domain structure prediction, showing a signal peptide (SP), followed by a bipartite nuclear localisation signal (bipartite NLS), a C-terminal transmembrane domain (TMD), and a KKXX-like motif 'GKAA'.

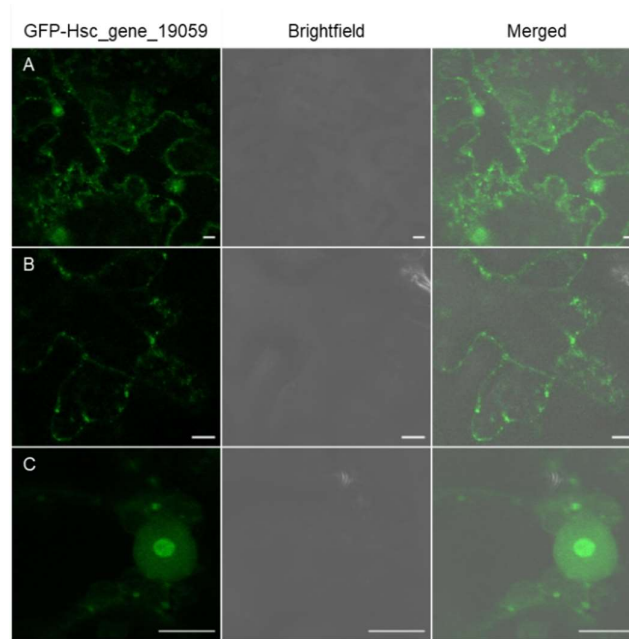


Figure 5. 32. Tobacco leaf epidermal cells *Agro*-infiltrated with GFP-Hsc_gene_19059. Localisation to the nucleus and punctae was observed. **A.** An overview of infiltrated cells. **B.** A view of the centre of an infiltrated cell, showing punctae and weak cytoplasm localisation. **C.** A close up image of the nucleus, showing brighter fluorescence of GFP-Hsc_gene_19059 at the nucleolus. Scale bars represent 10 μ m.

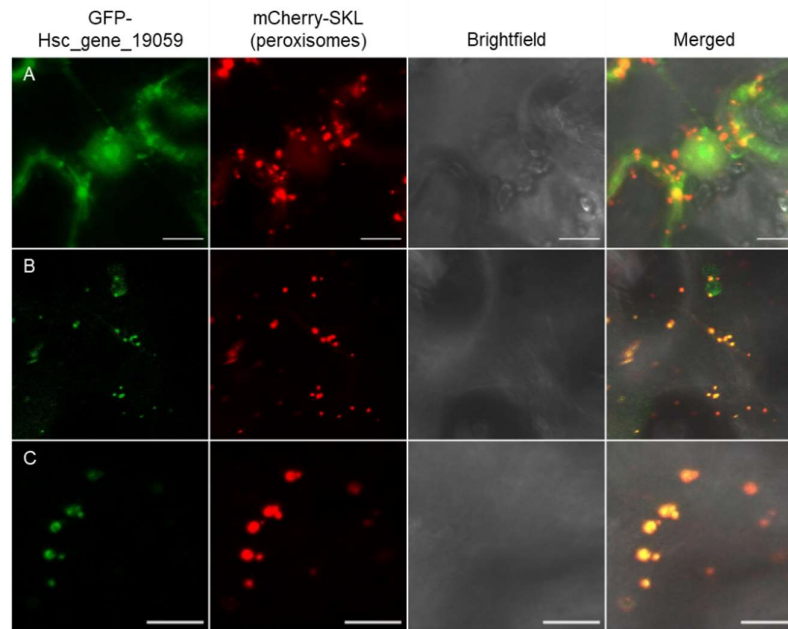


Figure 5. 33. Tobacco leaf epidermal cells of GFP-Hsc_gene_19059 co-infiltrated with the peroxisome marker mCherry-SKL. Co-localisation between GFP-Hsc_gene_19059 and mCherry-SKL was observed. **A.** A close up image of a GFP-Hsc_gene_19059 labelled nucleus. **B.** The cortical cytoplasm of a cell, showing co-localisation between GFP-Hsc_gene_19059 and the peroxisome marker. **C.** A close up image of the cortical cytoplasm to further show the co-localisation. Scale bars represent 10 μ m.

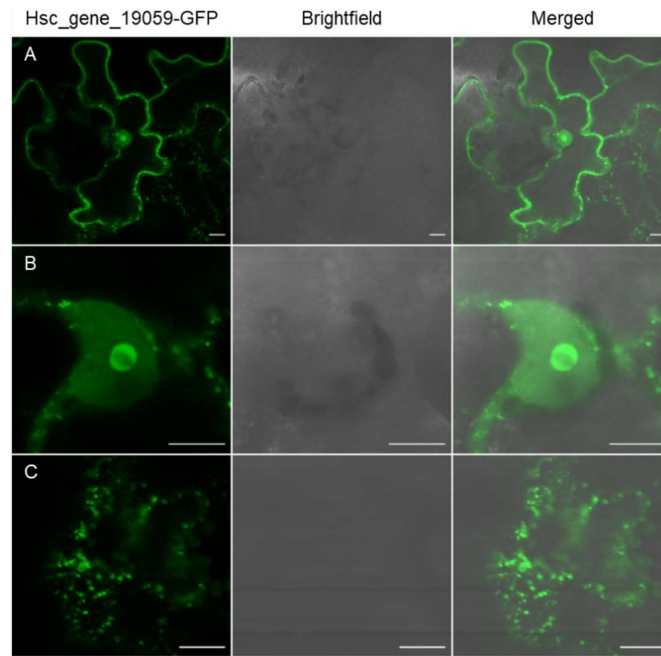


Figure 5. 34. Tobacco leaf epidermal cells *Agro*-infiltrated with Hsc_gene_19059-GFP. Localisation to the nucleus and punctae was observed, similar to the N-terminal GFP fusion. **A.** An overview of infiltrated cells. **B.** A close up of a labelled nucleus, showing brighter fluorescence at the nucleolus, and punctae around the periphery of the nucleoplasm. **C.** Labelled punctae dispersed through the cortical cytoplasm of a cell. Scale bars represent 10 μm .

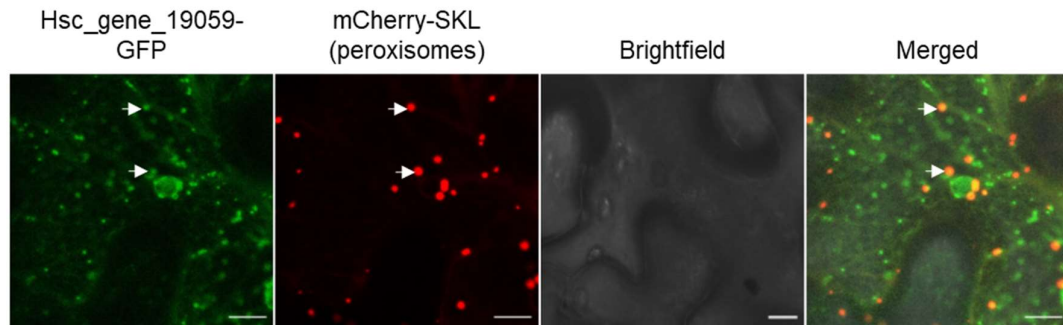


Figure 5. 35. Tobacco leaf epidermal cells co-infiltrated with Hsc_gene_19059-GFP and the peroxisome marker mCherry-SKL. Although some Hsc_gene_19059-GFP punctae are closely associated with mCherry-SKL punctae (white arrows), there were many more Hsc_gene_19059-GFP punctae in the cells than mCherry-SKL, with several punctae which did not co-localise. Scale bars represent 10 μm .

5.3.11 Hsc_gene_14672

Hsc_gene_14672 was selected due to its similarity to the cyst nematode SPRY-SEC effectors. This gene had a predicted B30.2/SPRY domain and a predicted mitochondrial presequence cleavage site KRA|EI following the signal peptide (**Figure 5.36C**). Ninety-nine NCBI BLAST hits for Hsc_gene_14672 were identified, all *G. pallida* genes. BLAST hits included Ran-Binding proteins and SPRY domain containing proteins. One of the BLAST hits identified was the *G. pallida* SPRY-SEC effector RBP-1, sharing 34.47 % sequence identity (e-value $3e-25$). This protein induces effector triggered immunity through binding to the potato cell surface receptor, Gpa2 (Sacco et al, 2009). BLAST hits were also identified for the *G. rostochiensis* SPRY-SEC effectors GrSPRYSEC-4 (34.74 % identity, e-value $3e-23$), GrSPRYSEC-18 (40.11 % identity, e-value $1e-26$), and GrSPRYSEC-19 (43.02 % identity, e-value $2e-24$), all of which suppress plant cell death (Ali et al, 2015). Using the WormBase genome database, similar BLAST hits were identified, although SPRY domain containing proteins from cyst nematode species other than *G. pallida* were identified: *H. schachtii*, *H. glycines* and *G. rostochiensis*.

The expression of Hsc_gene_14672 was consistently low across the early parasitic stages, disputing effector activity of this gene (**Figure 5.36A**). For example, the mean normalised expression values for the cyst, J2, 10 hpi and 48 hpi life stages were below 50. This increased at the 12 dpi female stage (77.9 ± 15.4), to peak at the 12 dpi male stage (227.9 ± 9.1), and the 24 dpi stage (147.4 ± 18.8). In line with this, no staining was detected for the J2 in-situ hybridisations (**Figure 5.36B**). Also, contrasting subcellular localisations were identified for the N- and C- terminal Hsc_gene_14672 GFP fusions. For GFP-Hsc_gene_14672, weak cytoplasm localisation was observed (**Figure 5.37**). 35S:GFP was infiltrated on its own to use as a comparison for cytoplasm localisation (**Figure 5.38**). Labelling of the nucleoplasm was observed for both GFP-Hsc_gene_14672 and 35S:GFP, in addition to weak cytoplasmic strands and a diffused signal across the cortical cytoplasm. Contrastingly, for Hsc_gene_14672-GFP, the cytoplasm was labelled in addition to punctate structures (**Figure 5.39**). As the peroxisome was the most likely predicted punctate structure for Hsc_gene_14672-GFP, mCherry-SKL was used for co-infiltrations, although no co-localisation was observed (**Figure 5.40**). Instead, these punctae could localise to the mitochondria, as predicted by the PSORTII and MultiLoc2 servers (**Table 5.7**), and the presence of a mitochondrial pre-sequence cleavage site.

Hsc_gene_14672 Ran binding protein-1

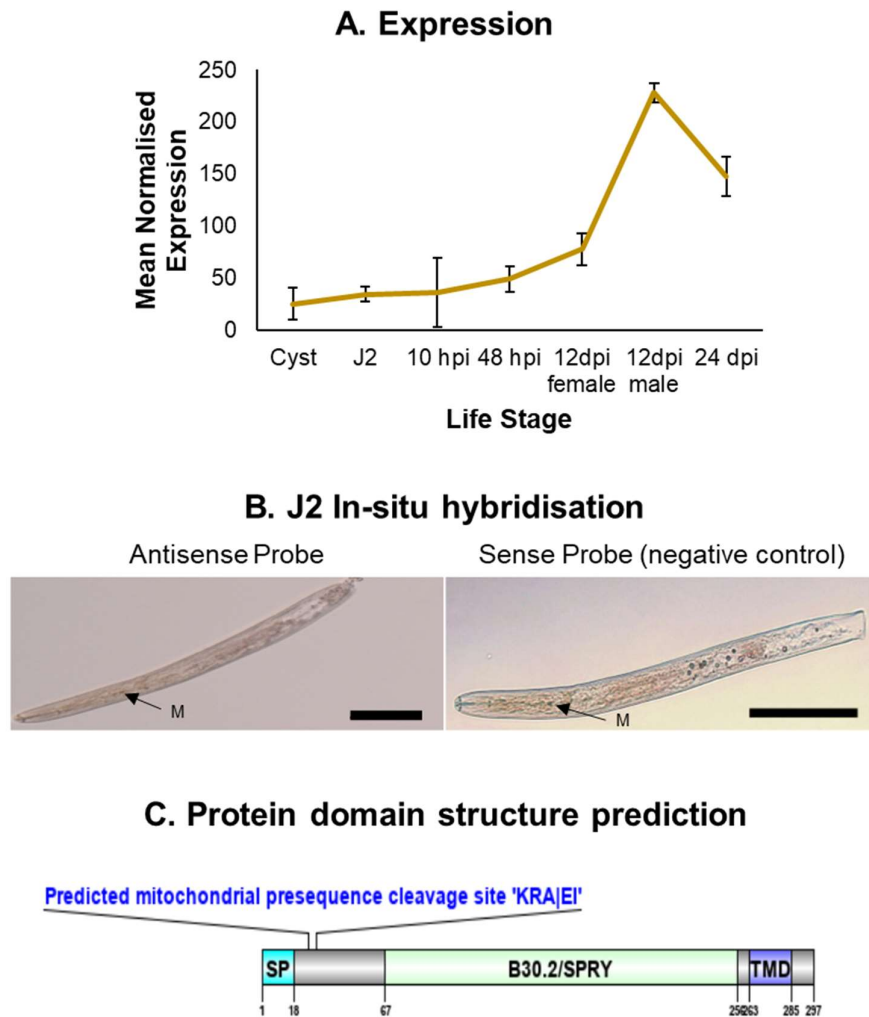


Figure 5. 36. The analysis of Hsc_gene_14672, the Ran binding protein-1. A. The normalised expression of Hsc_gene_14672 across the various life stages. For each life stage, the mean expression is shown, with error bars representing the standard deviation. Expression was highest in 12 dpi males and 24 dpi females. Hpi = hours post infection, dpi = days post infection. **B.** J2 in-situ hybridisation, with no staining detected in any part of the worm for the antisense or sense probe. Scale bars represent 100 μ m. The metacarpal bulb is labelled (M). **C.** Protein domain structure prediction, showing a predicted mitochondrial presequence cleavage site 'KRAE|' following the signal peptide, and a predicted B30.2/SPRY domain in the mid-portion of the gene. SP= signal peptide. TMD= transmembrane domain.

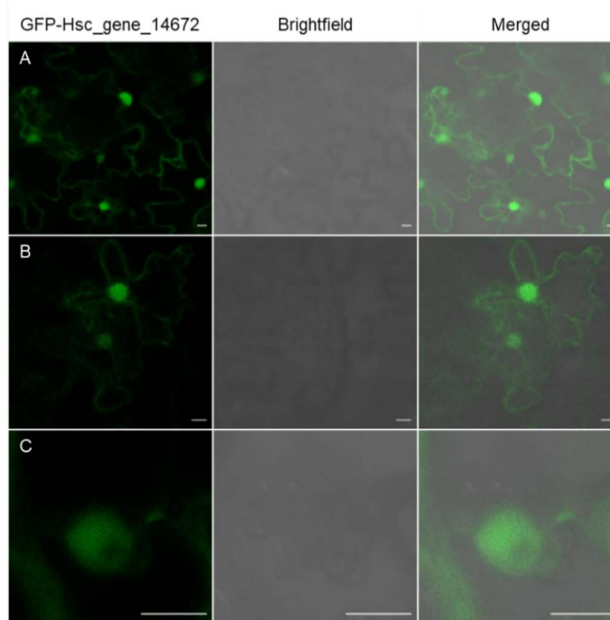


Figure 5. 37. Tobacco leaf epidermal cells *Agro*-infiltrated with GFP-Hsc_gene_14672. Cytoplasm localisation was predicted, with labelling of the nucleoplasm and a diffused GFP signal present in the cytoplasm. **A.** An overview of infiltrated cells. **B.** Infiltrated cells showing the labelled nucleoplasm and weak fluorescence diffused throughout the cytoplasm. **C.** A close up of a labelled nucleoplasm, with no fluorescence visible in the nucleolus. Scale bars represent 10 μ m.

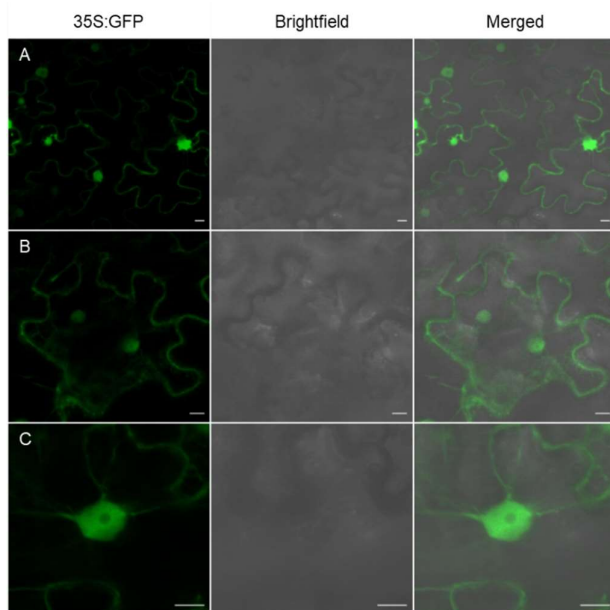


Figure 5. 38. Tobacco leaf epidermal cells *Agro*-infiltrated with 35S:GFP, used a control for cytoplasm localisation. **A.** An overview of infiltrated cells. **B.** An overview of two cells, showing the labelled nucleoplasm, and weak fluorescence diffused throughout the cytoplasm. **C.** A close up of a labelled nucleoplasm, with no fluorescence visible in the nucleolus, and cytoplasmic strands visible. Scale bars represent 10 μ m.

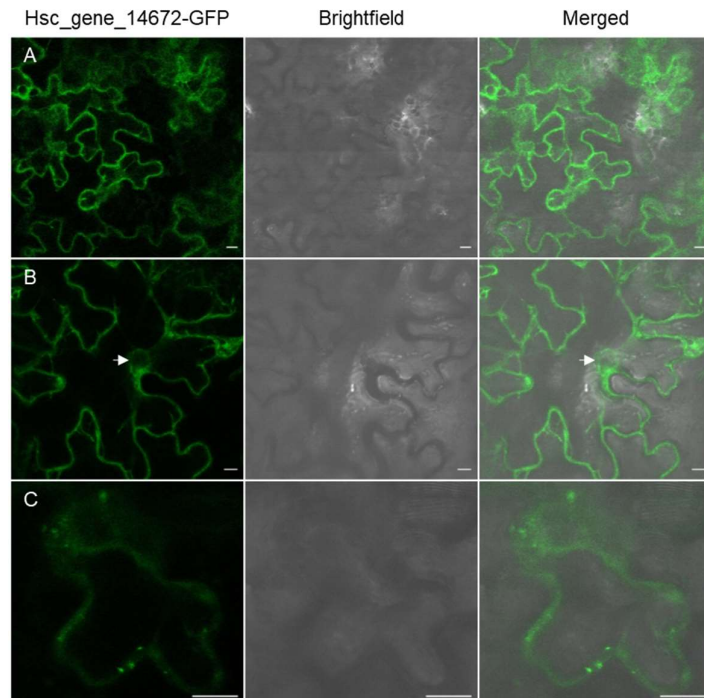


Figure 5. 39. Tobacco leaf epidermal cells *Agro*-infiltrated with Hsc_gene_14672-GFP. Cytoplasm and potentially weak ER localisation was predicted, in addition to the visualisation of punctae. **A.** An overview of infiltrated cells. **B.** The central focal plane of a cell, showing the labelled nuclear envelope (white arrow). Due to weak expression, no punctae were visible in this cell. **C.** A close up of a cell, showing punctae and a diffused fluorescence across the cortical cytoplasm. Scale bars represent 10 μm .

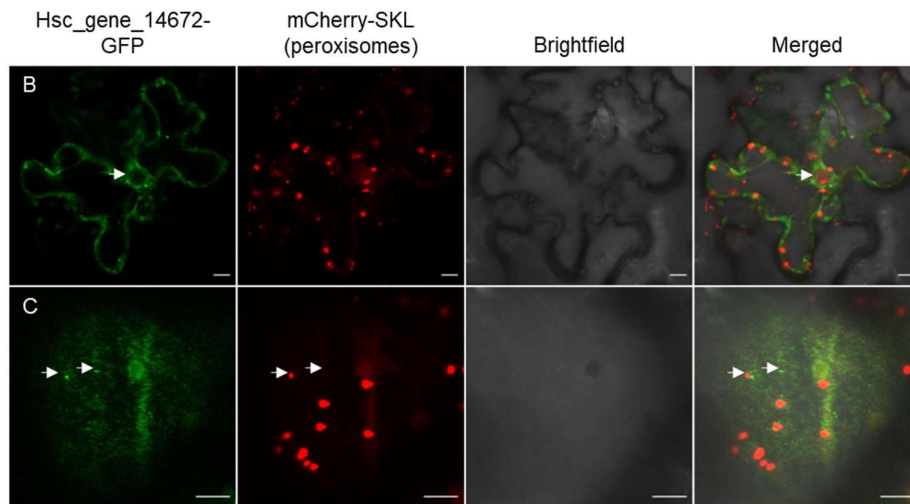


Figure 5. 40. Tobacco leaf epidermal cells co-infiltrated with Hsc_gene_14672-GFP and the peroxisome marker mCherry-SKL. No co-localisation between Hsc_gene_14672-GFP and the peroxisome marker was observed. **A.** The central focal plane of a cell, showing the labelled nuclear envelope (white arrow). **B.** The cortical cytoplasm of a cell, showing Hsc_gene_14672-GFP punctae which do not co-localise with mCherry-SKL punctae (white arrows). In both **A** and **B**, there was much more mCherrySKL punctae than Hsc_gene_14672-GFP punctae. Scale bars represent 10 μm .

5.3.12 Hsc_gene_10206

Hsc_gene_10206 was selected due to its annotation as a putative effector. In addition to the prerequisite N-terminal signal peptide and C-terminal TMD, a predicted histidine acid phosphatase domain and a leucine zipper pattern were identified at the N-terminus. A bipartite nuclear localisation signal was also predicted (**Figure 5.41D**). Using NCBI BLAST, 99 hits were identified for Hsc_gene_10206, all containing histidine acid phosphatase domains. These BLAST hits included genes from varied species, including plant parasitic and animal parasitic nematodes.

The expression of Hsc_gene_10206 was high throughout the parasitic stages (**Figure 5.41A**). This gene was moderately expressed at the cyst (75.4 ± 8.2) and J2 stages (216.8 ± 28.1), with expression increasing at 10 hpi (794.5 ± 130.8), to peak at 48 hpi (1129.7 ± 134.2). Expression was comparable at the 12 dpi female (940.4 ± 84.7) and 24 dpi female (938.5 ± 142.8) stages, and was lower at the 12 dpi male stage (605.6 ± 27.9) compared to the two female stages. From the J2 in-situ hybridisations, no staining was detected in the worms (**Figure 5.41B**). However, due to low expression at the J2 stage, parasitic stage in-situ were conducted. From this, staining of the intestines was observed, in addition to the staining of an adult male (**Figure 5.41C**).

The N- and C- terminal GFP fusion constructs of Hsc_gene_10206 showed different subcellular localisations. GFP-Hsc_gene_10206 showed cytoplasm localisation, with labelling of the nucleoplasm observed, but not the nucleolus. ER localisation was also suggested, with tubules visualised in the cortical cytoplasm, and the nuclear envelope was labelled (**Figure 5.42**). However, for Hsc_gene_10206-GFP, in addition to cytoplasm localisation, there were punctate structures at the plasma membrane and fluorescence in the apoplast (**Figure 5.43**). Consequently, the plasmodesmata marker PDCB-mCherry was co-infiltrated with Hsc_gene_10206-GFP. However, no co-localisation was shown (**Figure 5.44**). Instead, the punctae shown to be labelled by Hsc_gene_10206-GFP could be plastid autofluorescence.

Hsc_gene_10206
(*H. avenae* Ha-acp1 effector homologue)

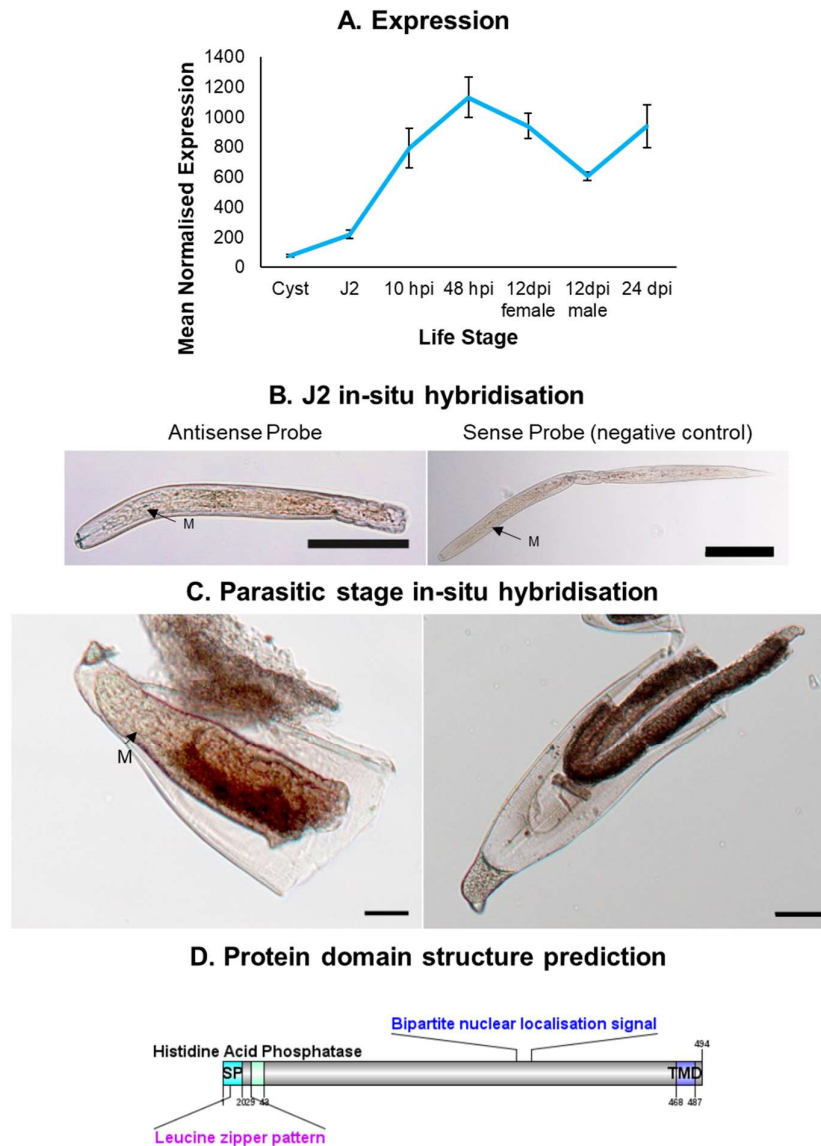


Figure 5. 41. The analysis of Hsc_gene_10206, predicted to be a homologue for the *H. avenae* effector Ha-acp1. A. The expression of Hsc_gene_10206 across the various life stages. For each life stage, the mean expression is shown, with error bars representing the standard deviation. Hsc_gene_10206 expression was shown to be high across all parasitic life stages. **B.** J2 in-situ hybridisations, showing no staining in worms with the antisense or sense probe. Scale bars represent 100 µm. The metacarpal bulb is labelled (M). **C.** Parasitic stage in-situ hybridisations, the image on the left showing staining of the intestinal regions. The image on the right shows a stained male inside a J4 cuticle. Scale bars represent 10 µm. The metacarpal bulb is labelled M. **D.** Protein domain structure prediction, showing a predicted leucine zipper pattern and histidine acid phosphatase domain following the signal peptide (SP). A predicted bipartite nuclear localisation signal was also predicted, prior to the C-terminal transmembrane domain (TMD).

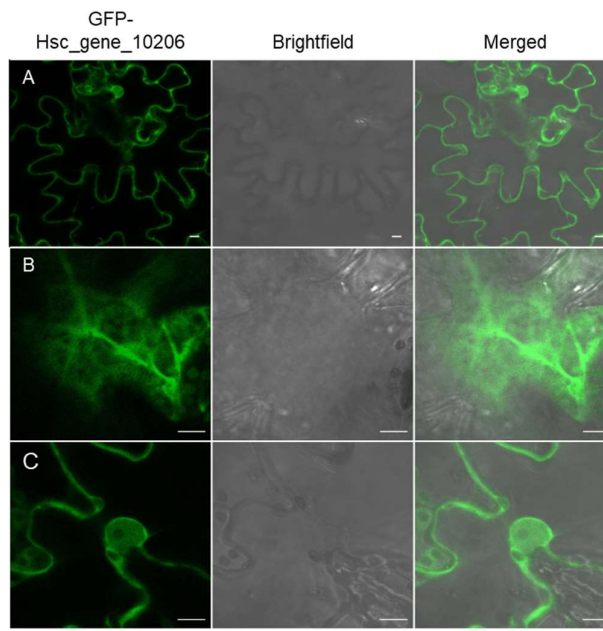


Figure 5. 42. Tobacco leaf epidermal cells *Agro*-infiltrated with GFP-Hsc_gene_10206. Cytoplasm and weak ER localisation was observed. **A.** An overview of infiltrated cells. **B.** The cortical cytoplasm of a cell, showing the labelled ER network. **C.** The central focal plane of a cell, showing the labelled nucleoplasm and nuclear envelope. Scale bars represent 10 μm .

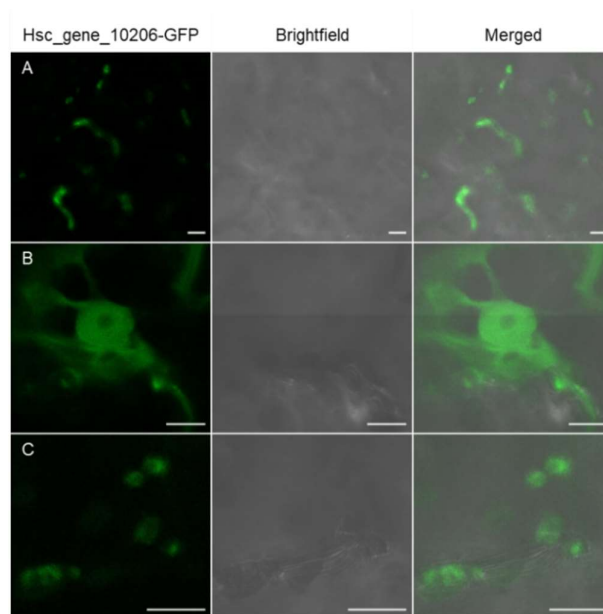


Figure 5. 43. Tobacco leaf epidermal cells *Agro*-infiltrated with Hsc_gene_10206-GFP. Cytoplasm and apoplast localisation was observed, in addition to structures at the plasma membrane which were predicted to be plasmodesmata. **A.** An overview of infiltrated cells, showing bright patches of fluorescence between the cells to indicate apoplast localisation. **B.** A close up image of the labelled nucleoplasm, characteristic of cytoplasm localisation. **C.** A close up of the plasma membrane, showing the labelling of spherical structures. Scale bars represent 10 μm .

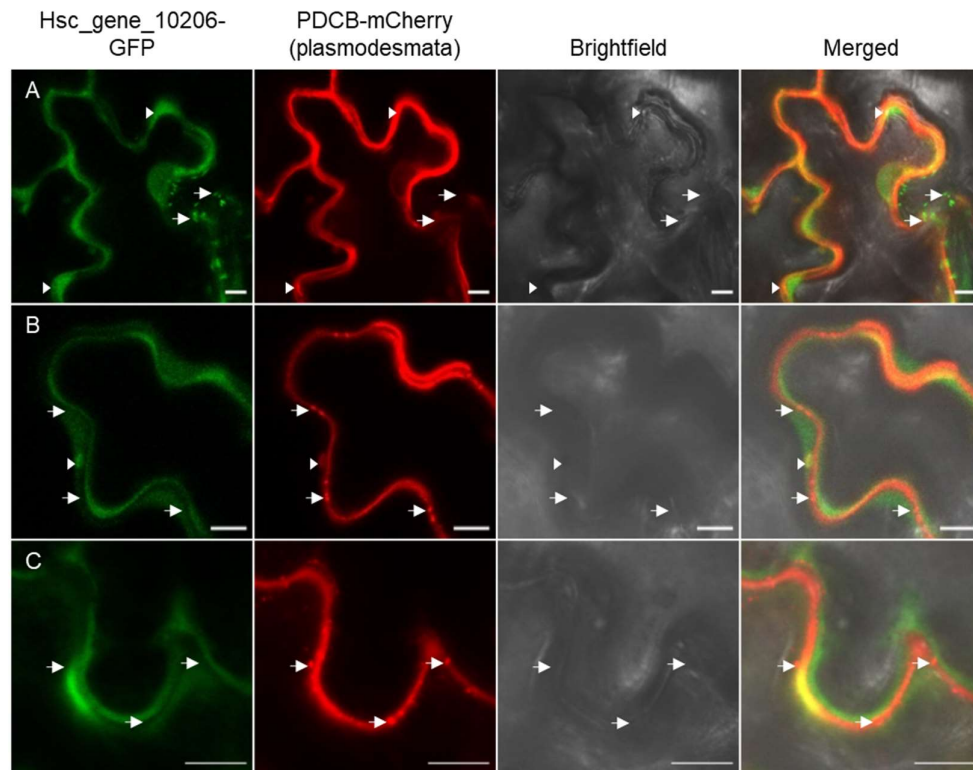


Figure 5. 44. Tobacco leaf epidermal cells co-infiltrated with Hsc_gene_10206-GFP and the plasmodesmata marker PDCB-mCherry. A. The central focal plane of a cell, showing Hsc_gene_10206-GFP label the nucleoplasm in addition to the apoplast (arrowheads). Punctate GFP labelled structures are also observed, which do not co-localise with PDCB-mCherry (arrows). **B.** and **C.** show two close up images of the plasma membrane, showing punctate PDCB-mCherry labelled plasmodesmata along the plasma membrane (arrows) which aren't labelled by Hsc_gene_10206-GFP. Plastid auto-fluorescence was also observed in both channels (arrow head), as shown in **B.** Scale bars represent 10 μ m.

5.3.13 GPLIN_000933000

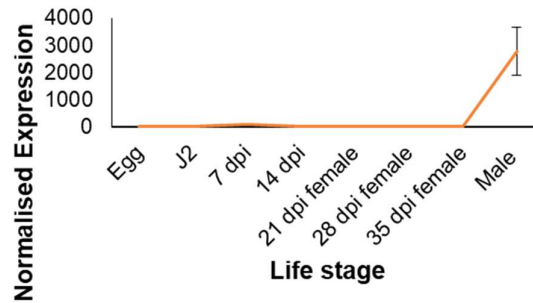
Although GPLIN_000933000 had three predicted TMDs rather than one, it was chosen due to its annotation as an effector homologue (**Figure 5.45C**). The homologous sequence was the *H. glycines* effector G17G01, sharing 74 % sequence identity with GPLIN_000933000 (e-value $2e-16$). In addition to G17G01, seven other NCBI BLAST hits were identified for GPLIN_000933000. Two of these were hypothetical proteins, the *Meloidogyne graminicola* Mgra_00006293 (e-value $1e-04$), and Mgra_00009757 (e-value 0.001). The other five BLAST hits were uncharacterised proteins from *Meloidogyne enterolobii*. Contrastingly, the WormBase BLAST search retrieved 75 hits, all of which were uncharacterised proteins from the cyst nematode species *G. pallida*, *G. rostochiensis*, *H. glycines* and *H. schachtii*.

Despite GPLIN_000933000 being an effector homologue, the expression of this protein peaked at the male stage (2789 ± 890.3). Much lower expression was observed at the egg (1.3 ± 0.2), J2 (1.2 ± 0.2), 7 dpi (89.7 ± 9.3), 14 dpi (16.8 ± 3.2), 21 dpi female (5.5 ± 0.4), 28 dpi female (2.9 ± 1.1) and 35 dpi female (4.7 ± 0.9) life stages (**Figure 5.45A**). Additionally, the J2 in-situ hybridisation was unsuccessful for this gene, with no staining detected in the worms (**Figure 5.45B**).

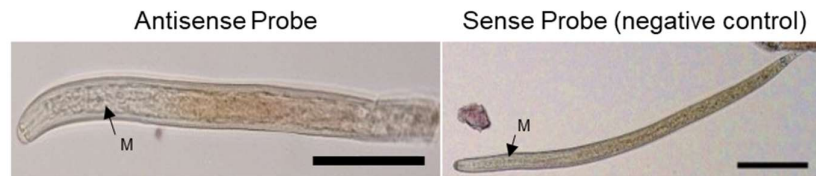
The N- and C- terminal GFP fusions with GPLIN_000933000 appeared to have the same subcellular localisation; labelling the ER and punctate structures. A network of tubules resembling the ER was observed in the cortical cytoplasm, and the nuclear envelope was labelled in the central focal plane of the cell, for both GFP constructs (**Figures 5.46 and 5.49**). ER localisation was supported by the co-infiltration of both GFP constructs with the ER marker secRFP-p24aTM (**Figures 5.48 and 5.51**). However, for both constructs, punctate structures were also observed which did not co-localise with the ER marker. As the Golgi was identified as the most likely subcellular localisation of the labelled punctate structures using the subcellular localisation prediction software (**Table 5.7**), both N- and C- terminal fusions of GPLIN_000933000 were co-infiltrated with the Golgi marker RFP-MNS3. However, no co-localisation was observed (**Figures 5.47 and 5.50**). Instead, this gene may localise to the mitochondria, with the presence of a predicted mitochondrial pre-sequence cleavage site. This was supported by the prediction of mitochondrial localisation using the PSORTII and MultiLoc2 servers (**Table 5.7**).

GPLIN_000933000 (G17G01 homologue)

A. Expression



B. J2 In-situ hybridisation



C. Protein domain structure prediction

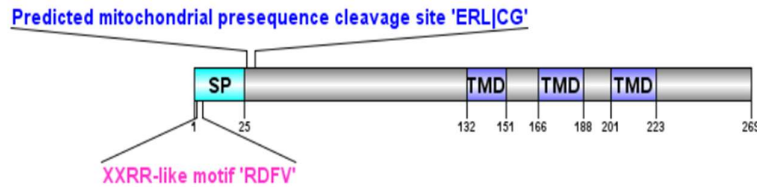


Figure 5. 45. The analysis of GPLIN_000933000, the *H. glycines* G17G01 effector homologue.
A. The expression of GPLIN_000933000 across the various life stages. For each life stage, the normalised mean expression is shown, with the error bars representing the standard deviation. The expression of this gene had a slight peak at 7 dpi (days post infection), although expression levels were much higher in males than any other life stage. **B.** J2 in-situ hybridisation, showing no specific staining of any structures in worms hybridised with the antisense or sense probe. Scale bars represent 100 μ m. The metacorpal bulb is labelled (M). **C.** Protein domain structure prediction, showing a XXRR-like motif, RDFV, and a predicted mitochondrial presequence cleavage site ERL|CG at either side of the signal peptide (SP). Three predicted transmembrane domains (TMDs) were present in the sequence, with a short C-terminal tail following the final TMD.

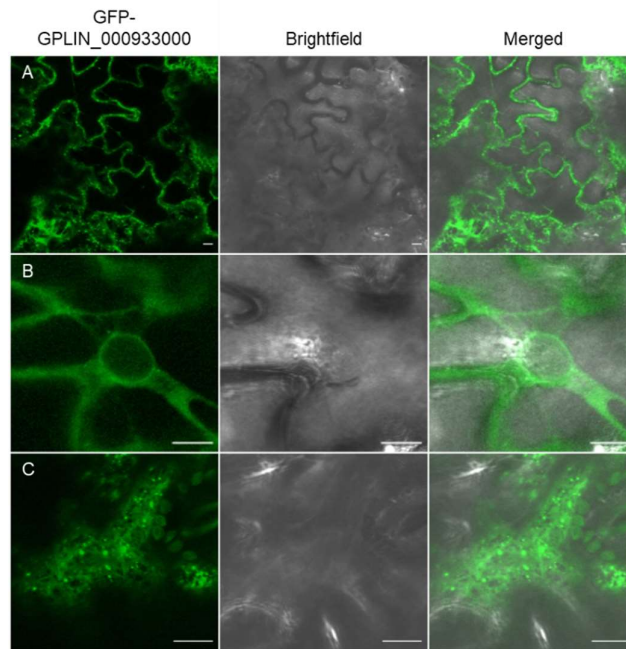


Figure 5. 46. Tobacco leaf epidermal cells *Agro*-infiltrated with GFP-GPLIN_000933000. Localisation to the ER and punctate structures was observed. **A.** An overview of infiltrated cells. **B.** A close up image of the labelled nuclear envelope. **C.** The cortical cytoplasm, showing the labelled ER network and punctae. Scale bars represent 10 μ m.

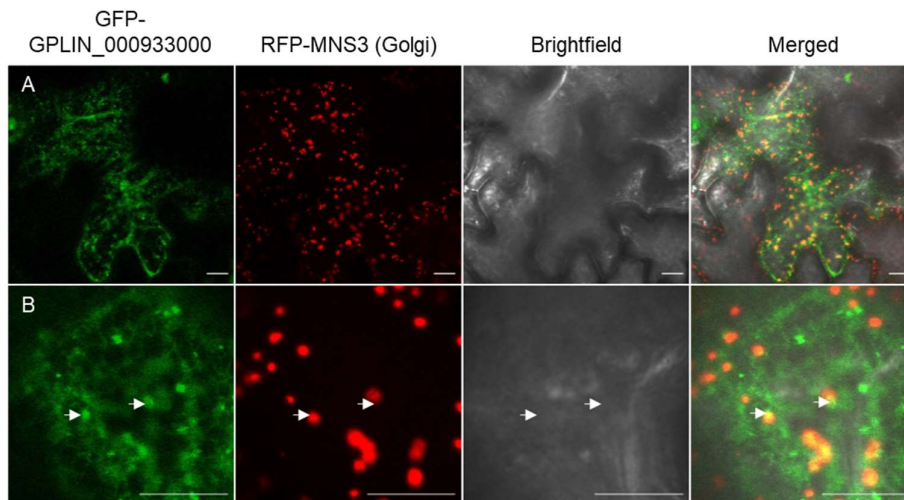


Figure 5. 47. Tobacco leaf epidermal cells co-infiltrated with GFP-GPLIN_000933000 and the Golgi marker RFP-MNS3. No co-localisation was observed **A.** An overview of an infiltrated cell. **B.** An image of the cortical cytoplasm, showing GFP-GPLIN_000933000 punctae which did not co-localise with RFP-MNS3 punctae, although some transiently were shown to be in close proximity to each other (arrows). Scale bars represent 10 μ m.

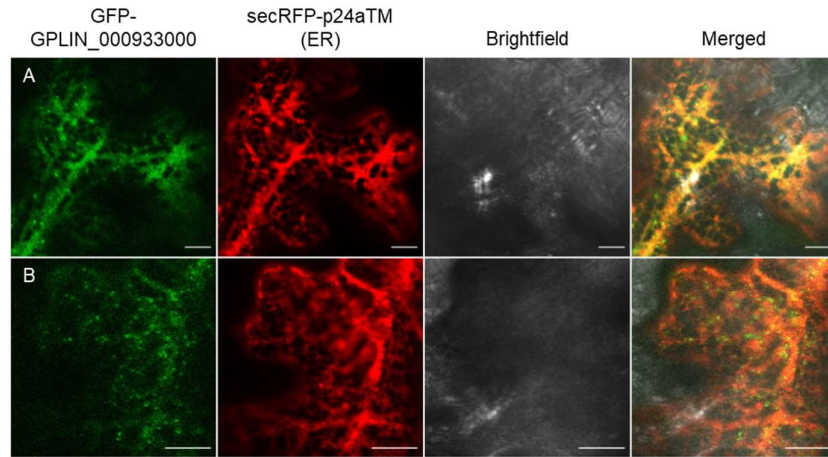


Figure 5. 48. Tobacco leaf epidermal cells co-infiltrated with GFP-GPLIN_000933000 and the ER marker secRFP-p24aTM. **A.** The cortical cytoplasm of a cell, showing both GFP-GPLIN_000933000 and secRFP-p24aTM labelling the ER network. **B.** The cortical cytoplasm of a cell, showing weaker ER localisation of GFP-GPLIN_000933000. Several punctate structures labelled by GFP-GPLIN_000933000 are also shown in both A and B. Scale bars represent 10 μm .

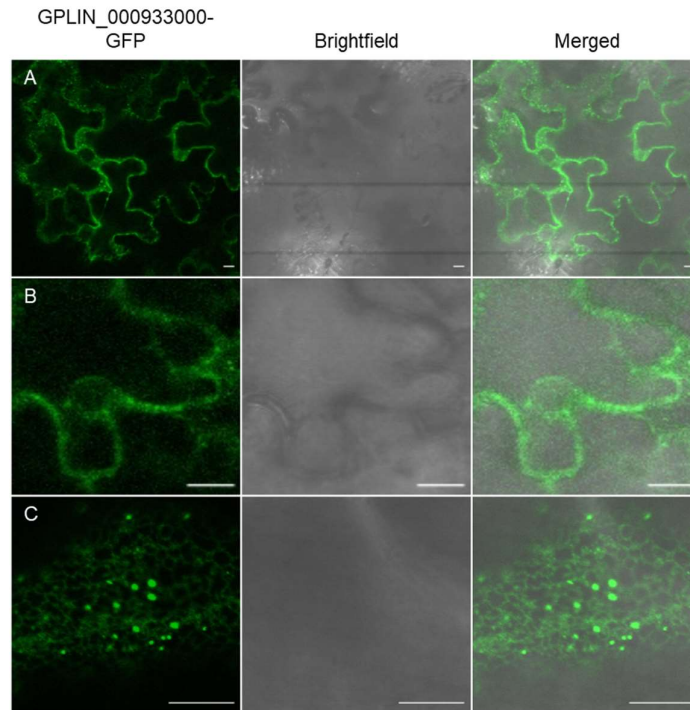


Figure 5. 49. Tobacco leaf epidermal cells *Agro*-infiltrated with GPLIN_000933000-GFP. As with the N-terminal GFP fusion, GPLIN_000933000-GFP localised to the ER and punctate structures. **A.** An overview of infiltrated cells. **B.** A close up of a labelled nuclear envelope. Resolution of this image was poor, with high laser power used as a result of low expression. **C.** The cortical cytoplasm, showing bright punctate structures and the ER network. Scale bars represent 10 μm .

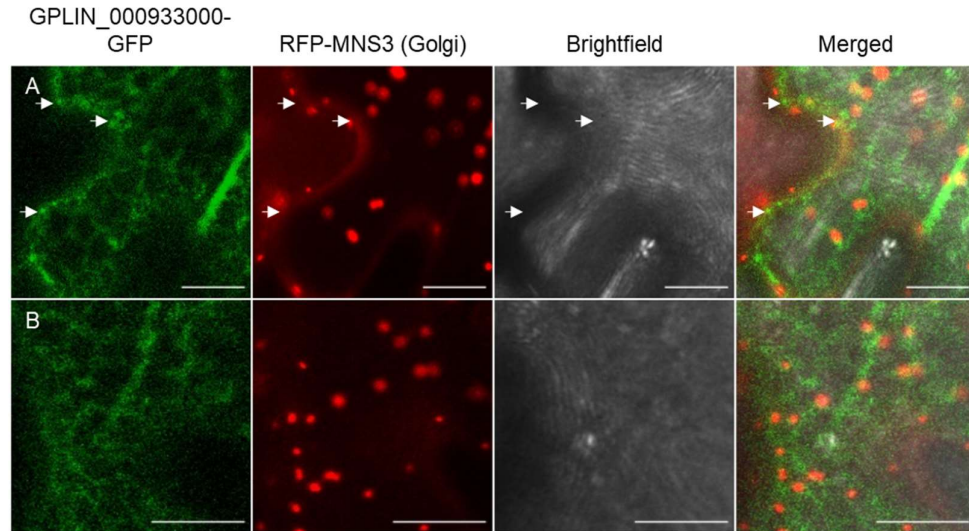


Figure 5. 50. Tobacco leaf epidermal cells co-infiltrated with GPLIN_000933000-GFP and the Golgi marker RFP-MNS3. No co-localisation was observed. A. The cortical cytoplasm, showing GPLIN_000933000-GFP punctae which do not co-localise with RFP-MNS3 punctae (arrows). **B.** Another image of the cortical cytoplasm, highlighting the low expression of GFP-GPLIN_000933000 which often impeded the imaging of punctate structures. Scale bars represent 10 μ m.

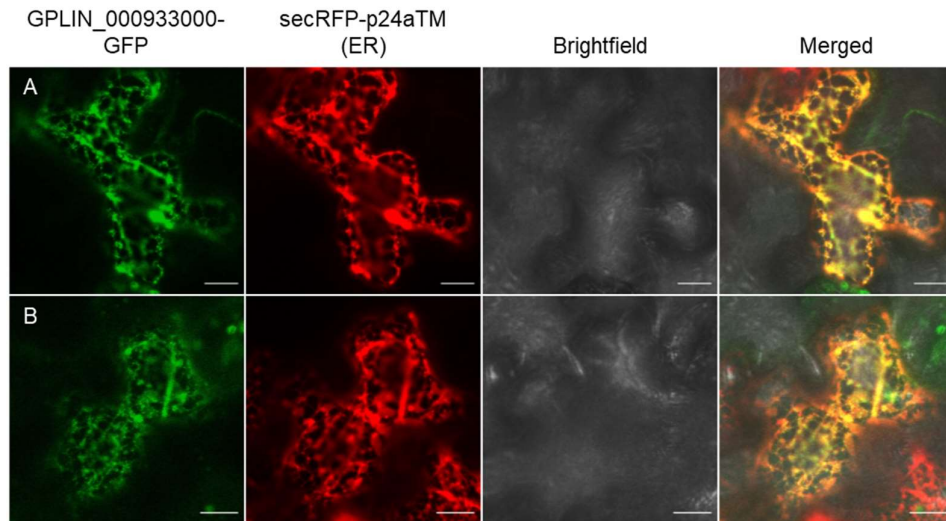


Figure 5. 51. Tobacco leaf epidermal cells co-infiltrated with GPLIN_000933000-GFP and the ER marker secRFP-p24aTM, showing co-localisation. A. and B. are two images of the cortical cytoplasm, showing GPLIN_000933000-GFP co-localising with secRFP-p24aTM. Scale bars represent 10 μ m.

5.4 Discussion

This effector screen aimed to identify novel putative cyst nematode effectors containing a C-terminal TMD, and to test if these had ER localisation. From this screen, a set of six *H. schachtii* and three *G. pallida* proteins was selected for further analysis. For each gene, an overview of the analysis is provided, discussing the annotation, protein domain prediction, BLAST hits, expression profiles, in-situ hybridisations and tobacco leaf infiltrations to validate effector activity of the genes, and to infer potential functions in the host.

5.4.1 Putative ER-targeting cyst nematode effectors

5.4.1.1 The positive control gene, GPLIN_000854400

The previously characterised *G. pallida* '16H02' effector, GPLIN_000854400, was used as a positive control, with tobacco leaf infiltrations confirming ER localisation, and in-situ hybridisations confirming dorsal gland expression. As this gene was expressed most highly at the egg and J2 stage, later parasitic stage in-situ hybridisations weren't conducted. However, the expression of this gene across all life stages was low. Additionally, the dorsal gland expression of this gene contrasts the peak in expression at the J2 life stage, as higher dorsal gland activity has previously been observed during sedentary parasitic stages rather than J2 (Hussey et al, 1990). However, the expression of GPLIN_000854400 may be highest between the J2 and 7 dpi time points measured. Therefore, the expression should be analysed at more regular time points through early syncytial formation.

This effector protein has previously been shown to bind to potato NAC transcription factors, using yeast two-hybrid screening and YFP bimolecular fluorescence complementation (M. Coke, personal communication). Binding of GPLIN_000854400 to the potato NAC TFs was hypothesised to prohibit their translocation from the ER to the nucleus, to prevent the activation of genes involved in defence responses. This is a novel function of cyst nematode effectors, and the first example of a cyst nematode effector containing TMDs. Due to this, future effector screens should include proteins with several TMDs.

5.4.1.2 Hsc_gene_15040, localising to the ER and cytoplasm

Hsc_gene_15040 was a putative effector localising to the ER and cytoplasm. Although C-terminal TMDs have previously been shown to be responsible for the ER localisation of plant pathogen effectors (Breeze et al, 2020), a C-terminal KKXX-like motif identified in Hsc_gene_15040 may also contribute towards ER localisation, as this motif has a

characterised role in ER retrieval (Vincent et al, 1998). *Hsc_gene_15040* was suggested to be an effector due to its upregulation in the gland cells at 10 hpi, which was further supported by the dorsal gland expression observed in the parasitic stage in-situ hybridisations. The dorsal gland expression of *Hsc_gene_15040* suggests a role of this gene in syncytial formation rather than migration and invasion, supported by the peak in expression in early parasitism. The structure of this gene, including a coiled-coil domain, could allude to one of several functions typical of this domain, including membrane fusion, protein folding and microtubule dynamics (Burkhard et al, 2001). However, no cyst nematode effector proteins containing a coiled-coil domain have previously been identified, suggesting that this gene has a novel function in the host.

5.4.1.3 GPLIN_001269700, localising to the ER, cytoplasm and punctae

GPLIN_001269700 was identified as a putative effector due to the presence of two DOG boxes upstream of the gene and the dorsal gland expression suggested from the J2 in-situ hybridisations. However, as dorsal gland effector proteins are typically involved in parasitic stages (Thorpe et al, 2014; Hussey et al, 2019), this contrasts the lack of expression that was observed from the J2 stage onwards. This further highlights the need for additional time points to measure the expression of the *G. pallida* genes between the J2 and 7 dpi life stage. The subcellular localisation of GPLIN_001269700 also requires further investigation. For instance, in addition to the ER and cytoplasm localisation of the N-terminal GFP fusion, additional punctate structures were labelled by the C-terminal GFP fusion.

5.4.2 Putative effectors targeting other subcellular compartments

5.4.2.1 *Hsc_gene_2739*, targeting the nucleus

Hsc_gene_2739 was identified as a putative effector targeting the nucleus. The localisation of this gene could be due to the presence of the pat 4 NLS, which should be tested by mutation of this signal and subsequent fusion of the gene to GFP. In the host, *Hsc_gene_2739* may act similarly to other nucleus-targeting cyst nematode effectors, which alter host transcription to promote syncytial development. This includes the *H. schachtii* 30D08 effector secreted by the dorsal gland. 30D08 interacts with an auxillary spliceosomal protein, SMU2, to alter the pre-mRNA splicing of Arabidopsis genes involved in transcription, development, and hormone signalling (Verma et al, 2018). Another nuclear-targeting *H. schachtii* effector is 32E03, which inhibits histone deacetylases that modulate host chromatin. In turn, this effector epigenetically regulates gene expression to promote parasitism (Vijayapalani et al, 2018).

The sequence analysis of Hsc_gene_2739 did not allude to any potential functions of this gene. Additionally, the BLAST searches for Hsc_gene_2739 did not identify any previously characterised proteins similar in sequence. This supports that Hsc_gene_2739 is specific to cyst nematodes, with a potential novel role in parasitism. The subventral gland staining from the J2 in-situ hybridisation also supports that this gene is a putative effector. However, other nucleus-targeting cyst nematode effectors are associated with dorsal gland expression (Verma et al, 2018; Vijayapalani et al, 2018).

5.4.2.2 Hsc_gene_19069, localising to the cytoplasm and punctae

Hsc_gene_19069, “putative esophageal gland cell secretory protein 28”, was validated as a putative effector protein. This gene was suggested to be expressed within the subventral glands, and had high expression at the J2 and later parasitic life stages, supporting a role of this gene in parasitism. Hsc_gene_19069 contained an EGF-like domain which can be found in a large variety of eukaryotic proteins.

In animals, EGF-like proteins are cell surface receptors with roles in calcium signalling and mitogenesis (Villalobo et al, 2000; Engel, 1989). As cyst nematode effectors including the *H. avenae* effector HaCRT1 alter calcium signalling in host cells (Liu et al, 2020), and *G. pallida* secretions alter mitogenic activity in tobacco leaf protoplasts (Goverse et al, 1999), effectors such as Hsc_gene_19069 could act as calcium signalling receptors to induce mitogenic activity in the host to enable cell proliferation. However, despite this evidence, rather than localising to the cell surface, Hsc_gene_19069 localised to the cytoplasm and punctae, which is atypical of animal proteins containing EGF-like domains. Therefore, Hsc_gene_19069 could have a similar role to plant EGF-like proteins. In plants, these domains are present within several plant vacuolar sorting receptors (Ahmed et al, 2000; Shimada et al, 1997). Therefore, Hsc_gene_19069 could mimic plant EGF-like proteins to manipulate vacuolar sorting. To test this, markers for the post-Golgi organelles could be co-infiltrated with this gene.

5.4.2.3 Hsc_gene_19059, localising to the nucleus, peroxisomes and punctae

Hsc_gene_19059 was another gene identified as a putative effector expressed during early parasitism, although gland cell expression was not confirmed with J2 in-situ hybridisations. This gene localised to the nucleus and peroxisomes, with the C-terminal GFP fusion localising to additional punctate structures. Although the nucleus is a common subcellular target of cyst nematode effectors, only two peroxisome targeting cyst nematode effectors have been identified, the *G. pallida* GPLIN_000662500 and GPLIN_000457000, which are yet to be functionally characterised (Thorpe et al, 2014). The dual localisation of Hsc_gene_19059 to the nucleus and peroxisomes could infer its

function in the cell. Localisation to both the nucleus and peroxisomes has been observed for catalase proteins, which translocate from the peroxisomes to the nucleus to regulate the transcription of genes associated with H₂O₂ production (Zhang et al, 2015). Therefore, Hsc_gene_19059 may similarly translocate from the peroxisomes to the nucleus to alter the expression of H₂O₂ related genes.

5.4.3 Proteins discounted as putative effectors

5.4.3.1 Hsc_gene_14672, localising to the cytoplasm, ER and punctae

Hsc_gene_14672 is a SPRY-SEC protein annotated as ran-binding protein-1. SPRY-SEC proteins have varied roles in the cell, mediating protein-protein interactions (Diaz-Granados et al, 2016), suggesting many potential roles of Hsc_gene_14672. The similarity of Hsc_gene_14672 to several SPRY-SEC effectors could suggest a role for this gene in parasitism. However, this gene was discounted as a putative effector for several reasons. This includes its subcellular localisation, which was within the cytoplasm, or ER and punctae, for N- and C- terminal GFP fusions respectively. This contrasts the localisation of previously characterised SPRY-SECs, which localise to the cytoplasm, nucleus and nucleolus (Carpentier et al, 2012; Jones et al, 2009; Rehman et al, 2009). Additionally, the expression profile and J2 in-situ hybridisations suggested that this gene is not a putative effector, with a suggested role in adult development rather than establishment or maintenance of the syncytium.

5.4.3.2 Hsc_gene_10206, localising to the cytoplasm, ER, apoplast and punctae

Hsc_gene_10206 was chosen due to its similarity to the *H. avenae* effector Ha-acp1 (Liu et al, 2014). Acid-phosphatase effectors are also secreted by other plant-parasitic nematode species, including *Meloidogyne incognita* (Huang et al, 2003), hypothesised to have a digestive role in the host cells. However, acid phosphatase genes are also common housekeeping genes, present across nematodes with varying feeding strategies (Rigden, 2008). Hsc_gene_10206 had subcellular localisations resembling that of an acid phosphatase, which typically localise to the lysosomes, extracellular space and cytoplasm (Veeramani et al, 2009; Rigden, 2008). For this Hsc_gene_10206, cytoplasm and ER localisation, or cytoplasm, apoplast and punctae localisation was observed for the N- and C- terminal GFP fusions respectively. Due to the digestive role of acid phosphatases, the punctate structures labelled by Hsc_gene_10206-GFP may represent the lysosomes, which should be tested with future tobacco leaf infiltrations.

The intestinal expression, suggested from the parasitic stage in-situ hybridisations, discounts this gene as a putative effector and could indicate a role of this gene in digestive processes. This is supported by the histidine acid phosphatase, *pho-1*, being

expressed in the intestines of the *C. elegans* nematode, having a role in digestion (Beh et al, 1991). The in-situ hybridisations of Hsc_gene_10206 also contrasts those for the *H. avenae* effector *Ha-acp1*, which showed staining in the subventral glands (Liu et al, 2014).

5.4.3.3 GPLIN_000933000, localising to the ER and punctae

GPLIN_000933000, the G17G01 effector homologue, localised to the ER and punctae. This gene was specific to sedentary plant-parasitic nematodes, which could indicate a role in parasitism. However, this gene was discounted as a putative effector, due to the lack of gland cell staining observed in the J2 in-situ hybridisations, and the expression of this gene peaking in 12 dpi males. This contrasts the expression of the *H. glycines* effector G17G01, which was upregulated in J2s prior to soybean infection (Klink et al, 2009).

5.4.4 The efficacy of the effector screen

5.4.4.1 Limitations of the in-situ hybridisations

In-situ hybridisations suggested that four out of the eight screened *G. pallida* and *H. schachtii* genes were expressed in the gland cells. Although to confirm this, microscope images with higher resolution of the nematode's anatomy should be obtained. For the other four genes, the in-situ hybridisations were unable to show the staining of any structures. This could occur for several reasons. For instance, gland cell expression may still be present, but it could be below the detection threshold for the staining method that was used. To help solve this, fluorescence in-situ hybridisations could be conducted, as this technique has been shown to improve the sensitivity of RNA detection in nematode tissues (Ruark-Seward et al, 2019).

Additionally, suboptimal probe design could account for the unsuccessful in-situ hybridisations. As only one probe was used for each gene, the number of probes tested on the worms could be increased to help improve the success of the in-situ hybridisations. These additional probes could be designed to hybridise to different regions of the RNA transcript, and could have shortened lengths to improve permeability into the worms (Kud et al, 2019). Another limitation of the in-situ hybridisations was the use of J2s, as these were the most convenient life stage to use. However, several of the screened genes had higher levels of expression during parasitic life stages. This includes Hsc_gene_19059, which had the highest expression at 10 hpi and 48 hpi, Hsc_gene_14672, which had the highest expression at 12 dpi male and 24 dpi female, and GPLIN_000933000, which peaked at the adult male life stage. Therefore, further in-situ hybridisations for these genes should be conducted at these parasitic life stages to

increase the likelihood of probe detection. Finally, to help to further validate the in-situ hybridisations, *in planta* immunolocalisation within infected plant roots should also be conducted. This would verify the secretion of the genes from the nematode gland cells into the syncytium.

5.4.4.2 Limitations of the gene expression analysis

RNA-seq data was used to analyse the expression of the screened *G. pallida* and *H. schachtii* genes (Siddique et al, 2021; Cotton et al, 2014). However, protein levels within a cell often poorly correlate with transcript levels (Fukao, 2015). Therefore, the RNA transcript abundance that was inferred from the RNA-seq data may not accurately reflect gene expression at the different nematode life stages. To validate the RNA-seq data, methods for protein quantification, including selected reaction monitoring (SRM) mass spectrometry could be used, which has previously quantified protein abundance in animal parasitic nematode species (Wang and Gasser, 2021). Another limitation of the RNA-seq data was the need for more frequent time points to be measured. For example, with the *H. schachtii* data set, no time points between 48 hpi and 12 dpi were obtained (Siddique et al, 2021), and for the *G. pallida* data set, no time points between the J2 and 7 dpi life stages were obtained (Cotton et al, 2014). As effector genes may only be expressed during early parasitic time points that weren't measured in these datasets, this may have resulted in effectors being missed from the screen.

5.4.4.3 Limitations of the subcellular localisation prediction

None of the cloned genes displayed sole ER localisation, other than the previously identified 16H02 gene that was used as a control. This contrasts evidence that transmembrane domains between 17-22 residues in length are associated with ER localisation in plant cells (Brandizzi et al, 2002). Also, the results from this screen are contrasted by the localisation of seven out of fifteen *Phytophthora infestans* effectors only to the ER, when the same screening parameters were used (Breeze et al, 2020). Additionally, the subcellular localisation prediction servers used in this effector screen, PSORTII, MuLocDeep and MultiLoc2, gave conflicting and inaccurate results. This contrasts evidence that these servers can accurately predict the subcellular localisations of plant, animal and fungi species (Horton and Nakai, 1997; Blum et al, 2009; Jiang et al, 2021). This may be due to the removal of the signal peptide from the cloned nematode proteins, as the N-terminal portion of the protein is part of the subcellular localisation prediction algorithms used by each of the servers (Horton and Nakai, 1997; Blum et al, 2009; Jiang et al, 2021).

Streamlined cyst nematode effector identification may be achieved from the development of effector prediction software. This has already been developed for fungal

and oomycete effectors. Named EffectorP 3.0, this software can distinguish between apoplastic and cytoplasmic effectors (Sperschneider and Dodds, 2022). EffectorP 3.0 screens proteins based on the presence of an RxLR motif that is responsible for the secretion of fungal and oomycete effectors into host cells (Liu et al, 2019). However, cyst nematode effectors don't contain this motif or any similar protein coding region. Therefore, EffectorP 3.0 wouldn't be suitable for the identification of cyst nematode effectors, highlighting the need for the development of a cyst nematode specific effector prediction software. Also, the EffectorP 3.0 software excludes transmembrane proteins (Sperschneider and Dodds, 2022), thus wouldn't be suitable for the identification of plant pathogen effectors containing C-terminal TMDs.

5.4.4.4 Limitations of the tobacco leaf infiltrations

Tobacco leaf infiltrations were conducted to infer the *in planta* subcellular localisation of the screened cyst nematode proteins. Although this is the standard method for the subcellular localisation analyses of cyst nematode effector proteins (Jones et al, 2009), there are limitations associated with this technique. For example, the correct localisation of cyst nematode effectors may require the presence of genes that are specific to the host species, and root tissue. Therefore, as tobacco isn't a host for *G. pallida* or *H. schachtii*, the screened nematode proteins may be unable to localise to their target compartment. Thus, to validate the subcellular localisation analyses, immunolocalisations could be performed on the roots of transgenic host lines overexpressing the putative effectors (Vijayapalani et al, 2018).

Another limitation of the subcellular localisation analysis was the addition of fluorescent protein tags including GFP. This can alter the localisation of the protein of interest, through interfering with its binding activity, subcellular trafficking or stability (Palmer and Freeman, 2004). To test this, both N- and C- terminal GFP constructs were developed for each screened cyst nematode gene. Four of the genes, Hsc_gene_15040, Hsc_gene_2739, Hsc_gene_19069 and GPLIN_000933000, displayed the same subcellular localisation when GFP was fused to the N- and C- terminus. However, for the four other genes, GPLIN_001269700, Hsc_gene_19059, Hsc_gene_14672 and Hsc_gene_10206, additional subcellular structures were observed when GFP was fused to the C-terminus. As these proteins contain C-terminal TMDs that were predicted to act as tail anchors, adding a GFP onto the C-terminus could be expected to alter the ability of the transmembrane region to anchor to the target membrane, thereby altering the localisation. Therefore, the subcellular localisations of the N-terminal GFP constructs for these genes were hypothesised to be the most reliable.

Another limitation of the tobacco leaf infiltrations was the expression of the genes without their signal peptides, due to the assumption that these are cleaved in nematode esophageal glands (Mitchum et al, 2013). To further validate this, immunoblots could be

conducted using antibodies specific to the screened putative effectors, with and without their signal peptides. This would further confirm that the signal peptide is cleaved within the gland cells prior to secretion (Chen et al, 2015).

5.4.5 Conclusions

This effector screen aimed to identify a set of novel putative effectors from the model cyst nematode species *H. schachtii*, and the economically important potato cyst nematode, *G. pallida*. This screen also aimed to test if these genes would localise to the ER, as was previously shown with *Phytophthora* effectors (Breeze et al, 2020). The set of screened cyst nematode proteins had varying subcellular localisations, contradicting the hypothesis of putative effectors containing C-terminal TMD proteins typically localising to the ER. However, this screen has provided further evidence that cyst nematode effectors can have TMDs. This screen has also shown that the use of subcellular localisation prediction servers retrieves variable results, and aren't an accurate predictor for the subcellular localisation of cyst nematode proteins lacking a signal peptide, acting outside of their synthesising cell.

Putative effector proteins, from the in-situ hybridisations and expression data:

- The ER targeting **Hsc_gene_15040** and **GPLIN_001269700**
- The nucleus targeting **Hsc_gene_2739**
- **Hsc_gene_19069**, the EGF-like protein with an unidentified subcellular localisation
- The nucleus and peroxisome targeting **Hsc_gene_19059**, although further in-situ hybridisations are required to verify gland cell expression

Non-likely effector proteins, with low expression during parasitism and unsuccessful J2 in-situ hybridisations:

- **Hsc_gene_14672**, a putative ran-binding protein with an unidentified subcellular localisation
- **Hsc_gene_10206**, a putative histidine acid phosphatase with an unidentified subcellular localisation
- **GPLIN_000933000**, the *H. glycines* G17G01 homologue localising to the ER and an unidentified subcellular compartment

Chapter 6 General Discussion

There are two main parts to the work described; the characterisation of the plant secretory pathway in *Arabidopsis* syncytia induced by *H. schachtii*, and the identification of novel putative cyst nematode effector proteins containing a C-terminal TMD, which may target the endoplasmic reticulum. The increased knowledge of the plant secretory pathway in plant-cyst nematode interactions that has been gained from this work could be used to identify potential host susceptibility genes, and potential cyst nematode genes as targets for RNAi.

6.1 Dual fluorescence reporters provide new insight into the plant secretory pathway

The set of dual fluorescence organelle marker constructs has been developed for use in both transient and stable expression assays. These are novel, as no dual fluorescence constructs labelling the full secretory pathway have previously been published. These constructs are also customisable, sharing a common vector system containing a large choice of restriction sites. This allows for easy construct modification using traditional restriction cloning (Bertero et al, 2017), with the ability to change the promoter, fluorescent protein, marker gene and terminator sequence.

Tobacco leaf infiltrations of the dual fluorescence organelle markers has furthered knowledge on the plant secretory pathway. For instance, the ER marker RFP-HDEL was unexpectedly retained in the Golgi when co-expressed with the Golgi marker secYFP-ERD2b. This finding could be used to uncover novel information about K/HDEL mediated ER retention via the ERD2 receptor protein. Also, the comparison of marker expression in traditional transient expression assays vs stable expression in *Arabidopsis* has provided novel information on the plant secretory pathway in different expression systems and tissue types. One key observation was the localisation of the ER marker secRFP-p24aTM in the vacuoles of *Arabidopsis* roots but not *Arabidopsis* cotyledon cells, or tobacco leaf epidermal cells. This could suggest altered vacuolar sorting or ER-Golgi trafficking mechanisms specific to plant roots. Several other differences in marker expression were observed between the different expression systems. This includes the presence of punctae for the tonoplast marker CBL6-RFP and the vacuole marker Aleu-RFP only in the tobacco leaf infiltrations, and the unexpected lack of punctate PVC localisation for the PVC marker TR2:RFP-BP80, only when stably expressed in *Arabidopsis* tissue. This indicates that aspects of the plant secretory pathway differ across different expression systems, species and tissue types.

This work has highlighted the need to characterise plant secretory pathway markers in varied cellular contexts. So far, knowledge on the plant endomembrane system has

mostly relied on transient expression assays in tobacco leaf epidermal cells, although stable marker expression has been analysed in seeds (Ichino et al, 2020; Galili and Herman, 1997) pollen tubes (Grebnev et al, 2017), and root hairs (Grierson et al, 2014). However, this work describes the first study of plant secretory markers in primary root tissues, highlighting areas requiring further research, including the root-specific vacuole localisation of the ER marker secRFP-p24aTM. However, despite the differences observed in marker localisation, each organelle marker apart from the ER marker secRFP-p24aTM and the PVC marker TR2:RFP-BP80 was suggested to localise to their intended subcellular compartment in both transient and stable expression systems. Therefore, the set of dual fluorescence constructs and Arabidopsis lines are a valid novel resource that could be used to further knowledge on the plant secretory pathway across different tissue types, developmental contexts or in response to biotic or abiotic stresses.

6.2 Common aspects of the plant secretory pathway across plant-pathogen interactions

Cyst nematodes are economically important plant pathogens that induce vast subcellular changes in their host during syncytial formation. The dual fluorescence Arabidopsis lines were infected with syncytia to further knowledge on the plant secretory pathway during cyst nematode infection, which so far has relied on 2D electron microscopy. Previously published Arabidopsis RNA-seq data was used to complement fluorescence microscopy observations. To support the hypotheses developed from this work, knowledge on the plant secretory pathway in response to other biotrophic pathogens can be used, due to similarities in plant defence responses, and common pathways being targeted by plant pathogen effectors. This can support the suggested endomembrane trafficking pathways identified to be involved in plant-cyst nematode interactions, and could also be used to postulate future experiments.

6.2.1 The early secretory pathway reveals features of both plant defence and susceptibility

Gene expression analysis identified downregulated ER stress related genes, bZIPs and calreticulins in Arabidopsis syncytia, which are commonly involved in plant defence responses to biotrophic plant pathogens (Moreno et al, 2012; Qiu et al, 2012; Caplan et al, 2009). This suggests that cyst nematodes target ER stress pathways involved in defence responses. This is supported by the identification of plant pathogen effectors targeting BIPs and calreticulins. For example, the oomycete *Phytophthora sojae* effector PsAvh262 binds to BIP to suppress the activation of ER stress and programmed cell death (Jing et al, 2016), and there are several plant-parasitic nematodes effectors from *H. avenae* (Liu et al, 2020), *Meloidogyne incognita* (Jaouannet et al, 2013), and *Radopholus similis* (Li et al, 2015) that mimic calreticulins. Similarly, *H. schachtii* could

secrete effectors which target BIPs or calreticulins to suppress the induction of ER stress-induced PCD.

Disruption of ER-Golgi trafficking was suggested from the fluorescence microscopy and gene expression analysis of *Arabidopsis* syncytia, and could also indicate a common feature of pathogen manipulation. This includes the downregulation of *SEC22*, previously characterised in the resistant plant-cyst nematode interaction soybean-*H. glycines* (Sharma et al, 2016), and the downregulation of *SAR1B*, that contributes to basal defence against biotrophic pathogens (Wang et al, 2007). However, other ER and Golgi trafficking components, including COPI coatomer subunits and COG subunits, were progressively upregulated in response to cyst nematodes. These are also involved in defence to other plant pathogens. For example, γ 1-COP and COG subunit genes are involved in barley resistance to the fungi *Blumeria* (Ostertag et al, 2013). However, with the progressive downregulation of ER stress and ER-Golgi trafficking genes in syncytia, the role of the early secretory pathway is likely to be a complex amalgamation of plant defence responses and mechanisms of pathogen manipulation.

6.2.2 Atypical secretion and vacuolar sorting occurs across plant-pathogen interactions

Golgi-PM trafficking components that are involved in resistance to biotrophic plant pathogens were progressively downregulated in *Arabidopsis* syncytia. This includes the syntaxins *SYP71*, *SYP122* and *SYP132* (Liu et al, 2016; Zhang et al, 2008; Kalde et al, 2007). The downregulation of these genes in *Arabidopsis* syncytia could reflect a mechanism of the pathogen to suppress secretion. This is supported by the downregulation of *RABA1A* in *Arabidopsis* syncytia, as this gene is also targeted by the RxLR24 effector secreted by the oomycete *Phytophthora brassicae* (Tomczynska et al, 2018). There is also evidence that cyst nematode effectors can interact with subcellular trafficking components involved in secretion. For instance, the CLE effectors secreted by *Heterodera* spp. are hypothesised to be delivered into the plant cell, then use the plant subcellular trafficking machinery to be secreted to the apoplast (Wang et al, 2021a). This mechanism hasn't been reported for any other plant pathogen effectors. For post-Golgi trafficking to the vacuoles, fluorescence microscopy and downregulated trafficking components could indicate that unconventional fusion of the PVCs with the plasma membrane occurs, as in the response to fungi (An et al, 2006) and bacteria (Wang et al, 2014). The fusion of PVCs with the PM in *Arabidopsis* syncytia is also supported by EM observations (Golinowski et al, 1996). Therefore, evidence suggests that post-Golgi trafficking plays common roles in plant responses to pathogens including cyst nematodes, displaying features of both plant defence and susceptibility. This is to be expected, as secretion is key to delivering antimicrobial or cell-wall related compounds to the site of the invading pathogen.

6.2.3 The vacuoles of syncytia have both unique and common features to other plant-pathogen interactions

A unique aspect of cyst nematode infection is the fragmentation of the large central vacuole, which was confirmed with fluorescence microscopy. Rather than a common response to plant pathogens, fragmented vacuoles are often observed in cells with high biosynthetic activity (Rodiuc et al, 2014). This coincides with the proliferation of the ER and Golgi in syncytia, that are also features of highly metabolically active cells (Ferrero et al, 2015; Abiodun and Matsuoka, 2013). Therefore, the ultrastructural changes to the ER, Golgi and vacuoles during syncytial formation could reflect a unique pathogenic mechanism of cyst nematodes to increase nutrient and metabolite production in syncytial cells. Despite this, the expression of vacuole-related genes in *Arabidopsis* syncytia is comparable to that within other plant-pathogen interactions. For example, TIPs are targeted by root-knot nematode *Meloidogyne incognita* Mi8D05 effector (Xue et al, 2013), and are downregulated in response to the fungus *Fusarium oxysporum* (Gupta et al, 2017). Additionally, the upregulation of vacuolar processing enzymes (VPEs) is shown in response to several biotrophic pathogens, including bacteria (Zhang et al, 2010), fungi (Kumar et al, 2015) and oomycetes (Misas-Villamil et al, 2013), and is hypothesised to be associated with PCD. Therefore, despite the unique ultrastructure of vacuoles, the downregulation of TIPs in *Arabidopsis* syncytia could reflect a common mechanism of susceptibility, while the upregulation of VPEs could be induced as part of a conserved plant defence response.

6.2.4 A novel model for the plant secretory pathway in syncytia

From the live fluorescence microscopy and gene expression analysis in *Arabidopsis* syncytia, and the conclusions drawn from the comparison against different plant-pathogen interactions, a model for the changes to the secretory pathway during infection with cyst nematodes is presented in **Figure 6.1**.

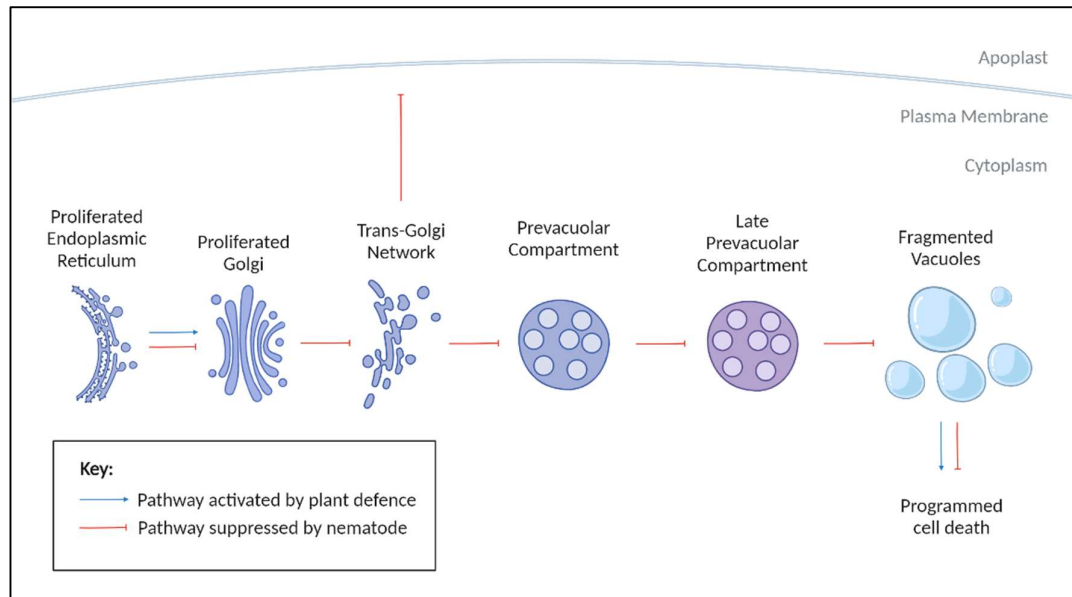


Figure 6. 1. A novel model for the plant secretory pathway in *Arabidopsis* syncytia induced by *H. schachtii*. Novel hypotheses include the nematode-induced suppression of ER stress, in addition to the suppression of components of ER-Golgi trafficking, secretion, vacuolar trafficking and vacuole function, which all typically function in plant pathogen responses. Contrastingly, other components involved in ER-Golgi trafficking and vacuole mediated immune responses were suggested to be activated in syncytia, as part of defence responses against *H. schachtii*.

Many aspects of the secretory pathway were hypothesised to be suppressed by *H. schachtii* in *Arabidopsis* syncytia, to prevent the activation of immune responses. This includes the suppression of components of ER stress, ER-Golgi trafficking, exocytosis, vacuolar trafficking and vacuole-mediated calcium signalling (**Figure 6.1**). These changes were suggested by the downregulation of genes that are related to these processes, which are typically upregulated in response to plant pathogens. This was also supported the lack of fluorescence of the ER marker secRFP-p24aTM, Golgi marker secYFP-ERD2b, TGN marker RFP-SYP61, PVC marker RFP-BP80 and LPVC marker RFP-Rha1 in syncytial cells. Contrastingly, this work highlighted aspects of the plant secretory pathway that may be activated in syncytia to support host defence responses. This was evidenced by the upregulation of genes involved in Golgi-ER trafficking, the COG complex and vacuole-mediated programmed cell death.

This new model for subcellular trafficking in *Arabidopsis* syncytia has helped to unravel the complex interplay between mechanisms of plant defence and pathogen manipulation within susceptible plant-cyst nematode interactions. Future experiments should be conducted to confirm this model and to help close the research gaps on the secretory pathway within syncytia. This could include further work to validate the roles of this set of secretory pathway genes in syncytia, in addition to further advanced microscopy to understand how the structure of organelles in syncytia, such as the proliferation of the ER, Golgi and the fragmentation of vacuoles relates to the hypothesised alterations in

subcellular trafficking. Additionally, the ultrastructure of post-Golgi organelles including the TGN, PVC and LPVCs should be characterised to support the hypothesis that vacuolar sorting is suppressed in syncytia, and to support previous claims of unconventional secretion in *Arabidopsis* syncytia (Golinowski et al, 1996).

6.3 Nematode effectors target diverse subcellular compartments in the host

The effector screen identified a set of *H. schachtii* and *G. pallida* proteins containing signal peptides and C-terminal TMDs, due to increasing evidence that plant pathogen effectors can contain TMDs (Fungi- Carreón-Anguiano et al, 2020; oomycetes- Breeze et al, 2020). Novel putative effectors identified from this screen had various subcellular localisations, including the ER, cytoplasm, nucleus, peroxisomes, and unidentified subcellular compartments. If studied further, these proteins could reveal novel host pathways targeted by cyst nematodes. Comparison of these putative effector proteins with other characterised plant pathogen effectors could be used to infer subcellular targets of the screened putative effectors, to aid future experiments. Also from this work, effector screens could be conducted to identify additional effectors that contain TMDs. These screens could be conducted across several plant pathogen species, as transmembrane proteins have typically been discounted from the effector screens in plant-parasitic nematodes (Thorpe et al, 2014; Haegeman et al, 2012), fungi and oomycetes (Sperschneider et al, 2015 & 2016).

6.3.1 ER-targeting cyst nematode effectors reveal conserved and potentially unique functions

GPLIN_000854400, used as a control in the effector screen, evidences that cyst nematode effectors target similar host signalling pathways to other biotrophic plant pathogen effectors. GPLIN_000854400 interacts with potato NAC transcription factors in the ER to prevent their relocalisation to the nucleus (unpublished), which is similar to effectors containing TMDs from the oomycetes *Phytophthora infestans*, *Hyaloperonospora arabidopsidis* and *Plasmopara halstedii*, which also bind to host NAC transcription factors (Breeze et al, 2020; McLellan et al, 2013). These effectors have been hypothesised to suppress the expression of plant defence-related genes. All screened putative effectors apart from Hsc_gene_2739 and Hsc_gene_19069 partially localised to the ER. However, the different subcellular localisation of these genes suggests a different mechanism of action to GPLIN_000854400 and other plant pathogen effectors that bind to NAC TFs. Therefore, the functional characterisation of these proteins could identify novel mechanisms of pathogenicity.

6.3.2 A putative *H. schachtii* effector with potential ROS-modulating function

The localisation of Hsc_gene_19059 was unique amongst other previously characterised cyst nematode effectors, with GFP-Hsc_gene_19059 localising to the nucleus and peroxisomes, and Hsc_gene_19059-GFP localising to an additional unidentified subcellular compartment. Although two *G. pallida* peroxisome targeting effectors have previously been identified, these don't contain a TMD and only localise to the peroxisomes (Thorpe et al, 2014). Interestingly, other plant pathogen effectors have dual nucleus and peroxisome localisation, including those from the bacteria *Phytophthora sojae*, the cucumber mosaic virus, and the fungus *Blumeria graminis*, that bind to peroxisome localised catalases. This induces the translocation of effector-bound catalases to the nucleus, and alters the transcription of genes associated with PCD (Yuan et al, 2021; Zhang et al, 2015; Inaba et al, 2011; Murota et al, 2017). Using evidence from other plant pathogen effectors, the unidentified subcellular compartment of Hsc_gene_19059-GFP was most likely predicted to be the mitochondria. Tail anchored proteins commonly localise to both the peroxisomes and mitochondria (Costello et al, 2017), therefore, it is plausible for Hsc_gene_19059 to localise to both organelles. As the peroxisomes and mitochondria have closely linked roles in ROS production (Marthur et al, 2018), Hsc_gene_19059 may function to suppress the expression or activity of ROS-related genes.

6.3.3 A putative *H. schachtii* effector hypothesised to target host gene expression

The putative effector Hsc_gene_2739 localised to the nucleus, which is a common target of cyst nematode effectors (Elling et al, 2007) and other plant pathogen effectors, including fungi (de Mandal and Jeon, 2022), oomycetes (Fabro, 2022) and bacteria (Canonne and Rivas, 2012). However, no nucleus-targeting plant pathogen effectors containing TMDs have been previously identified. Non-transmembrane, nucleus-targeting effectors from *H. schachtii* have similar functions to other plant pathogen effectors targeting this organelle, including root-knot nematodes, bacteria, fungi and oomycetes. These functions include the suppression of plant defence-related genes through: DNA binding (Barnes et al, 2018; Zhang et al, 2015; Kim et al, 2008; Song et al, 2015; Ahmed et al, 2018), interaction with pre-mRNA splicing machinery (Verma et al 2018; Mejias et al, 2021; Tang et al, 2022; Huang et al, 2017), and modification of histone acetylation (Vijayapalani et al, 2018; Miller et al, 2010; Kong et al, 2017; Chen et al, 2022). Therefore, the common targets of plant pathogen nuclear-targeting effectors could be used to identify the function of Hsc_gene_2739. Although, the presence of a C-terminal TMD could suggest a novel function of this gene within the nucleus.

6.3.4 Putative effectors potentially targeting COPII and COPI cycling, or vacuolar sorting

Putative cyst nematode effectors were identified that localised to the ER, plus an additional subcellular compartment predicted to be the Golgi or a post-Golgi organelle. This includes GPLIN_001269700; with the C-terminal GFP fusion of this gene localising to punctate structures predicted to be the Golgi. Dual ER and Golgi localisation has been identified for other plant pathogen effectors containing a C-terminal TMD, including five effectors from the oomycete *Phytophthora infestans*, although these are yet to be functionally characterised (Breeze et al, 2020). Non-transmembrane plant pathogen effectors localising to both of these organelles have been identified which disrupt COPI and COPII vesicle trafficking, including those from the red clover necrotic mosaic virus (Hyodo et al, 2014). Therefore similarly, GPLIN_001269700 may function to disrupt COPI and COPII cycling.

Another screened cyst nematode protein, Hsc_gene_19069, had predicted ER and Golgi or post-Golgi organelle localisation, due to the presence of an EGF-like domain which is involved in plant vacuolar sorting. Many other plant pathogen effectors have been shown to manipulate vacuolar sorting, including those secreted by oomycetes (Bozkurt et al, 2011), fungi (Schmidt et al, 2014) and bacteria (Nomura et al, 2006). Although no plant pathogen effectors have been identified containing EGF-like domains, altered subcellular trafficking is involved in soybean resistance to the cyst nematode *H. glycines* (Bayless et al, 2018). Therefore, it is plausible that cyst nematode effectors, such as Hsc_gene_19069, manipulate vacuolar trafficking to suppress plant defence.

6.3.5 Research gaps on plant pathogen effector delivery

The analyses of putative cyst nematode effectors in this work was based on the assumption that the signal peptides of the effectors were cleaved in the nematode gland cell, as they entered the conventional secretory pathway at the ER. The effectors were then hypothesised to travel through the nematode's secretory pathway and exit the gland cell via exocytosis (Liu et al, 2018; Mitchum et al, 2013). Evidence to support this model for effector delivery in cyst nematodes has been provided by immunodetection studies; with the mature versions of effectors lacking a signal peptide being detected in the nematode's gland cells (Chen et al, 2015). Moreover, in addition to cyst nematodes, this is thought to be the conventional mode of effector delivery for other biotrophic plant pathogens, including root-knot nematodes, fungi and oomycetes (Rizzo et al, 2020; Lee et al, 2011).

However, this model for effector delivery currently doesn't explain how the transmembrane effectors are able to insert themselves into the membrane of the secretory vesicles, to then dissociate from the membrane once within the host cell and

reach their target membranes. Thus, alternative mechanisms of effector delivery may explain the trafficking of transmembrane effectors into host cells. Unconventional effector delivery has been suggested across several plant pathogens, from the identification of effector proteins that lack signal peptides from root knot nematodes, fungi and oomycetes (Qin et al, 2021; Liu et al, 2014). Additionally, the signal peptide of the *H. avenae* effector HaEXP2 isn't cleaved in the nematode; instead it is required within the host cell for its correct subcellular localisation and function (Liu et al, 2016).

An alternative model for the delivery of effectors could be extracellular vesicles (EVs). These are secreted by various plant pathogens including bacteria, fungi and oomycetes (Zhou et al, 2022; Rizzo et al, 2020). Recently, EVs from several animal pathogen species and the plant pathogenic fungi *Ustilago maydis* have been found to contain mRNAs that encode pathogen virulence genes (Lécrivain and Beckmann, 2020; Kwon et al, 2021). Therefore, EVs secreted by cyst nematodes may contain the mRNAs of effector proteins that are translated and processed within the host, rather than within the pathogen. This could explain how plant pathogen effectors containing transmembrane effectors, including those studied in this work, are trafficked into host cells, which could be confirmed with immunoblotting experiments. Therefore, studying this set of putative cyst nematode transmembrane effectors further would help to close the research gaps on plant pathogen effector delivery, while furthering knowledge on the mechanisms of cyst nematode parasitism.

6.4 Conclusions

The role of the plant secretory pathway in plant-pathogen interactions is beginning to be unravelled, emerging as an exciting, up-and-coming field of research. Here, fluorescence microscopy and gene expression analysis in syncytia identified components of the endomembrane system that may be involved in host defence or pathogenicity, which are common to other plant-pathogen interactions. This includes the potential suppression of defence related genes involved in ER stress, ER-Golgi trafficking, secretion and vacuolar trafficking. Contrastingly, other plant defence related genes were upregulated in Arabidopsis syncytia, including COPI coatomer subunits, COG subunits and VPE genes, suggesting the role of the early secretory pathway and vacuole-mediated cell death in plant defence during cyst nematode infection. When studied further, the role of these differentially expressed genes in syncytia could deepen understanding of the plant secretory pathway in plant-pathogen responses, and could identify potential cyst nematode resistance genes to be introduced into economically important crops.

Another main aim of this work was to identify novel putative cyst nematode effectors containing a C-terminal TMD. From this screen, several putative cyst nematode effectors were identified, which targeted various subcellular compartments. Although some of these didn't target the ER as predicted, this set of putative effectors has provided further

evidence to suggest cyst nematode effectors can contain TMDs, which could aid the identification of novel effectors across plant pathogen species. These effectors targeted subcellular compartments such as the nucleus, which is unique to other characterised plant pathogen effectors containing TMDs. Some screened putative effectors also had multiple subcellular localisations, including the nucleus, peroxisomes, and potentially the mitochondria, which is unique amongst characterised plant pathogen effectors. Therefore, the functional characterisation of these proteins could identify novel host mechanisms targeted by plant pathogen effectors to enhance understanding of plant-pathogen interactions. In turn, this could help to identify genes for silencing in the pathogen, via commonly used RNAi strategies.

References

- Abad, P. and Williamson, V.M. 2010. Plant Nematode Interaction: A Sophisticated Dialogue. In: Kader, J.-C. and Delseny, M. eds. *Advances in Botanical Research*. Academic Press, pp.147-192.
- Abd El Samad, A.A 2019. Transmission Electron Tomography: Intracellular Insight for the Future of Medicine. In: *Electron Microscopy-Novel Microscopy Trends* (p. 59).
- Abiodun, M.O. and Matsuoka, K. 2013. Evidence that proliferation of golgi apparatus depends on both de novo generation from the endoplasmic reticulum and formation from pre-existing stacks during the growth of tobacco BY-2 cells. *Plant Cell Physiol.* **54**(4), pp.541-554.
- Acedo, J.R. and Dropkin, V.H. 1982. Technique for Obtaining Eggs and Juveniles of Heterodera glycines. *J Nematol.* **14**(3), pp.418-420.
- Aditya, J., Lewis, J., Shirley, N.J., Tan, H.T., Henderson, M., Fincher, G.B., Burton, R.A., Mather, D.E. and Tucker, M.R. 2015. The dynamics of cereal cyst nematode infection differ between susceptible and resistant barley cultivars and lead to changes in (1,3;1,4)- β -glucan levels and HvCslF gene transcript abundance. *New Phytologist.* **207**(1), pp.135-147.
- Ahmed, M.B., Santos, K.C.G.D., Sanchez, I.B., Petre, B., Lorrain, C., Plourde, M.B., Duplessis, S., Desgagné-Penix, I. and Germain, H. 2018. A rust fungal effector binds plant DNA and modulates transcription. *Sci Rep.* **8**(1), p14718.
- Ahmed, S.U., Rojo, E., Kovaleva, V., Venkataraman, S., Dombrowski, J.E., Matsuoka, K. and Raikhel, N.V. 2000. The plant vacuolar sorting receptor AtELP is involved in transport of NH(2)-terminal propeptide-containing vacuolar proteins in Arabidopsis thaliana. *J Cell Biol.* **149**(7), pp.1335-1344.
- Alexandersson, E., Ali, A., Resjö, S. and Andreasson, E. 2013. Plant secretome proteomics. *Front Plant Sci.* **4**, p9.

- Ali, M.A., Anjam, M.S., Nawaz, M.A., Lam, H.M. and Chung, G. 2018. Signal Transduction in Plant-Nematode Interactions. *Int J Mol Sci.* **19**(6).
- Ali, M.A., Azeem, F., Abbas, A., Joyia, F.A., Li, H. and Dababat, A.A. 2017a. Transgenic Strategies for Enhancement of Nematode Resistance in Plants. *Front Plant Sci.* **8**, p750.
- Ali, M.A., Azeem, F., Li, H. and Bohlmann, H. 2017b. Smart Parasitic Nematodes Use Multifaceted Strategies to Parasitize Plants. *Front Plant Sci.* **8**, p1699.
- Ali, S., Magne, M., Chen, S., Côté, O., Stare, B.G., Obradovic, N., Jamshaid, L., Wang, X., Bélair, G. and Moffett, P. 2015a. Analysis of putative apoplastic effectors from the nematode, *Globodera rostochiensis*, and identification of an expansin-like protein that can induce and suppress host defenses. *PLoS One.* **10**(1), pe0115042.
- Ali, S., Magne, M., Chen, S., Obradovic, N., Jamshaid, L., Wang, X., Bélair, G. and Moffett, P. 2015b. Analysis of *Globodera rostochiensis* effectors reveals conserved functions of SPRYSEC proteins in suppressing and eliciting plant immune responses. *Front Plant Sci.* **6**, p623.
- Aljaafri, W., Alfadhil, F., Naji Hussein, A. and Al-Jouburi, H. 2018. Analysis of the Glycine max role of Syntaxin (SYP22) in resistance to *Rotylenchulus reniformis*. *International Journal of Pharmaceutical Quality Assurance.* **9**(3), pp.324-331
- Aljuaifari, W.A., Alshimaysawe, U.A.A., Mohammed, A.E. and Al-Abedy, A.N. 2019. Evaluate the ability of Syntaxin genes to enhance resistance against *Fusarium virguliforme* and *Heterodera glycines*. *IOP Conference Series: Earth and Environmental Science.* **388**(1), p012014.
- Almagro Armenteros, J.J., Tsirigos, K.D., Sønderby, C.K., Petersen, T.N., Winther, O., Brunak, S., von Heijne, G. and Nielsen, H. 2019. SignalP 5.0 improves signal peptide predictions using deep neural networks. *Nat Biotechnol.* **37**(4), pp.420-423.

- Alvim, J.C. 2018. On the mechanisms of receptor-mediated retention of soluble endoplasmic reticulum resident proteins in eukaryotes. (Doctoral dissertation, University of Leeds).
- Amack, S.C. and Antunes, M.S. 2020. CaMV35S promoter – A plant biology and biotechnology workhorse in the era of synthetic biology. *Current Plant Biology*. **24**, p100179.
- An, Q., Ehlers, K., Kogel, K.H., van Bel, A.J. and Hückelhoven, R. 2006b. Multivesicular compartments proliferate in susceptible and resistant MLA12-barley leaves in response to infection by the biotrophic powdery mildew fungus. *New Phytol.* **172**(3), pp.563-576.
- An, Q., Hückelhoven, R., Kogel, K.H. and van Bel, A.J. 2006a. Multivesicular bodies participate in a cell wall-associated defence response in barley leaves attacked by the pathogenic powdery mildew fungus. *Cell Microbiol.* **8**(6), pp.1009-1019.
- Andres, M.F., Melillo, M.T., Delibes, A., Romero, M.D. and Bleve-Zacheo, T. 2001. Changes in wheat root enzymes correlated with resistance to cereal cyst nematodes. *New Phytologist.* **152**(2), pp.343-354.
- Angelos, E. and Brandizzi, F. 2018. NADPH oxidase activity is required for ER stress survival in plants. *Plant J.* **96**(6), pp.1106-1120.
- Angenon, G., Uotila, J., Kurkela, S.A., Teeri, T.H., Botterman, J., Van Montagu, M. and Depicker, A. 1989. Expression of dicistronic transcriptional units in transgenic tobacco. *Mol Cell Biol.* **9**(12), pp.5676-5684.
- Anlar, B. and Gunel-Ozcan, A. 2012. Tenascin-R: role in the central nervous system. *Int J Biochem Cell Biol.* **44**(9), pp.1385-1389.
- Austin, H.W., McNeece, B.T., Sharma, K., Niraula, P.M., Lawrence, K.S. and Klink, V.P. 2019. An expanded role of the SNARE-containing regulon as it relates to the defense process that Glycine max has to Heterodera glycines. *Journal of Plant Interactions.* **14**(1), pp.276-283.

- Baars, T.L., Petri, S., Peters, C. and Mayer, A. 2007. Role of the V-ATPase in regulation of the vacuolar fission-fusion equilibrium. *Mol Biol Cell*. **18**(10), pp.3873-3882.
- Banerjee, S., Banerjee, A., Gill, S.S., Gupta, O.P., Dahuja, A., Jain, P.K. and Sirohi, A. 2017. RNA Interference: A Novel Source of Resistance to Combat Plant Parasitic Nematodes. *Front Plant Sci*. **8**, p834.
- Baranowski, Ł., Róžańska, E., Sańko-Sawczenko, I., Matuszkiewicz, M., Znojek, E., Filipecki, M., Grundler, F.M.W. and Sobczak, M. 2019. Arabidopsis tonoplast intrinsic protein and vacuolar H. *Protoplasma*. **256**(2), pp.419-429.
- Barnes, S.N., Wram, C.L., Mitchum, M.G. and Baum, T.J. 2018. The plant-parasitic cyst nematode effector GLAND4 is a DNA-binding protein. *Mol Plant Pathol*. **19**(10), pp.2263-2276.
- Barthels, N., van der Lee, F.M., Klap, J., Goddijn, O.J., Karimi, M., Puzio, P., Grundler, F.M., Ohl, S.A., Lindsey, K., Robertson, L., Robertson, W.M., Van Montagu, M., Gheysen, G. and Sijmons, P.C. 1997. Regulatory sequences of Arabidopsis drive reporter gene expression in nematode feeding structures. *Plant Cell*. **9**(12), pp.2119-2134.
- Barton, D.A., Cole, L., Collings, D.A., Liu, D.Y., Smith, P.M., Day, D.A. and Overall, R.L. 2011. Cell-to-cell transport via the lumen of the endoplasmic reticulum. *Plant J*. **66**(5), pp.806-817.
- Bassham, D.C., Brandizzi, F., Otegui, M.S. and Sanderfoot, A.A. 2008. The secretory system of Arabidopsis. *Arabidopsis Book*. **6**, pe0116.
- Bayless, A.M., Smith, J.M., Song, J., McMinn, P.H., Teillet, A., August, B.K. and Bent, A.F. 2016. Disease resistance through impairment of α -SNAP-NSF interaction and vesicular trafficking by soybean Rhg1. *Proc Natl Acad Sci U S A*. **113**(47), pp.E7375-E7382.
- Bayless, A.M., Zapotocny, R.W., Grunwald, D.J., Amundson, K.K., Diers, B.W. and Bent, A.F. 2018. An atypical N-ethylmaleimide sensitive factor enables

the viability of nematode-resistant. *Proc Natl Acad Sci U S A*. **115**(19), pp.E4512-E4521.

- Beaugelin, I., Chevalier, A., D'Alessandro, S., Ksas, B. and Havaux, M. 2020. Endoplasmic reticulum-mediated unfolded protein response is an integral part of singlet oxygen signalling in plants. *Plant J*. **102**(6), pp.1266-1280.
- Beh, C.T., Ferrari, D.C., Chung, M.A. and McGhee, J.D. 1991. An acid phosphatase as a biochemical marker for intestinal development in the nematode *Caenorhabditis elegans*. *Dev Biol*. **147**(1), pp.133-143.
- Bekal, S., Domier, L.L., Gonfa, B., Lakhssassi, N., Meksem, K. and Lambert, K.N. 2015. A SNARE-Like Protein and Biotin Are Implicated in Soybean Cyst Nematode Virulence. *PLOS ONE*. **10**(12), pe0145601.
- Benitez-Alfonso, Y., Faulkner, C., Pendle, A., Miyashima, S., Helariutta, Y. and Maule, A. 2013. Symplastic intercellular connectivity regulates lateral root patterning. *Dev Cell*. **26**(2), pp.136-147.
- Berg, R.H. and Beachy, R.N. 2008. Fluorescent Protein Applications in Plants. *Methods in Cell Biology*. Academic Press, pp.153-177.
- Berka, M., Kopecká, R., Berková, V., Brzobohatý, B. and Černý, M. 2022. Regulation of heat shock proteins 70 and their role in plant immunity. *J Exp Bot*. **73**(7), pp.1894-1909.
- Bertero, A., Brown, S. and Vallier, L. 2017. Methods of cloning. *Basic science methods for clinical researchers*. Elsevier, pp.19-39.
- Bian, Z., Gao, H. and Wang, C. 2020. NAC Transcription Factors as Positive or Negative Regulators during Ongoing Battle between Pathogens and Our Food Crops. *Int J Mol Sci*. **22**(1).
- Bitto, E., Bingman, C.A., Kondrashov, D.A., McCoy, J.G., Bannen, R.M., Wesenberg, G.E. and Phillips Jr., G.N. 2008. Structure and dynamics of γ -SNAP: Insight into flexibility of proteins from the SNAP family. *Proteins: Structure, Function, and Bioinformatics*. **70**(1), pp.93-104.

- Blackburn, J.B., Kudlyk, T., Pokrovskaya, I. and Lupashin, V.V. 2018. More than just sugars: Conserved oligomeric Golgi complex deficiency causes glycosylation-independent cellular defects. *Traffic*. **19**(6), pp.463-480.
- Bleve-Zacheo, T. and Zacheo, G. 1987. Cytological studies of the susceptible reaction of sugarbeet roots to *Heterodera schachtii*. *Physiological and Molecular Plant Pathology*. **30**(1), pp.13-25.
- Block, A., Toruño, T.Y., Elowsky, C.G., Zhang, C., Steinbrenner, J., Beynon, J. and Alfano, J.R. 2014. The *Pseudomonas syringae* type III effector HopD1 suppresses effector-triggered immunity, localizes to the endoplasmic reticulum, and targets the Arabidopsis transcription factor NTL9. *New Phytol*. **201**(4), pp.1358-1370.
- Blum, T., Briesemeister, S. and Kohlbacher, O. 2009. MultiLoc2: integrating phylogeny and Gene Ontology terms improves subcellular protein localization prediction. *BMC Bioinformatics*. **10**, p274.
- Bobardt, S.D., Dillman, A.R. and Nair, M.G. 2020. The Two Faces of Nematode Infection: Virulence and Immunomodulatory Molecules From Nematode Parasites of Mammals, Insects and Plants. *Front Microbiol*. **11**, p577846.
- Böckenhoff, A. and Grundler, F.M.W. 1994. Studies on the nutrient uptake by the beet cyst nematode *Heterodera schachtii* by in situ microinjection of fluorescent probes into the feeding structures in *Arabidopsis thaliana*. *Parasitology*. **109**(2), pp.249-255.
- Böhlenius, H., Mørch, S.M., Godfrey, D., Nielsen, M.E. and Thordal-Christensen, H. 2010. The multivesicular body-localized GTPase ARFA1b/1c is important for callose deposition and ROR2 syntaxin-dependent preinvasive basal defense in barley. *Plant Cell*. **22**(11), pp.3831-3844.
- Bohlmann, H. and Sobczak, M. 2014. The plant cell wall in the feeding sites of cyst nematodes. *Front Plant Sci*. **5**, p89.
- Bohlmann, H. and Wieczorek, K. 2015. Infection assay of cyst nematodes on *Arabidopsis* roots. *Bio-protocol*. **5**, pe1596.

- Bongers, T. and Ferris, H. 1999. Nematode community structure as a bioindicator in environmental monitoring. *Trends Ecol Evol.* **14**(6), pp.224-228.
- Bonifacino, J.S. and Glick, B.S. 2004. The mechanisms of vesicle budding and fusion. *Cell.* **116**(2), pp.153-166.
- Bottanelli, F., Foresti, O., Hanton, S. and Denecke, J. 2011. Vacuolar transport in tobacco leaf epidermis cells involves a single route for soluble cargo and multiple routes for membrane cargo. *Plant Cell.* **23**(8), pp.3007-3025.
- Bottanelli, F., Gershlick, D.C. and Denecke, J. 2012. Evidence for sequential action of Rab5 and Rab7 GTPases in prevacuolar organelle partitioning. *Traffic.* **13**(2), pp.338-354.
- Boutté, Y., Vernhettes, S. and Satiat-Jeunemaitre, B. 2007. Involvement of the cytoskeleton in the secretory pathway and plasma membrane organisation of higher plant cells. *Cell Biol Int.* **31**(7), pp.649-654.
- Bozkurt, T.O., Schornack, S., Win, J., Shindo, T., Ilyas, M., Oliva, R., Cano, L.M., Jones, A.M., Huitema, E., van der Hoorn, R.A. and Kamoun, S. 2011. Phytophthora infestans effector AVRblb2 prevents secretion of a plant immune protease at the haustorial interface. *Proc Natl Acad Sci U S A.* **108**(51), pp.20832-20837.
- Brandizzi, F. and Barlowe, C. 2013. Organization of the ER-Golgi interface for membrane traffic control. *Nat Rev Mol Cell Biol.* **14**(6), pp.382-392.
- Brandizzi, F., Frangne, N., Marc-Martin, S., Hawes, C., Neuhaus, J.M. and Paris, N. 2002. The destination for single-pass membrane proteins is influenced markedly by the length of the hydrophobic domain. *Plant Cell.* **14**(5), pp.1077-1092.
- Brandizzi, F., Hanton, S., DaSilva, L.L., Boevink, P., Evans, D., Oparka, K., Denecke, J. and Hawes, C. 2003. ER quality control can lead to retrograde transport from the ER lumen to the cytosol and the nucleoplasm in plants. *Plant J.* **34**(3), pp.269-281.

- Breeze, E., Dzimitrowicz, N., Kriechbaumer, V., Brooks, R., Botchway, S.W., Brady, J.P., Hawes, C., Dixon, A.M., Schnell, J.R., Fricker, M.D. and Frigerio, L. 2016. A C-terminal amphipathic helix is necessary for the in vivo tubule-shaping function of a plant reticulon. *Proceedings of the National Academy of Sciences*. **113**(39), pp.10902-10907.
- Breeze, E., Vale, V., Mclellan, H., Godiard, L., Grant, M. and Frigerio, L. 2020. The plant endoplasmic reticulum is both receptive and responsive to pathogen effectors. *BioRxiv*, pp.2020-06.
- Bruce, T.J.A. 2010. Tackling the threat to food security caused by crop pests in the new millennium. *Food Security*. **2**(2), pp.133-141.
- Bubeck, J., Scheuring, D., Hummel, E., Langhans, M., Viotti, C., Foresti, O., Denecke, J., Banfield, D.K. and Robinson, D.G. 2008. The syntaxins SYP31 and SYP81 control ER-Golgi trafficking in the plant secretory pathway. *Traffic*. **9**(10), pp.1629-1652.
- Burkhard, P., Stetefeld, J. and Strelkov, S.V. 2001. Coiled coils: a highly versatile protein folding motif. *Trends Cell Biol.* **11**(2), pp.82-88.
- Burrows, P.R. 1992. Molecular Analysis of the Interactions between Cyst Nematodes and Their Hosts. *J Nematol.* **24**(3), pp.338-342.
- Burton, Y. 1991. Ultrastructure of initial responses of susceptible and resistant soybean roots to infection by *Heterodera glycines*. *Revue Nétnatol.* **4**, pp.73-94.
- Butler, K.J., Fliege, C., Zapotocny, R., Diers, B., Hudson, M. and Bent, A.F. 2021. Soybean Cyst Nematode Resistance Quantitative Trait Locus. *Mol Plant Microbe Interact.* **34**(12), pp.1433-1445.
- Cai, Y., Zhuang, X., Gao, C., Wang, X. and Jiang, L. 2014. The Arabidopsis Endosomal Sorting Complex Required for Transport III Regulates Internal Vesicle Formation of the Prevacuolar Compartment and Is Required for Plant Development. *Plant Physiol.* **165**(3), pp.1328-1343.

- Çakır Aydemir, B., Yüksel Özmen, C., Kibar, U., Mutaf, F., Büyük, P.B., Bakır, M. and Ergül, A. 2020. Salt stress induces endoplasmic reticulum stress-responsive genes in a grapevine rootstock. *PLoS One*. **15**(7), pe0236424.
- Camacho, M.J., Mota, M., Lima, A., Rusinque, L. and Inácio, M.L. 2018. Extraction of potato cyst nematodes from soil samples: Cobb's decanting and sieving method vs. Fenwick's method. *Revista de Ciências Agrárias*. **41**(spe), pp.8-14.
- Canonne, J. and Rivas, S. 2012. Bacterial effectors target the plant cell nucleus to subvert host transcription. *Plant Signal Behav.* **7**(2), pp.217-221.
- Caplan, J.L., Zhu, X., Mamillapalli, P., Marathe, R., Anandalakshmi, R. and Dinesh-Kumar, S.P. 2009. Induced ER chaperones regulate a receptor-like kinase to mediate antiviral innate immune response in plants. *Cell Host Microbe*. **6**(5), pp.457-469.
- Carpentier, J., Esquibet, M., Fouville, D., Manzanares-Dauleux, M.J., Kerlan, M.C. and Grenier, E. 2012. The evolution of the Gp-Rbp-1 gene in *Globodera pallida* includes multiple selective replacements. *Mol Plant Pathol*. **13**(6), pp.546-555.
- Carreón-Anguiano, K.G., Islas-Flores, I., Vega-Arreguín, J., Sáenz-Carbonell, L. and Canto-Canché, B. 2020. EffHunter: A Tool for Prediction of Effector Protein Candidates in Fungal Proteomic Databases. *Biomolecules*. **10**(5).
- Chakraborty, R., Macoy, D.M., Lee, S.Y., Kim, W.-Y. and Kim, M.G. 2017. Tunicamycin-induced endoplasmic reticulum stress suppresses plant immunity. *Applied Biological Chemistry*. **60**(6), pp.623-630.
- Chatre, L., Brandizzi, F., Hocquellet, A., Hawes, C. and Moreau, P. 2005. Sec22 and Memb11 are v-SNAREs of the anterograde endoplasmic reticulum-Golgi pathway in tobacco leaf epidermal cells. *Plant Physiol*. **139**(3), pp.1244-1254.
- Chauvin, C., Dorel, M., Villenave, C., Roger-Estrade, J., Thuries, L. and Risède, J.-M. 2015. Biochemical characteristics of cover crop litter affect the soil

food web, organic matter decomposition, and regulation of plant-parasitic nematodes in a banana field soil. *Applied Soil Ecology*. **96**, pp.131-140.

Chen, J., Doyle, C., Qi, X. and Zheng, H. 2012. The endoplasmic reticulum: a social network in plant cells. *J Integr Plant Biol*. **54**(11), pp.840-850.

Chen, X., Duan, Y., Qiao, F., Liu, H., Huang, J., Luo, C., Li, G., Xie, K., Hsiang, T. and Zheng, L. 2022. A secreted fungal effector suppresses rice immunity through host histone hypoacetylation. *New Phytol*. **235**(5), pp.1977-1994.

Cheng, F.Y., Blackburn, K., Lin, Y.M., Goshe, M.B. and Williamson, J.D. 2009. Absolute protein quantification by LC/MS(E) for global analysis of salicylic acid-induced plant protein secretion responses. *J Proteome Res*. **8**(1), pp.82-93.

Cho, Y. and Kanehara, K. 2017. Endoplasmic Reticulum Stress Response in Arabidopsis Roots. *Front Plant Sci*. **8**, p144.

Choi, S.W., Tamaki, T., Ebine, K., Uemura, T., Ueda, T. and Nakano, A. 2013. RABA members act in distinct steps of subcellular trafficking of the FLAGELLIN SENSING2 receptor. *Plant Cell*. **25**(3), pp.1174-1187.

Choi, U.B., Zhao, M., White, K.I., Zhou, Q., Pfuetzner, R. and Brunger, A.T. 2018. Single SNARE complex recycling by NSF. *Biophysical Journal*. **114**(3), p282a.

Chopra, D., Hasan, M.S., Matera, C., Chitambo, O., Mendy, B., Mahlitz, S.V., Naz, A.A., Szumski, S., Janakowski, S., Sobczak, M., Mithöfer, A., Kyndt, T., Grundler, F.M.W. and Siddique, S. 2021. Plant parasitic cyst nematodes redirect host indole metabolism via NADPH oxidase-mediated ROS to promote infection. *New Phytol*. **232**(1), pp.318-331.

Clemens, C.D., Aumann, J., Spiegel, Y. and Wyss, U. 1994. Attractant-mediated behaviour of mobile stages of *Heterodera schachtii*. *Fundamental and Applied Nematology*. **17**.

- Clough, S.J. and Bent, A.F. 1998. Floral dip: a simplified method for *Agrobacterium*-mediated transformation of *Arabidopsis thaliana*. *Plant J.* **16**(6), pp.735-743.
- Coemans, B., Takahashi, Y., Berberich, T., Ito, A., Kanzaki, H., Matsumura, H., Saitoh, H., Tsuda, S., Kamoun, S., Sági, L., Swennen, R. and Terauchi, R. 2008. High-throughput in planta expression screening identifies an ADP-ribosylation factor (ARF1) involved in non-host resistance and R gene-mediated resistance. *Mol Plant Pathol.* **9**(1), pp.25-36.
- Cohen, M.J., Chirico, W.J. and Lipke, P.N. 2020. Through the back door: Unconventional protein secretion. *Cell Surf.* **6**, p100045.
- Cook, D.E., Lee, T.G., Guo, X., Melito, S., Wang, K., Bayless, A.M., Wang, J., Hughes, T.J., Willis, D.K., Clemente, T.E., Diers, B.W., Jiang, J., Hudson, M.E. and Bent, A.F. 2012. Copy number variation of multiple genes at *Rhg1* mediates nematode resistance in soybean. *Science.* **338**(6111), pp.1206-1209.
- Costello, J.L., Castro, I.G., Camões, F., Schrader, T.A., McNeall, D., Yang, J., Giannopoulou, E.A., Gomes, S., Pogenberg, V., Bonekamp, N.A., Ribeiro, D., Wilmanns, M., Jedd, G., Islinger, M. and Schrader, M. 2017. Predicting the targeting of tail-anchored proteins to subcellular compartments in mammalian cells. *J Cell Sci.* **130**(9), pp.1675-1687.
- Cotton, J.A., Lilley, C.J., Jones, L.M., Kikuchi, T., Reid, A.J., Thorpe, P., Tsai, I.J., Beasley, H., Blok, V., Cock, P.J., Eves-van den Akker, S., Holroyd, N., Hunt, M., Mantelin, S., Naghra, H., Pain, A., Palomares-Rius, J.E., Zarowiecki, M., Berriman, M., Jones, J.T. and Urwin, P.E. 2014. The genome and life-stage specific transcriptomes of *Globodera pallida* elucidate key aspects of plant parasitism by a cyst nematode. *Genome Biol.* **15**(3), pR43.
- Cui, Y., Shen, J., Gao, C., Zhuang, X., Wang, J. and Jiang, L. 2016. Biogenesis of Plant Prevacuolar Multivesicular Bodies. *Mol Plant.* **9**(6), pp.774-786.

- Cvjetkovic, A., Jang, S.C., Konečná, B., Höög, J.L., Sihlbom, C., Lässer, C. and Lötvall, J. 2016. Detailed Analysis of Protein Topology of Extracellular Vesicles-Evidence of Unconventional Membrane Protein Orientation. *Sci Rep.* **6**, p36338.
- daSilva, L.L., Foresti, O. and Denecke, J. 2006. Targeting of the plant vacuolar sorting receptor BP80 is dependent on multiple sorting signals in the cytosolic tail. *Plant Cell.* **18**(6), pp.1477-1497.
- daSilva, L.L., Taylor, J.P., Hadlington, J.L., Hanton, S.L., Snowden, C.J., Fox, S.J., Foresti, O., Brandizzi, F. and Denecke, J. 2005. Receptor salvage from the prevacuolar compartment is essential for efficient vacuolar protein targeting. *Plant Cell.* **17**(1), pp.132-148.
- Davies, L.J. and Urwin, P.E. 2012. The cell walls of syncytia formed by *Heterodera schachtii* in *Arabidopsis thaliana* are abundant in methyl-esterified pectin. *Plant Signal Behav.* **7**(11), pp.1404-1406.
- Davies, L.J., Lilley, C.J., Paul Knox, J. and Urwin, P.E. 2012. Syncytia formed by adult female *Heterodera schachtii* in *Arabidopsis thaliana* roots have a distinct cell wall molecular architecture. *New Phytol.* **196**(1), pp.238-246.
- Davis, D.J., Kang, B.H., Heringer, A.S., Wilkop, T.E. and Drakakaki, G. 2016. Unconventional Protein Secretion in Plants. *Methods Mol Biol.* **1459**, pp.47-63.
- de Almeida Engler, J. and Gheysen, G. 2013. Nematode-induced endoreduplication in plant host cells: why and how? *Mol Plant Microbe Interact.* **26**(1), pp.17-24.
- de Almeida Engler, J., De Vleeschauwer, V., Burssens, S., Celenza, J.L., Inzé, D., Van Montagu, M., Engler, G. and Gheysen, G. 1999. Molecular markers and cell cycle inhibitors show the importance of cell cycle progression in nematode-induced galls and syncytia. *Plant Cell.* **11**(5), pp.793-808.

- de Almeida Engler, J., Van Poucke, K., Karimi, M., De Groodt, R., Gheysen, G. and Engler, G. 2004. Dynamic cytoskeleton rearrangements in giant cells and syncytia of nematode-infected roots. *Plant J.* **38**(1), pp.12-26.
- De Benedictis, M., Bleve, G., Faraco, M., Stigliano, E., Grieco, F., Piro, G., Dalessandro, G. and Di Sansebastiano, G.P. 2013. AtSYP51/52 functions diverge in the post-Golgi traffic and differently affect vacuolar sorting. *Mol Plant.* **6**(3), pp.916-930.
- de Boer, J.M., Yan, Y., Smant, G., Davis, E.L. and Baum, T.J. 1998. In-situ Hybridization to Messenger RNA in *Heterodera glycines*. *J Nematol.* **30**(3), pp.309-312.
- de Jonge, N. and Peckys, D.B. 2016. Live Cell Electron Microscopy Is Probably Impossible. *ACS Nano.* **10**(10), pp.9061-9063.
- De Mandal, S. and Jeon, J. 2022. Nuclear Effectors in Plant Pathogenic Fungi. *Mycobiology.* **50**(5), pp.259-268.
- De Marcos Lousa, C., Soubeyrand, E., Bolognese, P., Wattelet-Boyer, V., Bouyssou, G., Marais, C., Boutté, Y., Filippini, F. and Moreau, P. 2016. Subcellular localization and trafficking of phytolongins (non-SNARE longins) in the plant secretory pathway. *J Exp Bot.* **67**(9), pp.2627-2639.
- De Saeger, J., Park, J., Thoris, K., De Bruyn, C., Chung, H.S., Inzé, D. and Depuydt, S. 2022. IMPLANT: a new technique for transgene copy number estimation in plants using a single end-point PCR reaction. *Plant Methods.* **18**(1), p132.
- Demaurex, N., Furuya, W., D'Souza, S., Bonifacino, J.S. and Grinstein, S. 1998. Mechanism of acidification of the trans-Golgi network (TGN). In situ measurements of pH using retrieval of TGN38 and furin from the cell surface. *J Biol Chem.* **273**(4), pp.2044-2051.
- Denecke, J., Aniento, F., Frigerio, L., Hawes, C., Hwang, I., Mathur, J., Neuhaus, J.M. and Robinson, D.G. 2012. Secretory pathway research: the more experimental systems the better. *Plant Cell.* **24**(4), pp.1316-1326.

- Denecke, J., Botterman, J. and Deblaere, R. 1990. Protein secretion in plant cells can occur via a default pathway. *Plant Cell*. **2**(1), pp.51-59.
- Deng, Y., Srivastava, R. and Howell, S.H. 2013. Endoplasmic reticulum (ER) stress response and its physiological roles in plants. *Int J Mol Sci*. **14**(4), pp.8188-8212.
- Denic, V., Dötsch, V. and Sinning, I. 2013. Endoplasmic reticulum targeting and insertion of tail-anchored membrane proteins by the GET pathway. *Cold Spring Harb Perspect Biol*. **5**(8), pa013334.
- Di Sansebastiano, G.P., Paris, N., Marc-Martin, S. and Neuhaus, J.M. 2001. Regeneration of a lytic central vacuole and of neutral peripheral vacuoles can be visualized by green fluorescent proteins targeted to either type of vacuoles. *Plant Physiol*. **126**(1), pp.78-86.
- Diaz-Granados, A., Petrescu, A.J., Goverse, A. and Smant, G. 2016. SPRYSEC Effectors: A Versatile Protein-Binding Platform to Disrupt Plant Innate Immunity. *Front Plant Sci*. **7**, p1575.
- Ding, Y., Robinson, D.G. and Jiang, L. 2014. Unconventional protein secretion (UPS) pathways in plants. *Curr Opin Cell Biol*. **29**, pp.107-115.
- Dinh, T.T., Luscher, E., Li, S., Liu, X., Won, S.Y. and Chen, X. 2014. Genetic screens for floral mutants in *Arabidopsis thaliana*: enhancers and suppressors. *Methods Mol Biol*. **1110**, pp.127-156.
- Dixit, R., Cyr, R. and Gilroy, S. 2006. Using intrinsically fluorescent proteins for plant cell imaging. *Plant J*. **45**(4), pp.599-615.
- Dixon, D.C., Cutt, J.R. and Klessig, D.F. 1991. Differential targeting of the tobacco PR-1 pathogenesis-related proteins to the extracellular space and vacuoles of crystal idioblasts. *EMBO J*. **10**(6), pp.1317-1324.
- Dong, J., Zielinski, R.E. and Hudson, M.E. 2020. t-SNAREs bind the Rhg1 α -SNAP and mediate soybean cyst nematode resistance. *Plant J*. **104**(2), pp.318-331.

- Dong, O.X. and Ronald, P.C. 2021. Targeted DNA insertion in plants. *Proc Natl Acad Sci U S A.* 118(22).
- Doucet, M.E., Angeli, R.V. and Lorenzo, E. 2004. Histopathology of two tobacco cultivars infected by *Globodera tabacum* in Argentina. *Nematologia Mediterranea.*
- Drakakaki, G. and Dandekar, A. 2013. Protein secretion: how many secretory routes does a plant cell have? *Plant Sci.* **203-204**, pp.74-78.
- Drakakaki, G., van de Ven, W., Pan, S., Miao, Y., Wang, J., Keinath, N.F., Weatherly, B., Jiang, L., Schumacher, K., Hicks, G. and Raikhel, N. 2012. Isolation and proteomic analysis of the SYP61 compartment reveal its role in exocytic trafficking in Arabidopsis. *Cell Res.* **22**(2), pp.413-424.
- Driouich, A., Follet-Gueye, M.L., Bernard, S., Kousar, S., Chevalier, L., Vicré-Gibouin, M. and Lerouxel, O. 2012. Golgi-mediated synthesis and secretion of matrix polysaccharides of the primary cell wall of higher plants. *Front Plant Sci.* **3**, p79.
- D'Souza-Schorey, C. and Chavrier, P. 2006. ARF proteins: roles in membrane traffic and beyond. *Nat Rev Mol Cell Biol.* **7**(5), pp.347-358.
- Du, Y., Overdijk, E.J.R., Berg, J.A., Govers, F. and Bouwmeester, K. 2018. Solanaceous exocyst subunits are involved in immunity to diverse plant pathogens. *J Exp Bot.* **69**(3), pp.655-666.
- Du, Y., Tejos, R., Beck, M., Himschoot, E., Li, H., Robatzek, S., Vanneste, S. and Friml, J. 2013. Salicylic acid interferes with clathrin-mediated endocytic protein trafficking. *Proc Natl Acad Sci U S A.* **110**(19), pp.7946-7951.
- Duan, Z. and Tominaga, M. 2018. Actin-myosin XI: an intracellular control network in plants. *Biochem Biophys Res Commun.* **506**(2), pp.403-408.
- Eichmann, R. and Schäfer, P. 2012. The endoplasmic reticulum in plant immunity and cell death. *Front Plant Sci.* **3**, p200.

- Ekanayake, G., LaMontagne, E.D. and Heese, A. 2019. Never Walk Alone: Clathrin-Coated Vesicle (CCV) Components in Plant Immunity. *Annu Rev Phytopathol.* **57**, pp.387-409.
- El-kereamy, A., El-sharkawy, I., Ramamoorthy, R., Taheri, A., Errampalli, D., Kumar, P. and Jayasankar, S. 2011. *Prunus domestica* pathogenesis-related protein-5 activates the defense response pathway and enhances the resistance to fungal infection. *PLoS One.* **6**(3), pe17973.
- Elling, A.A., Davis, E.L., Hussey, R.S. and Baum, T.J. 2007. Active uptake of cyst nematode parasitism proteins into the plant cell nucleus. *Int J Parasitol.* **37**(11), pp.1269-1279.
- Ellinger, D., Glöckner, A., Koch, J., Naumann, M., Stürtz, V., Schütt, K., Manisseri, C., Somerville, S.C. and Voigt, C.A. 2014. Interaction of the Arabidopsis GTPase RabA4c with its effector PMR4 results in complete penetration resistance to powdery mildew. *Plant Cell.* **26**(7), pp.3185-3200.
- Elowsky, C., Wamboldt, Y. and Mackenzie, S. 2017. Laser Scanning Confocal Microscopy for. *Bio Protoc.* **7**(5), pe2150.
- Endo, B.Y. 1987. Ultrastructure of Esophageal Gland Secretory Granules in Juveniles of *Heterodera glycines*. *J Nematol.* **19**(4), pp.469-483.
- Engel, J. 1989. EGF-like domains in extracellular matrix proteins: localized signals for growth and differentiation? *FEBS Lett.* **251**(1-2), pp.1-7.
- Evans, K. and Stone, A.R. 1977. A review of the distribution and biology of the potato cyst-nematodes *Globodera rostochiensis* and *G. pallida*. *Pans.* **23**(2), pp.178-189.
- Eves-van den Akker, S., Laetsch, D.R., Thorpe, P., Lilley, C.J., Danchin, E.G., Da Rocha, M., Rancurel, C., Holroyd, N.E., Cotton, J.A., Szitenberg, A., Grenier, E., Montarry, J., Mimee, B., Duceppe, M.O., Boyes, I., Marvin, J.M., Jones, L.M., Yusup, H.B., Lafond-Lapalme, J., Esquibet, M., Sabehe, M., Rott, M., Overmars, H., Finkers-Tomczak, A., Smant, G.,

- Koutsovoulos, G., Blok, V., Mantelin, S., Cock, P.J., Phillips, W., Henrissat, B., Urwin, P.E., Blaxter, M. and Jones, J.T. 2016. The genome of the yellow potato cyst nematode, *Globodera rostochiensis*, reveals insights into the basis of parasitism and virulence. *Genome Biol.* **17**(1), p124.
- Fabro, G. 2022. Oomycete intracellular effectors: specialised weapons targeting strategic plant processes. *New Phytologist.* **233**(3), pp.1074-1082.
- Fan, G., Yang, Y., Li, T., Lu, W., Du, Y., Qiang, X., Wen, Q. and Shan, W. 2018. A *Phytophthora capsici* RXLR Effector Targets and Inhibits a Plant PPIase to Suppress Endoplasmic Reticulum-Mediated Immunity. *Mol Plant.* **11**(8), pp.1067-1083.
- Fan, L., Li, R., Pan, J., Ding, Z. and Lin, J. 2015. Endocytosis and its regulation in plants. *Trends Plant Sci.* **20**(6), pp.388-397.
- Fenwick, D.W. 1940. Methods for the recovery and counting of cysts of *Heterodera schachtii* from soil. *Journal of helminthology.* **18**(4), pp.155-172.
- Ferrero, S., Grados-Torrez, R.E., Leivar, P., Antolín-Llovera, M., López-Iglesias, C., Cortadellas, N., Ferrer, J.C. and Campos, N. 2015. Proliferation and Morphogenesis of the Endoplasmic Reticulum Driven by the Membrane Domain of 3-Hydroxy-3-Methylglutaryl Coenzyme A Reductase in Plant Cells. *Plant Physiol.* **168**(3), pp.899-914.
- Filipecki, M., Żurczak, M., Matuszkiewicz, M., Święcicka, M., Kurek, W., Olszewski, J., Koter, M.D., Lamont, D. and Sobczak, M. 2021. Profiling the Proteome of Cyst Nematode-Induced Syncytia on Tomato Roots. *Int J Mol Sci.* **22**(22).
- Fluckiger, R., De Caroli, M., Piro, G., Dalessandro, G., Neuhaus, J.M. and Di Sansebastiano, G.P. 2003. Vacuolar system distribution in *Arabidopsis* tissues, visualized using GFP fusion proteins. *J Exp Bot.* **54**(387), pp.1577-1584.

- Foresti, O. and Denecke, J. 2008. Intermediate organelles of the plant secretory pathway: identity and function. *Traffic*. **9**(10), pp.1599-1612.
- Foresti, O., Gershlick, D.C., Bottanelli, F., Hummel, E., Hawes, C. and Denecke, J. 2010. A recycling-defective vacuolar sorting receptor reveals an intermediate compartment situated between prevacuoles and vacuoles in tobacco. *Plant Cell*. **22**(12), pp.3992-4008.
- Franco, A.L.C., Gherardi, L.A., de Tomasel, C.M., Andriuzzi, W.S., Ankrom, K.E., Shaw, E.A., Bach, E.M., Sala, O.E. and Wall, D.H. 2019. Drought suppresses soil predators and promotes root herbivores in mesic, but not in xeric grasslands. *Proc Natl Acad Sci U S A*. **116**(26), pp.12883-12888.
- Friedman, J.R. and Voeltz, G.K. 2011. The ER in 3D: a multifunctional dynamic membrane network. *Trends Cell Biol*. **21**(12), pp.709-717.
- Fudali, S. and Golinowski, W. 2007. The reorganization of root anatomy and ultrastructure of syncytial cells in tomato [*Lycopersicon esculentum* Mill.] infected with potato cyst nematode [*Globodera rostochiensis* Woll.]. *Acta Societatis Botanicorum Poloniae*. **76**(3).
- Fujisaki, K., Abe, Y., Ito, A., Saitoh, H., Yoshida, K., Kanzaki, H., Kanzaki, E., Utsushi, H., Yamashita, T., Kamoun, S. and Terauchi, R. 2015. Rice Exo70 interacts with a fungal effector, AVR-Pii, and is required for AVR-Pii-triggered immunity. *Plant J*. **83**(5), pp.875-887.
- Fukao, Y. 2015. Discordance between protein and transcript levels detected by selected reaction monitoring. *Plant Signal Behav*. **10**(5), pe1017697.
- Galili, G. and Herman, E.M. 1997. Protein bodies: storage vacuoles in seeds. *Advances in Botanical Research*. **25**, pp.113-140.
- Gamir, J., Pastor, V., Sánchez-Bel, P., Agut, B., Mateu, D., García-Andrade, J. and Flors, V. 2018. Starch degradation, abscisic acid and vesicular trafficking are important elements in callose priming by indole-3-carboxylic acid in response to *Plectosphaerella cucumerina* infection. *The Plant Journal*. **96**(3), pp.518-531.

- Gardner, M., Dhroso, A., Johnson, N., Davis, E.L., Baum, T.J., Korkein, D. and Mitchum, M.G. 2018. Novel global effector mining from the transcriptome of early life stages of the soybean cyst nematode *Heterodera glycines*. *Sci Rep.* **8**(1), p2505.
- Gee, H.Y., Kim, J. and Lee, M.G. 2018. Unconventional secretion of transmembrane proteins. *Semin Cell Dev Biol.* **83**, pp.59-66.
- Geldner, N., Dénervaud-Tendon, V., Hyman, D.L., Mayer, U., Stierhof, Y.D. and Chory, J. 2009. Rapid, combinatorial analysis of membrane compartments in intact plants with a multicolor marker set. *Plant J.* **59**(1), pp.169-178.
- Gelvin, S.B. 2003. Agrobacterium-mediated plant transformation: the biology behind the "gene-jockeying" tool. *Microbiol Mol Biol Rev.* **67**(1), pp.16-37, table of contents.
- Gerdes, H.H. and Kaether, C. 1996. Green fluorescent protein: applications in cell biology. *FEBS Lett.* **389**(1), pp.44-47.
- Gershlick, D.C., de Marcos Lousa, C., Foresti, O., Lee, A.J., Pereira, E.A., daSilva, L.L., Bottanelli, F. and Denecke, J. 2014. Golgi-dependent transport of vacuolar sorting receptors is regulated by COPII, AP1, and AP4 protein complexes in tobacco. *Plant Cell.* **26**(3), pp.1308-1329.
- Ghini, R., Hamada, E., Pedro Júnior, M.J., Marengo, J.A. and Gonçalves, R.R.d.V. 2008. Risk analysis of climate change on coffee nematodes and leaf miner in Brazil. *Pesquisa Agropecuária brasileira.* **43**, pp.187-194.
- Giepmans, B.N. 2008. Bridging fluorescence microscopy and electron microscopy. *Histochem Cell Biol.* **130**(2), pp.211-217.
- Glick, B.S. and Luini, A. 2011. Models for Golgi traffic: a critical assessment. *Cold Spring Harb Perspect Biol.* **3**(11), pa005215.
- Glover, D.M. 1985. DNA cloning: a practical approach. Volume 1.
- Goddijn, O.J., Lindsey, K., van der Lee, F.M., Klap, J.C. and Sijmons, P.C. 1993. Differential gene expression in nematode-induced feeding structures of

transgenic plants harbouring promoter-gusA fusion constructs. *Plant J.* **4**(5), pp.863-873.

Godfray, H.C., Beddington, J.R., Crute, I.R., Haddad, L., Lawrence, D., Muir, J.F., Pretty, J., Robinson, S., Thomas, S.M. and Toulmin, C. 2010. Food security: the challenge of feeding 9 billion people. *Science.* **327**(5967), pp.812-818.

Goheen, C, S. and Donal, P. 2013. Nutritional Requirements of Soybean Cyst Nematodes. *InTech.*

Golinowski, W., Grundler, F.M.W. and Sobczak, M. 1996. Changes in the structure of *Arabidopsis thaliana* during female development of the plant-parasitic nematode *Heterodera schachtii*. *Protoplasma.* **194**, pp.103-116.

Gomord, V., Denmat, L.A., Fitchette-Lainé, A.C., Satiat-Jeunemaitre, B., Hawes, C. and Faye, L. 1997. The C-terminal HDEL sequence is sufficient for retention of secretory proteins in the endoplasmic reticulum (ER) but promotes vacuolar targeting of proteins that escape the ER. *Plant J.* **11**(2), pp.313-325.

González, E., Solano, R., Rubio, V., Leyva, A. and Paz-Ares, J. 2005. PHOSPHATE TRANSPORTER TRAFFIC FACILITATOR1 is a plant-specific SEC12-related protein that enables the endoplasmic reticulum exit of a high-affinity phosphate transporter in *Arabidopsis*. *Plant Cell.* **17**(12), pp.3500-3512.

Gotté, M., Bénard, M., Kiefer-Meyer, M.C., Jaber, R., Moore, J.P., Vicré-Gibouin, M. and Driouich, A. 2016. Endoplasmic Reticulum Body-Related Gene Expression in Different Root Zones of *Arabidopsis* Isolated by Laser-Assisted Microdissection. *Plant Genome.* **9**(2).

Goverse, A., Biesheuvel, J., Wijers, G.J., Gommers, F.J., Bakker, J., Schots, A. and Helder, J. 1998. In plant monitoring of the activity of two constitutive promoters, CaMV 35S and TR2', in developing feeding cells induced by *Globodera rostochiensis* using green fluorescent protein in combination

with confocal laser scanning microscopy. *Physiological and Molecular Plant Pathology*. **52**(4), pp.275-284.

Goverse, A., Overmars, H., Engelbertink, J., Schots, A., Bakker, J. and Helder, J. 2000. Both induction and morphogenesis of cyst nematode feeding cells are mediated by auxin. *Mol Plant Microbe Interact*. **13**(10), pp.1121-1129.

Goverse, A., Rouppe van der Voort, J., Roppe van der Voort, C., Kavelaars, A., Smant, G., Schots, A., Bakker, J. and Helder, J. 1999. Naturally induced secretions of the potato cyst nematode co-stimulate the proliferation of both tobacco leaf protoplasts and human peripheral blood mononuclear cells. *Mol Plant Microbe Interact*. **12**(10), pp.872-881.

Grebnev, G., Ntefidou, M. and Kost, B. 2017. Secretion and Endocytosis in Pollen Tubes: Models of Tip Growth in the Spot Light. *Front Plant Sci*. **8**, p154.

Grefen, C., Donald, N., Hashimoto, K., Kudla, J., Schumacher, K. and Blatt, M.R. 2010. A ubiquitin-10 promoter-based vector set for fluorescent protein tagging facilitates temporal stability and native protein distribution in transient and stable expression studies. *Plant J*. **64**(2), pp.355-365.

Grierson, C., Nielsen, E., Ketelaarc, T. and Schiefelbein, J. 2014. Root hairs. *Arabidopsis Book*. **12**, pe0172.

Grundler, F.M.W., Sobczak, M. and Golinowski, W. 1998. Formation of wall openings in root cells of *Arabidopsis thaliana* following infection by the plant-parasitic nematode *Heterodera schachtii*. *European Journal of Plant Pathology*. **104**, pp.545-551.

Grunwald, D.J., Zapotocny, R.W., Ozer, S., Diers, B.W. and Bent, A.F. 2022. Detection of rare nematode resistance Rhg1 haplotypes in *Glycine soja* and a novel Rhg1 α -SNAP. *Plant Genome*. **15**(1), pe20152.

Gu, Y., Zavaliev, R. and Dong, X. 2017. Membrane Trafficking in Plant Immunity. *Mol Plant*. **10**(8), pp.1026-1034.

Gunning, B.E.S. 1998. The identity of mystery organelles in *Arabidopsis* plants expressing GFP. *Trends in Plant Science*. **3**(11), p417.

- Gunning, B.E.S. and Pate, J.S. 1969. "Transfer cells" plant cells with wall ingrowths, specialized in relation to short distance transport of solutes—their occurrence, structure, and development. *Protoplasma*. **68**, pp.107-133.
- Guo, W., Roth, D., Walch-Solimena, C. and Novick, P. 1999. The exocyst is an effector for Sec4p, targeting secretory vesicles to sites of exocytosis. *EMBO J*. **18**(4), pp.1071-1080.
- Guo, X., Wang, J., Gardner, M., Fukuda, H., Kondo, Y., Etchells, J.P., Wang, X. and Mitchum, M.G. 2017. Identification of cyst nematode B-type CLE peptides and modulation of the vascular stem cell pathway for feeding cell formation. *PLoS Pathog*. **13**(2), pe1006142.
- Gupta, R. and Deswal, R. 2012. Low temperature stress modulated secretome analysis and purification of antifreeze protein from *Hippophae rhamnoides*, a Himalayan wonder plant. *J Proteome Res*. **11**(5), pp.2684-2696.
- Gupta, S., Bhar, A., Chatterjee, M., Ghosh, A. and Das, S. 2017. Transcriptomic dissection reveals wide spread differential expression in chickpea during early time points of *Fusarium oxysporum* f. sp. *ciceri* Race 1 attack. *PLoS One*. **12**(5), pe0178164.
- Habash, S.S., Radakovic, Z.S., Vankova, R., Siddique, S., Dobrev, P., Gleason, C., Grundler, F.M.W. and Elashry, A. 2017a. *Heterodera schachtii* Tyrosinase-like protein - a novel nematode effector modulating plant hormone homeostasis. *Sci Rep*. **7**(1), p6874.
- Habash, S.S., Sobczak, M., Siddique, S., Voigt, B., Elashry, A. and Grundler, F.M.W. 2017b. Identification and characterization of a putative protein disulfide isomerase (HsPDI) as an alleged effector of *Heterodera schachtii*. *Scientific Reports*. **7**(1), pp.1-14.
- Hachez, C., Laloux, T., Reinhardt, H., Cavez, D., Degand, H., Grefen, C., De Rycke, R., Inzé, D., Blatt, M.R., Russinova, E. and Chaumont, F. 2014. *Arabidopsis* SNAREs SYP61 and SYP121 coordinate the trafficking of

plasma membrane aquaporin PIP2;7 to modulate the cell membrane water permeability. *Plant Cell*. **26**(7), pp.3132-3147.

Hadlington, J.L. and Denecke, J. 2000. Sorting of soluble proteins in the secretory pathway of plants. *Curr Opin Plant Biol*. **3**(6), pp.461-468.

Haegeman, A., Mantelin, S., Jones, J.T. and Gheysen, G. 2012. Functional roles of effectors of plant-parasitic nematodes. *Gene*. **492**(1), pp.19-31.

Hanton, S.L. and Brandizzi, F. 2006. Fluorescent proteins as markers in the plant secretory pathway. *Microsc Res Tech*. **69**(3), pp.152-159.

Hanton, S.L., Chatre, L., Matheson, L.A., Rossi, M., Held, M.A. and Brandizzi, F. 2008. Plant Sar1 isoforms with near-identical protein sequences exhibit different localisations and effects on secretion. *Plant Mol Biol*. **67**(3), pp.283-294.

Hanton, S.L., Chatre, L., Renna, L., Matheson, L.A. and Brandizzi, F. 2007. De novo formation of plant endoplasmic reticulum export sites is membrane cargo induced and signal mediated. *Plant Physiol*. **143**(4), pp.1640-1650.

Hara-Nishimura, I. and Hatsugai, N. 2011. The role of vacuole in plant cell death. *Cell Death Differ*. **18**(8), pp.1298-1304.

Hara-Nishimura, I., Shimada, T., Hatano, K., Takeuchi, Y. and Nishimura, M. 1998. Transport of storage proteins to protein storage vacuoles is mediated by large precursor-accumulating vesicles. *Plant Cell*. **10**(5), pp.825-836.

Hardham, A.R. 2007. Cell biology of plant-oomycete interactions. *Cell Microbiol*. **9**(1), pp.31-39.

Hatsugai, N., Kuroyanagi, M., Yamada, K., Meshi, T., Tsuda, S., Kondo, M., Nishimura, M. and Hara-Nishimura, I. 2004. A plant vacuolar protease, VPE, mediates virus-induced hypersensitive cell death. *Science*. **305**(5685), pp.855-858.

- Hatsugai, N., Nakatsuji, A., Unten, O., Ogasawara, K., Kondo, M., Nishimura, M., Shimada, T., Katagiri, F. and Hara-Nishimura, I. 2018. Involvement of Adapter Protein Complex 4 in Hypersensitive Cell Death Induced by Avirulent Bacteria. *Plant Physiol.* **176**(2), pp.1824-1834.
- Hatsugai, N., Yamada, K., Goto-Yamada, S. and Hara-Nishimura, I. 2015. Vacuolar processing enzyme in plant programmed cell death. *Front Plant Sci.* **6**, p234.
- Häweker, H., Rips, S., Koiwa, H., Salomon, S., Saijo, Y., Chinchilla, D., Robatzek, S. and von Schaewen, A. 2010. Pattern recognition receptors require N-glycosylation to mediate plant immunity. *J Biol Chem.* **285**(7), pp.4629-4636.
- Hawes, C. and Satiat-Jeunemaitre, B. 2005. The plant Golgi apparatus--going with the flow. *Biochim Biophys Acta.* **1744**(3), pp.466-480.
- Hawes, C., Kiviniemi, P. and Kriechbaumer, V. 2015. The endoplasmic reticulum: a dynamic and well-connected organelle. *J Integr Plant Biol.* **57**(1), pp.50-62.
- Hayashi, Y., Yamada, K., Shimada, T., Matsushima, R., Nishizawa, N.K., Nishimura, M. and Hara-Nishimura, I. 2001. A proteinase-storing body that prepares for cell death or stresses in the epidermal cells of Arabidopsis. *Plant Cell Physiol.* **42**(9), pp.894-899.
- Haydock, P.P.J. and Evans, K. 1998. Management of potato cyst nematodes in the UK: an integrated approach? *Outlook on Agriculture.* **27**(4), pp.253-260.
- Hinz, G., Hillmer, S., Baumer, M. and Hohl, I. 1999. Vacuolar storage proteins and the putative vacuolar sorting receptor BP-80 exit the golgi apparatus of developing pea cotyledons in different transport vesicles. *Plant Cell.* **11**(8), pp.1509-1524.
- Hodda, M. 2022. Phylum Nematoda: a classification, catalogue and index of valid genera, with a census of valid species. *Zootaxa.* **5114**(1), pp.1-289.

- Hodda, M., Peters, L. and Traunspurger, W. 2009. Nematode diversity in terrestrial, freshwater aquatic and marine systems. *Nematodes as environmental indicators*. CABI Wallingford UK, pp.45-93.
- Hofmann, J. and Grundler, F.M. 2006. Females and males of root-parasitic cyst nematodes induce different symplasmic connections between their syncytial feeding cells and the phloem in *Arabidopsis thaliana*. *Plant Physiol Biochem.* **44**(5-6), pp.430-433.
- Holtmann, B., Kleine, M. and Grundler, F.M.W. 2000. Ultrastructure and anatomy of nematode-induced syncytia in roots of susceptible and resistant sugar beet. *Protoplasma.* **211**, pp.39-50.
- Horton, P. and Nakai, K. 1997. Better prediction of protein cellular localization sites with the k nearest neighbors classifier. *Proc Int Conf Intell Syst Mol Biol.* **5**, pp.147-152.
- Horton, P., Park, K.J., Obayashi, T., Fujita, N., Harada, H., Adams-Collier, C.J. and Nakai, K. 2007. WoLF PSORT: protein localization predictor. *Nucleic Acids Res.* **35**(Web Server issue), pp.W585-587.
- Hoth, S., Stadler, R., Sauer, N. and Hammes, U.Z. 2008. Differential vascularization of nematode-induced feeding sites. *Proc Natl Acad Sci U S A.* **105**(34), pp.12617-12622.
- Hou, H., Fang, J., Liang, J., Diao, Z., Wang, W., Yang, D., Li, S. and Tang, D. 2020. OsExo70B1 Positively Regulates Disease Resistance to *Magnaporthe oryzae* in Rice. *Int J Mol Sci.* **21**(19).
- Howe, K.L., Bolt, B.J., Shafie, M., Kersey, P. and Berriman, M. 2017. WormBase ParaSite - a comprehensive resource for helminth genomics. *Mol Biochem Parasitol.* **215**, pp.2-10.
- Howell, S.H. 2021. Evolution of the unfolded protein response in plants. *Plant Cell Environ.* **44**(8), pp.2625-2635.
- Hu, X.L., Lu, H., Hassan, M.M., Zhang, J., Yuan, G., Abraham, P.E., Shrestha, H.K., Villalobos Solis, M.I., Chen, J.G., Tschaplinski, T.J., Doktycz, M.J.,

- Tuskan, G.A., Cheng, Z.M. and Yang, X. 2021. Advances and perspectives in discovery and functional analysis of small secreted proteins in plants. *Hortic Res.* **8**(1), p130.
- Huang, G., Gao, B., Maier, T., Allen, R., Davis, E.L., Baum, T.J. and Hussey, R.S. 2003. A profile of putative parasitism genes expressed in the esophageal gland cells of the root-knot nematode *Meloidogyne incognita*. *Mol Plant Microbe Interact.* **16**(5), pp.376-381.
- Huang, J., Gu, L., Zhang, Y., Yan, T., Kong, G., Kong, L., Guo, B., Qiu, M., Wang, Y., Jing, M., Xing, W., Ye, W., Wu, Z., Zhang, Z., Zheng, X., Gijzen, M. and Dong, S. 2017. An oomycete plant pathogen reprograms host pre-mRNA splicing to subvert immunity. *Nat Commun.* **8**(1), p2051.
- Hussey, R.S. and Grundler, F.M.W. 1998. Nematode parasitism of plants. *The physiology and biochemistry of free-living and plant-parasitic nematodes.*, pp.213-243.
- Hussey, R.S. and Mims, C.W. 1990. Ultrastructure of esophageal glands and their secretory granules in the root-knot nematode *Meloidogyne incognita*. *Protoplasma.* **156**, pp.9-18.
- Hwang, H.H., Yu, M. and Lai, E.M. 2017. Agrobacterium-mediated plant transformation: biology and applications. *Arabidopsis Book.* **15**, pe0186.
- Hyodo, K., Kaido, M. and Okuno, T. 2014. Traffic jam on the cellular secretory pathway generated by a replication protein from a plant RNA virus. *Plant Signal Behav.* **9**(3), pe28644.
- Hyodo, K., Mine, A., Taniguchi, T., Kaido, M., Mise, K., Taniguchi, H. and Okuno, T. 2013. ADP ribosylation factor 1 plays an essential role in the replication of a plant RNA virus. *J Virol.* **87**(1), pp.163-176.
- Ichino, T., Maeda, K., Hara-Nishimura, I. and Shimada, T. 2020. Arabidopsis ECHIDNA protein is involved in seed coloration, protein trafficking to vacuoles, and vacuolar biogenesis. *J Exp Bot.* **71**(14), pp.3999-4009.

- Inaba, J., Kim, B.M., Shimura, H. and Masuta, C. 2011. Virus-induced necrosis is a consequence of direct protein-protein interaction between a viral RNA-silencing suppressor and a host catalase. *Plant Physiol.* **156**(4), pp.2026-2036.
- Ito, J. and Fukuda, H. 2002. ZEN1 is a key enzyme in the degradation of nuclear DNA during programmed cell death of tracheary elements. *Plant Cell.* **14**(12), pp.3201-3211.
- Ivanov, S. and Harrison, M.J. 2014. A set of fluorescent protein-based markers expressed from constitutive and arbuscular mycorrhiza-inducible promoters to label organelles, membranes and cytoskeletal elements in *Medicago truncatula*. *Plant J.* **80**(6), pp.1151-1163.
- Ivanov, S., Fedorova, E. and Bisseling, T. 2010. Intracellular plant microbe associations: secretory pathways and the formation of perimicrobial compartments. *Curr Opin Plant Biol.* **13**(4), pp.372-377.
- Jacquemyn, J., Cascalho, A. and Goodchild, R.E. 2017. The ins and outs of endoplasmic reticulum-controlled lipid biosynthesis. *EMBO Rep.* **18**(11), pp.1905-1921.
- Jafree, D.J., Long, D.A., Scambler, P.J. and Moulding, D. 2020. Tissue Clearing and Deep Imaging of the Kidney Using Confocal and Two-Photon Microscopy. *Methods Mol Biol.* **2067**, pp.103-126.
- Jaouannet, M. and Rosso, M.N. 2013. Effectors of root sedentary nematodes target diverse plant cell compartments to manipulate plant functions and promote infection. *Plant Signal Behav.* **8**(9).
- Jasmer, D.P., Goverse, A. and Smant, G. 2003. Parasitic nematode interactions with mammals and plants. *Annu Rev Phytopathol.* **41**, pp.245-270.
- Jauh, G.Y., Fischer, A.M., Grimes, H.D., Ryan, C.A. and Rogers, J.C. 1998. delta-Tonoplast intrinsic protein defines unique plant vacuole functions. *Proc Natl Acad Sci U S A.* **95**(22), pp.12995-12999.

- Jauh, G.Y., Phillips, T.E. and Rogers, J.C. 1999. Tonoplast intrinsic protein isoforms as markers for vacuolar functions. *Plant Cell*. **11**(10), pp.1867-1882.
- Jelly, N.S., Valat, L., Walter, B. and Maillot, P. 2014. Transient expression assays in grapevine: a step towards genetic improvement. *Plant Biotechnol J*. **12**(9), pp.1231-1245.
- Jiang, L., Phillips, T.E., Rogers, S.W. and Rogers, J.C. 2000. Biogenesis of the protein storage vacuole crystalloid. *J Cell Biol*. **150**(4), pp.755-770.
- Jiang, Y., Wang, D., Yao, Y., Eubel, H., Künzler, P., Møller, I.M. and Xu, D. 2021. MULocDeep: A deep-learning framework for protein subcellular and suborganellar localization prediction with residue-level interpretation. *Comput Struct Biotechnol J*. **19**, pp.4825-4839.
- Jin, H., Yan, Z., Nam, K.H. and Li, J. 2007. Allele-specific suppression of a defective brassinosteroid receptor reveals a physiological role of UGGT in ER quality control. *Mol Cell*. **26**(6), pp.821-830.
- Jing, M. and Wang, Y. 2020. Plant pathogens utilize effectors to hijack the host endoplasmic reticulum as part of their infection strategy. *Engineering*. **6**(5), pp.500-504.
- Jing, M., Guo, B., Li, H., Yang, B., Wang, H., Kong, G., Zhao, Y., Xu, H., Wang, Y., Ye, W., Dong, S., Qiao, Y., Tyler, B.M. and Ma, W. 2016. A *Phytophthora sojae* effector suppresses endoplasmic reticulum stress-mediated immunity by stabilizing plant Binding immunoglobulin Proteins. *Nat Commun*. **7**, p11685.
- Johannes, L. and Popoff, V. 2008. Tracing the retrograde route in protein trafficking. *Cell*. **135**(7), pp.1175-1187.
- Johansson, I., Karlsson, M., Johanson, U., Larsson, C. and Kjellbom, P. 2000. The role of aquaporins in cellular and whole plant water balance. *Biochim Biophys Acta*. **1465**(1-2), pp.324-342.

- Johansson, O.N., Fantozzi, E., Fahlberg, P., Nilsson, A.K., Buhot, N., Tör, M. and Andersson, M.X. 2014. Role of the penetration-resistance genes PEN1, PEN2 and PEN3 in the hypersensitive response and race-specific resistance in *Arabidopsis thaliana*. *Plant J.* **79**(3), pp.466-476.
- Jones, J.T., Curtis, R.H., Wightman, P.J. and Burrows, P.R. 1996. Isolation and characterization of a putative collagen gene from the potato cyst nematode *Globodera pallida*. *Parasitology.* **113** (Pt 6), pp.581-588.
- Jones, J.T., Haegeman, A., Danchin, E.G., Gaur, H.S., Helder, J., Jones, M.G., Kikuchi, T., Manzanilla-López, R., Palomares-Rius, J.E., Wesemael, W.M. and Perry, R.N. 2013. Top 10 plant-parasitic nematodes in molecular plant pathology. *Mol Plant Pathol.* **14**(9), pp.946-961.
- Jones, J.T., Kumar, A., Pylypenko, L.A., Thirugnanasambandam, A., Castelli, L., Chapman, S., Cock, P.J., Grenier, E., Lilley, C.J., Phillips, M.S. and Blok, V.C. 2009. Identification and functional characterization of effectors in expressed sequence tags from various life cycle stages of the potato cyst nematode *Globodera pallida*. *Mol Plant Pathol.* **10**(6), pp.815-828.
- Jones, J.T., Reavy, B., Smant, G. and Prior, A.E. 2004. Glutathione peroxidases of the potato cyst nematode *Globodera Rostochiensis*. *Gene.* **324**, pp.47-54.
- Jones, M.G. and Northcote, D.H. 1972. Nematode-induced syncytium--a multinucleate transfer cell. *J Cell Sci.* **10**(3), pp.789-809.
- Jones, M.G. and Payne, H.L. 1978. Early stages of nematode-induced giant-cell formation in roots of *Impatiens balsamina*. *J Nematol.* **10**(1), pp.70-84.
- Jones, M.G.K. and Dropkin, V.H. 1975. Scanning electron microscopy of syncytial transfer cells induced in roots by cyst-nematodes. *Physiological Plant Pathology.* **7**(3), pp.259-263.
- Joshi, I., Kohli, D., Pal, A., Chaudhury, A., Sirohi, A. and Jain, P.K. 2022. Host delivered-RNAi of effector genes for imparting resistance against root-knot

and cyst nematodes in plants. *Physiological and Molecular Plant Pathology*. p101802.

Juergensen, K., Scholz-Starke, J., Sauer, N., Hess, P., van Bel, A.J. and Grundler, F.M. 2003. The companion cell-specific Arabidopsis disaccharide carrier AtSUC2 is expressed in nematode-induced syncytia. *Plant Physiol.* **131**(1), pp.61-69.

Kalde, M., Nühse, T.S., Findlay, K. and Peck, S.C. 2007. The syntaxin SYP132 contributes to plant resistance against bacteria and secretion of pathogenesis-related protein 1. *Proc Natl Acad Sci U S A.* **104**(28), pp.11850-11855.

Kandath, P.K., Ithal, N., Recknor, J., Maier, T., Nettleton, D., Baum, T.J. and Mitchum, M.G. 2011. The Soybean Rhg1 locus for resistance to the soybean cyst nematode *Heterodera glycines* regulates the expression of a large number of stress- and defense-related genes in degenerating feeding cells. *Plant Physiol.* **155**(4), pp.1960-1975.

Kang, B.H., Nielsen, E., Preuss, M.L., Mastrorarde, D. and Staehelin, L.A. 2011. Electron tomography of RabA4b- and PI-4K β 1-labeled trans Golgi network compartments in Arabidopsis. *Traffic.* **12**(3), pp.313-329.

Kang, B.S., Baek, J.H., Macoy, D.M., Chakraborty, R., Cha, J.-Y., Hwang, D.-J., Lee, Y.H., Lee, S.Y., Kim, W.-Y. and Kim, M.G. 2015. N-glycosylation process in both ER and Golgi plays pivotal role in plant immunity. *Journal of plant biology.* **58**, pp.374-382.

Karimi, M., Inzé, D. and Depicker, A. 2002. GATEWAY vectors for Agrobacterium-mediated plant transformation. *Trends Plant Sci.* **7**(5), pp.193-195.

Karnik, R., Zhang, B., Waghmare, S., Aderhold, C., Grefen, C. and Blatt, M.R. 2015. Binding of SEC11 indicates its role in SNARE recycling after vesicle fusion and identifies two pathways for vesicular traffic to the plasma membrane. *Plant Cell.* **27**(3), pp.675-694.

- Khoei, M.A., Karimi, M., Karamian, R., Amini, S. and Soorni, A. 2021. Identification of the Complex Interplay Between Nematode-Related lncRNAs and Their Target Genes in. *Front Plant Sci.* **12**, p779597.
- Kim, J.G., Taylor, K.W., Hotson, A., Keegan, M., Schmelz, E.A. and Mudgett, M.B. 2008. XopD SUMO protease affects host transcription, promotes pathogen growth, and delays symptom development in xanthomonas-infected tomato leaves. *Plant Cell.* **20**(7), pp.1915-1929.
- Kim, J.S., Yamaguchi-Shinozaki, K. and Shinozaki, K. 2018. ER-Anchored Transcription Factors bZIP17 and bZIP28 Regulate Root Elongation. *Plant Physiol.* **176**(3), pp.2221-2230.
- Kim, S.J. and Brandizzi, F. 2012. News and Views into the SNARE Complexity in Arabidopsis. *Front Plant Sci.* **3**, p28.
- Kim, S.J. and Brandizzi, F. 2014. The plant secretory pathway: an essential factory for building the plant cell wall. *Plant Cell Physiol.* **55**(4), pp.687-693.
- Kim, S.J., Held, M.A., Zemelis, S., Wilkerson, C. and Brandizzi, F. 2015. CGR2 and CGR3 have critical overlapping roles in pectin methylesterification and plant growth in Arabidopsis thaliana. *Plant J.* **82**(2), pp.208-220.
- Kim, Y.H., Kim, K.S. and Riggs, R.D. 2010. Differential subcellular responses in resistance soybeans infected with soybean cyst nematode races. *The Plant Pathology Journal.* **26**(2), pp.154-158.
- Kim, Y.H., Kim, K.S. and Riggs, R.D. 2012. Initial subcellular responses of susceptible and resistant soybeans infected with the soybean cyst nematode. *The Plant Pathology Journal.* **28**(4), pp.401-408.
- Kim, Y.H., Riggs, R.D. and Kim, K.S. 1987. Structural Changes Associated with Resistance of Soybean to *Heterodera glycines*. *J Nematol.* **19**(2), pp.177-187.
- Kiselev, K.V., Aleynova, O.A., Ogneva, Z.V., Suprun, A.R. and Dubrovina, A.S. 2021. 35S promoter-driven transgenes are variably expressed in different

organs of *Arabidopsis thaliana* and in response to abiotic stress. *Mol Biol Rep.* **48**(3), pp.2235-2241.

Klink, V.P., Darwish, O., Alkharouf, N.W., Lawaju, B.R., Khatri, R. and Lawrence, K.S. 2021. Conserved oligomeric Golgi (COG) complex genes functioning in defense are expressed in root cells undergoing a defense response to a pathogenic infection and exhibit regulation by MAPKs. *PLoS One.* **16**(8), pe0256472.

Klink, V.P., Hosseini, P., MacDonald, M.H., Alkharouf, N.W. and Matthews, B.F. 2009. Population-specific gene expression in the plant pathogenic nematode *Heterodera glycines* exists prior to infection and during the onset of a resistant or susceptible reaction in the roots of the *Glycine max* genotype Peking. *BMC Genomics.* **10**, p111.

Klink, V.P., Lawaju, B.R., Niraula, P.M., Sharma, K., McNeece, B.T., Pant, S.R., Troell, H.A., Acharya, S., Khatri, R. and Rose, A.H. 2022. The conserved oligomeric Golgi (COG) complex, a window into plant-pathogen interactions. *Journal of Plant Interactions.* **17**(1), pp.344-360.

Klink, V.P., Sharma, K., Pant, S.R., McNeece, B., Niraula, P. and Lawrence, G.W. 2017. Components of the SNARE-containing regulon are co-regulated in root cells undergoing defense. *Plant Signal Behav.* **12**(2), pe1274481.

Kofsky, J., Zhang, H. and Song, B.H. 2021. Novel resistance strategies to soybean cyst nematode (SCN) in wild soybean. *Sci Rep.* **11**(1), p7967.

Koga, D., Ushiki, T. and Watanabe, T. 2017. Novel scanning electron microscopy methods for analyzing the 3D structure of the Golgi apparatus. *Anat Sci Int.* **92**(1), pp.37-49.

Komis, G., Novák, D., Ovečka, M., Šamajová, O. and Šamaj, J. 2018. Advances in Imaging Plant Cell Dynamics. *Plant Physiol.* **176**(1), pp.80-93.

Kong, L., Qiu, X., Kang, J., Wang, Y., Chen, H., Huang, J., Qiu, M., Zhao, Y., Kong, G., Ma, Z., Ye, W., Dong, S. and Ma, W. 2017. A *Phytophthora*

Effector Manipulates Host Histone Acetylation and Reprograms Defense Gene Expression to Promote Infection. *Curr Biol.* **27**(7), pp.981-991.

Kong, L.A., Wu, D.Q., Huang, W.K., Peng, H., Wang, G.F., Cui, J.K., Liu, S.M., Li, Z.G., Yang, J. and Peng, D.L. 2015. Large-scale identification of wheat genes resistant to cereal cyst nematode *Heterodera avenae* using comparative transcriptomic analysis. *BMC Genomics.* **16**, p801.

Kørner, C.J., Du, X., Vollmer, M.E. and Pajeroska-Mukhtar, K.M. 2015. Endoplasmic Reticulum Stress Signaling in Plant Immunity--At the Crossroad of Life and Death. *Int J Mol Sci.* **16**(11), pp.26582-26598.

Krogh, A., Larsson, B., von Heijne, G. and Sonnhammer, E.L. 2001. Predicting transmembrane protein topology with a hidden Markov model: application to complete genomes. *J Mol Biol.* **305**(3), pp.567-580.

Kud, J., Solo, N., Caplan, A., Kuhl, J.C., Dandurand, L.M. and Xiao, F. 2019. Hybridization of Plant-parasitic Nematode. *Bio Protoc.* **9**(18), pe3372.

Kumar, D., Rampuria, S., Singh, N.K., Shukla, P. and Kirti, P.B. 2015. Characterization of a vacuolar processing enzyme expressed in *Arachis diogeni* in resistance responses against late leaf spot pathogen, *Phaeoisariopsis personata*. *Plant Mol Biol.* **88**(1-2), pp.177-191.

Kunze, I., Hillmer, S., Kunze, G. and Müntz, K. 1995. Brefeldin A differentially affects protein secretion from suspension-cultured tobacco cells (*Nicotiana tabacum* L.). *Journal of plant physiology.* **146**(1-2), pp.71-80.

Kuroyanagi, M., Yamada, K., Hatsugai, N., Kondo, M., Nishimura, M. and Hara-Nishimura, I. 2005. Vacuolar processing enzyme is essential for mycotoxin-induced cell death in *Arabidopsis thaliana*. *J Biol Chem.* **280**(38), pp.32914-32920.

Kutay, U., Hartmann, E. and Rapoport, T.A. 1993. A class of membrane proteins with a C-terminal anchor. *Trends Cell Biol.* **3**(3), pp.72-75.

Kwon, C., Bednarek, P. and Schulze-Lefert, P. 2008a. Secretory pathways in plant immune responses. *Plant Physiol.* **147**(4), pp.1575-1583.

- Kwon, C., Lee, J.H. and Yun, H.S. 2020. SNAREs in Plant Biotic and Abiotic Stress Responses. *Mol Cells*. **43**(6), pp.501-508.
- Kwon, C., Neu, C., Pajonk, S., Yun, H.S., Lipka, U., Humphry, M., Bau, S., Straus, M., Kwaaitaal, M., Rampelt, H., El Kasmi, F., Jürgens, G., Parker, J., Panstruga, R., Lipka, V. and Schulze-Lefert, P. 2008b. Co-option of a default secretory pathway for plant immune responses. *Nature*. **451**(7180), pp.835-840.
- Kwon, S., Rupp, O., Brachmann, A., Blum, C.F., Kraege, A., Goesmann, A. and Feldbrügge, M. 2021. mRNA Inventory of Extracellular Vesicles from *Ustilago maydis*. *J Fungi (Basel)*. **7**(7).
- Kyndt, T., Vieira, P., Gheysen, G. and de Almeida-Engler, J. 2013. Nematode feeding sites: unique organs in plant roots. *Planta*. **238**(5), pp.807-818.
- Lam, S.K., Tse, Y.C., Robinson, D.G. and Jiang, L. 2007. Tracking down the elusive early endosome. *Trends Plant Sci*. **12**(11), pp.497-505.
- LaMontagne, E.D. and Heese, A. 2017. Trans-Golgi network/early endosome: a central sorting station for cargo proteins in plant immunity. *Curr Opin Plant Biol*. **40**, pp.114-121.
- Lampl, N., Alkan, N., Davydov, O. and Fluhr, R. 2013. Set-point control of RD21 protease activity by AtSerpin1 controls cell death in Arabidopsis. *Plant J*. **74**(3), pp.498-510.
- Langhans, M., Marcote, M.J., Pimpl, P., Virgili-López, G., Robinson, D.G. and Aniento, F. 2008. In vivo trafficking and localization of p24 proteins in plant cells. *Traffic*. **9**(5), pp.770-785.
- Lawaju, B.R., Niraula, P., Lawrence, G.W., Lawrence, K.S. and Klink, V.P. 2020. The. *Front Plant Sci*. **11**, p564495.
- Leborgne-Castel, N., Adam, T. and Bouhidel, K. 2010. Endocytosis in plant-microbe interactions. *Protoplasma*. **247**(3-4), pp.177-193.

- Lecourieux, D., Ranjeva, R. and Pugin, A. 2006. Calcium in plant defence-signalling pathways. *New Phytol.* **171**(2), pp.249-269.
- Lécrivain, A.L. and Beckmann, B.M. 2020. Bacterial RNA in extracellular vesicles: A new regulator of host-pathogen interactions? *Biochim Biophys Acta Gene Regul Mech.* **1863**(7), p194519.
- Lee, C., Chronis, D., Kenning, C., Peret, B., Hewezi, T., Davis, E.L., Baum, T.J., Hussey, R., Bennett, M. and Mitchum, M.G. 2011. The novel cyst nematode effector protein 19C07 interacts with the Arabidopsis auxin influx transporter LAX3 to control feeding site development. *Plant Physiol.* **155**(2), pp.866-880.
- Lee, D.L. 2002. *The biology of nematodes*. CRC Press.
- Lee, G.J., Sohn, E.J., Lee, M.H. and Hwang, I. 2004. The Arabidopsis rab5 homologs rha1 and ara7 localize to the prevacuolar compartment. *Plant Cell Physiol.* **45**(9), pp.1211-1220.
- Lee, H.C., Carroll, A., Crossett, B., Connolly, A., Batarseh, A. and Djordjevic, M.A. 2020. Improving the Identification and Coverage of Plant Transmembrane Proteins in Medicago Using Bottom-Up Proteomics. *Front Plant Sci.* **11**, p595726.
- Leffel, S.M., Mabon, S.A. and Stewart, C.N. 1997. Applications of green fluorescent protein in plants. *Biotechniques.* **23**(5), pp.912-918.
- Levin, K.A., Tucker, M.R., Bird, D.M. and Mather, D.E. 2020. Infection by cyst nematodes induces rapid remodelling of developing xylem vessels in wheat roots. *Sci Rep.* **10**(1), p9025.
- Levin, K.A., Tucker, M.R., Strock, C.F., Lynch, J.P. and Mather, D.E. 2021. Three-dimensional imaging reveals that positions of cyst nematode feeding sites relative to xylem vessels differ between susceptible and resistant wheat. *Plant Cell Rep.* **40**(2), pp.393-403.
- Levine, T. and Loewen, C. 2006. Inter-organelle membrane contact sites: through a glass, darkly. *Curr Opin Cell Biol.* **18**(4), pp.371-378.

- Li, X., Bao, H., Wang, Z., Wang, M., Fan, B., Zhu, C. and Chen, Z. 2018. Biogenesis and Function of Multivesicular Bodies in Plant Immunity. *Front Plant Sci.* **9**, p979.
- Li, Y., Wang, K., Xie, H., Wang, Y.T., Wang, D.W., Xu, C.L., Huang, X. and Wang, D.S. 2015. A Nematode Calreticulin, Rs-CRT, Is a Key Effector in Reproduction and Pathogenicity of *Radopholus similis*. *PLoS One.* **10**(6), pe0129351.
- Lia, A., Gallo, A., Marti, L., Roversi, P. and Santino, A. 2018. EFR-Mediated Innate Immune Response in *Arabidopsis thaliana* is a Useful Tool for Identification of Novel ERQC Modulators. *Genes (Basel).* **10**(1).
- Liebrand, T.W., Smit, P., Abd-El-Haliem, A., de Jonge, R., Cordewener, J.H., America, A.H., Sklenar, J., Jones, A.M., Robatzek, S., Thomma, B.P., Tameling, W.I. and Joosten, M.H. 2012. Endoplasmic reticulum-quality control chaperones facilitate the biogenesis of Cf receptor-like proteins involved in pathogen resistance of tomato. *Plant Physiol.* **159**(4), pp.1819-1833.
- Lilley, C.J., Atkinson, H.J. and Urwin, P.E. 2005. Molecular aspects of cyst nematodes. *Mol Plant Pathol.* **6**(6), pp.577-588.
- Lilley, C.J., Maqbool, A., Wu, D., Yusup, H.B., Jones, L.M., Birch, P.R.J., Banfield, M.J., Urwin, P.E. and Eves-van den Akker, S. 2018. Effector gene birth in plant parasitic nematodes: Neofunctionalization of a housekeeping glutathione synthetase gene. *PLoS Genet.* **14**(4), pe1007310.
- Lin, B., Qing, X., Liao, J. and Zhuo, K. 2020. Role of Protein Glycosylation in Host-Pathogen Interaction. *Cells.* **9**(4).
- Lippincott-Schwartz, J., Yuan, L.C., Bonifacino, J.S. and Klausner, R.D. 1989. Rapid redistribution of Golgi proteins into the ER in cells treated with brefeldin A: evidence for membrane cycling from Golgi to ER. *Cell.* **56**(5), pp.801-813.

- Liu, C., Talbot, N.J. and Chen, X.L. 2021. Protein glycosylation during infection by plant pathogenic fungi. *New Phytol.* **230**(4), pp.1329-1335.
- Liu, J., Peng, H., Cui, J., Huang, W., Kong, L., Clarke, J.L., Jian, H., Wang, G.L. and Peng, D. 2016. Molecular Characterization of A Novel Effector Expansin-like Protein from *Heterodera avenae* that Induces Cell Death in *Nicotiana benthamiana*. *Sci Rep.* **6**, p35677.
- Liu, J., Peng, H., Su, W., Liu, M., Huang, W., Dai, L. and Peng, D. 2020. HaCRT1 of. *Front Plant Sci.* **11**, p583584.
- Liu, L., Xu, L., Jia, Q., Pan, R., Oelmüller, R., Zhang, W. and Wu, C. 2019. Arms race: diverse effector proteins with conserved motifs. *Plant Signal Behav.* **14**(2), p1557008.
- Liu, S., Kandoth, P.K., Lakhssassi, N., Kang, J., Colantonio, V., Heinz, R., Yeckel, G., Zhou, Z., Bekal, S., Dapprich, J., Rotter, B., Cianzio, S., Mitchum, M.G. and Meksem, K. 2017. The soybean GmSNAP18 gene underlies two types of resistance to soybean cyst nematode. *Nat Commun.* **8**, p14822.
- Liu, T., Song, T., Zhang, X., Yuan, H., Su, L., Li, W., Xu, J., Liu, S., Chen, L., Chen, T., Zhang, M., Gu, L., Zhang, B. and Dou, D. 2014. Unconventionally secreted effectors of two filamentous pathogens target plant salicylate biosynthesis. *Nat Commun.* **5**, p4686.
- Liu, W., Mazarei, M., Peng, Y., Fethe, M.H., Rudis, M.R., Lin, J., Millwood, R.J., Arelli, P.R. and Stewart, C.N. 2014. Computational discovery of soybean promoter cis-regulatory elements for the construction of soybean cyst nematode-inducible synthetic promoters. *Plant Biotechnol J.* **12**(8), pp.1015-1026.
- Liu, Y. and Li, J. 2013. A conserved basic residue cluster is essential for the protein quality control function of the *Arabidopsis* calreticulin 3. *Plant Signal Behav.* **8**(4), pe23864.
- Liu, Y., Burgos, J.S., Deng, Y., Srivastava, R., Howell, S.H. and Bassham, D.C. 2012. Degradation of the endoplasmic reticulum by autophagy during

endoplasmic reticulum stress in Arabidopsis. *Plant Cell*. **24**(11), pp.4635-4651.

Liu, Y., Lan, X., Song, S., Yin, L., Dry, I.B., Qu, J., Xiang, J. and Lu, J. 2018. Functional Analysis and Subcellular Localization of the Oomycete Pathogen. *Front Plant Sci*. **9**, p286.

Liu, Y.-k., Huang, W.-k., Long, H.-b., Huan, P., He, W.-t. and Peng, D.-l. 2014. Molecular characterization and functional analysis of a new acid phosphatase gene (Ha-acp1) from *Heterodera avenae*. *Journal of Integrative Agriculture*. **13**(6), pp.1303-1310.

Lu, C., Zainal, Z., Tucker, G.A. and Lycett, G.W. 2001. Developmental abnormalities and reduced fruit softening in tomato plants expressing an antisense Rab11 GTPase gene. *Plant Cell*. **13**(8), pp.1819-1833.

Luo, F., Fong, Y.H., Zeng, Y., Shen, J., Jiang, L. and Wong, K.B. 2014. How vacuolar sorting receptor proteins interact with their cargo proteins: crystal structures of apo and cargo-bound forms of the protease-associated domain from an Arabidopsis vacuolar sorting receptor. *Plant Cell*. **26**(9), pp.3693-3708.

Ma, S., Quist, T.M., Ulanov, A., Joly, R. and Bohnert, H.J. 2004. Loss of TIP1;1 aquaporin in Arabidopsis leads to cell and plant death. *Plant J*. **40**(6), pp.845-859.

Magnusson, C. and Golinowski, W. 1991. Ultrastructural relationships of the developing syncytium induced by *Heterodera schachtii* (Nematoda) in root tissues of rape. *Canadian journal of botany*. **69**(1), pp.44-52.

Manghwar, H. and Li, J. 2022. Endoplasmic Reticulum Stress and Unfolded Protein Response Signaling in Plants. *Int J Mol Sci*. **23**(2).

Marchant, R. and Robards, A.W. 1968. Membrane systems associated with the plasmalemma of plant cells. *Annals of Botany*. **32**(3), pp.457-471.

- Martinière, A. and Moreau, P. 2020. Complex roles of Rab5 and SNAREs in the secretory pathway and plant development: a never-ending story. *J Microsc.* **280**(2), pp.140-157.
- Martinoia, E., Maeshima, M. and Neuhaus, H.E. 2007. Vacuolar transporters and their essential role in plant metabolism. *J Exp Bot.* **58**(1), pp.83-102.
- Marty, F. 1999. Plant vacuoles. *Plant Cell.* **11**(4), pp.587-600.
- Marz, K.E., Lauer, J.M. and Hanson, P.I. 2003. Defining the SNARE complex binding surface of alpha-SNAP: implications for SNARE complex disassembly. *J Biol Chem.* **278**(29), pp.27000-27008.
- Mathur, J., Shaikh, A. and Mathur, N. 2018. Peroxisome Mitochondria Interrelations in Plants. *Subcell Biochem.* **89**, pp.417-433.
- Matsuoka, K. and Nakamura, K. 1991. Propeptide of a precursor to a plant vacuolar protein required for vacuolar targeting. *Proc Natl Acad Sci U S A.* **88**(3), pp.834-838.
- Matsushima, R., Hayashi, Y., Kondo, M., Shimada, T., Nishimura, M. and Hara-Nishimura, I. 2002. An endoplasmic reticulum-derived structure that is induced under stress conditions in Arabidopsis. *Plant Physiol.* **130**(4), pp.1807-1814.
- Matsushima, R., Hayashi, Y., Yamada, K., Shimada, T., Nishimura, M. and Hara-Nishimura, I. 2003. The ER body, a novel endoplasmic reticulum-derived structure in Arabidopsis. *Plant Cell Physiol.* **44**(7), pp.661-666.
- Matsye, P.D., Lawrence, G.W., Youssef, R.M., Kim, K.H., Lawrence, K.S., Matthews, B.F. and Klink, V.P. 2012. The expression of a naturally occurring, truncated allele of an α -SNAP gene suppresses plant parasitic nematode infection. *Plant Mol Biol.* **80**(2), pp.131-155.
- Matuszkiewicz, M., Sobczak, M., Cabrera, J., Escobar, C., Karpiński, S. and Filipecki, M. 2018. The Role of Programmed Cell Death Regulator. *Front Plant Sci.* **9**, p314.

- Mbengue, M., Bourdais, G., Gervasi, F., Beck, M., Zhou, J., Spallek, T., Bartels, S., Boller, T., Ueda, T., Kuhn, H. and Robatzek, S. 2016. Clathrin-dependent endocytosis is required for immunity mediated by pattern recognition receptor kinases. *Proc Natl Acad Sci U S A*. **113**(39), pp.11034-11039.
- McLellan, H., Boevink, P.C., Armstrong, M.R., Pritchard, L., Gomez, S., Morales, J., Whisson, S.C., Beynon, J.L. and Birch, P.R. 2013. An RxLR effector from *Phytophthora infestans* prevents re-localisation of two plant NAC transcription factors from the endoplasmic reticulum to the nucleus. *PLoS Pathog*. **9**(10), pe1003670.
- McMahon, H.T. and Boucrot, E. 2011. Molecular mechanism and physiological functions of clathrin-mediated endocytosis. *Nat Rev Mol Cell Biol*. **12**(8), pp.517-533.
- McNew, J.A., Parlati, F., Fukuda, R., Johnston, R.J., Paz, K., Paumet, F., Söllner, T.H. and Rothman, J.E. 2000. Compartmental specificity of cellular membrane fusion encoded in SNARE proteins. *Nature*. **407**(6801), pp.153-159.
- Mei, Y., Wright, K.M., Haegeman, A., Bauters, L., Diaz-Granados, A., Goverse, A., Gheysen, G., Jones, J.T. and Mantelin, S. 2018. The *Globodera pallida* SPRYSEC Effector Gp SPRY-414-2 That Suppresses Plant Defenses Targets a Regulatory Component of the Dynamic Microtubule Network. *Front Plant Sci*. **9**, p1019.
- Meisrimler, C.N., Pelgrom, A.J.E., Oud, B., Out, S. and Van den Ackerveken, G. 2019. Multiple downy mildew effectors target the stress-related NAC transcription factor LsNAC069 in lettuce. *Plant J*. **99**(6), pp.1098-1115.
- Mejias, J., Bazin, J., Truong, N.M., Chen, Y., Marteu, N., Bouteiller, N., Sawa, S., Crespi, M.D., Vaucheret, H., Abad, P., Favery, B. and Quentin, M. 2021. The root-knot nematode effector MiEFF18 interacts with the plant core spliceosomal protein SmD1 required for giant cell formation. *New Phytol*. **229**(6), pp.3408-3423.

- Melillo, M.T., Bleve-Zacheo, T. and Zacheo, G. 1990. Ultrastructural response of potato roots susceptible to cyst nematode *Globodera pallida* pathotype Pa3. *Revue Nematol.* **13**, pp.17-28.
- Meyer, D., Pajonk, S., Micali, C., O'Connell, R. and Schulze-Lefert, P. 2009. Extracellular transport and integration of plant secretory proteins into pathogen-induced cell wall compartments. *Plant J.* **57**(6), pp.986-999.
- Miao, Y., Li, K.Y., Li, H.Y., Yao, X. and Jiang, L. 2008. The vacuolar transport of aleurain-GFP and 2S albumin-GFP fusions is mediated by the same pre-vacuolar compartments in tobacco BY-2 and Arabidopsis suspension cultured cells. *Plant J.* **56**(5), pp.824-839.
- Micali, C.O., Neumann, U., Grunewald, D., Panstruga, R. and O'Connell, R. 2011. Biogenesis of a specialized plant-fungal interface during host cell internalization of *Golovinomyces orontii* haustoria. *Cell Microbiol.* **13**(2), pp.210-226.
- Michalak, M., Corbett, E.F., Mesaeli, N., Nakamura, K. and Opas, M. 1999. Calreticulin: one protein, one gene, many functions. *Biochem J.* **344 Pt 2**(Pt 2), pp.281-292.
- Miles, G.P., Samuel, M.A., Zhang, Y. and Ellis, B.E. 2005. RNA interference-based (RNAi) suppression of AtMPK6, an Arabidopsis mitogen-activated protein kinase, results in hypersensitivity to ozone and misregulation of AtMPK3. *Environ Pollut.* **138**(2), pp.230-237.
- Min, M.K., Kim, S.J., Miao, Y., Shin, J., Jiang, L. and Hwang, I. 2007. Overexpression of Arabidopsis AGD7 causes relocation of Golgi-localized proteins to the endoplasmic reticulum and inhibits protein trafficking in plant cells. *Plant Physiol.* **143**(4), pp.1601-1614.
- Miranda, K., Girard-Dias, W., Attias, M., de Souza, W. and Ramos, I. 2015. Three dimensional reconstruction by electron microscopy in the life sciences: An introduction for cell and tissue biologists. *Mol Reprod Dev.* **82**(7-8), pp.530-547.

- Misas-Villamil, J.C., Toenges, G., Kolodziejek, I., Sadaghiani, A.M., Kaschani, F., Colby, T., Bogyo, M. and van der Hoorn, R.A. 2013. Activity profiling of vacuolar processing enzymes reveals a role for VPE during oomycete infection. *Plant J.* **73**(4), pp.689-700.
- Mitchum, M.G., Hussey, R.S., Baum, T.J., Wang, X., Elling, A.A., Wubben, M. and Davis, E.L. 2013. Nematode effector proteins: an emerging paradigm of parasitism. *New Phytol.* **199**(4), pp.879-894.
- Moens, M. and Perry, R.N. 2009. Migratory plant endoparasitic nematodes: a group rich in contrasts and divergence. *Annu Rev Phytopathol.* **47**, pp.313-332.
- Moens, T., Braeckman, U., Derycke, S., Fonseca, G., Gallucci, F., Gingold, R., Guillini, K., Ingels, J., Leduc, D. and Vanaverbeke, J. 2013. Ecology of free-living marine nematodes. *Nematoda.* **2**, pp.109-152.
- Montesinos, J.C., Pastor-Cantizano, N., Robinson, D.G., Marcote, M.J. and Aniento, F. 2014. Arabidopsis p24 δ 5 and p24 δ 9 facilitate Coat Protein I-dependent transport of the K/HDEL receptor ERD2 from the Golgi to the endoplasmic reticulum. *Plant J.* **80**(6), pp.1014-1030.
- Montesinos, J.C., Sturm, S., Langhans, M., Hillmer, S., Marcote, M.J., Robinson, D.G. and Aniento, F. 2012. Coupled transport of Arabidopsis p24 proteins at the ER-Golgi interface. *J Exp Bot.* **63**(11), pp.4243-4261.
- Mor, M., Spiegel, Y. and Oka, Y. 2008. Histological study of syncytia induced in cereals by the Mediterranean cereal cyst nematode *Heterodera latipons*. *Nematology.* **10**(2), pp.279-287.
- Morel, J.B., Mourrain, P., Béclin, C. and Vaucheret, H. 2000. DNA methylation and chromatin structure affect transcriptional and post-transcriptional transgene silencing in Arabidopsis. *Curr Biol.* **10**(24), pp.1591-1594.
- Moreno, A.A., Mukhtar, M.S., Blanco, F., Boatwright, J.L., Moreno, I., Jordan, M.R., Chen, Y., Brandizzi, F., Dong, X., Orellana, A. and Pajeroska-Mukhtar, K.M. 2012. IRE1/bZIP60-mediated unfolded protein response

plays distinct roles in plant immunity and abiotic stress responses. *PLoS One*. **7**(2), pe31944.

Mosesso, N., Bläske, T., Nagel, M.K., Laumann, M. and Isono, E. 2018. Preparation of Clathrin-Coated Vesicles From. *Front Plant Sci*. **9**, p1972.

Mukhtar, M.S., Carvunis, A.R., Dreze, M., Epple, P., Steinbrenner, J., Moore, J., Tasan, M., Galli, M., Hao, T., Nishimura, M.T., Pevzner, S.J., Donovan, S.E., Ghamsari, L., Santhanam, B., Romero, V., Poulin, M.M., Gebreab, F., Gutierrez, B.J., Tam, S., Monachello, D., Boxem, M., Harbort, C.J., McDonald, N., Gai, L., Chen, H., He, Y., Vandenhoute, J., Roth, F.P., Hill, D.E., Ecker, J.R., Vidal, M., Beynon, J., Braun, P., Dangl, J.L. and Consortium, E.U.E. 2011. Independently evolved virulence effectors converge onto hubs in a plant immune system network. *Science*. **333**(6042), pp.596-601.

Muller, J. 1999. The economic importance of *Heterodera schachtii* in Europe. *Helminthologia*. **36**(3), pp.205-213.

Munch, D., Teh, O.K., Malinovsky, F.G., Liu, Q., Vetukuri, R.R., El Kasmi, F., Brodersen, P., Hara-Nishimura, I., Dangl, J.L., Petersen, M., Mundy, J. and Hofius, D. 2015. Retromer contributes to immunity-associated cell death in *Arabidopsis*. *Plant Cell*. **27**(2), pp.463-479.

Murota, K., Shimura, H., Takeshita, M. and Masuta, C. 2017. Interaction between Cucumber mosaic virus 2b protein and plant catalase induces a specific necrosis in association with proteasome activity. *Plant Cell Rep*. **36**(1), pp.37-47.

Musielak, T.J., Slane, D., Liebig, C. and Bayer, M. 2016. A Versatile Optical Clearing Protocol for Deep Tissue Imaging of Fluorescent Proteins in *Arabidopsis thaliana*. *PLoS One*. **11**(8), pe0161107.

Nagashima, Y., Mishiba, K., Suzuki, E., Shimada, Y., Iwata, Y. and Koizumi, N. 2011. *Arabidopsis* IRE1 catalyses unconventional splicing of bZIP60 mRNA to produce the active transcription factor. *Sci Rep*. **1**, p29.

- Nakai, W., Kondo, Y., Saitoh, A., Naito, T., Nakayama, K. and Shin, H.W. 2013. ARF1 and ARF4 regulate recycling endosomal morphology and retrograde transport from endosomes to the Golgi apparatus. *Mol Biol Cell*. **24**(16), pp.2570-2581.
- Nakano, R.T., Yamada, K., Bednarek, P., Nishimura, M. and Hara-Nishimura, I. 2014. ER bodies in plants of the Brassicales order: biogenesis and association with innate immunity. *Front Plant Sci*. **5**, p73.
- Napier, R.M., Fowke, L.C., Hawes, C., Lewis, M. and Pelham, H.R. 1992. Immunological evidence that plants use both HDEL and KDEL for targeting proteins to the endoplasmic reticulum. *J Cell Sci*. **102 (Pt 2)**, pp.261-271.
- Nebenführ, A. and Staehelin, L.A. 2001. Mobile factories: Golgi dynamics in plant cells. *Trends Plant Sci*. **6**(4), pp.160-167.
- Neher, D.A. 2010. Ecology of plant and free-living nematodes in natural and agricultural soil. *Annu Rev Phytopathol*. **48**, pp.371-394.
- Nelson, B.K., Cai, X. and Nebenführ, A. 2007. A multicolored set of in vivo organelle markers for co-localization studies in Arabidopsis and other plants. *Plant J*. **51**(6), pp.1126-1136.
- Nickel, W. 2010. Pathways of unconventional protein secretion. *Curr Opin Biotechnol*. **21**(5), pp.621-626.
- Nicol, J.M., Turner, S.J., Coyne, D.L., Nijs, L.d., Hockland, S. and Maafi, Z.T. 2011. Current nematode threats to world agriculture. *Genomics and molecular genetics of plant-nematode interactions*. pp.21-43.
- Nielsen, M.E., Feechan, A., Böhlenius, H., Ueda, T. and Thordal-Christensen, H. 2012. Arabidopsis ARF-GTP exchange factor, GNOM, mediates transport required for innate immunity and focal accumulation of syntaxin PEN1. *Proc Natl Acad Sci U S A*. **109**(28), pp.11443-11448.
- Niemes, S., Labs, M., Scheuring, D., Krueger, F., Langhans, M., Jesenofsky, B., Robinson, D.G. and Pimpl, P. 2010. Sorting of plant vacuolar proteins is initiated in the ER. *Plant J*. **62**(4), pp.601-614.

- Niraula, P.M., Sharma, K., McNeece, B.T., Troell, H.A., Darwish, O., Alkharouf, N.W., Lawrence, K.S. and Klink, V.P. 2020. Mitogen activated protein kinase (MAPK)-regulated genes with predicted signal peptides function in the Glycine max defense response to the root pathogenic nematode *Heterodera glycines*. *PLoS One*. **15**(11), pe0241678.
- Nishimura, M.T. and Dangl, J.L. 2010. Arabidopsis and the plant immune system. *Plant J*. **61**(6), pp.1053-1066.
- Nodzynski, T., Feraru, M.I., Hirsch, S., De Rycke, R., Niculaes, C., Boerjan, W., Van Leene, J., De Jaeger, G., Vanneste, S. and Friml, J. 2013. Retromer subunits VPS35A and VPS29 mediate prevacuolar compartment (PVC) function in Arabidopsis. *Mol Plant*. **6**(6), pp.1849-1862.
- Nomura, K., Debroy, S., Lee, Y.H., Pumplin, N., Jones, J. and He, S.Y. 2006. A bacterial virulence protein suppresses host innate immunity to cause plant disease. *Science*. **313**(5784), pp.220-223.
- Nvyss, U., Stender, C. and Lehmann, H. 1984. Ultrastructure of feeding sites of the cyst nematode *Heterodera schachtii* Schmidt in roots of susceptible and resistant *Raphanus sativus* L. var. *oleiformis* Pers. cultivars. *Physiological Plant Pathology*. **25**(1), pp.21-37.
- Oerke, E.C. 2006. Crop losses to pests. *The Journal of Agricultural Science*. **144**(1), pp.31-43.
- Ohtsu, M., Sato, Y., Kurihara, D., Suzaki, T., Kawaguchi, M., Maruyama, D. and Higashiyama, T. 2017. Spatiotemporal deep imaging of syncytium induced by the soybean cyst nematode *Heterodera glycines*. *Protoplasma*. **254**(6), pp.2107-2115.
- Oka, Y. 2020. From old-generation to next-generation nematicides. *Agronomy*. **10**(9), p1387.
- Oka, Y., Nacar, S., Putievsky, E., Ravid, U., Yaniv, Z. and Spiegel, Y. 2000. Nematicidal activity of essential oils and their components against the root-knot nematode. *Phytopathology*. **90**(7), pp.710-715.

- Osterrieder, A., Sparkes, I.A., Botchway, S.W., Ward, A., Ketelaar, T., de Ruijter, N. and Hawes, C. 2017. Stacks off tracks: a role for the golgin AtCASP in plant endoplasmic reticulum-Golgi apparatus tethering. *J Exp Bot.* **68**(13), pp.3339-3350.
- Ostertag, M., Stammler, J., Douchkov, D., Eichmann, R. and Hüchelhoven, R. 2013. The conserved oligomeric Golgi complex is involved in penetration resistance of barley to the barley powdery mildew fungus. *Mol Plant Pathol.* **14**(3), pp.230-240.
- Pain, C., Kriechbaumer, V., Kittelmann, M., Hawes, C. and Fricker, M. 2019. Quantitative analysis of plant ER architecture and dynamics. *Nat Commun.* **10**(1), p984.
- Pakdel, M. and von Blume, J. 2018. Exploring new routes for secretory protein export from the. *Mol Biol Cell.* **29**(3), pp.235-240.
- Palmer, E. and Freeman, T. 2004. Investigation into the use of C- and N-terminal GFP fusion proteins for subcellular localization studies using reverse transfection microarrays. *Comp Funct Genomics.* **5**(4), pp.342-353.
- Pant, S.R., Krishnavajhala, A., McNeece, B.T., Lawrence, G.W. and Klink, V.P. 2015. The syntaxin 31-induced gene, LESION SIMULATING DISEASE1 (LSD1), functions in Glycine max defense to the root parasite *Heterodera glycines*. *Plant Signal Behav.* **10**(1), pe977737.
- Pant, S.R., Matsye, P.D., McNeece, B.T., Sharma, K., Krishnavajhala, A., Lawrence, G.W. and Klink, V.P. 2014. Syntaxin 31 functions in Glycine max resistance to the plant parasitic nematode *Heterodera glycines*. *Plant Mol Biol.* **85**(1-2), pp.107-121.
- Paris, N., Rogers, S.W., Jiang, L., Kirsch, T., Beevers, L., Phillips, T.E. and Rogers, J.C. 1997. Molecular cloning and further characterization of a probable plant vacuolar sorting receptor. *Plant Physiol.* **115**(1), pp.29-39.

- Park, C.J. and Park, J.M. 2019. Endoplasmic Reticulum Plays a Critical Role in Integrating Signals Generated by Both Biotic and Abiotic Stress in Plants. *Front Plant Sci.* **10**, p399.
- Park, C.J., Bart, R., Chern, M., Canlas, P.E., Bai, W. and Ronald, P.C. 2010. Overexpression of the endoplasmic reticulum chaperone BiP3 regulates XA21-mediated innate immunity in rice. *PLoS One.* **5**(2), pe9262.
- Pasternak, T. and Pérez-Pérez, J.M. 2021. Methods of In Situ Quantitative Root Biology. *Plants (Basel).* **10**(11).
- Pecenková, T., Hála, M., Kulich, I., Kocourková, D., Drdová, E., Fendrych, M., Toupalová, H. and Zársky, V. 2011. The role for the exocyst complex subunits Exo70B2 and Exo70H1 in the plant-pathogen interaction. *J Exp Bot.* **62**(6), pp.2107-2116.
- Pedrazzini, E. 2009. Tail-anchored proteins in plants. *Journal of Plant Biology.* **52**, pp.88-101.
- Peter, F., Wong, S.H., Subramaniam, V.N., Tang, B.L. and Hong, W. 1998. Alpha-SNAP but not gamma-SNAP is required for ER-Golgi transport after vesicle budding and the Rab1-requiring step but before the EGTA-sensitive step. *J Cell Sci.* **111 (Pt 17)**, pp.2625-2633.
- Philippe, G., De Bellis, D., Rose, J.K.C. and Nawrath, C. 2021. Trafficking Processes and Secretion Pathways Underlying the Formation of Plant Cuticles. *Front Plant Sci.* **12**, p786874.
- Pinheiro, H., Samalova, M., Geldner, N., Chory, J., Martinez, A. and Moore, I. 2009. Genetic evidence that the higher plant Rab-D1 and Rab-D2 GTPases exhibit distinct but overlapping interactions in the early secretory pathway. *J Cell Sci.* **122**(Pt 20), pp.3749-3758.
- Pogorelko, G.V., Juvale, P.S., Rutter, W.B., Hütten, M., Maier, T.R., Hewezi, T., Paulus, J., van der Hoorn, R.A., Grundler, F.M., Siddique, S., Lionetti, V., Zabortina, O.A. and Baum, T.J. 2019. Re-targeting of a plant defense protease by a cyst nematode effector. *Plant J.* **98**(6), pp.1000-1014.

- Poulsen, C.P., Dilokpimol, A., Mouille, G., Burow, M. and Geshi, N. 2014. Arabinogalactan glycosyltransferases target to a unique subcellular compartment that may function in unconventional secretion in plants. *Traffic*. **15**(11), pp.1219-1234.
- Preuss, M.L., Serna, J., Falbel, T.G., Bednarek, S.Y. and Nielsen, E. 2004. The Arabidopsis Rab GTPase RabA4b localizes to the tips of growing root hair cells. *Plant Cell*. **16**(6), pp.1589-1603.
- Qiao, F., Kong, L.A., Peng, H., Huang, W.K., Wu, D.Q., Liu, S.M., Clarke, J.L., Qiu, D.W. and Peng, D.L. 2019. Transcriptional profiling of wheat (*Triticum aestivum* L.) during a compatible interaction with the cereal cyst nematode *Heterodera avenae*. *Sci Rep*. **9**(1), p2184.
- Qin, X., Xue, B., Tian, H., Fang, C., Yu, J., Chen, C., Xue, Q., Jones, J. and Wang, X. 2022. An unconventionally secreted effector from the root knot nematode *Meloidogyne incognita*, Mi-ISC-1, promotes parasitism by disrupting salicylic acid biosynthesis in host plants. *Mol Plant Pathol*. **23**(4), pp.516-529.
- Qiu, Y., Xi, J., Du, L., Roje, S. and Poovaiah, B.W. 2012. A dual regulatory role of Arabidopsis calreticulin-2 in plant innate immunity. *Plant J*. **69**(3), pp.489-500.
- Rabouille, C. 2017. Pathways of Unconventional Protein Secretion. *Trends Cell Biol*. **27**(3), pp.230-240.
- Rashidifard, M., Ashrafi, S., Claassens, S., Thünen, T. and Fourie, H. 2021. A Pilot Approach Investigating the Potential of Crop Rotation With Sainfoin to Reduce. *Front Plant Sci*. **12**, p659322.
- Raza, A., Charagh, S., Sadaqat, N. and Jin, W. 2020. Arabidopsis thaliana: Model plant for the study of abiotic stress responses. *The Plant Family Brassicaceae: Biology and Physiological Responses to Environmental Stresses*. pp.129-180.

- Read, A. and Schröder, M. 2021. The Unfolded Protein Response: An Overview. *Biology (Basel)*. **10**(5).
- Regon, P., Panda, P., Kshetrimayum, E. and Panda, S.K. 2014. Genome-wide comparative analysis of tonoplast intrinsic protein (TIP) genes in plants. *Funct Integr Genomics*. **14**(4), pp.617-629.
- Rehman, S., Postma, W., Tytgat, T., Prins, P., Qin, L., Overmars, H., Vossen, J., Spiridon, L.N., Petrescu, A.J., Goverse, A., Bakker, J. and Smant, G. 2009. A secreted SPRY domain-containing protein (SPRYSEC) from the plant-parasitic nematode *Globodera rostochiensis* interacts with a CC-NB-LRR protein from a susceptible tomato. *Mol Plant Microbe Interact*. **22**(3), pp.330-340.
- Reigoto, A.M., Andrade, S.A., Seixas, M.C.R.R., Costa, M.L. and Mermelstein, C. 2021. A comparative study on the use of microscopy in pharmacology and cell biology research. *PLoS One*. **16**(1), pe0245795.
- Ren, J., Wen, L., Gao, X., Jin, C., Xue, Y. and Yao, X. 2009. DOG 1.0: illustrator of protein domain structures. *Cell Res*. **19**(2), pp.271-273.
- Renna, L. and Brandizzi, F. 2020. The mysterious life of the plant trans-Golgi network: advances and tools to understand it better. *J Microsc*. **278**(3), pp.154-163.
- Reumann, S. and Bartel, B. 2016. Plant peroxisomes: recent discoveries in functional complexity, organelle homeostasis, and morphological dynamics. *Curr Opin Plant Biol*. **34**, pp.17-26.
- Reyes, F.C., Buono, R. and Otegui, M.S. 2011. Plant endosomal trafficking pathways. *Curr Opin Plant Biol*. **14**(6), pp.666-673.
- Rigden, D.J. 2008. The histidine phosphatase superfamily: structure and function. *Biochem J*. **409**(2), pp.333-348.
- Riggs, R.D., Kim, K.S. and Gipson, I. 1973. Ultrastructural changes in Peking soybeans infected with *Heterodera glycines*. *Phytopathology*. **63**(1), pp.76-84.

- Rivera, A.L., Gómez-Lim, M., Fernández, F. and Loske, A.M. 2012. Physical methods for genetic plant transformation. *Phys Life Rev.* **9**(3), pp.308-345.
- Rizzo, J., Rodrigues, M.L. and Janbon, G. 2020. Extracellular Vesicles in Fungi: Past, Present, and Future Perspectives. *Front Cell Infect Microbiol.* **10**, p346.
- Robatzek, S. 2007. Vesicle trafficking in plant immune responses. *Cell Microbiol.* **9**(1), pp.1-8.
- Robin, G.P., Kleemann, J., Neumann, U., Cabre, L., Dallery, J.F., Lapalu, N. and O'Connell, R.J. 2018. Subcellular Localization Screening of *Colletotrichum higginsianum* effector candidates identifies fungal proteins targeted to plant peroxisomes, golgi bodies, and microtubules. *Front Plant Sci.* **9**, p562.
- Robinson, D.G. 2020. Plant Golgi ultrastructure. *J Microsc.* **280**(2), pp.111-121.
- Robinson, D.G., Ding, Y. and Jiang, L. 2016. Unconventional protein secretion in plants: a critical assessment. *Protoplasma.* **253**(1), pp.31-43.
- Robinson, D.G., Scheuring, D., Naramoto, S. and Friml, J. 2011. ARF1 localizes to the golgi and the trans-golgi network. *Plant Cell.* **23**(3), pp.846-849; author reply 849-850.
- Rodiuc, N., Vieira, P., Banora, M.Y. and de Almeida Engler, J. 2014. On the track of transfer cell formation by specialized plant-parasitic nematodes. *Front Plant Sci.* **5**, p160.
- Rodriguez-Furlan, C., Domozych, D., Qian, W., Enquist, P.A., Li, X., Zhang, C., Schenk, R., Winbigler, H.S., Jackson, W., Raikhel, N.V. and Hicks, G.R. 2019. Interaction between VPS35 and RABG3f is necessary as a checkpoint to control fusion of late compartments with the vacuole. *Proc Natl Acad Sci U S A.* **116**(42), pp.21291-21301.
- Rogers, S.W., Burks, M. and Rogers, J.C. 1997. Monoclonal antibodies to barley aleurain and homologs from other plants. *Plant J.* **11**(6), pp.1359-1368.

- Rojo, E. and Denecke, J. 2008. What is moving in the secretory pathway of plants? *Plant Physiol.* **147**(4), pp.1493-1503.
- Rojo, E., Martín, R., Carter, C., Zouhar, J., Pan, S., Plotnikova, J., Jin, H., Paneque, M., Sánchez-Serrano, J.J., Baker, B., Ausubel, F.M. and Raikhel, N.V. 2004. VPEgamma exhibits a caspase-like activity that contributes to defense against pathogens. *Curr Biol.* **14**(21), pp.1897-1906.
- Rothman, J.E. 1981. The golgi apparatus: two organelles in tandem. *Science.* **213**(4513), pp.1212-1219.
- Ruano, G. and Scheuring, D. 2020. Plant Cells under Attack: Unconventional Endomembrane Trafficking during Plant Defense. *Plants (Basel).* **9**(3).
- Ruark-Seward, C.L., Davis, E.L. and Sit, T.L. 2019. Electroporation-based fluorescence. *MethodsX.* **6**, pp.2720-2728.
- Rufián, J.S., Elmore, J.M., Bejarano, E.R., Beuzon, C.R. and Coaker, G.L. 2021. ER Bodies Are Induced by. *Mol Plant Microbe Interact.* **34**(9), pp.1001-1009.
- Rui, Q., Tan, X., Liu, F., Li, Y., Liu, X., Li, B., Wang, J., Yang, H., Qiao, L., Li, T., Fang, S., Gao, R., Wang, W., Bednarek, S.Y. and Bao, Y. 2021. Syntaxin of plants31 (SYP31) and SYP32 is essential for Golgi morphology maintenance and pollen development. *Plant Physiol.* **186**(1), pp.330-343.
- Rui, Q., Wang, J., Li, Y., Tan, X. and Bao, Y. 2020. Arabidopsis COG6 is essential for pollen tube growth and Golgi structure maintenance. *Biochem Biophys Res Commun.* **528**(3), pp.447-452.
- Sacco, M.A., Koropacka, K., Grenier, E., Jaubert, M.J., Blanchard, A., Goverse, A., Smant, G. and Moffett, P. 2009. The cyst nematode SPRYSEC protein RBP-1 elicits Gpa2- and RanGAP2-dependent plant cell death. *PLoS Pathog.* **5**(8), pe1000564.

- Saito, K., Maeda, M. and Katada, T. 2017. Regulation of the Sar1 GTPase Cycle Is Necessary for Large Cargo Secretion from the Endoplasmic Reticulum. *Front Cell Dev Biol.* **5**, p75.
- Saito, K., Yamazaki, M., Kaneko, H., Murakoshi, I., Fukuda, Y. and Van Montagu, M. 1991. Tissue-specific and stress-enhancing expression of the TR promoter for mannopine synthase in transgenic medicinal plants. *Planta.* **184**(1), pp.40-46.
- Samaj, J., Müller, J., Beck, M., Böhm, N. and Menzel, D. 2006. Vesicular trafficking, cytoskeleton and signalling in root hairs and pollen tubes. *Trends Plant Sci.* **11**(12), pp.594-600.
- Sampaio, M., Neves, J., Cardoso, T., Pissarra, J., Pereira, S. and Pereira, C. 2022. Coping with Abiotic Stress in Plants-An Endomembrane Trafficking Perspective. *Plants (Basel).* **11**(3).
- Sánchez-Simarro, J., Bernat-Silvestre, C., Gimeno-Ferrer, F., Selvi-Martínez, P., Montero-Pau, J., Aniento, F. and Marcote, M.J. 2020. Loss of. *Front Plant Sci.* **11**, p430.
- Sanderfoot, A.A., Ahmed, S.U., Marty-Mazars, D., Rapoport, I., Kirchhausen, T., Marty, F. and Raikhel, N.V. 1998. A putative vacuolar cargo receptor partially colocalizes with AtPEP12p on a prevacuolar compartment in Arabidopsis roots. *Proc Natl Acad Sci U S A.* **95**(17), pp.9920-9925.
- Sanger, M., Daubert, S. and Goodman, R.M. 1990. Characteristics of a strong promoter from figwort mosaic virus: comparison with the analogous 35S promoter from cauliflower mosaic virus and the regulated mannopine synthase promoter. *Plant Mol Biol.* **14**(3), pp.433-443.
- Sardar, A., Nandi, A.K. and Chattopadhyay, D. 2017. CBL-interacting protein kinase 6 negatively regulates immune response to *Pseudomonas syringae* in Arabidopsis. *J Exp Bot.* **68**(13), pp.3573-3584.

- Savary, S., Willocquet, L., Pethybridge, S.J., Esker, P., McRoberts, N. and Nelson, A. 2019. The global burden of pathogens and pests on major food crops. *Nat Ecol Evol.* **3**(3), pp.430-439.
- Schlüter, A., Fourcade, S., Ripp, R., Mandel, J.L., Poch, O. and Pujol, A. 2006. The evolutionary origin of peroxisomes: an ER-peroxisome connection. *Mol Biol Evol.* **23**(4), pp.838-845.
- Schmidt, S.M., Kuhn, H., Micali, C., Liller, C., Kwaaitaal, M. and Panstruga, R. 2014. Interaction of a *Blumeria graminis* f. sp. *hordei* effector candidate with a barley ARF-GAP suggests that host vesicle trafficking is a fungal pathogenicity target. *Mol Plant Pathol.* **15**(6), pp.535-549.
- Schoberer, J., König, J., Veit, C., Vavra, U., Liebminger, E., Botchway, S.W., Altmann, F., Kriechbaumer, V., Hawes, C. and Strasser, R. 2019. A signal motif retains Arabidopsis ER- α -mannosidase I in the cis-Golgi and prevents enhanced glycoprotein ERAD. *Nat Commun.* **10**(1), p3701.
- Schutze, M.P., Peterson, P.A. and Jackson, M.R. 1994. An N-terminal double-arginine motif maintains type II membrane proteins in the endoplasmic reticulum. *EMBO J.* **13**(7), pp.1696-1705.
- Sharma, K., Niraula, P.M., Troell, H.A., Adhikari, M., Alshehri, H.A., Alkharouf, N.W., Lawrence, K.S. and Klink, V.P. 2020. Exocyst components promote an incompatible interaction between *Glycine max* (soybean) and *Heterodera glycines* (the soybean cyst nematode). *Sci Rep.* **10**(1), p15003.
- Sharma, K., Pant, S.R., McNeece, B.T., Lawrence, G.W. and Klink, V.P. 2016. Co-regulation of the *Glycine max* soluble N-ethylmaleimide-sensitive fusion protein attachment protein receptor (SNARE)-containing regulon occurs during defense to a root pathogen. *Journal of plant interactions.* **11**(1), pp.74-93.
- Shen, J., Zeng, Y., Zhuang, X., Sun, L., Yao, X., Pimpl, P. and Jiang, L. 2013. Organelle pH in the Arabidopsis endomembrane system. *Mol Plant.* **6**(5), pp.1419-1437.

- Shestakova, A., Suvorova, E., Pavliv, O., Khaidakova, G. and Lupashin, V. 2007. Interaction of the conserved oligomeric Golgi complex with t-SNARE Syntaxin5a/Sed5 enhances intra-Golgi SNARE complex stability. *J Cell Biol.* **179**(6), pp.1179-1192.
- Shi, S., Ma, T. and Xi, Y. 2020. A Pan-Cancer Study of Epidermal Growth Factor-Like Domains 6/7/8 as Therapeutic Targets in Cancer. *Front Genet.* **11**, p598743.
- Shi, X., Halder, P., Yavuz, H., Jahn, R. and Shuman, H.A. 2016. Direct targeting of membrane fusion by SNARE mimicry: Convergent evolution of Legionella effectors. *Proc Natl Acad Sci U S A.* **113**(31), pp.8807-8812.
- Shimada, T., Kuroyanagi, M., Nishimura, M. and Hara-Nishimura, I. 1997. A pumpkin 72-kDa membrane protein of precursor-accumulating vesicles has characteristics of a vacuolar sorting receptor. *Plant Cell Physiol.* **38**(12), pp.1414-1420.
- Shimada, T., Yamada, K., Kataoka, M., Nakaune, S., Koumoto, Y., Kuroyanagi, M., Tabata, S., Kato, T., Shinozaki, K., Seki, M., Kobayashi, M., Kondo, M., Nishimura, M. and Hara-Nishimura, I. 2003. Vacuolar processing enzymes are essential for proper processing of seed storage proteins in *Arabidopsis thaliana*. *J Biol Chem.* **278**(34), pp.32292-32299.
- Siddique, S. and Grundler, F.M. 2018. Parasitic nematodes manipulate plant development to establish feeding sites. *Curr Opin Microbiol.* **46**, pp.102-108.
- Siddique, S., Endres, S., Atkins, J.M., Szakasits, D., Wieczorek, K., Hofmann, J., Blaukopf, C., Urwin, P.E., Tenhaken, R., Grundler, F.M.W., Kreil, D.P. and Bohlmann, H. 2009. Myo-inositol oxygenase genes are involved in the development of syncytia induced by *Heterodera schachtii* in *Arabidopsis* roots. *New Phytol.* **184**(2), pp.457-472.
- Siddique, S., Matera, C., Radakovic, Z.S., Hasan, M.S., Gutbrod, P., Rozanska, E., Sobczak, M., Torres, M.A. and Grundler, F.M. 2014. Parasitic worms

stimulate host NADPH oxidases to produce reactive oxygen species that limit plant cell death and promote infection. *Sci Signal.* **7**(320), pra33.

Siddique, S., Radakovic, Z.S., De La Torre, C.M., Chronis, D., Novák, O., Ramireddy, E., Holbein, J., Matera, C., Hütten, M., Gutbrod, P., Anjam, M.S., Rozanska, E., Habash, S., Elashry, A., Sobczak, M., Kakimoto, T., Strnad, M., Schmülling, T., Mitchum, M.G. and Grundler, F.M. 2015. A parasitic nematode releases cytokinin that controls cell division and orchestrates feeding site formation in host plants. *Proc Natl Acad Sci U S A.* **112**(41), pp.12669-12674.

Siddique, S., Radakovic, Z.S., Hiltl, C., Pellegrin, C., Baum, T.J., Beasley, H., Bent, A.F., Chitambo, O., Chopra, D. and Danchin, E.G.J. 2022. The genome and lifestage-specific transcriptomes of a plant-parasitic nematode and its host reveal susceptibility genes involved in trans-kingdom synthesis of vitamin B5. *Nature Communications.* **13**(1), p6190.

Siddique, S., Sobczak, M., Tenhaken, R., Grundler, F.M. and Bohlmann, H. 2012. Cell wall ingrowths in nematode induced syncytia require UGD2 and UGD3. *PLoS One.* **7**(7), pe41515.

Siddique, S., Wieczorek, K., Szakasits, D., Kreil, D.P. and Bohlmann, H. 2011. The promoter of a plant defensin gene directs specific expression in nematode-induced syncytia in *Arabidopsis* roots. *Plant Physiol Biochem.* **49**(10), pp.1100-1107.

Sijmons, P.C., Grundler, F.M.W., von Mende, N., Burrows, P.R. and Wyss, U. 1991. *Arabidopsis thaliana* as a new model host for plant-parasitic nematodes. *The Plant Journal.* **1**(2), pp.245-254.

Silady, R.A., Ehrhardt, D.W., Jackson, K., Faulkner, C., Oparka, K. and Somerville, C.R. 2008. The GRV2/RME-8 protein of *Arabidopsis* functions in the late endocytic pathway and is required for vacuolar membrane flow. *The Plant Journal.* **53**(1), pp.29-41.

Silva-Alvim, F.A.L., An, J., Alvim, J.C., Foresti, O., Grippa, A., Pelgrom, A., Adams, T.L., Hawes, C. and Denecke, J. 2018. Predominant Golgi

Residency of the Plant K/HDEL Receptor Is Essential for Its Function in Mediating ER Retention. *Plant Cell*. **30**(9), pp.2174-2196.

Simoni, E.B., Oliveira, C.C., Fraga, O.T., Reis, P.A.B. and Fontes, E.P.B. 2022. Cell Death Signaling From Endoplasmic Reticulum Stress: Plant-Specific and Conserved Features. *Front Plant Sci*. **13**, p835738.

Singh, S. and Mittal, A. 2016. Transmembrane Domain Lengths Serve as Signatures of Organismal Complexity and Viral Transport Mechanisms. *Sci Rep*. **6**, p22352.

Sipes, B.S., Schmitt, D.P. and Barker, K.R. 1992. Fertility of three parasitic biotypes of *Heterodera glycines*. *PHYTOPATHOLOGY-NEW YORK AND BALTIMORE THEN ST PAUL*. **82**, pp.999-999.

Smant, G., Stokkermans, J.P., Yan, Y., de Boer, J.M., Baum, T.J., Wang, X., Hussey, R.S., Gommers, F.J., Henrissat, B., Davis, E.L., Helder, J., Schots, A. and Bakker, J. 1998. Endogenous cellulases in animals: isolation of beta-1, 4-endoglucanase genes from two species of plant-parasitic cyst nematodes. *Proc Natl Acad Sci U S A*. **95**(9), pp.4906-4911.

Smith, R.D. and Lupashin, V.V. 2008. Role of the conserved oligomeric Golgi (COG) complex in protein glycosylation. *Carbohydr Res*. **343**(12), pp.2024-2031.

Sobczak, M. and Golinowski, W. 2009. Structure of Cyst Nematode Feeding Sites. In: Berg, R.H. and Taylor, C.G. eds. *Cell Biology of Plant Nematode Parasitism*. Berlin, Heidelberg: Springer Berlin Heidelberg, pp.153-187.

Sobczak, M., Golinowski, W. and Grundler, F.M.W. 1997. Changes in the structure of *Arabidopsis thaliana* roots induced during development of males of the plant parasitic nematode *Heterodera schachtii*. *European Journal of Plant Pathology*. **103**(2), pp.113-124.

Sobczak, M., Golinowski, W. and Grundler, F.M.W. 1999. Ultrastructure of feeding plugs and feeding tubes formed by *Heterodera schachtii*. *Nematology*. **1**(4), pp.363-374.

- Sohn, E.J., Kim, E.S., Zhao, M., Kim, S.J., Kim, H., Kim, Y.W., Lee, Y.J., Hillmer, S., Sohn, U., Jiang, L. and Hwang, I. 2003. Rha1, an Arabidopsis Rab5 homolog, plays a critical role in the vacuolar trafficking of soluble cargo proteins. *Plant Cell*. **15**(5), pp.1057-1070.
- Song, J., Lee, M.H., Lee, G.J., Yoo, C.M. and Hwang, I. 2006. Arabidopsis EPSIN1 plays an important role in vacuolar trafficking of soluble cargo proteins in plant cells via interactions with clathrin, AP-1, VTI11, and VSR1. *Plant Cell*. **18**(9), pp.2258-2274.
- Song, T., Ma, Z., Shen, D., Li, Q., Li, W., Su, L., Ye, T., Zhang, M., Wang, Y. and Dou, D. 2015. An Oomycete CRN Effector Reprograms Expression of Plant HSP Genes by Targeting their Promoters. *PLoS Pathog*. **11**(12), pe1005348.
- Sotta, N. and Fujiwara, T. 2017. Preparing thin cross sections of Arabidopsis roots without embedding. *Biotechniques*. **63**(6), pp.281-283.
- Spallek, T., Beck, M., Ben Khaled, S., Salomon, S., Bourdais, G., Schellmann, S. and Robatzek, S. 2013. ESCRT-I mediates FLS2 endosomal sorting and plant immunity. *PLoS Genet*. **9**(12), pe1004035.
- Sparkes, I.A., Runions, J., Kearns, A. and Hawes, C. 2006. Rapid, transient expression of fluorescent fusion proteins in tobacco plants and generation of stably transformed plants. *Nat Protoc*. **1**(4), pp.2019-2025.
- Sperschneider, J. and Dodds, P.N. 2022. EffectorP 3.0: Prediction of Apoplastic and Cytoplasmic Effectors in Fungi and Oomycetes. *Mol Plant Microbe Interact*. **35**(2), pp.146-156.
- Sperschneider, J., Dodds, P.N., Gardiner, D.M., Manners, J.M., Singh, K.B. and Taylor, J.M. 2015. Advances and challenges in computational prediction of effectors from plant pathogenic fungi. *PLoS Pathog*. **11**(5), pe1004806.
- Sperschneider, J., Gardiner, D.M., Dodds, P.N., Tini, F., Covarelli, L., Singh, K.B., Manners, J.M. and Taylor, J.M. 2016. EffectorP: predicting fungal effector

proteins from secretomes using machine learning. *New Phytol.* **210**(2), pp.743-761.

Stanley, P. 2011. Golgi glycosylation. *Cold Spring Harb Perspect Biol.* **3**(4).

Stegmann, M., Anderson, R.G., Westphal, L., Rosahl, S., McDowell, J.M. and Trujillo, M. 2013. The exocyst subunit Exo70B1 is involved in the immune response of *Arabidopsis thaliana* to different pathogens and cell death. *Plant Signal Behav.* **8**(12), pe27421.

Stein, M., Dittgen, J., Sánchez-Rodríguez, C., Hou, B.H., Molina, A., Schulze-Lefert, P., Lipka, V. and Somerville, S. 2006. Arabidopsis PEN3/PDR8, an ATP binding cassette transporter, contributes to nonhost resistance to inappropriate pathogens that enter by direct penetration. *Plant Cell.* **18**(3), pp.731-746.

Sticher, L. and Metraux, J.P. 2000. Inhibitors of N-linked glycosylation induce systemic acquired resistance in cucumber. *Physiological and Molecular Plant Pathology.* **56**(6), pp.245-252.

Su, T., Li, W., Wang, P. and Ma, C. 2019. Dynamics of Peroxisome Homeostasis and Its Role in Stress Response and Signaling in Plants. *Front Plant Sci.* **10**, p705.

Sumit, R., Sahu, B.B., Xu, M., Sandhu, D. and Bhattacharyya, M.K. 2012. Arabidopsis nonhost resistance gene PSS1 confers immunity against an oomycete and a fungal pathogen but not a bacterial pathogen that cause diseases in soybean. *BMC Plant Biol.* **12**, p87.

Sun, L., Lu, S.J., Zhang, S.S., Zhou, S.F. and Liu, J.X. 2013. The lumen-facing domain is important for the biological function and organelle-to-organelle movement of bZIP28 during ER stress in *Arabidopsis*. *Mol Plant.* **6**(5), pp.1605-1615.

Szakasits, D., Heinen, P., Wieczorek, K., Hofmann, J., Wagner, F., Kreil, D.P., Sykacek, P., Grundler, F.M. and Bohlmann, H. 2009. The transcriptome of

syncytia induced by the cyst nematode *Heterodera schachtii* in *Arabidopsis* roots. *Plant J.* **57**(5), pp.771-784.

Tan, X., Cao, K., Liu, F., Li, Y., Li, P., Gao, C., Ding, Y., Lan, Z., Shi, Z., Rui, Q., Feng, Y., Liu, Y., Zhao, Y., Wu, C., Zhang, Q., Jiang, L. and Bao, Y. 2016. *Arabidopsis* COG Complex Subunits COG3 and COG8 Modulate Golgi Morphology, Vesicle Trafficking Homeostasis and Are Essential for Pollen Tube Growth. *PLoS Genet.* **12**(7), pe1006140.

Tang, C., Xu, Q., Zhao, J., Yue, M., Wang, J., Wang, X. and Kang, Z. 2022. A rust fungus effector directly binds plant pre-mRNA splice site to reprogram alternative splicing and suppress host immunity. *Plant Biotechnol J.* **20**(6), pp.1167-1181.

Tao-Cheng, J.H., Crocker, V., Moreira, S.L. and Azzam, R. 2021. Optimization of protocols for pre-embedding immunogold electron microscopy of neurons in cell cultures and brains. *Mol Brain.* **14**(1), p86.

Teng, P.S. and Krupa, S.V. 1980. *Crop loss assessment*. Minnesota Agricultural Experiment Station: Retrieved from the University of Minnesota Digital Conservancy. Available from: <https://hdl.handle.net/11299/110181>

Thapa, S., Gates, M.K., Reuter-Carlson, U., Androwski, R.J. and Schroeder, N.E. 2019. Convergent evolution of saccate body shapes in nematodes through distinct developmental mechanisms. *Evodevo.* **10**, p5.

Thorpe, P., Mantelin, S., Cock, P.J., Blok, V.C., Coke, M.C., Eves-van den Akker, S., Guzeeva, E., Lilley, C.J., Smant, G., Reid, A.J., Wright, K.M., Urwin, P.E. and Jones, J.T. 2014. Genomic characterisation of the effector complement of the potato cyst nematode *Globodera pallida*. *BMC Genomics.* **15**(1), p923.

Tilman, D., Balzer, C., Hill, J. and Belfort, B.L. 2011. Global food demand and the sustainable intensification of agriculture. *Proc Natl Acad Sci U S A.* **108**(50), pp.20260-20264.

- Tolley, N., Sparkes, I.A., Hunter, P.R., Craddock, C.P., Nuttall, J., Roberts, L.M., Hawes, C., Pedrazzini, E. and Frigerio, L. 2008. Overexpression of a plant reticulon remodels the lumen of the cortical endoplasmic reticulum but does not perturb protein transport. *Traffic*. **9**(1), pp.94-102.
- Tomczynska, I., Stumpe, M. and Mauch, F. 2018. A conserved RxLR effector interacts with host RABA-type GTPases to inhibit vesicle-mediated secretion of antimicrobial proteins. *Plant J*. **95**(2), pp.187-203.
- Torrens-Spence, M.P., Bobokalonova, A., Carballo, V., Glinkerman, C.M., Pluskal, T., Shen, A. and Weng, J.K. 2019. PBS3 and EPS1 Complete Salicylic Acid Biosynthesis from Isochorismate in Arabidopsis. *Mol Plant*. **12**(12), pp.1577-1586.
- Torres, M.A., Dangl, J.L. and Jones, J.D. 2002. Arabidopsis gp91phox homologues AtrbohD and AtrbohF are required for accumulation of reactive oxygen intermediates in the plant defense response. *Proc Natl Acad Sci U S A*. **99**(1), pp.517-522.
- Torto-Alalibo, T., Collmer, C.W., Lindeberg, M., Bird, D., Collmer, A. and Tyler, B.M. 2009. Common and contrasting themes in host cell-targeted effectors from bacterial, fungal, oomycete and nematode plant symbionts described using the Gene Ontology. *BMC Microbiology*. **9**(1), pS3.
- Tsao, H.E., Lui, S.N., Lo, A.H., Chen, S., Wong, H.Y., Wong, C.K., Jiang, L. and Wong, K.B. 2022. Structural insights into how vacuolar sorting receptors recognize the sorting determinants of seed storage proteins. *Proc Natl Acad Sci U S A*. **119**(1).
- Tse, Y.C., Mo, B., Hillmer, S., Zhao, M., Lo, S.W., Robinson, D.G. and Jiang, L. 2004. Identification of multivesicular bodies as prevacuolar compartments in *Nicotiana tabacum* BY-2 cells. *Plant Cell*. **16**(3), pp.672-693.
- Tytgat, T., De Meutter, J., Vanholme, B., Claeys, M., Verreijdt, L., Gheysen, G. and Coomans, A. 2002. Development and pharyngeal gland activities of *Heterodera schachtii* infecting *Arabidopsis thaliana* roots. *Nematology*. **4**(8), pp.899-908.

- Tytgat, T., Meutter, J.D., Gheysen, G. and Coomans, A. 2000. Sedentary endoparasitic nematodes as a model for other plant parasitic nematodes. *Nematology*. **2**(1), pp.113-121.
- Uemura, T. 2016. Physiological Roles of Plant Post-Golgi Transport Pathways in Membrane Trafficking. *Plant Cell Physiol.* **57**(10), pp.2013-2019.
- Uemura, T., Kim, H., Saito, C., Ebine, K., Ueda, T., Schulze-Lefert, P. and Nakano, A. 2012. Qa-SNAREs localized to the trans-Golgi network regulate multiple transport pathways and extracellular disease resistance in plants. *Proc Natl Acad Sci U S A.* **109**(5), pp.1784-1789.
- Uemura, T., Morita, M.T., Ebine, K., Okatani, Y., Yano, D., Saito, C., Ueda, T. and Nakano, A. 2010. Vacuolar/pre-vacuolar compartment Qa-SNAREs VAM3/SYP22 and PEP12/SYP21 have interchangeable functions in Arabidopsis. *Plant J.* **64**(5), pp.864-873.
- Urwin, P.E., Lilley, C.J., McPherson, M.J. and Atkinson, H.J. 1997a. Resistance to both cyst and root-knot nematodes conferred by transgenic Arabidopsis expressing a modified plant cystatin. *Plant J.* **12**(2), pp.455-461.
- Urwin, P.E., Møller, S.G., Lilley, C.J., McPherson, M.J. and Atkinson, H.J. 1997b. Continual green-fluorescent protein monitoring of cauliflower mosaic virus 35S promoter activity in nematode-induced feeding cells in Arabidopsis thaliana. *Mol Plant Microbe Interact.* **10**(3), pp.394-400.
- van de Meene, A.M., Doblin, M.S. and Bacic, A. 2017. The plant secretory pathway seen through the lens of the cell wall. *Protoplasma.* **254**(1), pp.75-94.
- van der Fits, L., Deakin, E.A., Hoge, J.H. and Memelink, J. 2000. The ternary transformation system: constitutive virG on a compatible plasmid dramatically increases Agrobacterium-mediated plant transformation. *Plant Mol Biol.* **43**(4), pp.495-502.
- van Doorn, W.G. 2011. Classes of programmed cell death in plants, compared to those in animals. *J Exp Bot.* **62**(14), pp.4749-4761.

- Van Loock, B., Markakis, M.N., Verbelen, J.P. and Vissenberg, K. 2010. High-throughput transient transformation of Arabidopsis roots enables systematic colocalization analysis of GFP-tagged proteins. *Plant Signal Behav.* **5**(3), pp.261-263.
- van Weering, J.R., Brown, E., Sharp, T.H., Mantell, J., Cullen, P.J. and Verkade, P. 2010. Intracellular membrane traffic at high resolution. *Methods Cell Biol.* **96**, pp.619-648.
- Veeramani, S., Lee, M.S. and Lin, M.F. 2009. Revisiting histidine-dependent acid phosphatases: a distinct group of tyrosine phosphatases. *Trends Biochem Sci.* **34**(6), pp.273-278.
- Velten, J., Velten, L., Hain, R. and Schell, J. 1984. Isolation of a dual plant promoter fragment from the Ti plasmid of *Agrobacterium tumefaciens*. *EMBO J.* **3**(12), pp.2723-2730.
- Verica, J.A., Chae, L., Tong, H., Ingmire, P. and He, Z.H. 2003. Tissue-specific and developmentally regulated expression of a cluster of tandemly arrayed cell wall-associated kinase-like kinase genes in Arabidopsis. *Plant Physiol.* **133**(4), pp.1732-1746.
- Verma, A., Lee, C., Morriss, S., Odu, F., Kenning, C., Rizzo, N., Spollen, W.G., Lin, M., McRae, A.G., Givan, S.A., Hewezi, T., Hussey, R., Davis, E.L., Baum, T.J. and Mitchum, M.G. 2018. The novel cyst nematode effector protein 30D08 targets host nuclear functions to alter gene expression in feeding sites. *New Phytol.* **219**(2), pp.697-713.
- Vieira, P. and Gleason, C. 2019. Plant-parasitic nematode effectors - insights into their diversity and new tools for their identification. *Curr Opin Plant Biol.* **50**, pp.37-43.
- Vijayapalani, P., Hewezi, T., Pontvianne, F. and Baum, T.J. 2018. An Effector from the Cyst Nematode. *Plant Cell.* **30**(11), pp.2795-2812.

- Villalobo, A., Ruano, M.J., Palomo-Jiménez, P.I., Li, H. and Martín-Nieto, J. 2000. The epidermal growth factor receptor and the calcium signal. *Calcium: The molecular basis of calcium action in biology and medicine*. pp.287-303.
- Vincent, M.J., Martin, A.S. and Compans, R.W. 1998. Function of the KKXX motif in endoplasmic reticulum retrieval of a transmembrane protein depends on the length and structure of the cytoplasmic domain. *J Biol Chem*. **273**(2), pp.950-956.
- Vitale, A. and Boston, R.S. 2008. Endoplasmic reticulum quality control and the unfolded protein response: insights from plants. *Traffic*. **9**(10), pp.1581-1588.
- Vitale, A. and Denecke, J. 1999. The endoplasmic reticulum-gateway of the secretory pathway. *Plant Cell*. **11**(4), pp.615-628.
- Vitale, A., Ceriotti, A. and Denecke, J. 1993. The Role of the Endoplasmic Reticulum in Protein Synthesis, Modification and Intracellular Transport. *Journal of Experimental Botany*. **44**(9), pp.1417-1444.
- Vuttipongchaikij, S., Brocklehurst, D., Steele-King, C., Ashford, D.A., Gomez, L.D. and McQueen-Mason, S.J. 2012. Arabidopsis GT34 family contains five xyloglucan α -1,6-xylosyltransferases. *New Phytol*. **195**(3), pp.585-595.
- Waghmare, S., Lileikyte, E., Karnik, R., Goodman, J.K., Blatt, M.R. and Jones, A.M.E. 2018. SNAREs SYP121 and SYP122 Mediate the Secretion of Distinct Cargo Subsets. *Plant Physiol*. **178**(4), pp.1679-1688.
- Walter, P. and Lingappa, V.R. 1986. Mechanism of protein translocation across the endoplasmic reticulum membrane. *Annual review of cell biology*. **2**(1), pp.499-516.
- Wan, J., He, M., Hou, Q., Zou, L., Yang, Y., Wei, Y. and Chen, X. 2021. Cell wall associated immunity in plants. *Stress Biology*. **1**(1), p3.

- Wang, D., Weaver, N.D., Kesarwani, M. and Dong, X. 2005. Induction of protein secretory pathway is required for systemic acquired resistance. *Science*. **308**(5724), pp.1036-1040.
- Wang, F., Shang, Y., Fan, B., Yu, J.Q. and Chen, Z. 2014a. Arabidopsis LIP5, a positive regulator of multivesicular body biogenesis, is a critical target of pathogen-responsive MAPK cascade in plant basal defense. *PLoS Pathog*. **10**(7), pe1004243.
- Wang, H., Guo, B., Yang, B., Li, H., Xu, Y., Zhu, J., Wang, Y., Ye, W., Duan, K. and Zheng, X. 2021. An atypical *Phytophthora sojae* RxLR effector manipulates host vesicle trafficking to promote infection. *PLoS Pathog*. **17**(11), pe1010104.
- Wang, J., Dhroso, A., Liu, X., Baum, T.J., Hussey, R.S., Davis, E.L., Wang, X., Korkin, D. and Mitchum, M.G. 2021a. Phytonematode peptide effectors exploit a host post-translational trafficking mechanism to the ER using a novel translocation signal. *New Phytol*. **229**(1), pp.563-574.
- Wang, J., Lee, C., Replogle, A., Joshi, S., Korkin, D., Hussey, R., Baum, T.J., Davis, E.L., Wang, X. and Mitchum, M.G. 2010. Dual roles for the variable domain in protein trafficking and host-specific recognition of *Heterodera glycines* CLE effector proteins. *New Phytol*. **187**(4), pp.1003-1017.
- Wang, J., Yeckel, G., Kandoth, P.K., Wasala, L., Hussey, R.S., Davis, E.L., Baum, T.J. and Mitchum, M.G. 2020a. Targeted suppression of soybean BAG6-induced cell death in yeast by soybean cyst nematode effectors. *Mol Plant Pathol*. **21**(9), pp.1227-1239.
- Wang, R., Deng, M., Yang, C., Yu, Q., Zhang, L., Zhu, Q. and Guo, X. 2021b. A Qa-SNARE complex contributes to soybean cyst nematode resistance via regulation of mitochondria-mediated cell death. *J Exp Bot*. **72**(20), pp.7145-7162.
- Wang, T. and Gasser, R.B. 2021. Prospects of Using High-Throughput Proteomics to Underpin the Discovery of Animal Host-Nematode Interactions. *Pathogens*. **10**(7).

- Wang, W., Devoto, A., Turner, J.G. and Xiao, S. 2007. Expression of the membrane-associated resistance protein RPW8 enhances basal defense against biotrophic pathogens. *Mol Plant Microbe Interact.* **20**(8), pp.966-976.
- Wang, X., Chung, K.P., Lin, W. and Jiang, L. 2017. Protein secretion in plants: conventional and unconventional pathways and new techniques. *J Exp Bot.* **69**(1), pp.21-37.
- Wang, X., Deng, L., Chang, H., Dubcovsky, J., Feng, H., Han, Q., Huang, L. and Kang, Z. 2014b. Wheat TaNPSN SNARE homologues are involved in vesicle-mediated resistance to stripe rust (*Puccinia striiformis* f. sp. *tritici*). *J Exp Bot.* **65**(17), pp.4807-4820.
- Wang, X., Xu, M., Gao, C., Zeng, Y., Cui, Y., Shen, W. and Jiang, L. 2020b. The roles of endomembrane trafficking in plant abiotic stress responses. *J Integr Plant Biol.* **62**(1), pp.55-69.
- Watanabe, N. and Lam, E. 2008. BAX inhibitor-1 modulates endoplasmic reticulum stress-mediated programmed cell death in Arabidopsis. *J Biol Chem.* **283**(6), pp.3200-3210.
- Wee, E.G., Sherrier, D.J., Prime, T.A. and Dupree, P. 1998. Targeting of active sialyltransferase to the plant Golgi apparatus. *Plant Cell.* **10**(10), pp.1759-1768.
- Weßling, R., Epple, P., Altmann, S., He, Y., Yang, L., Henz, S.R., McDonald, N., Wiley, K., Bader, K.C., Gläßer, C., Mukhtar, M.S., Haigis, S., Ghamsari, L., Stephens, A.E., Ecker, J.R., Vidal, M., Jones, J.D., Mayer, K.F., Ver Loren van Themaat, E., Weigel, D., Schulze-Lefert, P., Dangl, J.L., Panstruga, R. and Braun, P. 2014. Convergent targeting of a common host protein-network by pathogen effectors from three kingdoms of life. *Cell Host Microbe.* **16**(3), pp.364-375.
- Wilkop, T., Pattathil, S., Ren, G., Davis, D.J., Bao, W., Duan, D., Peralta, A.G., Domozych, D.S., Hahn, M.G. and Drakakaki, G. 2019. A Hybrid Approach

Enabling Large-Scale Glycomic Analysis of Post-Golgi Vesicles Reveals a Transport Route for Polysaccharides. *Plant Cell*. **31**(3), pp.627-644.

Williams, K.J. and Fisher, J.M. 1993. Development of *Heterodera avenae* Woll. and host cellular responses in susceptible and resistant wheat. *Fundamental and applied nematology*. **16**(5), pp.417-423.

Wilson, D.W., Lewis, M.J. and Pelham, H.R. 1993. pH-dependent binding of KDEL to its receptor in vitro. *J Biol Chem*. **268**(10), pp.7465-7468.

Winey, M., Meehl, J.B., O'Toole, E.T. and Giddings, T.H. 2014. Conventional transmission electron microscopy. *Mol Biol Cell*. **25**(3), pp.319-323.

Wrather, J.A., Anderson, T.R., Arsyad, D.M., Gai, J., Ploper, L.D., Porta-Puglia, A., Ram, H.H. and Yorinori, J.T. 1997. Soybean Disease Loss Estimates for the Top 10 Soybean Producing Countries in 1994. *Plant Dis*. **81**(1), pp.107-110.

Wu, G., Liu, S., Zhao, Y., Wang, W., Kong, Z. and Tang, D. 2015. ENHANCED DISEASE RESISTANCE4 associates with CLATHRIN HEAVY CHAIN2 and modulates plant immunity by regulating relocation of EDR1 in *Arabidopsis*. *Plant Cell*. **27**(3), pp.857-873.

Wu, T.M., Lin, K.C., Liao, W.S., Chao, Y.Y., Yang, L.H., Chen, S.Y., Lu, C.A. and Hong, C.Y. 2016. A set of GFP-based organelle marker lines combined with DsRed-based gateway vectors for subcellular localization study in rice (*Oryza sativa* L.). *Plant Mol Biol*. **90**(1-2), pp.107-115.

Wyss, U. 1981. Ectoparasitic root nematodes: feeding behaviour and plant cell responses. *Plant parasitic nematodes*. **3**, pp.325-351.

Wyss, U. and Grundler, F.M.W. 1992. Feeding behavior of sedentary plant parasitic nematodes. *Netherlands Journal of Plant Pathology*. **98**, pp.165-173.

Wyss, U. and Zunke, U. 1986. Observations on the behaviour of second stage juveniles of *Hetero* inside host roots. *Rev Nematol*. **9**, pp.153-165.

- Xu, R. and Li, Q.Q. 2008. Protocol: Streamline cloning of genes into binary vectors in *Agrobacterium* via the Gateway(R) TOPO vector system. *Plant Methods*. **4**, p4.
- Xue, B., Hamamouch, N., Li, C., Huang, G., Hussey, R.S., Baum, T.J. and Davis, E.L. 2013. The 8D05 parasitism gene of *Meloidogyne incognita* is required for successful infection of host roots. *Phytopathology*. **103**(2), pp.175-181.
- Yamada, K., Goto-Yamada, S., Nakazaki, A., Kunieda, T., Kuwata, K., Nagano, A.J., Nishimura, M. and Hara-Nishimura, I. 2020. Endoplasmic reticulum-derived bodies enable a single-cell chemical defense in Brassicaceae plants. *Commun Biol*. **3**(1), p21.
- Yang, J., Zhang, T., Li, J., Wu, N., Wu, G., Chen, X., He, L. and Chen, J. 2020. Chinese wheat mosaic virus-derived vsiRNA-20 can regulate virus infection in wheat through inhibition of vacuolar- (H. *New Phytol*. **226**(1), pp.205-220.
- Yang, J.S., Lee, S.Y., Gao, M., Bourgoin, S., Randazzo, P.A., Premont, R.T. and Hsu, V.W. 2002. ARFGAP1 promotes the formation of COPI vesicles, suggesting function as a component of the coat. *J Cell Biol*. **159**(1), pp.69-78.
- Yang, Z.T., Wang, M.J., Sun, L., Lu, S.J., Bi, D.L., Song, Z.T., Zhang, S.S., Zhou, S.F. and Liu, J.X. 2014. The membrane-associated transcription factor NAC089 controls ER-stress-induced programmed cell death in plants. *PLoS Genet*. **10**(3), pe1004243.
- Ye, F. and Signer, E.R. 1996. RIGS (repeat-induced gene silencing) in *Arabidopsis* is transcriptional and alters chromatin configuration. *Proc Natl Acad Sci U S A*. **93**(20), pp.10881-10886.
- Yuan, P., Qian, W., Jiang, L., Jia, C., Ma, X., Kang, Z. and Liu, J. 2021. A secreted catalase contributes to *Puccinia striiformis* resistance to host-derived oxidative stress. *Stress Biology*. **1**(1), p22.

- Yuan, X., Wang, H., Cai, J., Li, D. and Song, F. 2019. NAC transcription factors in plant immunity. *Phytopathology Research*. **1**(1), pp.1-13.
- Yun, H.S. and Kwon, C. 2017. Vesicle trafficking in plant immunity. *Curr Opin Plant Biol*. **40**, pp.34-42.
- Yun, H.S., Kang, B.G. and Kwon, C. 2016. Arabidopsis immune secretory pathways to powdery mildew fungi. *Plant Signal Behav*. **11**(10), pe1226456.
- Zárský, V., Kulich, I., Fendrych, M. and Pečenková, T. 2013. Exocyst complexes multiple functions in plant cells secretory pathways. *Curr Opin Plant Biol*. **16**(6), pp.726-733.
- Zeng, W., Ford, K.L., Bacic, A. and Heazlewood, J.L. 2018. -linked Glycan Microheterogeneity in Glycoproteins of Arabidopsis. *Mol Cell Proteomics*. **17**(3), pp.413-421.
- Zhang, B., Liu, X., Qian, Q., Liu, L., Dong, G., Xiong, G., Zeng, D. and Zhou, Y. 2011. Golgi nucleotide sugar transporter modulates cell wall biosynthesis and plant growth in rice. *Proc Natl Acad Sci U S A*. **108**(12), pp.5110-5115.
- Zhang, C., Beckmann, L., Kudla, J. and Batistič, O. 2017a. N-terminal S-acylation facilitates tonoplast targeting of the calcium sensor CBL6. *FEBS Lett*. **591**(22), pp.3745-3756.
- Zhang, C., Hicks, G.R. and Raikhel, N.V. 2014. Plant vacuole morphology and vacuolar trafficking. *Front Plant Sci*. **5**, p476.
- Zhang, L., Lilley, C.J., Imren, M., Knox, J.P. and Urwin, P.E. 2017b. The Complex Cell Wall Composition of Syncytia Induced by Plant Parasitic Cyst Nematodes Reflects Both Function and Host Plant. *Front Plant Sci*. **8**, p1087.
- Zhang, L., Liu, Y., Zhu, X.F., Jung, J.H., Sun, Q., Li, T.Y., Chen, L.J., Duan, Y.X. and Xuan, Y.H. 2019a. SYP22 and VAMP727 regulate BRI1 plasma membrane targeting to control plant growth in Arabidopsis. *New Phytol*. **223**(3), pp.1059-1065.

- Zhang, L., Xing, J. and Lin, J. 2019b. At the intersection of exocytosis and endocytosis in plants. *New Phytol.* **224**(4), pp.1479-1489.
- Zhang, M., Hu, S., Yi, F., Gao, Y., Zhu, D., Wang, Y., Cai, Y., Hou, D., Lin, X. and Shen, J. 2021a. Organelle Visualization With Multicolored Fluorescent Markers in Bamboo. *Front Plant Sci.* **12**, p658836.
- Zhang, M., Li, Q., Liu, T., Liu, L., Shen, D., Zhu, Y., Liu, P., Zhou, J.M. and Dou, D. 2015. Two cytoplasmic effectors of *Phytophthora sojae* regulate plant cell death via interactions with plant catalases. *Plant Physiol.* **167**(1), pp.164-175.
- Zhang, X., Li, H., Lu, H. and Hwang, I. 2021b. The trafficking machinery of lytic and protein storage vacuoles: how much is shared and how much is distinct? *J Exp Bot.* **72**(10), pp.3504-3512.
- Zhang, Z., Lenk, A., Andersson, M.X., Gjetting, T., Pedersen, C., Nielsen, M.E., Newman, M.A., Hou, B.H., Somerville, S.C. and Thordal-Christensen, H. 2008. A lesion-mimic syntaxin double mutant in *Arabidopsis* reveals novel complexity of pathogen defense signaling. *Mol Plant.* **1**(3), pp.510-527.
- Zhao, J. and Liu, S. 2022. Beet cyst nematode HsSNARE1 interacts with both AtSNAP2 and AtPR1 and promotes disease in *Arabidopsis*. *J Adv Res.*
- Zhao, J., Zhang, X., Wan, W., Zhang, H., Liu, J., Li, M., Wang, H., Xiao, J. and Wang, X. 2018. Identification and Characterization of the. *Int J Mol Sci.* **20**(1).
- Zheng, Q., Putker, V. and Goverse, A. 2021. Molecular and Cellular Mechanisms Involved in Host-Specific Resistance to Cyst Nematodes in Crops. *Front Plant Sci.* **12**, p641582.
- Zheng, Z., Qualley, A., Fan, B., Dudareva, N. and Chen, Z. 2009. An important role of a BAHD acyl transferase-like protein in plant innate immunity. *Plant J.* **57**(6), pp.1040-1053.

- Zhong, L., Zhang, Y., Liu, H., Sun, G., Chen, R. and Song, S. 2016. *Agrobacterium*-mediated transient expression via root absorption in flowering Chinese cabbage. *Springerplus*. **5**(1), p1825.
- Zhou, L., Bokhari, S.A., Dong, C.J. and Liu, J.Y. 2011. Comparative proteomics analysis of the root apoplasts of rice seedlings in response to hydrogen peroxide. *PLoS One*. **6**(2), pe16723.
- Zhou, Q., Ma, K., Hu, H., Xing, X., Huang, X. and Gao, H. 2022. Extracellular vesicles: Their functions in plant-pathogen interactions. *Mol Plant Pathol*. **23**(6), pp.760-771.
- Zhu, X.F., Liu, Y., Gai, X.T., Zhou, Y., Xia, Z.Y., Chen, L.J., Duan, Y.X. and Xuan, Y.H. 2019. SNARE proteins SYP22 and VAMP727 negatively regulate plant defense. *Plant Signal Behav*. **14**(7), p1610300.
- Zuppini, A., Navazio, L. and Mariani, P. 2004. Endoplasmic reticulum stress-induced programmed cell death in soybean cells. *J Cell Sci*. **117**(Pt 12), pp.2591-2598.